รายงานวิจัยฉบับสมบูรณ์

โครงการเพียโซอิเล็กตริกเซรามิกที่อุณหภูมิต่ำ

LOW TEMPERATRUE SINTERING PIEZOELECTRIC CERAMICS

โดย ศาสตราจารย์ ดร.ทวี ตันฆศิริ และคณะ

สิงหาคม 2548

สัญญาเลขที่ RTA 4580004

รายงานวิจัยฉบับสมบูรณ์

โครงการเพียโซอิเล็กตริกเซรามิกที่อุณหภูมิต่ำ

LOW TEMPERATURE SINTERING PIEZOELECTRIC CERAMICS

โดย ศาสตราจารย์ ดร.ทวี ตันฆศิริ และคณะ

ภาควิชาฟิสิกส์ คณะวิทยาศาสตร์

มหาวิทยาลัยเชียงใหม่

สนับสนุนโดยกองทุนสนับสนุนการวิจัย

สัญญาเลขที่ RTA4580004

รายงานฉบับสมบูรณ์

โครงการเพียโซอิเล็กตริกเซรามิกที่อุณหภูมิต่ำ

Low Temperature Sintering Piezoelectric Ceramics

	คณะผู้วิจัย	สังกัด
1.	ศ.ดร.ทวี ตันฆศิริ	คณะวิทยาศาสตร์ มหาวิทยาลัยเชียงใหม่
2.	รศ.ดร.จีระพงษ์ ตันตระกูล	คณะวิทยาศาสตร์ มหาวิทยาลัยเชียงใหม่
3.	รศ.ดร.นรินทร์ สิริกุลรัตน์	คณะวิทยาศาสตร์ มหาวิทยาลัยเชียงใหม่
4.	ดร.วิม เหนือเพ็ง	คณะวิทยาศาสตร์ มหาวิทยาลัยเชียงใหม่
5.	ดร.วิมล ไสยสมบัติ	คณะวิทยาศาสตร์ มหาวิทยาลัยเชียงใหม่
6.	อ.อรวรรณ คำมั่น	คณะวิทยาศาสตร์ มหาวิทยาลัยเชียงใหม่
7.	รศ.ดร.ศุภสโรช หมื่นสิทธิ์	คณะวิทยาศาสตร์ มหาวิทยาลัยสงขลานครินทร์
8.	ดร.สมนึก ศิริสุนทร	ศูนย์เทคโนโลยีโลหะและวัสดุแห่งชาติ กรุงเทพฯ
9.	นายสุวิทย์ ชัยสุพรรณ	คณะวิทยาศาสตร์ มหาวิทยาลัยเชียงใหม่

สนับสนุนโดยสำนักงานกองทุนสนับสนุนการวิจัย

(ความเห็นในรายงานนี้เป็นของผู้วิจัย สกว. ไม่จำเป็นต้องเห็นด้วยเสมอไป)

กิตติกรรมประกาศ

คณะวิจัย ขอขอบพระคุณ สำนักงานสนับสนุนการวิจัย (สกว.) ที่สนับสนุนให้ทุนโครงการวิจัยเมธีอาวุโส "เพียโซอิเล็กตริกเซรามิกที่อุณหภูมิซินเตอร์ต่ำ (Low Temperature Sintering Piezoelectric Ceramics)"

โครงการนี้สำเร็จลุล่วงไปด้วยการสนับสนุนและความร่วมมือจากหลายท่าน หลายหน่วยงาน ได้แก่ อาจารย์ นักวิจัย และนักศึกษา (ซึ่งมีส่วนร่วมอย่างมาก) ทำให้เกิดผลงานวิจัยอันมีคุณภาพและคุณค่า ขอขอบคุณ เจ้าหน้าที่ สกว. และเจ้าหน้าที่ห้องปฏิบัติการเซรามิกประยุกต์ คณะวิทยาศาสตร์ มหาวิทยาลัยเชียงใหม่ ที่ช่วยในงานด้านเอกสารต่างๆ

ขอขอบคุณการสนับสนุนเพิ่มเติมจากแหล่งอื่นๆ ที่ช่วยเสริมการทำวิจัย ทำให้มีประสิทธิภาพยิ่งขึ้น ได้แก่ The Royal Golden Jubilee (RGJ), Ph.D. program (TRF), ศูนย์เทคโนโลยีโลหะและวัสดุแห่งชาติ (MTEC), The Post-graduate Education Development (PED) Program (The Commission on Higher Education) สำนักงานคณะกรรมการวิจัยแห่งชาติ (NRC)

ขอขอบคุณผู้บริหารทุกท่าน ได้แก่ ผู้อำนวยการ สกว. อธิการบดีมหาวิทยาลัยเชียงใหม่ คณบดีคณะวิทยาศาสตร์ หัวหน้าภาควิชาฟิสิกส์ ที่ให้การสนับสนุน และทุกท่านที่มีส่วนร่วมทั้งในทางตรงและทางอ้อม แต่ไม่ได้เอ่ยนามในที่นี้

ศาสตราจารย์ ดร.ทวี ตันฆศิริ
หัวหน้าโครงการ

บทคัดย่อ

โครงการเพียโซอิเล็กตริกเซรามิกที่อุณหภูมิซินเตอร์ต่ำ

โครงการเมธีวิจัยอาวุโส สกว. สัญญาเลขที่ RTA 4580004

หัวหน้าโครงการ: ศาสตราจารย์ ดร.ทวี ตันฑศิริ

โครงการนี้เป็นงานวิจัยที่จะดำเนินการลดอุณหภูมิที่เผาผนึก (เผาให้เป็นเซรามิก, ซินเตอร์) ของกลุ่มเพียโซอิเล็กตริกเซรามิก โครงการนี้อาจแยกเป็น 4 โครงการย่อย

โครงการย่อยที่ 1 แผ่นฟิล์มเซรามิกหนาที่มีสารช่วยหลอม

ในโครงการย่อยนี้ ได้ดำเนินการสังเคราะห์แผ่นฟิล์มเซรามิกหนา (< 0.5 มม) ของ $BaTi_4O_9$, $BaTi_2O_5$ และ $BaTi_5O_{11}$ ด้วยวิธีดั้งเดิม (เผาโดยตรงจากการผสมของออกไซด์ของโลหะ) โซล-เจล และการตกผลึกร่วม อุณหภูมิซินเตอร์ของ $BaTi_2O_5$ และ $BaTi_5O_{11}$ (เตรียมจากวิธีเคมี, โซล-เจลและการตกผลึกร่วม) จะต่ำเมื่อเทียบกับ $BaTi_4O_9$, เซรามิกที่ได้จะมีความหนาแน่นสูงเมื่อเทียบกับทางทฤษฎี และมีการตอบสนองที่ดีมากต่อความถี่คลื่นช่วงไมโครเวฟ

เลดเซอร์โคเนตไทเทเนต ($Pb(Zr_{0.52}Ti_{0.48})O_3$, PZT) ที่มีขนาดอนุภาคเล็กกว่าไมครอน สามารถเตรียมได้โดยวิธีสเปรย์สารละลาย PZT ผ่านความร้อน (Spray dry) นำผง PZT ที่ได้ไปทำเป็นเซรามิก ซึ่งการเผาเป็นเซรามิกนี้สามารถเผาที่อุณหภูมิน้อยกว่า 1200 °ซ และสมบัติทางกายภาพ (ไดอิเล็กตริกและเพียโซอิเล็กตริก) โครงการนี้ได้ศึกษาการเปลี่ยนเฟสของสารที่มีตะกั่วเป็นฐานด้วย ตลอดทั้งการลดอุณหภูมิซินเตอร์โดยการใส่สารช่วยหลอมในสารเหล่านี้ และสามารถลดอุณหภูมิลงถึง 1000 °ซ และยังมีสมบัติที่ดี

โครงการย่อยที่ 2 ฟิล์มบาง PLZT

เตรียมฟิล์มบางของ PLZT (~ 500 nm) โดยวิธีโซล-เจล และสปินโคตติง เผาผนึกที่ 600 °ซ มีความหนาแน่นมากและความพรุนน้อย และสมบัติที่ดี ผลจากโครงการย่อยที่ 1 ทำให้ศึกษาการเกิดเฟสของ PZ, ZT, ZT และเตรียมแผ่นฟิล์มบาง PLZT ที่ได้จากการใช้วิธีการรีดด้วยเครื่องรีดเทป (ความหนาประมาณ 100 ไมครอน) ได้ แล้วเผาให้เป็นเซรามิก ซึ่งได้ฟิล์มที่สมบัติทางไฟฟ้าที่ดี และความสูญเสียทางไฟฟ้าที่น้อยมาก

โครงการย่อยที่ 3 วัสดุผสม

วัสดุผสมจะประกอบด้วยวัสดุมากกว่า 2 ชนิด ผสมกัน ในแบบสัมผัสต่างๆ (connectivity) ในโครงการย่อยนี้ได้เตรียมเซรามิกพรุนของ PT และ PZT แล้วให้อีพอกซี (epoxy) ซึมเข้าในรูต่างๆ สมบัติทางไฟฟ้าจะอยู่ระหว่างสารทั้งสองชนิด ซึ่งเหมาะสำหรับใช้เป็นตัวกลางให้คลื่น (เชิงกล) วิ่งผ่านได้ระหว่างตัวกลางสองชนิดที่ความหนาแน่นต่างกัน เช่น เซรามิก และผิวของมนุษย์

วัสดุผสมเซรามิก-เซรามิก (PZT+PZN, PZT+BFN และ BMN+BT) สามารถเตรียมได้และมีค่าคงที่ไดอิเล็กตริกที่สูงและอุณหภูมิซินเตอร์ที่ต่ำ

โครงการย่อยที่ 4 สารเพียโซอิเล็กตริกไร้ตะกั่ว

งานในโครงการย่อยนี้มุ่งไปที่การสังเคราะห์สารประกอบที่ไม่มีตะกั่วเป็นฐาน เช่น บิสมัทโซเดียมไทเทเนต (BiNT) แบเรียมสตรอนเชียมไทเทเนต (BST) และ BMN+BT ที่ผสมด้วยสารช่วยหลอม โครงการนี้ยังได้ดำเนินงานวิจัยสร้างแผ่นฟิล์มบาง เซลล์สุริยะ แคดเมียมซัลไฟด์ (CdS) ที่มี Ni เจือปนด้วยวิธีการยึดเกาะเป็นแผ่นของสารละลายบนแผ่นรองรับ (Chemical bath deposition) ความไวต่อแสงของแผ่นฟิล์มอยู่ในเกณฑ์ดี ขณะนี้กำลังทดสอบความสม่ำเสมอของความไวต่อแสง

Keywords: piezoelectric, dielectric, low sintering temperature, low sintering aids, composite

Abstract

LOW TEMPERATURE SINTERING PIEZOELECTRIC CERAMICS

TRF SENIOR RESEARCH SCHOLAR GRANT CONTACT NO. RTA 4580004

Principal Investigator: Prof.Dr.Tawee Tunkasiri

In this project, attempt to reduce densifying (sintering) temperature of the piezoelectric ceramics has been carried out.

This project can be divided into 4 subprojects, as follow:

Subproject I Thick Film Ceramics With Sintering Aids

In this subproject, thick film microware ceramics of $BaTi_4O_9$, $BaTi_2O_5$ and $BaTi_5O_{11}$ were synthesized employing conventional mixed oxide, sol-gel and co-precipitation methods respectively. Sintering temperature $BaTi_2O_5$ and $BaTi_5O_{11}$ powders (which prepared via chemical route, sol-gel and co-precipitation) are relatively low compared to that of $BaTi_4O_9$. Single phase of these ceramics were obtained with exceptional high densities compared with that of theoretical densities. Responses to the microwave frequencies were also excellent.

Submicro size particle of lead zirconate titanate ($Pb(Zr_{0.52}Ti_{0.48})O_3$, PZT) were obtained via spray drying of the mixed solution. The corresponding ceramics were sintered at low temperatures (< 1200 °C) as expected, with exceptional good physical properties (dielectric and piezoelectric,...etc.). Phase evolution of other lead based compounds were also studied. Sintering aids were mixed to the lead based compounds and it was found that they can reduced the sintering temperature (~ 1000 °C) with reasonable physical properties.

Subproject II Thin Film PLZT

Thin film of PZLT (~ 500 nm) can be produced by sol gel and spin coating methods. Annealing was accomplished at 600 °C resulting in very dense, ferroelectric phase with PLZT films of ~ 500 nm with exceptional low porosity and good electrical properties. Results from subproject I, study of phase evolution PZ, PT and ZT was carried out. Forming of thin film PLZT

green sheets (~ 100 μm) was done via tape casting. The corresponding ceramics showed good dielectric constant and low dielectric loss.

Subproject III Composite Materials

Composites are at least 2 compounds mixed together in various connectivities. In this subproject, epoxy was impregnated into porous ceramic of PT and PZT. Their electrical properties lie between the individual property of each compound, which is appropriate for using as a medium for acoustic wave penetration between 2 different density media such as human body and ceramics.

Ceramic-ceramic composites (PZT+PZN, PZT+BFN and BMN+BT) were also prepared inorder to obtain high dielectric constant for capacitor applications. All composites show high dielectric constants (> 10,000), especially, BMN+BT shows very high dielectric constant with low dielectric loss.

Subproject IV: Lead Free Piezoelectric compounds

Work in this subproject was concentrated on the lead free piezoelectric compounds, such as bismuth sodium titanate (BNT), barium strontium titanate ($BaSrTiO_3$) and BMN+BT with sintering aids. However, attempt was carried out to produce thin film Ni doped CdS solar cell via chemical both deposition. The films showed good sensitivity to light. Now, consistence of these films is being tested.

Keywords: piezoelectric, dielectric, low sintering temperature, low sintering aids, composite.

Executive Summary

TRF Senior Research Scholar Grant (No. RTA 4580004)

1. Title เพียโซอิเล็กตริกเซรามิกที่อุณหภูมิซินเตอร์ต่ำ

   Low Temperature Sintering Piezoelectric Ceramics

2. Principal Investigator

ศาสตราจารย์ ดร.ทวี ตันฑศิริ

Professor Dr.Tawee Tunkasiri

Department of Physics, Faculty of Science

Chiang Mai University, Chiang Mai 50200

E-mail: tawee@chiangmai.ac.th

3. Research Field: Physical Properties of Materials

4. Budget: 7,400,000.- Baht

5. Research Period: 3 yrs. (1 August 20002 – 31 July 2005)

6. Support from other Agencies:

   6.1 The Royal Golden Jubilee (RGJ), Ph.D. Program, TRF.

   6.2 The Post-graduate Education Development (PED) Program (The Commission on Higher Education)

   6.3 National Metal and Materials Technology Center (MTEC)

   6.4 National Research Council (NRC)

7. Research Work

The research work was aimed to develop processing techniques and materials for producing piezoelectric and dielectric ceramics. Production of composite and cadmium sulphide solar cells were also the objectives of this research. Emphasis was on low sintering temperature of these materials with comparatively good physical properties inorder to reduce the cost of production.

This project consisted of 4 subprojects as follow:

1. Thick film ceramics synthesized with sintering aids.
2. Thin film PLZT
3. Composite materials and

4. Lead free piezoelectric compounds

8. Outputs

This research has resulted in:

- 20 papers (14 published, 6 in press)
- 3 submitted
- 1 patent
- 23 presentation international meeting

These were carried out by professors, associate professors, reader, lectures, researchers and students from universities, institute. These are Chiang Mai university, Prince Songkla University, National Metal and Materials Technology Center (MTEC), Ceramics division, Leeds University (UK) and Victoria University of Wellington (NewZealand).

Industrial linkage has been established with the Uyemura Ltd. (Japan).

There was an annual meeting on "TRF Senior Research Scholar on : Low Temperature Sintering Piezoelectric Ceramics" (16 July 2003). Research members all presented their work, Dr.S.J. Milne of Leeds University, UK. also joined the meeting and presented a topic of the work of his research program. The team has received honors to arrange (jointly with Fac. of Science, CMU and MTEC) an international seminar on "Smart/Intelligent Materials and Nanotechnology" (1-3 December 2004). Leading scientist of the world joined the events, such as Prof.R.E. Newnham, Supaporn Seraphin, Kenji Uchino USA, and Prof.A.J. Cheetham, Ron Stevens (UK), Ram P. Tandon, Yao Xi , Brian J. Tighe, John Wang, Amar S. Bhalla, David P. Cann, Derek C. Sinclair, Geoffrey R. Mitchell, Qi Zhang, Weiguang Zhu, Ahmad Safari

Members of the team have received various awards as follow:

- Member of the executive board in Asian Ferroelectric Association (AFA), (Prof.Dr.Tawee Tunkasiri)
- Reviewer of Journal of Materials Research (JMR) and Nuclear Instrumentation Measurement, Nuclear, Instruments and Methods in Physics Research Section B: Beam Interactions with Materials and Atoms (NIMB) (Prof.Dr.Tawee Tunkasiri)
- Micrograph Award 2003, LM: Materials Science 1st Prize Arranged by the Electron Microscopy Society of Thailand (2-4 February 2005)

- Best Poster Presentation 2003, 3rd Prize Arranged by the Electron Microscopy Society of Thailand
- Out standing researcher of the Institute for Science and Technology Research and Development Chiang Mai University
- Lecturer of the year 2002 (Prof.Dr.Tawee Tunkasiri) in science and technology of the Council of the University Faculty Senates of Thailand

การวิจัย "เพียโซอิเล็กตริกที่อุณหภูมิซินเตอร์ต่ำ"

ความสำคัญและที่มาของปัญหา

สารเพียโซอิเล็กตริกเซรามิกเป็นผลิตภัณฑ์ที่อำนวยประโยชน์ใช้ในอุปกรณ์อิเล็กทรอนิกส์ทั่วไป เช่น ในโทรศัพท์ทุกชนิด อุปกรณ์ที่ร้องเตือนเวลารถถอยหลัง เครื่องทำความสะอาดเหนือเสียง ซึ่งสารเพียโซที่ใช้กันในปัจจุบันส่วนใหญ่จะมีสารตะกั่วเป็นฐาน และจะต้องเผาในอุณหภูมิสูงกว่า (1200 °ซ) ในการผลิต อันเป็นเหตุให้ไอตะกั่วจะแพร่ออกไปในบรรยากาศ และเป็นพิษต่อร่างกาย งานวิจัยนี้ได้ดำเนินการลดการแพร่ของตะกั่วโดยใช้หลัก 2 ประการ กล่าวคือ 1) ลดอุณหภูมิการเผาโดยทำให้สารเพียโซก่อนขึ้นรูปให้เล็กลงขนาด 1000 นาโนเมตร และการทำให้เป็นแผ่นบางในกระบวนการที่เรียกว่า sol-gel ปัจจุบันสามารถลดอุณหภูมิการเผาลงไป < 800 °ซ แต่อย่างไรก็ตามกระบวนการ sol-gel ผลิตได้เนื้อสารไม่มากนักในครั้งหนึ่งๆ คณะวิจัยกำลังทดลองดำเนินการทำเป็นแผ่นบางๆ โดยใช้กระบวนการอื่น 2) ไม่ใช้สารตะกั่วเป็นฐาน ซึ่งต้องใช้สารอื่นแทน ขณะนี้ได้ใช้สารแบเรียมหรือบิสมัทไทเทเนต ทำให้ไม่ต้องกังวลถึงการแพร่ของตะกั่ว อย่างไรก็ดีหากใช้สารอื่นก็เผาที่อุณหภูมิสูง (> 1500 °ซ) ซึ่งจะสิ้นเปลืองงบลงทุน ปัจจุบันทีมวิจัยกำลังทดลองเพื่อลดอุณหภูมิเผาให้ต่ำลงอีก โดยการนำวิธีการผสมสารหลายตัวที่สามารถลดอุณหภูมิการเผาลง

โครงการนี้ยังแยกเป็น 4 โครงการย่อย ดังนี้

1. Thick film ceramics synthesized with sintering aids.
2. Thin film PLZT
3. Composite materials and
4. Lead free piezoelectric compounds

โครงการย่อยที่ 1. Thick Film Ceramics with Sintering Aids

โครงการนี้อาจแบ่งเป็น 2 ส่วน

ส่วนแรก การเตรียมสารเพียโซโดยใช้เป็นอุปกรณ์ด้านอิเล็กทรอนิกส์ในช่วงความถี่ไมโครเวฟ โดยมุ่งเน้นวิธีการเตรียมให้ได้อนุภาคเล็กมาก จะเป็นกลุ่มของ Barium Titanium Oxide ซึ่งจะทำให้อุณหภูมิซินเตอร์ต่ำ (1200 °ซ) และเจือด้วยสารช่วยในการ sinter

ส่วนที่สอง เป็นการเตรียมสารเพียโซอิเล็กตริกในกลุ่มของ PZT ในสูตร $PbZr_{0.52}Ti_{0.48}O_3$ และกลุ่มของสารที่มีตะกั่วเป็นฐานซึ่งจะเป็นการเตรียมสารตั้งต้นที่เล็กมาก โดยวิธี spray dry และทำแผ่นฟิล์มบางโดยการรีด (Tape casting) เพื่อให้ได้อุณหภูมิ sinter ที่ต่ำ

ส่วนแรก เป็นกลุ่มของเซรามิกในตระกูล Barium Titanium Oxide เป็นการเตรียมแบเรียมไททาเนียมที่สัดส่วนต่างๆ ได้แก่ $BaTi_2O_5$, $BaTi_4O_9$ และ $BaTi_5O_{11}$ ด้วยวิธีต่างๆ เช่น solid state reaction , co-precipitation และ sol-gel เพื่อให้ได้อนุภาคที่เล็กๆ และใช้อุณหภูมิซินเตอร์ที่ต่ำ การวิเคราะห์ใช้เทคนิควิธีการเปลี่ยนเฟสกับความร้อน (Differential Thermal Analyzer (DTA), Scanning Calorimeter (DSC) และ Thermogravimetric Analyzer (TGA) ศึกษาเฟสโดยใช้เครื่อง X-ray Diffractometer (XRD) และเทคนิคทาง Transform Infrared Spectroscopy (FTIR) เพื่อดูว่ามีโครงสร้างเป็นเช่นไร จากนั้นจึงนำมาวัดสมบัติทางไฟฟ้าที่ความถี่สูงๆ ควบคู่กับการศึกษาขนาดของเกรนในตัวเซรามิกด้วยกล้องจุลทรรศน์อิเล็กตรอนแบบส่องกราด (Scanning Electron Microscopy; SEM) จากการเตรียมอนุภาคของ $BaTi_2O_5$ โดยวิธี sol gel เผาแคลไซน์ที่ 800-1200 °ซ เป็นเวลา 4 ชั่วโมง ขนาดอนุภาควัดได้อยู่ในช่วง nm อนุภาคจะใหญ่ขึ้นถ้าอุณหภูมิ calcine สูงขึ้น ผลจากการตรวจเฟสของอนุภาคและเซรามิก (เผาซินเตอร์ที่ 1200 °ซ) ที่มีลักษณะเป็นฟิล์มหนา (อยู่ในลักษณะเหรียญบาท บางกว่า 0.8 มม) พบว่าทั้งอนุภาคและแผ่นเซรามิกเป็น $BaTi_2O_5$ เฟสเดี่ยว จากการวัดขนาดเกรนด้วยกล้องจุลทรรศน์อิเล็กตรอนแบบส่องกราด พบว่าเกรนมีขนาด 1-3 μm มีความหนาแน่นสูงกว่า 90 % ของความหนาแน่นทางทฤษฎี

สารประกอบ $BaTi_4O_9$ เตรียมได้โดยวิธี solid state reaction (นำผงออกไซด์มารวมกันแล้วเผา) ผลจากการตรวจเฟส, โครงสร้างด้วยวิธี DTA และ XRD พบว่าเกิด $BaTi_4O_9$ ที่อุณหภูมิประมาณ 1000 °ซ จากการศึกษาด้วย SEM พบว่าสารประกอบเป็นลักษณะของอนุภาคขนาด 0.5-2 μm เกาะติดกันเป็นก้อนใหญ่ และเป็นเฟสของ Orthorhombic sinter เป็นเซรามิกได้ที่อุณหภูมิสูงกว่า 1250 °ซ หากอุณหภูมิซินเตอร์สูงถึง 1400 °ซ ก้อนเซรามิก $BaTi_4O_9$ มีความหนาแน่นถึง 98% ของความหนาแน่นทางทฤษฎี

อนุภาคของ $BaTi_5O_{11}$ สามารถเตรียมจากทางเคมีด้วยวิธีตกตะกอนร่วม (Co-precipitation) ซึ่งจะได้อนุภาคที่เล็กมาก และเผาอุณหภูมิไม่สูง (700 - 1150 °ซ) ขนาดอนุภาคที่วัดได้ประมาณ 0.1 μm เมื่อเผาที่ 800 °ซ ฟิล์มหนาของเซรามิก $BaTi_5O_{11}$ จะเตรียมได้ด้วยการเผาประมาณ 1150 °ซ ด้วยขนาดเกรนอยู่ในช่วง 0.4 – 1 μm ด้วยความหนาแน่นของเซรามิกมี 75% ของความหนาแน่นทางทฤษฎี

จากการตรวจค่าทางไฟฟ้า (dielectric constant, ε_r) ของความถี่สูงๆ ประมาณ 10^5 Hz ขึ้นไป พบว่าค่า ε_r และการสูญเสีย (dissipation factor, tanδ) อยู่ในช่วงที่ค่อนข้างดี ผลงานส่วนนี้แสดงให้เห็นว่าสามารถดำเนินการเตรียมเซรามิกใช้ความถี่ในช่วงสูงๆ (ย่านไมโครเวฟ) ได้ โดยการเตรียมไม่ต้องเผาสูงมากนัก และได้นำผลงานส่วนนี้ไปเผยแพร่เป็นสิ่งตีพิมพ์ในวารสารต่างประเทศ ประกอบทั้งบรรยายในการประชุมในประเทศ

ส่วนที่สอง

เป็นการเตรียมกลุ่มของสารเพียโซที่มีสารตะกั่วเป็นฐานกลุ่มเหล่านี้ได้แก่ กลุ่ม PZT, Lead titanate (PT), Lead barium zirconate (PBZ), Lead magnesium niobate (PMN) และการนำมาผสมกัน และผสมกับสารช่วยซินเตอร์ (sintering aids) เพื่อลดอุณหภูมิซินเตอร์

ในส่วนของการเตรียมสาร PZT ในงานวิจัยนี้ได้ดำเนินการผสมสารละลายทางเคมีประกอบด้วย $Pb(NO_3)_2$, $ZrO(NO_3)_2$, $C_{12}H_{28}O_4Ti$ และ $MnCl_2$ ตามสัดส่วนที่ต้องการ ควบคุม pH ของสารละลายที่ผสมกัน จากนั้นนำสารละลายมาผ่านกระบวนการ spray dry ซึ่งเป็นการทำให้สารละลายเป็นฝอยพ่นผ่านความร้อนก็จะได้ผงที่ตกตะกอนในขนาดเล็กมาก (0.1μm) จากนั้นนำมาเผาให้เป็นอนุภาค PZT เนื่องจากว่าขนาดของอนุภาคเล็กมาก สมบัติต่างๆจึงจะไม่เหมือนอนุภาคที่ใหญ่ จากการศึกษาการเปลี่ยนแปลงของ phase พบว่าผง PZT ขนาดเล็ก จะเป็น cubic phase ตามคาด เมื่อเผาที่อุณหภูมิ 500 °ซ ขึ้นไป และการเผาซินเตอร์ที่ 900 - 1250 °ซ พบว่าเฟสของ cubic จะเปลี่ยนไปเป็น tetragonal เมื่อขนาดเกรนใหญ่ขึ้น ซึ่งเป็นการเปลี่ยนจาก paraelectric เป็น ferroelectric และจากการวัดค่าอัตราการเปลี่ยนของพลังงาน (planar coupling constant, Kp) และค่าการสร้างประจุ (piezoelectric constant, d_{33}) และค่าทางกายภาพอื่นๆ ก็มีค่าที่ดีกว่าเซรามิกที่ได้จากการเตรียมแบบ solid state sintering ซึ่งอาจจะเป็นผลมาจากการเตรียมให้อนุภาคมีขนาดเล็กลง โดยวิธี spray dry ในการวัดขนาดอนุภาคได้ประยุกต์การวัดโดยใช้ Fourier Series ซึ่งวัดได้ใกล้เคียงกับความเป็นจริง

งานวิจัยส่วนนี้ได้ขยายไปถึงการค้นหา phase อื่น เช่น antiferrolelectric phase ซึ่งพบในเซรามิก PBZ ในสารที่เตรียมด้วยกระบวนการแตกต่างไป กล่าวคือใช้การ calcine สองครั้ง อย่างไรก็ดี ค่า d_{33} และ K_p มีค่าต่ำกว่าที่ได้จาก PZT

คณะวิจัยได้มีความพยายามในการทำแผ่นฟิล์มหนาของ PZT โดยใช้กระบวนการรีดเป็นแผ่นบาง (0.1 mm) โดยใช้ tape casting เพื่อจะได้ลดอุณหภูมิซินเตอร์โดยใช้ binder ชนิดต่างๆ อย่างไรก็ตามแม้จะลดอุณหภูมิซินเตอร์ลงไปบ้าง (< 1200 °ซ) แต่ยังมีค่า dissipation factor (tanδ) สูงอยู่มาก จึงต้องดำเนินการปรับปรุงแก้ไขในส่วนนี้อยู่

ได้มีความพยายามในการลดอุณหภูมิซินเตอร์ด้วยวิธีใส่สารช่วยหลอมกล่าวคือใส่ sintering aids เข้าไป ส่วนสารเซรามิกได้แก่ส่วนผสมของ PT และ PMN ในอัตรา 1:9 สารช่วยหลอมได้แก่ B_2O_3+Bi_2O_3+CdO V_2O_5 และ $0.1Bi_2O_3$+$0.9Li_2CO_3$ (อัตราส่วนทั้งหมดเป็น wt%) พบว่าได้ลดอุณหภูมิซินเตอร์ลงมา ≤ 1000 °ซ อย่างไรก็ตามจากการวัดค่า dielectric constant (ε_r) และสมบัติทาง ferroelectric (ศึกษา hysteresis loop) และค่าทางฟิสิกส์อื่นๆ พบว่ามีค่าต่ำกว่าเซรามิกที่ไม่ใส่สารช่วยหลอมพอสมควร ได้รวบรวมผลงานแล้วส่งตีพิมพ์ที่ Journal of American

Ceramics แต่ได้รับการ comment ให้ปรับปรุงในงานบางส่วน ซึ่งได้แก้ไขเรียบร้อยและส่งไปตีพิมพ์ใหม่ (Journal ฉบับอื่น) อย่างไรก็ตามได้นำเสนองานส่วนนี้ในการประชุม The International conference on Smart Materials (SmartMat'-04) 1-3 ธันวาคม 2547

สรุปผลงานของโครงการย่อยที่ 1 Thick Film Ceramics with Sintering Aids สามารถสร้างผลงาน 8 papers ทั้งตีพิมพ์แล้ว, In press และ กำลังพิจารณา (แนบอยู่ในภาคผนวก)

1. S. Tangjuank and T. Tunkasiri, Effects of calcination temperature on phase and microstructure evolution of $BaTi_4O_9$ powders. *Mat. Res. Innovat.* **6** (2002) 256. (เอกสารหมายเลข 1.1)
2. T. Bongkarn, G. Rujijanagul and T. Tunkasiri, Microstructure, Piezoelectric Properties and Phase Transition of $(Pb_{0.90}Ba_{0.10})ZrO_3$ Ceramics Prepared by Solid State Reaction Method. *Ferroelectric Letters*. **29**(5-6) (2002) 105. (เอกสารหมายเลข 1.3)
3. S. Tangjuank, L.D Yu and T. Tunkasiri, Homogenaous precipitation synthesis and characterization of $BaTi_5O_{11}$ powders. *Smart Mater. Struct.* **12** (2003) 656. (เอกสารหมายเลข 1.4)
4. S. Tangjuank, T. Tunkasiri, Effects of heat treatment on structure evolution and morhphology of $BaTi_2O_{11}$ powder synthesized by the sol-gel method, *Mat. Sci. Eng. B.*, **108** (2004) 223. (เอกสารหมายเลข 1.10)
5. W. Thamjaree, W. Nhuapeng and T. Tunkasiri, Analysis of X-ray Diffraction Line Profiles of Lead Zirconate Titanate Using the Fourier Method, *Ferroelectrics Letters*, **31** (2004) 79. (เอกสารหมายเลข 1.12)
6. W. Thamjaree L.D. Yu, K. Pengpat and T. Tunkasiri, Preparation and Characterization of High-Purity PZT Powders and Ceramics Made by Modified Spray Drying Techniques. In press of Materials Research Innovation (เอกสารหมายเลข 2.2)
7. S. Tangjuank and T. Tunkasiri, Sol-gel synthesis and characterization of $BaTi_2O_5$ powder, In press of Appl. Phys. A. (เอกสารหมายเลข 2.3)
8. S. Sirisoonthorn, S. Budchan, K. Pengpat and T. Tunkasiri, Low Sintering Temperature of Lead Magnesium Niobate-Lead Titanate (0.9PMN-0.1PT) by adding oxide Additives, Submitted to Mater. Sci. Eng. B.

โครงการย่อยที่ 2 Thin Film PLZT

งานวิจัยในขั้นตอนนี้ได้ดำเนินการเตรียมแผ่นฟิล์มบางของ PZT โดยวิธี sol-gel กล่าวคือ ผสมสารละลายซึ่งมี 2 ประเภทคือ สารแขวนลอย อนุภาคของแข็งในของเหลว หรือกลุ่มของพอลิเมอร์ในของเหลว ผสมด้วย gel (gelatin) เป็นตัวเชื่อมต่อของแต่ละเฟสของสารเข้าด้วยกัน แผ่นฟิล์มบางของ PZT จะเตรียมได้ด้วยกระบวนการ hydrolysis และกระบวนการ condensation ซึ่งสองกระบวนการนี้อยู่ในขั้นตอนของ gelatin การเตรียม PZT ด้วย sol gel นี้มี 2 วิธี คือ diol-route และ triol-route 2 วิธีนี้แตกต่างกันที่สารตั้งต้นของการเตรียมแผ่นฟิล์มบาง การเตรียมโดย diol-route นั้นมี defect บนฟิล์มค่อนข้างมาก เนื่องจากกระบวนการ gelation มีอัตราการจัดเรียงตัวค่อนข้างเร็ว ดังนั้นในงานวิจัยนี้จึงใช้การเตรียมด้วยวิธี triol route ซึ่งยังไม่แพร่หลายนักและค่อนข้างยาก และเนื่องจากข้อมูลสารเคมีและกรรมวิธีบางส่วนต้องทดลองแบบ trial and error ในการเตรียม sol กระทำโดยผสมสาร Zirconium n-propoxide และ Acetylacetone เผาที่ 90 °ซ นาน 2 ชั่วโมง แล้วผสมสารละลาย TIAA THOME และผสมด้วย lead acetate trihydrate เผาที่ 70 °ซ นาน 4 ชั่วโมง ก็จะได้ stock solution จากนั้นนำ sol หยดลงบนแผ่น platinized substrate $Pt(111)/SiO_2/Si$ นำเข้า spin coater แล้ว spin ด้วยจำนวนรอบที่เหมาะสมกับความหนืดของสารละลาย หลังจากได้แผ่นฟิล์มบางของ PZT จึงนำไปเผาที่อุณหภูมิต่างๆ แล้วตรวจเฟสด้วย XRD พบว่าเฟสของ PZT จะเกิดที่การเผาอุณหภูมิที่ 600 °ซ และได้ฟิล์มบางมาก (~ 500 nm) จากการตรวจดูผิว พบว่า รูพรุนค่อนข้างน้อยเมื่อเทียบกับฟิล์มบาง PZT ที่เตรียมจากวิธี diol-route อนึ่งการเผาที่อุณหภูมิ 600 °ซ ไม่ทำให้ตะกั่วระเหยมารบกวน เนื่องจากตะกั่วจะระเหยที่อุณหภูมิในอัตราที่อาจเป็นพิษเมื่ออุณหภูมิมากกว่า 800 °ซ การศึกษาสมบัติเฟร์โรอิเล็กตริกแผ่นฟิล์มบางได้แก่การวัดค่า dielectric constant (ε_r) และ loss angle ($\tan\delta$) และตรวจดู hysteresis loop ซึ่งเนื่องจากเป็นแผ่นฟิล์มบางมากจึงต้องสร้างเครื่องมือขึ้นเอง เครื่องมือที่ใช้อยู่ใช้สำหรับวัดเซรามิกที่หนากว่า 0.5 มม. อย่างไรก็ตาม การวัดต่างๆ ได้แล้วเสร็จและได้ผลเป็นที่พอใจอยู่ระหว่างเขียนเป็นบทความสำหรับตีพิมพ์ในวารสาร

การศึกษาสมบัติของแผ่นฟิล์มบางของ PLZT เตรียมโดยวิธี sol-gel

แผ่นฟิล์มบางของ lead lanthanum zirconate titanate (PLZT) ก็สามารถเตรียมได้ด้วยวิธี sol-gel และ spin coating การเตรียม sol-gel อาศัยวิธีการ triol route ที่ดำเนินการจากการเตรียม sol-gel ของ PZT ซึ่งจะได้แผ่นฟิล์มบาง (~ 500 nm) บน substrate ที่ทำด้วย platinized substrate รายละเอียดการเตรียมได้บรรยายไว้ในรายงานฉบับที่ 4 และ 5 ได้ทำการศึกษาเฟสพบว่าเป็น PLZT และไม่มีเฟสอื่นเจือปน ดำเนินการเผาที่ preheat ที่ 400 °ซ และเผาที่ 600 °ซ จากนั้นนำฟิล์มมา

ศึกษาด้านไฟฟ้าและศึกษาลักษณะของผิว มีค่า dielectric constant ประมาณ 600 และ loss angle (tanδ) ค่อนข้างต่ำ จากการวัดค่าต่างๆทาง ferroelectric ได้ค่าเป็นที่น่าพอใจ ผลงานส่วนนี้ได้ดำเนินการนำเสนอ ในที่ประชุม The International Conference on Smart Materials (Smart Mat-04) 1-3 December 2004.

การเตรียมฟิล์ม PLZT ด้วยวิธี tape casting

ผลจากการใช้การรีดแผ่น (หนาระดับ 100 μm) ด้วยเครื่อง tape casting ของโครงการย่อยที่ 1 พบว่า มีรูพรุนมาก จึงต้องทำการศึกษาละเอียดเกี่ยวกับการเกิดเฟสของสารประกอบ PT, PZ และ ZT สาร PT ได้มีการศึกษาอยู่ก่อนหน้าแล้ว จึงศึกษาการเกิดเฟสของ ZT (Zirconate Titanate, $ZrTiO_3$), PZ (Lead Zirconate, $PbZrO_3$) และศึกษาสมบัติทาง Mechanics ซึ่งได้ดำเนินการแล้วเสร็จจาก literature พบว่า น่าจะผสม lanthanum ลงในส่วนผสมของผง PZT ก่อน เข้ากระบวนการรีดด้วยเครื่อง tape casting การเตรียม slurry สำหรับใช้ในการรีดก็ประกอบด้วยการเผา PbO, La_2O_3, ZrO_2 และ TiO_2 หลังจากการตรวจเฟสด้วย XRD แล้วนำมาผสมด้วย plasticizer solvent-binder เพื่อให้มีลักษณะเป็น slurry ที่ความหนืดที่เหมาะสม หลังจากรีดด้วย tape caster ได้ฟิล์มที่มีความหนาที่เหมาะสมแล้วจึงนำมาเผาซินเตอร์อุณหภูมิต่างๆ (รายละเอียดอยู่ที่รายงานฉบับที่ 4) และสามารถลดอุณหภูมิซินเตอร์ลงมาอยู่ที่ 1050 °ซ และมีสมบัติ ferroelectric ที่ดี สภาพผิวเซรามิกรูพรุนเพียงเล็กน้อย

สรุปผลงานของโครงการย่อยที่ 2 สามารถสร้างผลงาน 4 papers (แนบอยู่ในภาคผนวก)

1. Rungkan Pankumdal, Sarawut Thountom, Wimol Naksata , Manoch Naksata and Tawee Tunkasiri, Preparation of Lanthanum Doped Lead Zirconate Titanate Thin Film by Spin-Coating Technique,. The International Conference on Smart Materials: Smart/Intelligent Materials and Nanotechnology, Chiang Mai, Thailand, 1-3 December (2004).
2. S. Ananta, R. Tipakontitikul and T. Tunkasiri, "Synthesis Formation and Characterisation of Zirconium Titanate (ZT) Powders, *Mat. Lett.* **57** (2003) 2637-2642. (เอกสารหมายเลข 1.2)
3. C. Puchmark, S. Jiansirisomboon, G. Rujijanagul and T. Tunkasiri, Effect of sintering temperatures on phase transition of lead zirconate ceramics, *Current Appl. Phys*, **4** (2004) 179. (เอกสารหมายเลข 1.7)

4. C. Puchmark, G. Rujijanagul, S. Jiansirisomboon and T. Tunkasiri, Effect of Sintering Temperature on Phase Transition and Mechanical Properties of Lead Zirconate Ceramics, *Ferroelectric Letters*, **31** (2004) 1-13. (เอกสารหมายเลข 1.8)

โครงการย่อยที่ 3 Composite Materials

งานวิจัยในส่วนนี้มุ่งที่จะสร้าง composite Materials โดยการนำผงเซรามิก 2 ชนิด มาผสมกัน ซึ่งอาจทำได้หลายส่วนผสม ในงานวิจัยนี้ได้ผสมผงเซรามิกกับพอลิเมอร์, ผงเซรามิกกับเซรามิก ด้วยกัน โดยมีวัตถุประสงค์ที่จะลดอุณหภูมิซินเตอร์ เพื่อลดอันตรายที่จะเกิดจากการระเหยของตะกั่ว หรือเพิ่มค่า dielectric constant จากเซรามิก

ผลงานของโครงการย่อยที่ 3 มีดังนี้

1. เตรียม Porous ceramic ของ PT + PZT แล้วผสม epoxy เข้าใน pores โดยวิธี impregnation งานนี้เริ่มจากการเตรียมอนุภาคที่เป็นส่วนผสมของ PT-PZT โดยใช้วิธี mixed oxide route ซึ่งจะประกอบจาก PbO, ZrO_2 และ TiO_2 เผา calcine ให้อยู่ในรูปเหรียญบาท ซินเตอร์ที่อุณหภูมิ 1150 °ซ จะได้ porous ceramics จากนั้นผสม epoxy ด้วยวิธี impregnation จะได้ composite ที่ต้องการ ทำการวัด และศึกษาสมบัติต่างๆ นำผลงานไปเสนอที่ Asian Meeting on Ferroelectric (AMF4) และตีพิมพ์ในวารสาร

2. เตรียม composite ระหว่าง PZN และ PZT เซรามิก ในกรรมวิธี Columbite technique กล่าวคือเตรียมส่วนผสมให้อยู่ในลักษณะโครงสร้าง Columbite ก่อน แล้วจึงผสมกันแล้วซินเตอร์อีกทีหนึ่ง

3. เตรียม composite BMN $(BaMg_{1/3}Nb_{2/3})O_3$ กับ BT $(BaTiO_3)$ เพื่อศึกษาการเกิดเฟสร่วมใน composite

4. เตรียม composite ระหว่าง PZT และ BFN (Barium Ferro Niobate) ซึ่งคาดว่าจะได้ค่า ε_r ที่สูงมาก และอยู่ในช่วงอุณหภูมิที่กว้าง (-50 °ซ ถึง 300 °ซ) นำไปเสนอที่ The 2nd International Conference on Advanced Materials and Nanotechnology (AMN-2)

สรุปผลงานของโครงการย่อยที่ 3 สามารถสร้างผลงาน 4 papers (แนบอยู่ในภาคผนวก)

1. P. Auisui, S. Muensit, I.L. Guy, G. Rujijanagul and T. Tunkasiri, Piezoceramic-Polymer Composites for Detector Applications, In press of Ferroelectric and Integrated Ferroelectric. (เอกสารหมายเลข 2.1)
2. T. Tunkasiri, U. Intatha, S. Eitssayeam and K. Pengpat, Preparation and Characterization of Barium Iron Niobate ($BaFe_{0.5}Nb_{0.5}O_3$) Ceramics, The 2nd International Conference on Advanced Materials and Nanotechnology (AMN-2), Queenstown, New Zealand, 6-11 February (2005).
3. A. Munpakdee, J. Tontrakoon, K. Siriwittayakorn and T. Tunkasiri, "Effects of $Ba(Mg_{1/3}Nb_{2/3})O_3$ on microstructure and dielectric properties of Barium Titanate Ceramics, *J. Mat. Sci. Lett.* **22**(2003) 1307-1310. (เอกสารหมายเลข 1.5)
4. X. Tan, D.P. Cann, N. Vittayakorn, G. Rujijanagul, T. Tunkasiri, Perovskite phase formation and ferroelectric properties of the lead nickel niobate-lead zinc niobate-lead zirconate titanate ternary system, *J.Mater.Res.*, 18 [12] (2003) 2882. (เอกสารหมายเลข 1.6)
5. N. Vittayakorn, G. Rujijanagul, T. Tunkasiri, X. Tan and D.P. Cann, Influence of processing conditions on the phase transition and ferroelectric properties of $Pb(Zn_{1/3}Nb_{2/3})O_3$-$Pb(Zr_{1/2}Ti_{1/2})O_3$ ceramics, *Materials Science and Engineering: B.*, **108** (2004) 258. (เอกสารหมายเลข 1.9)
6. D.P. Cann, X. Tan, N. Vittayakorn, G. Rujijanagul and T. Tunkasiri, Influence of Processing Condition on the Morphotropic Phase Boundaries and Ferroelectric Properties of $Pb(ZN_{1/3}Nb_{2/3})O_3$-$Pb(Ni_{1/3}Nb_{2/3})O_3$-$Pb(Zr_{1/2}Ti_{1/2})O_3$ Solid Solutions. 2004 14th IEEE International symposium on applications of ferroelectric ISAF-04. (เอกสารหมายเลข 1.13)
7. W. Thamjaree, W. Nhuapeng, A. Chaipanich and T. Tunkasiri, Fabrication of Combined 0-3 and 1-3 Connectivities PZT/Epoxy Resin Composites. Appl. Phys. A. (on line) (เอกสารหมายเลข 1.14)

โครงการย่อยที่ 4 Lead Free Piezoelectric Compounds

งานในโครงการนี้เป็นการเตรียมสาร Piezoelectric ที่ไม่ใช่ตะกั่วเป็นฐาน ซึ่งงานในช่วงนี้ประกอบด้วย

1. การเตรียม Bismuth Sodium Titanate (BNT) ซึ่งเตรียมเป็นผงโดย mixed oxide route การบดผสมมี 2 วิธี กล่าวคือ วิธีผสม Bi_2O_3, Na_2O และ TiO_2 แล้วบดด้วย ball mill (แบบดั้งเดิม) และบดด้วย vibro mill จากนั้นเผาแคลไซน์แล้วเผาซินเตอร์เป็นเซรามิก แล้วนำผลการวัดค่าต่างๆ มาเปรียบเทียบกัน

2. สร้างแผ่นฟิล์มบางของ CdS sulphide (ใช้เป็น solar cell) โดยวิธี Chemical bath deposition ทำการทดสอบความไวกับแสงแดด

3. นำ composite จากโครงการย่อยที่ 3 มาผสม sintering aids เพื่อลดอุณหภูมิ sinter ซึ่งลดลงมาจาก 1350 °ซ เป็น 1000 °ซ ได้สำเร็จ

4. สร้าง Thermistor ที่มีความไวสูง ด้วยเซรามิก Barium Strontium Titanate ($BaSrTiO_3$) ที่มีส่วนผสมของ silicon สูง

สรุปผลงานของโครงการย่อยที่ 4 สามารถสร้างผลงาน 3 papers (แนบอยู่ในภาคผนวก)

1. S. Eitssayeam, U. Intatha, K. Pengpat and T. Tunkasiri, Properties of CdS:Ni films prepared by chemical bath deposition method. In press J. Mat. Sci. Lett. (เอกสารหมายเลข 2.4)
2. A. Munpakdee, J. Tontragoon and T. Tunkasiri, Dielectric properties of low firing $0.98BaTiO_3$-$0.02Ba(Mg_{1/2}Nb_{2/3})O_3$ with $Pb/LiCO_3$-Bi_2O_3 ceramics. In press J. Mat. Sci. Lett. (เอกสารหมายเลข 2.5)
3. P. Bomlai, N. Sirikulrat and T. Tunkasiri, Microstructures and Positive Temperature Coefficient Resistivity (PTCR) Characteristics of High Silicon Addition Barium-Strontium Titanate Ceramics, *J. of Mats. Science,* **39** (2004) 1831-1835. (เอกสารหมายเลข 1.11)

Out-put ที่ได้รับจากโครงการ

จากผลงานวิจัยที่กล่าวมาข้างต้นได้ตีพิมพ์ในวารสารแล้ว 20 เรื่อง (ตีพิมพ์แล้ว 14 เรื่อง อยู่ระหว่างตีพิมพ์ 6 เรื่อง) และอยู่ในระหว่างพิจารณาอีก 3 เรื่อง นอกจากนี้ได้นำเสนอผลงานในการประชุมนานาชาติ อีก 23 เรื่อง (ดังในภาคผนวก)

งานวิจัยดังกล่าวเป็นผลงานจากคณาจารย์ คณะวิจัย นักศึกษาจากมหาวิทยาลัย และสถาบันการศึกษาต่างๆ เช่น มหาวิทยาลัยเชียงใหม่ มหาวิทยาลัยสงขลานครินทร์ ศูนย์เทคโนโลยีโลหะและวัสดุแห่งชาติ นักวิจัยสาขาเซรามิกส์ มหาวิทยาลัยลีดส์ (ประเทศอังกฤษ) ภาควิชาฟิสิกส์ มหาวิทยาลัยวิคตอเรียแห่งเวลลิงตัน (ประเทศนิวซีแลนด์)

นอกจากนี้ยังมีการเชื่อมต่อกับภาคอุตสาหกรรม บริษัท Uyemura (ประเทศญี่ปุ่น)

คณะวิจัยยังได้จัดประชุมประจำปีเรื่อง Low Temperature Sintering Piezoelectric Ceramics (วันที่ 16 กรกฎาคม 2546) ซึ่งมีผู้เข้าร่วมประชุมจากภาครัฐ (คณาจารย์จากมหาวิทยาลัยต่างๆ) และอุตสาหกรรม นอกจากนี้ Dr.S.J. Milne จากมหาวิทยาลัยลีดส์ ได้เดินทางมาร่วมบรรยายด้วย นอกจากนี้ทางคณะวิจัยได้ร่วมจัดประชุม/สัมมนานานาชาติร่วมกับคณะวิทยาศาสตร์ มหาวิทยาลัยเชียงใหม่ และศูนย์เทคโนโลยีโลหะและวัสดุแห่งชาติ จัดประชุมเรื่อง Smart/Intelligent Materials Nanotechnology (1-3 ธันวาคม 2547) โดยมีนักวิทยาศาสตร์ชั้นนำของโลกมาร่วมบรรยายได้แก่

1.	Robert E. Newnham	Penn State University. (U.S.A)
2.	Supapan Seraphin	The University of Arizona. (U.S.A)
3.	Kenji Uchino	Penn State University. (U.S.A)
4.	Anthony K. Cheetham	University of California. (USA)
5.	Ron Stevens	University of Bath. (UK)
6.	Ram P. Tandon	University of Delhi. (India)
7.	Yao Xi	Tongji University. (China)
8.	Brian J. Tighe	Aston University. (UK)
9.	John Wang	National University of Singapore. (Singapore)
10.	Amar S. Bhalla	MRIPennsylvania State University, (USA)
11.	David P. Cann	Iowa State University. (USA)
12.	Derek C. Sinclair	University of Sheffield. (UK)
13.	Geoffrey R. Mitchell	University of Reading. (UK)

14.	Qi Zhang	Cranfield University. (UK)
15.	Weiguang Zhu	Nanyang Technological University. (Singapore)
16.	Ahmad Safari	Rutgers University. (USA)

สรุปผลงานที่ได้รับการตีพิมพ์แล้ว

1. S. Tangjuank and T. Tunkasiri, Effects of calcination temperature on phase and microstructure evolution of $BaTi_4O_9$ powders. *Mat. Res. Innovat.* **6** (2002) 256. (เอกสารหมายเลข 1.1)
2. S. Ananta, R. Tipakontitikul and T. Tunkasiri, "Synthesis, formation and characterisation of zirconium titanate (ZT) powders, *Mat. Lett.* **57** (2003) 2637. (เอกสารหมายเลข 1.2)
3. T. Bongkarn, G. Rujijanagul and T. Tunkasiri, Microstructure, Piezoelectric Properties and Phase Transition of $(Pb_{0.90}Ba_{0.10})ZrO_3$ Ceramics Prepared by Solid State Reaction Method. *Ferroelectric Letters*. **29**(5-6) (2002) 105. (เอกสารหมายเลข 1.3)
4. S. Tangjuank, L.D Yu and T. Tunkasiri, Homogenaous precipitation synthesis and characterization of $BaTi_5O_{11}$ powders. *Smart Mater. Struct.*. **12** (2003) 656. (เอกสารหมายเลข 1.4)
5. A. Munpakdee, J. Tontrakoon, K. Siriwittayakorn and T. Tunkasiri, "Effects of $Ba(Mg_{1/3}Nb_{2/3})O_3$ on microstructure and dielectric properties of Barium Titanate Ceramics, *J. Mat. Sci. Lett* .**22** (2003) 1307. (เอกสารหมายเลข 1.5)
6. X. Tan, D.P. Cann, N. Vittayakorn, G. Rujijanagul, T. Tunkasiri, Perovskite phase formation and ferroelectric properties of the lead nickel niobate-lead zinc niobate-lead zirconate titanate ternary system, *J.Mater.Res.*, **18** [12] (2003) 2882. (เอกสารหมายเลข 1.6)
7. C. Puchmark, S. Jiansirisomboon, G. Rujijanagul and T. Tunkasiri, Effect of sintering temperatures on phase transition of lead zirconate ceramics, *Current Appl. Phys*, **4** (2004) 179. (เอกสารหมายเลข 1.7)
8. C. Puchmark, G. Rujijanagul, S. Jiansirisomboon and T. Tunkasiri, Effect of Sintering Temperature on Phase Transition and Mechanical Properties of Lead Zirconate Ceramics, *Ferroelectric Letters*, **31** (2004) 1-13. (เอกสารหมายเลข 1.8)

9. N. Vittayakorn, G. Rujijanagul, T. Tunkasiri, X. Tan, D. Cann, Influence of processing conditions on the phase transition and ferroelectric properties of $Pb(Zn_{1/3}Nb_{2/3})O_3$-$Pb(Zr_{1/2}Ti_{1/2})O_3$ ceramics, *Mat. Sci. Eng. B.*, **108** (2004) 258. (เอกสารหมายเลข 1.9)

10. S. Tangjuank, T. Tunkasiri, Effects of heat treatment on structure evolution and morhphology of $BaTi_2O_{11}$ powder synthesized by the sol-gel method, *Mat. Sci. Eng. B.*, **108** (2004) 223. (เอกสารหมายเลข 1.10)

11. P. Bomlai, N. Sirikulrat and T. Tunkasiri, Microstructures and positive temperature coefficient resistivity (PTCR) characteristics of high silicon addition barium-strontium titanate ceramics, *J. of Mats. Science*, **39** (2004) 1831. (เอกสารหมายเลข 1.11)

12. W. Thamjaree, W. Nhuapeng and T. Tunkasiri, Analysis of X-ray Diffraction Line Profiles of Lead Zirconate Titanate Using the Fourier Method, *Ferroelectrics Letters*, **31** (2004) 79. (เอกสารหมายเลข 1.12)

13. D.P. Cann, X. Tan, N. Vittayakorn, G. Rujijanagul and T. Tunkasiri, Influence of Processing Condition on the Morphotropic Phase Boundaries and Ferroelectric Properties of $Pb(ZN_{1/3}Nb_{2/3})O_3$-$Pb(Ni_{1/3}Nb_{2/3})O_3$-$Pb(Zr_{1/2}Ti_{1/2})O_3$ Solid Solutions. 2004 14^{th} IEEE International symposium on applications of ferroelectric ISAF-04. (เอกสารหมายเลข 1.13)

14. W. Thamjaree, W. Nhuapeng, A. Chaipanich and T. Tunkasiri, Fabrication of Combined 0-3 and 1-3 Connectivities PZT/Epoxy Resin Composites. Appl. Phys. A. (on line) (เอกสารหมายเลข 1.14)

สรุปผลงานที่ได้รับการตอบรับการตีพิมพ์แล้ว

1. P. Auisui, S. Muensit, I.L. Guy, G. Rujijanagul and T. Tunkasiri, Piezoceramic-Polymer Composites for Detector Applications, In press of Ferroelectric and Integrated Ferroelectric. (เอกสารหมายเลข 2.1)
2. W. Thamjaree L.D. Yu, K. Pengpat and T. Tunkasiri, Preparation and Characterization of High-Purity PZT Powders and Ceramics Made by Modified Spray Drying Techniques. In press of Materials Research Innovation (เอกสารหมายเลข 2.2)
3. S. Tangjuank and T. Tunkasiri, Sol-gel synthesis and characterization of $BaTi_2O_5$ powder, In press of Appl. Phys. A. (เอกสารหมายเลข 2.3)
4. S. Eitssayeam, U. Intatha, K. Pengpat and T. Tunkasiri, Properties of CdS:Ni films prepared by Chemical bath deposition method. In press of J. Mat. Sci. Lett. (เอกสารหมายเลข 2.4)
5. A. Munpakdee, J. Tontragoon, K. Siriwitayakorn and T. Tunkasiri, Dielectric properties of low firing $0.98BaTiO_3$-$0.02Ba(Mg_{1/3}Nb_{2/3})O_3$ with Pb/Li_2CO_3-Bi_2O_3 ceramics. In press of J. Mat. Sci. Lett (เอกสารหมายเลข 2.5)
6. W. Thamjaree and T. Tunkasiri, Structural and physical properties of Nd-doped $Pb(Zr_{0.52}Ti_{0.48})O_3$ ceramics. In press of Ferroelectrics Letter. (เอกสารหมายเลข 2.6)

สรุปผลงานที่กำลังพิจารณา

1. S. Sirisoonthorn, S. Budchan, K. Pengpat and T. Tunkasiri, Low Sintering Temperature of Lead Magnesium Niobate-Lead Titanate (0.9PMN-0.1PT) by adding oxide Additives, Submitted to Mater. Sci. Eng. B.
2. A. Munpakdee, K. Pengpat, J. Tontrakoon and T. Tunkasiri, The Study of Dielectric Diffuseness in $Ba(Mg_{1/3}Nb_{2/3})O_3$- $BaTiO_3$ ceramic System, Submitted to Smart Materials and Structures.
3. S. Eitssayeam, U. Intatha, K. Pengpat and T. Tunkasiri, Structural and electrical properties characterization of (1-x) $PbZr_{0.52}Ti_{0.48}O_3$ $-xBaFe_{0.5}Nb_{0.5}O_3$ system, Submitted to J. of. Appl. Phy. A

สรุปการเข้าร่วมประชุมวิชาการระดับนานาชาติ (selected)

1. W. Chaisan, S. Ananta and T. Tunkasiri, Synthesis of Barium Titanate-Lead Zirconate Titanate Solid Solutions by a Modified Mixed-Oxide Synthetic Route, AMN-1 International Conference on Advanced Materials and Nanotechnology, Wellington, 9-14 February 2003.
2. C. Puchmark, G. Rujijanagul and T. Tunkasiri, Effect of Sintering Temperature on the Phase Transition of Lead Zirconate Ceramics, AMN-1 International Conference on Advanced Materials and Nanotechnology, Wellington, 9-14 February 2003.
3. W. Thamjaree, L.D. Yu, K. Pengpat and T. Tukasiri, Preparation of High-Purity Powders and Ceramics Made by Spray Drying Technique, ELECTROCERAMICS IX 2004 9th International Conference on Electroceramics & their Applications, Cherbourg, France.
4. A. Munpakdee, J. Tontragoon and T. Tunkasiri, Microstucture and Dielectric Properties of (1-x)$BaTiO_3$ -x$Ba(Mg_{1/3}Nb_{2/3})O_3$ Ceramics, ELECTROCERAMICS IX 2004 9th International Conference on Electroceramics & their Applications, Cherbourg, France.
5. S. Jiansirisomboon, K. Pengpat and T. Tunkasiri, Effect of Starting Precursor on Phase and Microstructural Characteristics of Ferroelectric Lead Magnesium Niobate Ceramics, The International Conference on Smart Materials: Smart/Intelligent Materials and Nanotechnology, Chiang Mai, Thailand, 1-3 December (2004).

6. A. Chaipanich and T. Tunkasiri, Effect of Particle Size of Starting Powders on the Properties of $Pb(Mg_{1/3}\ Nb_{2/3})O_3$ Ceramics, The International Conference on Smart Materials: Smart/Intelligent Materials and Nanotechnology, Chiang Mai, Thailand, 1-3 December (2004)

7. K. Pengpat, J. Srisuping, S. Eitssayeam, U. Intatha and T. Tunkasiri, Bismuth Titanate Glass Ceramics from $Bi_4Ti_3O_{12}$-B_2O_3 system, The International Conference on Smart Materials: Smart/Intelligent Materials and Nanotechnology, Chiang Mai, Thailand, 1-3 December (2004)

8. N. Sawangwan, J. Tontrakoon and T. Tunkasiri, Tape Casting Processing of MnO_2 Doped PZT Ceramic, The International Conference on Smart Materials: Smart/Intelligent Materials and Nanotechnology, Chiang Mai, Thailand, 1-3 December (2004)

9. W. Nhuapeng, W. Thamjaree and T. Tunkasiri, High Piezoelectric Coefficient Lead Lanthanum Zirconate Titanate for Piezoelectric Ceramic and Polymer Composites, The International Conference on Smart Materials: Smart/Intelligent Materials and Nanotechnology, Chiang Mai, Thailand, 1-3 December (2004)

10. S. Sirisoonthorn, K. Soponmanee and T. Tunkasiri Low Firing PZT (52/48) Tape Prepared for Bimorph Actuator, The International Conference on Smart Materials: Smart/Intelligent Materials and Nanotechnology, Chiang Mai, Thailand, 1-3 December (2004).

11. R. Pankumdal, S. Thountom, W. Naksata , M. Naksata and T. Tunkasiri Preparation of Lanthanum Doped Lead Zirconate Titanate Thin Film by Spin-Coating Technique, The International Conference on Smart Materials: Smart/Intelligent Materials and Nanotechnology, Chiang Mai, Thailand, 1-3 December (2004)

12. S. Kumfu, W. Nhuapeng and T. Tunkasiri Fabrication of Kevlar/epoxy resin laminate composites by using low-pressure technique, The International Conference on Smart Materials: Smart/Intelligent Materials and Nanotechnology, Chiang Mai, Thailand, 1-3 December (2004)

13. U. Intatha, S. Eitssayeam, K. Pengpat and T. Tunkasiri , Preparation and Characterization of 0.9PZT – 0.1BFN Ceramics, The International Conference on Smart Materials:

Smart/Intelligent Materials and Nanotechnology, Chiang Mai, Thailand, 1-3 December (2004).

14. N. Vittayakorn, G. Rujijanagul, T. Tunkasiri, X. Tan, David P. Cann Preparation and Ferroelectric Properties of $xPb(Zn_{1/3}Nb_{2/3})O_3$-(1-x)$Pb(Zr_{1/2}Ti_{1/2})O_3$ Ceramics, The International Conference on Smart Materials: Smart/Intelligent Materials and Nanotechnology, Chiang Mai, Thailand, 1-3 December (2004)

15. S. Sirisoonthorn, S. Budchan and T. Tunkasiri Low sintering temperature of Lead Magnesium Niobate –Lead Titanate (0.9PMN-0.1PT) by Various oxide additives, The International Conference on Smart Materials: Smart/Intelligent Materials and Nanotechnology, Chiang Mai, Thailand, 1-3 December (2004)

16. A. Munpakdee, J. Tontragoon, K. Pengpat, K. Siriwitayakorn and T. Tunkasiri, Phase Formation and Microstructure $Ba(0.98Ti-0.02(Mg_{1/3}Nb_{2/3})O_3$- Bi_2O_3/Li_2CO_3-PbO Ceramic System, The International Conference on Smart Materials: Smart/Intelligent Materials and Nanotechnology, Chiang Mai, Thailand, 1-3 December (2004)

17. W. Thamjaree, W. Nhuapeng, S. J. Milne and T. Tunkasiri, Phase Transformation of $Pb_{1-3(3x-2)}Nd_x(Zr_{0.52}Ti_{0.48})O_3$ Ceramics Prepared by Mixed Oxide Method, The International Conference on Smart Materials: Smart/Intelligent Materials and Nanotechnology, Chiang Mai, Thailand, 1-3 December (2004)

18. A. Munpakdee, J. Tontrakoon and T. Tunkasiri, Lead free and Low Temperature Sintered (1-x)$BaTiO_3$-x$Ba(Mg_{1/2}Nb_{2/3})O_3$ Ceramics, The International Conference on Smart Materials: Smart/Intelligent Materials and Nanotechnology, Chiang Mai, Thailand, 1-3 December (2004).

19. S. Jiansirisomboon, K. Songsiri and T. Tunkasiri, Mechanical Properties and Crack Growth Behavior in Unpoled and Poled Ferroelectric PMN-PZT Ceramics, AMN-2 Second International Conference on Advanced Materials and Nanotechnology, Queenstown, NewZealand, 6-11 February 2005.

20. T. Tunkasiri, U. Intatha, S. Eitssayeam and K. Pengpat, Preparation and Characterization of Bariium Iron Niobate ($BeFe_{0.5}Nb_{0.5}O_3$) Ceramics, AMN-2 Second International Conference on Advanced Materials and Nanotechnology, Queenstown, NewZealand, 6-11 February 2005.

21. A. Chaipanich and T. Tunkasiri, Effect of milling on the perovskite phase formation of $Pb(Mg_{1/3}Nb_{2/3})O_3$ using the starting precursors PbO and $MgNb_2O_6$, AMN-2 Second International Conference on Advanced Materials and Nanotechnology, Queenstown, NewZealand, 6-11 February 2005.
22. S. Jiansirisomboon and T. Tunkasiri, Fabrication of $BaTiO_3$-based Composite Dispersed with Al_2O_3 Nano-particulates, The 4th Asian Meeting on Electroceramics, Hangzhou, China, June 27-30, 2005.
23. A. Watcharapason and T. Tunkasiri, Effect of Sysprosium Oxide Addition in Bismuth Sodium Titanate Ceramics, The 4th Asian Meeting on Electroceramics, Hangzhou, China, June 27-30, 2005.

สิทธิบัตร

ได้รับสิทธิบัตรการประดิษฐ์ เรื่อง สารประกอบเพียโซอิเล็กทริกเซรามิกสำหรับใช้ในส่วนกระจายเสียงและกรรมวิธีผลิตสารประกอบดังกล่าว ตามเลขที่คำขอ 063593 เลขที่สิทธิบัตร 18359 ออกให้ ณ วันที่ 12 เมษายน 2548 หมดอายุวันที่ 14 กุมภาพันธ์ 2564 (เอกสารหมายเลข 3)

วิทยากรรับเชิญในการประชุมระดับนานาชาติ

1 A. Munpakdee, J. Tontrakoon and T. Tunkasiri, Lead free and Low Temperature Sintered $(1-x)BaTiO_3$-$xBa(Mg_{1/2}Nb_{2/3})O_3$ Ceramics, The International Conference on Smart Materials: Smart/Intelligent Materials and Nanotechnology, Chiang Mai, Thailand, 1-3 December (2004)

กรรมการต่างๆ และรางวัลที่ได้รับ

1. ศาสตราจารย์ ดร.ทวี ตันฑศิริ ได้รับการคัดเลือกให้เป็นตัวแทนประเทศไทย และเป็น Executive board ของ Asian Ferroelectric Association (เอกสารหมายเลข 4.1)
2. ศาสตราจารย์ ดร.ทวี ตันฑศิริ ได้รับการคัดเลือกให้เป็น reviewer ของ Journal Materials Research (เอกสารหมายเลข 4.2) และ Nuclear, Instruments and Methods in Physics Research Section B: Beam Interactions with Materials and Atoms (เอกสารหมายเลข 4.3)

3. Micrograph Award 2003 LM: Materials Science 1st Prize "Fracture Surface of A glass Rod". (การประชุมสมาคมจุลทรรศน์อิเล็กตรอน, รศ.ดร.กอบวุฒิ รุจิจนากุล และ ศ.ดร.ทวี ตันฆศิริ)
4. Best Poster Presentation 2003, 3rd Prize "Preparation and Preparations of Lead Zirconate Ceramics (การประชุมสมาคมจุลทรรศน์อิเล็กตรอน, ดร.สุกานดา เจียรศิริสมบูรณ์, ศ.ดร.ทวี ตันฆศิริ และ รศ.ดร.กอบวุฒิ รุจิจนากุล)
5. เหรียญทองนักวิจัยดีเด่น จากสถาบันวิจัยและพัฒนาวิทยาศาสตร์และเทคโนโลยี มหาวิทยาลัยเชียงใหม่ ประจำ 2545
6. อาจารย์ดีเด่นแห่งชาติ สาขาวิชาวิทยาศาสตร์และเทคโนโลยี จากที่ประชุมประธานสภาอาจารย์มหาวิทยาลัยเชียงใหม่ ประจำปี 2545

นักวิจัยในโครงการที่ได้รับรางวัลหรือได้รับทุนวิจัยอื่น

1. ชื่อนักวิจัย รองศาสตราจารย์ ดร.จีระพงษ์ ตันตระกูล และคณะ
   ได้รับทุนวิจัย จากบริษัท Uyemura ประเทศญี่ปุ่น ปีที่ได้รับ 2547
   เรื่อง การพัฒนาคุณภาพของสารทำความสะอาดผิวและสารชักเงานิกเกิล
2. ชื่อนักวิจัย รองศาสตราจารย์ ดร.จีระพงษ์ ตันตระกูล และคณะ
   ได้รับ ทุนวิจัย คณะวิทยาศาสตร์ มหาวิทยาลัยเชียงใหม่ ปีที่ได้รับ 2547
   เรื่อง การสร้างแก้วกันรังสีเอกซ์
3. ชื่อนักวิจัย ดร.วิม เหนือเพ็ง
   ได้รับทุนวิจัย สกว. ปีที่ได้รับ 2546-2548
   เรื่อง คุณสมบัติทางกลและทางกายภาพของวัสดุผสมเคฟลาร์/อีพ็อกซี/อะลูมินา สำหรับใช้เป็นชิ้นส่วนยานยนต์

การสร้างนักศึกษาระดับบัณฑิตศึกษา

นักศึกษาระดับปริญญาเอกที่สำเร็จการศึกษาแล้ว

1. นายสิงหเดช แตงจวง (มหาวิทยาลัยราชภัฏอุตรดิตถ์)
2. นางสาวอรวรรณ อุดมพร (มหาวิทยาลัยมหาสารคาม)
3. นางสาวพรสุดา บ่มไล่ (มหาวิทยาลัยสงขลานครินทร์)
4. นายธีรชัย บงการณ์ (มหาวิทยาลัยนเรศวร)
5. นางสาวรุ่งนภา ทิพากรฐิติกุล (มหาวิทยาลัยอุบลราชธานี)

6. นายนราธิป วิทยากร (สถาบันเทคโนโลยีพระจอมเกล้าเจ้าคุณทหารลาดกระบัง)
7. นางสาววันดี ธรรมจารี (มหาวิทยาลัยเชียงใหม่)
8. นางสาววันดี อ่อนเรียบร้อย (สถาบันเทคโนโลยีพระจอมเกล้าธนบุรี)

นักศึกษาระดับปริญญาโทที่สำเร็จการศึกษาแล้ว

1. นายสุขุม อิสเสงี่ยม
2. นางสาวอุไรวรรณ อินต๊ะถา
3. นางสาวเนติมา สว่างวรรณ
4. นางสาววันทนีย์ เชียรธานรักษ์
5. นางสาวขันทอง ทรงสิริ

รายการครุภัณฑ์ที่ได้รับการสนับสนุนจากโครงการนี้

1. DC Power Supply
2. เตาเผาไฟฟ้าอุณหภูมิสูงสุด 1750 °C
3. Analytical Balance and Density Determination Peripherals
4. AC Power Supply รุ่น 210-10R
5. Computer 2 ชุด
6. เครื่องวัดอุณหภูมิความแม่นยำสูง

การสร้างเครือข่าย

คณะวิจัยได้สร้างเครือข่ายงานวิจัยกับสถาบันและมหาวิทยาลัยต่างๆ ดังนี้

1. ศูนย์เทคโนโลยีโลหะและวัสดุแห่งชาติ
2. มหาวิทยาลัยสงขลานครินทร์
3. มหาวิทยาลัยแม่ฟ้าหลวง
4. มหาวิทยาลัยราชภัฏอุตรดิตถ์
5. มหาวิทยาลัยมหาสารคาม
6. มหาวิทยาลัยนเรศวร
7. มหาวิทยาลัยอุบลราชธานี
8. สถาบันเทคโนโลยีพระจอมเกล้าเจ้าคุณทหารลาดกระบัง
9. สถาบันเทคโนโลยีพระจอมเกล้าธนบุรี

10. University of Leeds. (UK)
11. Victoria University of Wellington. (NZ).
12. Penn State University. (U.S.A)
13. Iowa State University. (USA)

ภาคผนวก

เอกสารหมายเลข 1

เอกสารหมายเลข 1.1

Mat Res Innovat (2002) 6:256–259
DOI 10.1007/s10019-002-0208-0

ORIGINAL ARTICLE

Singhadej Tangjuank · Tawee Tunkasiri

Effects of calcination temperature on phase and microstructure evolution of $BaTi_4O_9$ powders

Received: 30 July 2002 / Revised: 27 September 2002 / Accepted: 25 September 2002 / Published online: 19 November 2002

Abstract Calcining of the mixture of $BaCO_3$ and TiO_2 with a ratio 1:4 at different temperatures was carried out to synthesize $BaTi_4O_9$ powders. Phase evolution of the samples was studied using the differential thermal analysis (DTA) and X-ray diffractometry (XRD). Both techniques confirmed that the formation of $BaTi_4O_9$ started around 1000 °C. The XRD peaks showed that $BaTi_4O_9$ was most pronounced at 1250 °C. X-ray line broadening methods were employed to study the variation of particle size and microstrain of the $BaTi_4O_9$ powders. The Voigt function in a single line and the pseudo-Voigt function in the variance methods were used in our case. We found that both functions resulted in the same trends, i.e., the particle size increased with the temperature with the biggest size of 180 and 160 nm, whilst the microstrain yielded the opposite trend with the lowest values of 6.2×10^{-3} and 1.1×10^{-3}. The scanning electron microscopy (SEM) study revealed the size of the large particles formed, due to agglomeration, to be about 0.5–1.9 μm. Furthermore, it was shown that irregular shapes of $BaTi_4O_9$ powders necked to each other appeared at 1000 °C and grew into ellipse and rod shapes at 1250 °C.

Keywords Solid state reaction · $BaTi_4O_9$ · X-ray line broadening method

Introduction

Barium tetratitanate ($BaTi_4O_9$) ceramic is of particular interest and subject to much research due to its many attractive properties. For example, its high temperature stability, low loss, high dielectric constant etc, make $BaTi_4O_9$ compatible with microwave circuits [1, 2]. It was Masse et al. [3] who first mentioned the suitability for $BaTi_4O_9$ to be employed as microwave dielectric material. This is because its dielectric contant (ε) and tanδ were reported to be about 38 and 10^{-4} respectively [3]. These are very close to the required values ε(35–40) and of tanδ(10^{-3}) in microwave applications. The effect of microstructure on the electrical properties of barium based ceramics has been studied by many authors. It has been confirmed by Mcneal et al. [4] that $BaTiO_3$ ceramic with an average grain size of 66 nm exhibits resonant behaviour. Tunkasiri and Rujijanagul [5] revealed that the relationship between the breakdown strength and grain size is in the same form as observed for the mechanical strength of ceramics. These may be due to the variation of the particle size and microstrain occurring in the ceramic powder during sintering. The degree of crystallinity and lattice disorder of materials may affect the stability of their properties. Therefore, the study of the variation of the particle size and microstrain of $BaTi_4O_9$ ceramics, especially as a function of the fabrication temperature, is of great importance for microwave ceramic fabrication.

Many techniques have been employed regarding the measurement of particle size of the $BaTi_4O_9$ powders prior to sintering. For example, Pfaff [6] employed the Brunauer, Emmett and Teller (BET) technique while Choy et al. [7] and Cernea et al. [8] employed transmission electron microscopy (TEM). Choy et al. [7] also used the Scherrer formula to calculate the crystallite size from the X-ray diffraction profile. Since different measurement methods would yield different results on the crystallite and particle, we decided to employ two methods for confirmation of the results. In the widely used X-ray line broadening techniques to measure the particle size and microstrain, different methods have shown their limitations. It is well known that the measurement based on the Scherrer formula does not yield microstrain values. Tunkasiri and Rujijanagul [9] and Pakokthom et al. [10] successfully employed Wagner method and pseudo-Voigt function in the variance method [11], respectively, to measure the particle size and microstrain of Ba-based compounds. Moreover, the pseudo-Voigt function in the variance method and the Voigt function in a single line method [12] can be applied on one single peak, thus

S. Tangjuank · T. Tunkasiri (✉)
Department of Physics, Faculty of Science,
Chiang Mai University, Chiang Mai 50200, Thailand,
e-mail: tawee@chiangmai.ac.th

avoiding the problem of the peak overlap, to estimate the particle size and microstrain. Therefore, we used the two methods in our measurement.

$BaTi_4O_9$ can be prepared by many techniques such as solid state reaction [13], sol gel process [14], citrate [7] and oxalate routes [8]. For simplicity, in this work, $BaTi_4O_9$ powder was prepared by the solid state reaction. X-ray diffraction (XRD) method was used to study the phase evolution of $BaTi_4O_9$. The heating rates were varied in order to obtain the best conditions of $BaTi_4O_9$ yield. Estimation of the particle size and microstrain were carried out. Electron microscopy was also used to study the morphology of the particles.

Relation to previous work

Barium based ceramics such as barium tetratitanate ($BaTi_4O_9$) and barium titanate ($BaTiO_3$) have become the most widely used microwave ceramics [1, 2, 3, 4]. These are due to the suitability of their properties such as high temperature stability, low loss, high dielectric contents,... etc. Results obtained from Tunkasiri and Rujijanagul [5] revealed close relationship between the grain size and other physical properties of $BaTiO_3$ ceramics. These may be due to the variation of the particle size and microstrain occurring in the ceramic powders prior to sintering. Many techniques such as Brunauer, Emmett and Teller (BET) [6], transmission electron microscopy (TEM) [7, 8] were employed to measure the particle size of $BaTi_4O_9$ powder. However, the methods used do not yield any information about the microstrain of $BaTi_4O_9$ powder. Both particle size and microstrain can be measured from the XRD line profiles of the powder using Wagner [9] and pseudo-Voigt function in variance method [10, 11]. Furthermore, the pseudo-Voigt function in the variance method and the Voigt function in a single line method can be applied on one single peak. These two methods were thus employed in the present work where there is only one clear single XRD peak in the case of $BaTi_4O_9$. Morphology of the particles was also studied using scanning electron microscopy.

Experimental

$BaTi_4O_9$ powder was prepared by conventional solid state reaction from $BaCO_3$ and TiO_2 with the mole ratio of barium carbonate ($BaCO_3$) and titanium oxide (TiO_2) at 1:4. The powders were mixed and milled for 24 h in a polyethylene container with zirconia balls. Ethanol was used as a milling medium. The mixture was then dried and calcined in air at temperatures of 1000 °C, 1050 °C, 1100 °C, 1200 °C and 1250 °C respectively, for 2 h. Heating rates were 3 °C/min, 10 °C/min and 15 °C/min respectively for each calcination temperature. A differential thermal analyzer (DTA, Dupont 9000) was used to study phase transformation of $BaTi_4O_9$. The mixed powder and αAl_2O_3 as a reference were put into a platinum cell and heated. The analysis was performed from room temperature up to 1200 °C with a heating rate of 20 °C/min. The X-ray diffraction profiles were obtained using a Siemens powder diffractometer with Ni-filtered CuK_α radiation. The X-ray scan speed was 2θ min^{-1} and the scan angle from 20–60° of 2θ was chosen. A slow scanning speed of 1/8 min^{-1} was also used on the (302) peak for measurement of the particle size and microstrain. Rachinger's method [15] was used to resolve the $K_{\alpha 1}$ and $K_{\alpha 2}$ lines. The Voigt function in a single line and the pseudo-Voigt function in the variance methods were employed to estimate the particle size and microstrain. The data treatments were performed according to the methods described by De Keijser et al. [12] and Sanchez-Bajo and Cumbrera [11] respectively. The (302) peak of $BaTi_4O_9$ was selected for measurement, since it was the only peak with high intensity and not overlapped by other peaks. Morphology of $BaTi_4O_9$ was studied from scanning electron micrographs.

Results and discussion

Figure 1 shows the DTA thermogram obtained from heating the mixture of $BaCO_3$ and TiO_2 to 1200 °C. It is indicated that moisture removal took place from room temperature to 250 °C and phase change approximately ocurred at about 950 °C, corresponding to forming of $BaTi_4O_9$. Figure 2 shows a series of the X-ray diffractograms, belonging to the as-mixed and calcined temperatures from 1000 °C (rate of 3 °C/min). The analysis of XRD patterns is based on the Joint Committee on Powders Diffraction Standard (JCPDS), card No.77-1565. Every peak can be attributed to $BaTi_4O_9$. The results show that the orthorhombic $BaTi_4O_9$ phase started to form at about 1000 °C and became most pronounced at 1250 °C. The heating rates and the temperature range of $BaTi_4O_9$ forming, obtained from our XRD results, are agreeable to those obtained by Pfaff [6, 14], Choy et al. [7], Cheng et al. [16] and Cernea et al. [8]. In these pre-

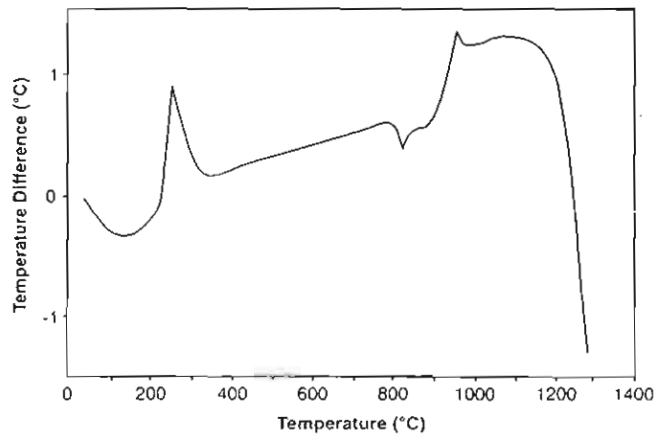

Fig. 1 SEM micrographs of $BaTi_4O_9$ powders calcined for 2 h at (a) 1000 °C (b) 1250 °C

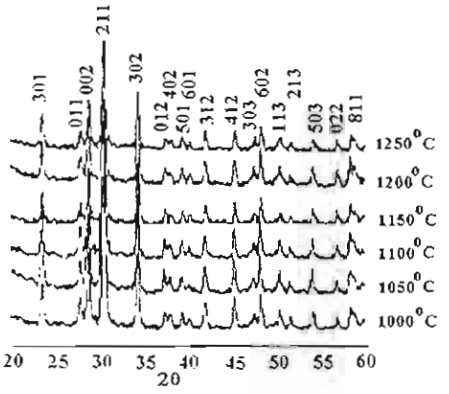

Fig. 2 X-ray diffractograms of $BaTi_4O_9$ calcined at 1000 to 1250 °C for 2 h with heating rate of 3 °C/min

vious investigations $BaTi_4O_9$ single phase was found at 900 °C [6], 1250 °C [7], 1200 °C [16], and 1300 °C [8] respectively. Furthermore, their results suggested that the longer heating time could enable $BaTi_4O_9$ to form at the lower annealing temperature, though most of their preparations were carried out via different routes such as peroxide [6], sol gel [14], citrate [7] and oxalate routes [8]. Figure 3 shows some of the scanning electron micrographs of the calcined $BaTi_4O_9$ powders. It can be seen that the $BaTi_4O_9$ powders consist of aggregated fine particles in almost irregular shape. They are slightly necked each other at 1000 °C and gradually grow larger at higher temperatures. At 1250 °C, large particles in ellipse and rod shapes were observed, resemble to that observed by Choy et al. [7]. The particle sizes obtained from our SEM techniques are in the range of 0.5–1.9 μm for the calcination temperatures from 1000–1250 °C. They are bigger than that observed from X-ray line broadening techniques. This may probably be due to agglomeration of the fine particles. However, their magnitudes are in the same order as that obtained from Pfaff [6], who employed BET method for measuring and prepared the powders via the peroxide route. Table 1 shows the particle size and microstrain values at each calcining temper-

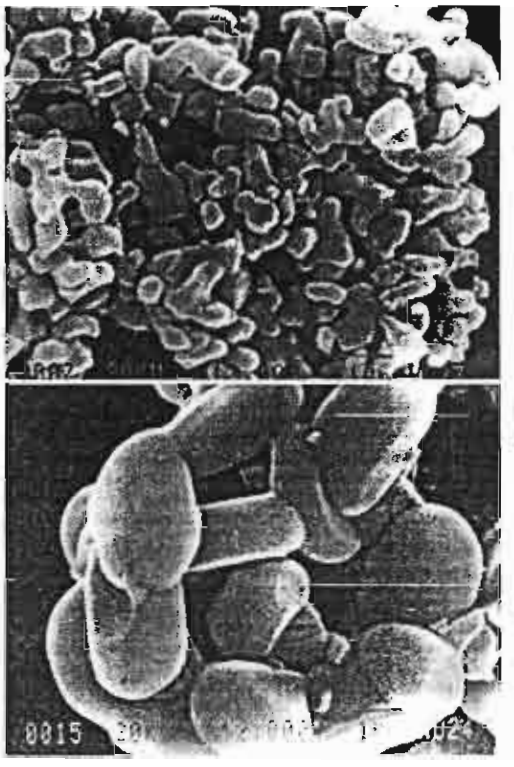

Fig. 3 DTA thermogram of the mixed powder from $BaCO_3$ and TiO_2 with the mole ratio 1:4 ($BaCO_3$:TiO_2)

ature. The particle sizes calculated from the pseudo-Voigt function in the variance method [11] were found smaller than that obtained from the Voigt function in a single line method [12]. This may be due to the different treatments of the two functions. However, they are in the same order and show the same trend, i.e., the particle size increases at higher temperatures. The microstrain values calculated from both functions show the opposite trend to that of the particle size, i.e., they decrease at higher temperatures. The particle sizes obtained from others [6, 7, 8] are also tabulated for comparison. The results show that the magnitudes of our particle size values

Table 1 Particle size and microstrain of the $BaTi_4O_9$ powders at various heating temperatures

Temp. (°C)	This work				Pfaff [6]	Choy et al. [7]	Cernea et al. [8]
	D_s (nm)	$\langle\varepsilon_s^2\rangle^{1/2}$ (×10⁻³)	D_{pv} (nm)	$\langle\varepsilon_{pv}^2\rangle^{1/2}$ (×10⁻³)	D_B (nm)	D_{sc} (nm)	D_T (nm)
900	–	–	–	–	90	36	–
1000	100	8.5	33	3.3	–	–	100
1050	107	8.3	40	3.1	–	–	–
1100	115	8.0	66	2.1	170	–	–
1150	130	7.4	94	1.6	–	–	–
1200	150	7.1	104	1.3	–	–	–
1250	180	6.2	160	1.1	–	–	–

D_s = Particle size by the Voigt function in a single line
D_{pv} = Particle size by the pseudo-voigt function in the variance method
D_B = Particle size by BET method
D_{sc} = Particle size by Scherrer formular
D_T = Particle size by TEM
$\langle\varepsilon_s^2\rangle^{1/2}$ = Microstrain by the Voigt function in a single line
$\langle\varepsilon_{pv}^2\rangle^{1/2}$ = Microstrain by the pseudo-voigt function in the variance method

are in the same order as that obtained from Pfaff [6], Choy et al. [7] and Cernea et al. [8], who though measured the size through BET technique, Scherrer formula and transmission electron microscopy respectively. The decrease of the strain is thought to have significant effects on some physical properties such as permittivity etc. of the $BaTi_4O_9$ ceramics.

Conclusions

$BaTi_4O_9$ powder was obtained from calcining the mixture of $BaCO_3$ and TiO_2 with the ratio 1:4 at different temperatures. Both DTA and XRD analysis reveal the formation of the crystalline $BaTi_4O_9$ powders at the temperature around 1000 °C. Estimation of the $BaTi_4O_9$ particle size and microstrain in the powder was carried out employing X-ray line broadening methods. The Voigt and pseudo-Voigt functions were used. The particle size values show that they increase at higher temperatures, whereas the values of the microstrain show the opposite trend, i.e., they decrease at higher temperatures. The biggest particle size and the lowest microstrain, estimated from the Voigt function, are 180 nm and 6.2×10^{-3}, respectively. From the microstructure analysis, it can be concluded that at 1000 °C the $BaTi_4O_9$ powders in irregular shape are necked to each other and eventually evolve into ellipse and rod shapes at 1250 °C. The agglomeration of the fine powders results in bigger particle sizes (~0.5–1.9 μm).

Acknowledgements The authors would like to express their sincere thanks to the Thailand Research Fund for the financial support. Thanks are also to Dr. L.D. Yu for his helpful comments and correction on the manuscript.

References

1. Negas T, Yeager G, Bell S, Coats N (1993) Am Ceram Soc Bull 72(1):80
2. Plourde K, Ren CL (1981) IEEE Trans Microwave Theory Tech MTT 29(8):754
3. Masse DJ, Pucel RA, Readey DW, Maguire EA, Hartwig CP (1971) Proc IEEE 59(11):1628
4. McNeal MP, Jang SJ, Newnham RE (1998) J Appl Phys 83(6):3288
5. Tunkasiri T, Rujijanagul G (1996) J Mater Sci Lett 15:1767
6. Pfaff G (1991) J Mater Sci Lett 10:129
7. Choy JH, Han YS, Sohn JH, Itoh M (1995) J Am Ceram Soc 78(5):1169
8. Cernea M, Chirtop E, Neacsu D, Pasuk I, Iordanescu S (2002) J Am Ceram Soc 85(2):499
9. Tunkasiri T, Rujijanagul G (1994) J Mater Sci Lett 13:165
10. Pakokthom C, Rujijanagul G, Tunkasiri T (1999) J Mater Sci Lett 18:747
11. Sanchez-Bajo F, Cumbrera GL (1997) J Appl Cryst 30:427
12. De Keijser TH, Langford JI, Mittemeijer EJ (1982) J Appl Cryst 15:308
13. Mhaisalkar SG, Lee WE, Readey DW (1989) J Am Ceram Soc 72(11):2154
14. Pfaff G (1992) J Mater Chem 2(6):591
15. Rachinger WA (1948) J Sci Inst 25:254
16. Cheng CM, Yang CF, Lo SH, Tseng TY (2000) J Euro Ceram Soc 20:1061

เอกสารหมายเลข 1.2

Available online at www.sciencedirect.com
SCIENCE DIRECT®
Materials Letters 57 (2003) 2637–2642
MATERIALS LETTERS
www.elsevier.com/locate/matlet

Synthesis, formation and characterization of zirconium titanate (ZT) powders

S. Ananta*, R. Tipakontitikul, T. Tunkasiri

Department of Physics, Faculty of Science, Chiang Mai University, Chiang Mai, 50200, Thailand

Received 30 May 2002; received in revised form 11 October 2002; accepted 25 October 2002

Abstract

Zirconium titanate ($ZrTiO_4$) powders have been prepared and characterised by differential thermal analysis (DTA), X-ray diffraction (XRD), scanning electron microscopy (SEM) and energy-dispersive X-ray (EDX) techniques. The effect of calcination temperature, dwell time and heating/cooling rates on phase formation, morphology and particle size distribution of the powders are examined. The calcination temperature and dwell time have been found to have a pronounced effect on the phase formation and particle size of the calcined zirconium titanate (ZT) powders. It has been found that the minor phases of ZrO_2 and TiO_2 tend to form together with $ZrTiO_4$, depending on calcination conditions. Optimisation of calcination conditions can lead to a single-phase $ZrTiO_4$ in an orthorhombic phase.

Keywords: Zirconium titanate; $ZrTiO_4$; Powder synthesis; Oxides; Calcination; X-ray diffraction

1. Introduction

Zirconium titanate-based compositions are extensively used as dielectric resonators for microwave telecommunications [1–3]. They also are of interest for a wide range of applications including catalysis, humidity sensors, high-temperature pigments and composites [4–8]. It is known that all forms of $ZrTiO_4$ have the orthorhombic structure [9]. Above 1200 °C, the high temperature phase of $ZrTiO_4$ was related to that of α-PbO_2, having random distributions of cations in available octahedral sites. On cooling within the temperature range 1200–1100 °C, a disorder–order transition has been observed; the reported phase transition is characterized by (1) a decrease in the length of the the *b* axis [10], (2) ordered arrangement of metal ions gives rise to a doubled axis along the *a* direction [11], and the reconstructive transition requiring a large scale rearrangement of the cations in the lattice [12].

The stoichiometry of zirconium titanate is known to be an important factor for ensuring good properties [2–5]. In order to obtain fine-grained, high quality and stoichiometric zirconium titanate powders at low processing temperatures, various chemical routes, for example, hydrolysis of alkoxides [13], sol–gel [14], Pechini [15], and co-precipitation [16], have been developed as alternatives to the conventional solid state reaction of mixed oxides [17]. All of these techniques are aimed at reducing the temperature of

* Corresponding author. Tel.: +66-53-943376; fax: +66-53-357512.
E-mail address: supon@chiangmai.ac.th (S. Ananta).

0167-577X/02/$ - see front matter
doi:10.1016/S0167-577X(02)01342-3

preparation of the compound even though they are more involved and complicated than the mixed oxide route. Generally, the mixed oxide method involves the heating of a mixture of zirconium oxide and titanium oxide above 1200–1600 °C for long times [17], and has been employed intensively in the last decade [18–20]. The optimisation of calcination conditions used in the mixed oxide process, however, have not received detailed attention, and the effects of applied dwell time and heating/cooling rates have not yet been studied extensively to our knowledge. The purpose of this work was to explore a simple mixed oxide synthetic route for the production of zirconium titanate (ZT) powders and perform a systematic study of the reaction between the starting zirconium oxide and titanium oxide precursors. The phase formation, morphology and particle size of the powder calcined at various conditions will be studied and discussed.

2. Experimental procedure

Laboratory grade purity oxides of zirconium oxide, ZrO_2 (baddeleyite: JCPDS file number 37-1484) and titanium oxide, TiO_2 (anatase: JCPDS file number 21-1272) (Fluka, 99.9% purity) were used in this study. The two oxide powders exhibited an average particle size in the range of 3.0–5.0 μm. $ZrTiO_4$ powder was synthesised by the solid state reaction of thoroughly ground mixtures of ZrO_2 and TiO_2 powders that were milled in the required stoichiometric ratio. The milling operation was carried out for 24 h in isopropanal. High purity zirconia balls with diameter of 10 mm were used as the milling media. After drying at 120 °C, various calcination conditions, i.e. temperatures ranging from 1100 to 1350 °C, dwell times ranging from 0.5 to 6 h and heating/cooling rates ranging from 2 to 20 °C/min., were applied, in order to investigate the formation of zirconium titanate. The reactions of the uncalcined ZT powders taking place during heat treatment were investigated by differential thermal analysis (DTA) (NETZSCH-Gerätebau GmbH Thermal Analysis STA 409) using a heating rate of 10 °C/min in air from room temperature up to 1400 °C. Calcined powders were subsequently examined by room temperature X-ray diffraction (XRD; Philips PW 1729 diffractometer) using CuK_α radiation to identify the phases formed and optimum calcination conditions for the manufacture of ZT powder. Powder morphologies and grain sizes were directly imaged using scanning electron microscopy (SEM; JEOL JSM-840A). The chemical compositions of the phases formed were elucidated by an energy-dispersive X-ray (EDX) analyser with an ultra-thin window. EDX spectra were quantified with the virtual standards peaks supplied with the Oxford Instruments eXL software.

3. Results and discussion

A DTA curve obtained for a powder mixed in the stoichiometric proportions of $ZrTiO_4$ is shown in Fig. 1. Two exothermic peaks with maxima at 1150 and 1240 °C, and two endothermic peaks centered at ca. 1200 and 1270 °C were observed in this profile. These temperatures having been obtained from the calibration of the sample thermocouple. It is to be noted that there is no obvious interpretation of the peaks, although it is likely to correspond to a phase transition reported by a number of workers [10–12]. These data were used to define the range of temperatures for XRD investigation to between 1100 and 1350 °C. Powder XRD patterns of the calcined ZT powders are given in Figs. 2–4. In general, the strongest reflections apparent in the majority of the XRD patterns indicate the formation of zirconium titanate phase, $ZrTiO_4$, which could be matched with JCPDS file no. 34-415. To a first approximation, this major phase has orthorhombic structure, space group *Pnab* (no. 60), with cell parameter $a = 503$ pm, $b = 549$ pm and $c = 480$ pm. It is also of interest that no evidence has been obtained for the existence of the α-PbO_2-like orthorhombic phase (space group *Pcnb*) reported by Newnham [9]. Depending on the calcination conditions, at least four minor phases were identified, i.e. monoclinic-ZrO_2 (*), tetragonal-ZrO_2 (∇), anatase-TiO_2 (•) and rutile-TiO_2 (÷), which can be correlated with JCPDS files numbers 37-1484, 17-923, 21-1272 and 21-1276, respectively. The precursor ZrO_2 has a baddeleyite-type structure with monoclinic unit cell ($a = 5.31$ Å, $b = 5.21$ Å, $c = 5.14$ Å and $\beta = 99.22°$), space group $P2_1/a$ (no. 14), whereas tetragonal symmetry ($a = 3.78$ Å and $c = 9.51$ Å) is associated with anatase-TiO_2 precursor, space group $I4_1/amd$ (no. 141). Both minor phases found in the calcined ZT powder of ZrO_2 (∇) and TiO_2 (•) have

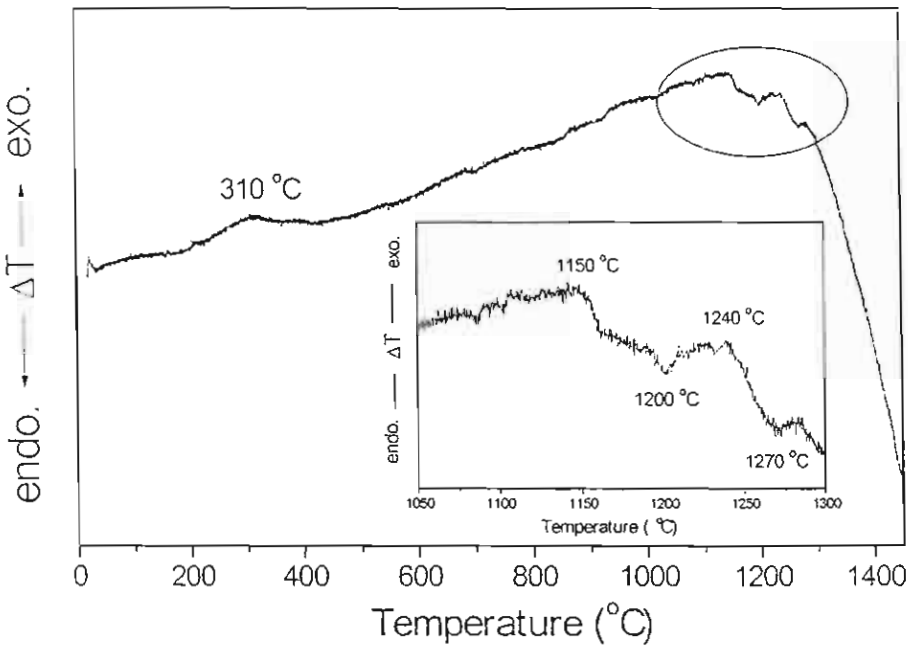

Fig. 1. A DTA curve for the mixture of ZrO_2-TiO_2 powder.

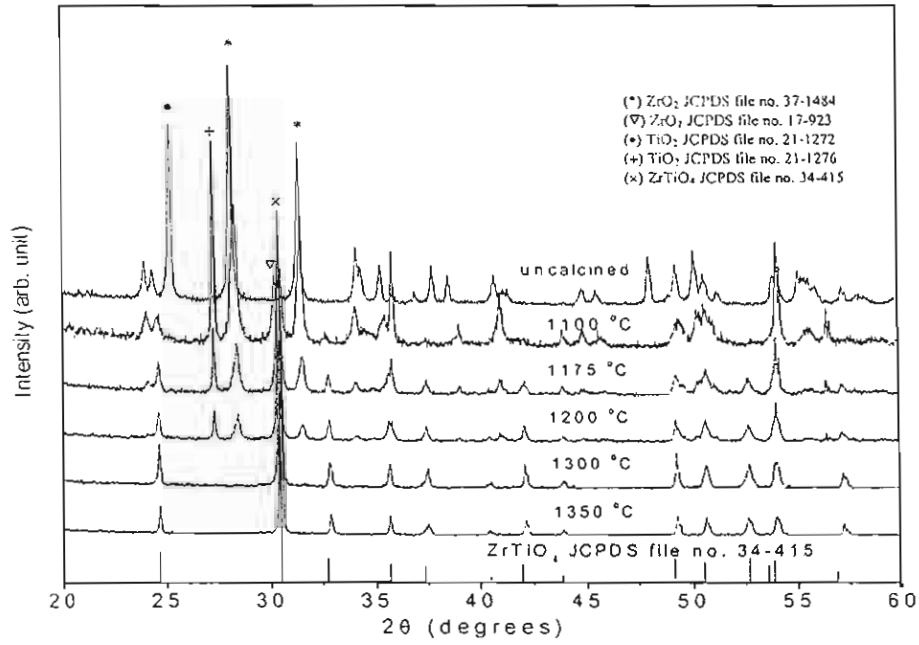

Fig. 2. XRD patterns of ZT powder calcined at various temperatures for 4 h with heating/cooling rates of 20 °C/min.

tetragonal symmetry with unit cell parameters: $a=5.12$ Å and $c=5.25$ Å, space group $P4m2$ (no. 115), and $a=3.78$ Å and $c=9.51$ Å, space group $P4_2/mnm$ (no.136), respectively. It is well established that there are a number of polymorphic forms of ZrO_2 and TiO_2 stable at different temperature and pressures. In the work reported here, monoclinic/tetragonal transformations of ZrO_2 and the anatase/rutile transformation of TiO_2 have been found. Monoclinic zirconia (*) is detected from the original mixture up to 1200 °C, whereas partial conversion to tetragonal zirconia (∇) was observed after heating at 1100 °C, which is associated to the DTA exothermic effect previously observed in Fig. 1. It is seen that completed conversion of anatase-TiO_2 (•) precursor to rutile (+) was found after calcination at 1100 °C, in agreement with other work [21]. No evidence of Ti_2ZrO was found, nor was there any indication of the orthorhombic phase of $Zr_5Ti_7O_{24}$ [22] being present.

This study shows that minor amounts of the ZrO_2 and TiO_2 phases tend to co-exist along with the zirconium titanate $ZrTiO_4$ phase, after calcinations in the range 1100–1200 °C. By increasing the calcination temperature, the yield of $ZrTiO_4$ phase increases significantly until 1300 °C, whereafter higher temperatures do not enhance the yield (Fig. 2). Apart from the calcination temperature, the effect of dwell time was also found to be quite significant (Fig. 3). It is seen that the single phase of $ZrTiO_4$ (yield of 100% within the limitations of the XRD technique) was found to be possible only in powders, calcined at 1300 °C with dwell time of 4 h or more. In the present study, an attempt was also made to calcine ZT powders under various heating/cooling rates (Fig. 4). In this connection, it is shown that the yield of $ZrTiO_4$ phase did not vary significantly with different heating/cooling rates ranging from 2 to 20 °C/min. It is to be noted that doublets observed in the XRD pattern for $ZrTiO_4$ at $2\theta=48°$, 50°, 52°, 54° and 57° could be attribute to the formation of minor phase $Zr_5Ti_7O_{24}$. This phase also has the α-PbO_2 type structure and a well-define superstructure with a tripled a-axis [23]. It is well established that zirconium titanate-based samples exhibiting difference degrees of ordering may be generated by employing high temperature treatment and different heating/cooling rates [23].

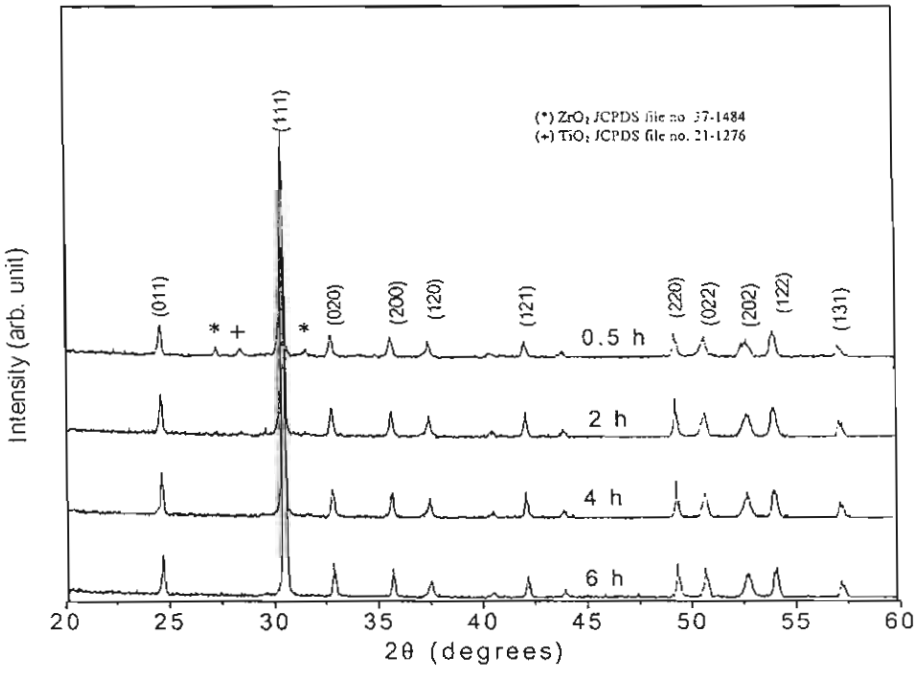

Fig. 3. XRD patterns of ZT powder calcined at 1300 °C with heating/cooling rates of 20 °C/min for various dwell times.

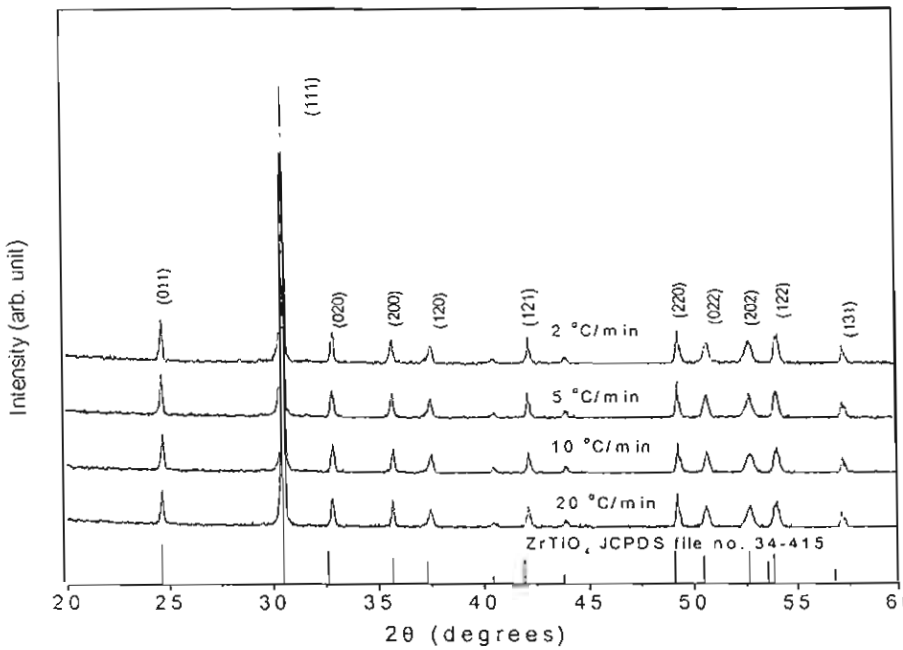

Fig. 4. XRD patterns of ZT powder calcined at 1300°C for 4 h with various heating/cooling rates.

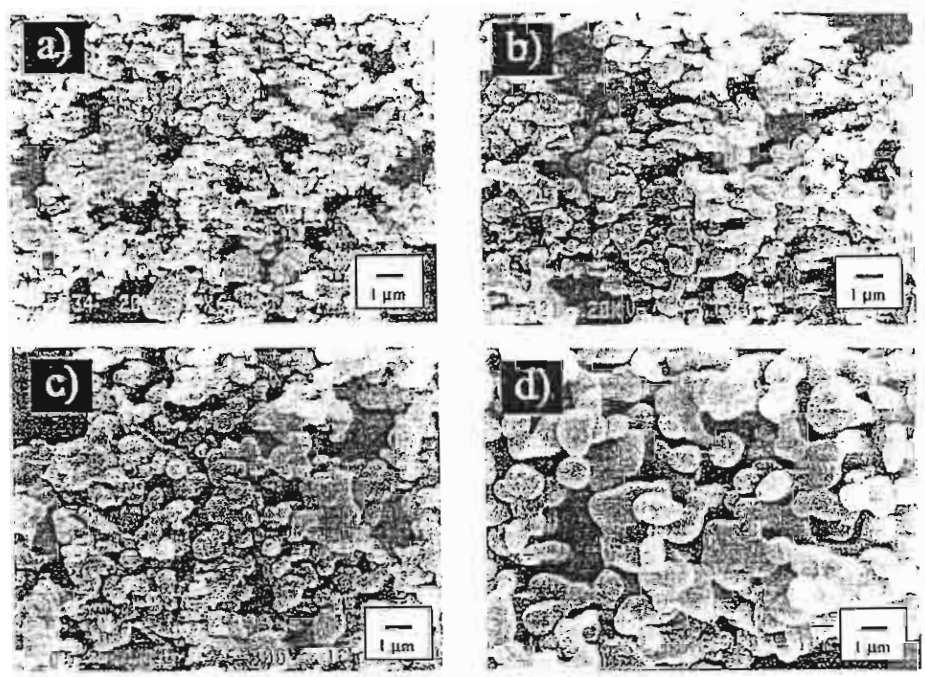

Fig. 5. SEM micrographs of the ZT powders calcined for 4 h at (a) 1100°C, (b) 1175°C, (c) 1200°C and (d) 1300°C.

Ferroelectrics Letters, 2002, Vol. 29(5–6), pp. 105–115
Reprints available directly from the publisher
Photocopying permitted by license only
DOI: 10.1080/07315170290033250

Microstructure, Piezoelectric Properties and Phase Transition of $(Pb_{0.90}Ba_{0.10})ZrO_3$ Ceramics Prepared by Solid State Reaction Method

T. BONGKARN, G. RUJIJANAGUL, and T. TUNKASIRI

Department of Physics, Faculty of Science, Chiang Mai University, Chiang Mai, Thailand 50200

Communicated by Dr. George W. Taylor

(Received August 24, 2002)

$(Pb_{0.90}Ba_{0.10})ZrO_3$ was prepared via the solid state reaction method under various heat treatment conditions. Microstructure, piezoelectric properties and phase transitions of $(Pb_{0.90}Ba_{0.10})ZrO_3$ were studied. Grain size of the samples is in the range of 0.5 to 1.3 μm. The d_{33} values of the samples are in the range of 19–27 pC/N while the planar coupling coefficient k_p is about 0.3 for all samples. Antiferroelectric to ferroelectric phase transition was found in samples re-calcined at 850°C and sintered at 1325°C and 1350°C. However, ferroelectric-to-antiferroelectric phase transition was not detected. The ferroelectric-to-paraelectric transition temperature slightly increases as the sintering temperature increases. This can be related to the characteristics of the grains in the ceramics.

Keywords: $(Pb_{0.90}Ba_{0.10})ZrO_3$; piezoelectric; phase transition

INTRODUCTION

$PbZrO_3$ (PZ) is an antiferroelectric (AFE) material which has an orthorhombic structure with lattice parameters $a = 5.87$A, $b = 11.74$A, $c = 8.20$A at room temperature. The phase transition temperature from AFE phase to paraelectric (PE) phase (cubic phase) of this material is around 230°C. The relative permittivity of the PZ ceramics is about 100 at room temperature and it shows a sharp maximum at the Curie point temperature [1]. This material is good for energy storage application. First characterization of the PZ as the AFE material was done by Sawaguchi et al. [2] in 1951. After that, many authors have studied its properties and tried to develop

methods for synthesis of the material [3–8]. It is well known that an intermediate phase forms when Pb sites in the PZ are partially replaced by Ba ions [9, 10]. The intermediate phase between the AFE and the FE phase in the $(Pb_{1-x}Ba_x)ZrO_3$ system is a ferroelectric (FE) phase. Because of a large volume change in the phase transition, modified PZ is selected as a candidate material for energy conversion. Shirane [9] found that the AFE to FE phase transition in the $(Pb_{1-x}Ba_x)ZrO_3$ (PBZ) system did not occur until x exceeded 0.05. However, the existence of the AFE phase at room temperature depends on the amount of x and the method of preparation [10, 11]. Furthermore, many authors reported that as the Ba ions in $(Pb_{1-x}Ba_x)ZrO_3$ increased, the Curie temperature of the PBZ shifted to a lower temperature [9, 12]. Recently, Pokharel and Pandey [11, 13, 14] have studied phase transitions of $(Pb_{0.9}Ba_{0.10})ZrO_3$(PBZ10). They prepared the PBZ10 by a chemical route to ensure a homogeneous distribution of Pb and Ba ions. They found that the AFE-to-FE phase transition in the PBZ10 ceramics is not fully reversible. The earlier researchers [12, 15] prepared PBZ10 by the conventional solid state route. However, the AFE-to-FE phase transition was not found in their samples. Properties of the modified PZ have been studied by many authors [11–16]. In the case of the PBZ10, Shirane [9] found that the AFE-to-FE phase transition occurred at the temperature of about 140°C, while Yoon et al. [12] and Ujima et al. [15] did not find the phase transition. However, Pokharel and Pandey [11, 13, 14] found that the AFE to FE transition temperature is 114°C on the heating cycle. They suggested that disappearing of the phase transition in the previous works might be due to the PbO loss during calcination at 1000°C in air. Evolution of these phases and their reversibility are of so much importance regarding to their physical properties. Heat treatment procedures can greatly affect the phase evolution on other lead based compound [17]. Although previous researchers have investigated the properties of the PBZ10 ceramics, the effects of heat treatment on microstructure and piezoelectric properties of the PBZ10 ceramics are not clearly understood. Therefore, in the present work, we studied the phase evolution, microstructure and piezoelectric properties of PBZ10, affected by heat treatment. Two steps of calcination at various temperatures were carried out, prior to sintering. PBZ10 powder was obtained via the conventional solid state reaction method. The first calcining temperature was 750°C, the second calcining temperatures were 800, 850, 900, 950 and 1000°C. Influence of the different sintering temperatures on microstructure, piezoelectric, and phase transition properties of the PBZ10 was studied. The results were discussed and compared to the previous works.

EXPERIMENTAL PROCEDURE

The conventional mixed oxide method was employed to prepare the PBZ10 powders. Commercial powder of PbO, $BaCO_3$, and ZrO_2 were mixed together. After ball milling in ethyl alcohol with zirconia grinding media for 24 h, the suspensions were dried and the powders were ground using an agate mortar and pestle into a fine powder. The crushed powders were calcined at 750°C in air for 6 h. Recalcination was done at 850–1000°C for 6 h, with a step of 50°C, and then grinding was done once more. Binder (0.5 wt% of PVA) was blended with the calcined powder to improve the compaction behaviour. The powders were pressed at 40 MPa into cylindrical pellets with 15 mm in diameter and 2 mm in thickness. The pellets were then sintered at various temperatures ranging from 1250°C to 1350°C for 4 h. The heat treatment conditions are shown in Table I. In order to minimize the loss of lead due to vaporization, the PbO atmosphere for the re-calcination and the sintering was maintained using $PbZrO_3$ as the spacer powder. Weight loss due to vaporization of lead escape at high temperatures was evaluated. The microstructures of the powders and the sintered samples were examined using scanning electron microscopy (SEM, JEOL 840A). The particle size and grain size were measured on the SEM photographs. The phase of the calcined powders and sintered samples was determined using a diffractometer (Bruker D8 ADVANCE $\theta - 2\theta$). The density of the sintered samples was measured by Archimedes' method with distilled water

TABLE I Heat treatment conditions and piezoelectric properties of PBZ10. (First calcination temperature is 750°C)

Heat treatment conditions		Piezoelectric properties	
Second calcination temperatures (°C)	Sintering temperatures (°C)	d_{33} (pC/N)	k_p
800	1325	19	0.30
850	1250	27	0.31
850	1275	27	0.31
850	1300	22	0.30
850	1325	19	0.30
850	1350	23	0.30
850	1325	19	0.30
900	1325	23	0.30
950	1325	24	0.30
1000	1325	24	0.37

as the fluid medium. The phase transition temperatures and enthalpy (ΔH) of the phase transitions were determined by a differential scanning calorimeter (DSC, PERKIN-ELMER DSC7). By using the DSC, the PBZ10 ceramics were heated up from room temperature to 275°C at a rate of 1°C/min, held at the final temperature for 1 h and then cooled down to room temperature at a rate of 0.5°C/min, following the conditions of Pokharel and Pandey [11]. The sintered samples were prepared for electrical property measurements by first polishing and then gold sputtering on to the clean pellet faces. The poling was done conventionally, in silicone oil bath at 170°C with a field of 25 kV/cm. After poling, the d_{33} coefficient was measured using a d_{33} meter (Piezometer System Model PM25). The planar coupling coefficient (k_p) was determined using a Hewlett Packard 4149A impedance analyzer.

RESULTS AND DISCUSSION

The XRD patterns of the calcined powder and the re-calcined powders are shown in Fig. 1. Trace of $BaCO_3$ appears in the diffactograms of the sample calcined at 750°C. At higher calcination temperatures, single phase of PBZ was detected in this work, showing similarity the results obtained by previous authors [11, 13].

Figure 2 shows SEM micrographs of the powders obtained under two of the calcination conditions, 850 and 1000°C. The particle size distribution at the lower calcination temperature is more uniform than that of the samples calcined at the higher temperature. The particle size and the PbO weight loss as a function of calcination temperature are shown in Fig. 3. The particle size increased with increasing the calcination temperature as expected. The weight loss due to vaporization of lead was found to be 0.42% for the sample re-calcined at 1000°C. Figure 4 shows SEM micrographs of the sintered samples in different heat treatment conditions. For the samples calcined at 850°C with various sintering temperatures, the grain size slightly increases with increasing the sintering temperature. Grain size at various sintering temperatures is shown in Fig. 5.

In the present work, we measured the transition temperatures by DSC. The heating and cooling were performed with the same conditions as that of Pookarel and Pandey [11]. It was found that the AFE-to-FE transition occurred for the samples re-calcined at 850°C and sintered at 1325 and 1350°C at 157 and 161°C respectively. However, the FE-to-AFE phase transition could not be observed on the cooling cycle in our samples.

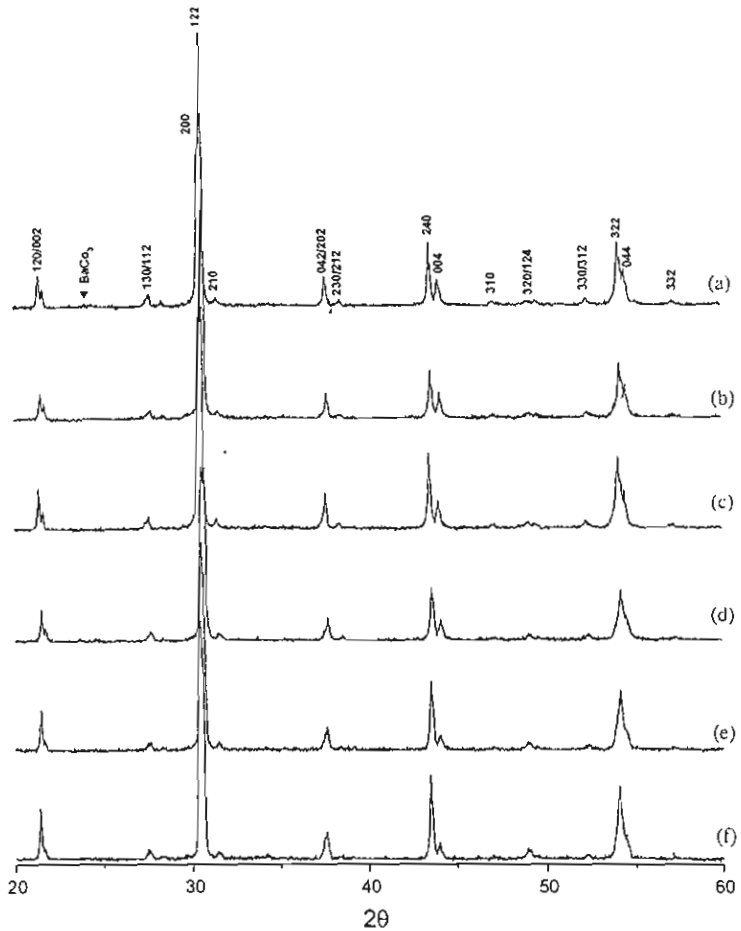

Figure 1. X-ray diffractograms of PBZ10 powders firing at various temperatures: (a) calcined at 750°C, (b) re-calcined at 800°C, (c) re-calcined at 850°C, (d) re-calcined at 900°C, (e) re-calcined at 950°C, and (f) re-calcined at 1000°C.

The calcined powders that we prepared were re-calcined at temperatures below 1100°C. The samples re-calcined at 850°C were well crystallized. In this condition, the PbO loss during calcination was 0.34 wt%. Moreover, at higher sintering temperatures, good compaction of grain and good crystallization were found, and the phase transition was observed in the samples. The FE-to-PE transition temperature was 187–190°C. This transition

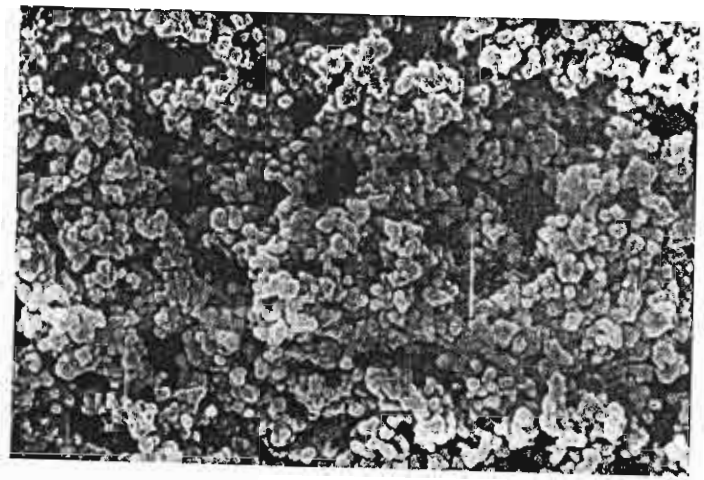

Figure 2. SEM photographs of PBZ10 powder re-calcined at (a) 850°C and (b) 1000°C.

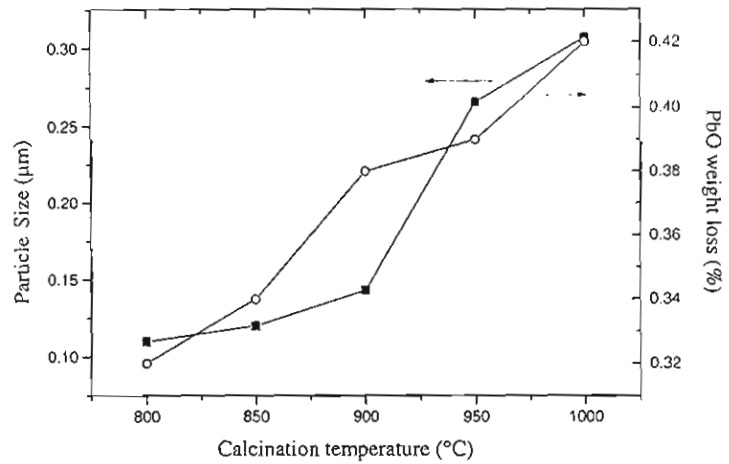

Figure 3. Particle size and PbO weight loss of PBZ10 powder calcined at various temperatures: (■) particle size and (○) PbO weight loss.

temperature slightly increased with the sintering temperature, as seen in Fig. 6. The PE-to-FE transition temperature is also shown in the same figure. The ΔH during the phase transitions was measured from the DSC peaks. The ΔHs of the FE-to-PE phase transition and the PE-to-FE phase transition increase with increasing the sintering temperature as seen in Fig. 7. High ΔH in the samples sintered at the higher temperature was observed, probably due to good compaction of the grains at the higher sintering temperature. Furthermore, the density of the ceramic samples is higher at the higher sintering temperature as seen in Fig. 5. Li and Shih [18] studied tetragonal-cubic phase transformation of $BaTiO_3$ particles. They found that ΔH as a function of particle size was proportional to cluster size and increased with increasing the particle size. They concluded that the stabilization of the tetragonal phase in the smaller particles was caused by clustering of the $BaTiO_3$ particles. This implies that the characteristics of particles and grains have an effect on the phase transformation behavior. Pookarel and Pandey [11, 13] have studied the FE-to-AFE phase transition in PBZ10. They did not find the phase transition in their samples. However, their X-Ray results showed that this transition was not fully reversible on the cooling cycle. In the present work, our DSC results agree that of Pookarel and Pandey, though their results were obtained dielectric measurement.

In order to study the piezoelectric properties, the d_{33} and the k_p coefficient of the sintered samples at room temperature were measured. The results are

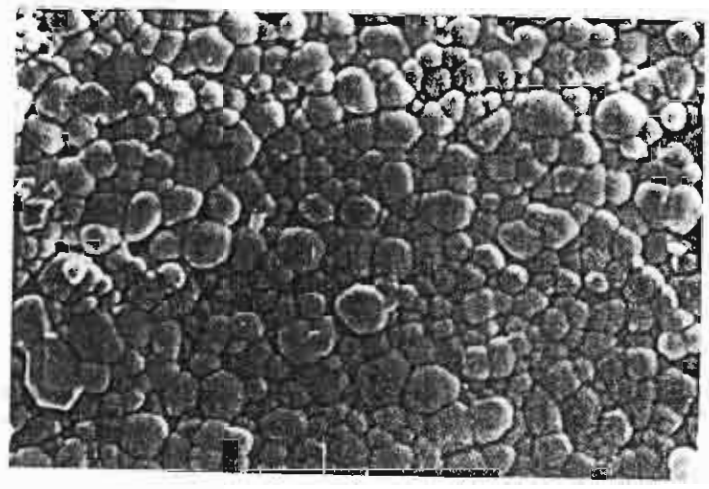

(a)

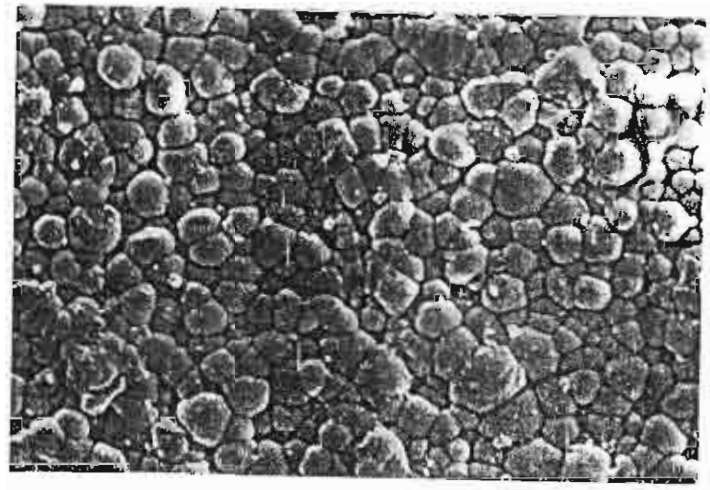

(b)

Figure 4. SEM photographs of sintered surfaces of PBZ10 ceramics re-calcined at 850 °C and sintered at (a) 1250 °C and (b) 1325 °C.

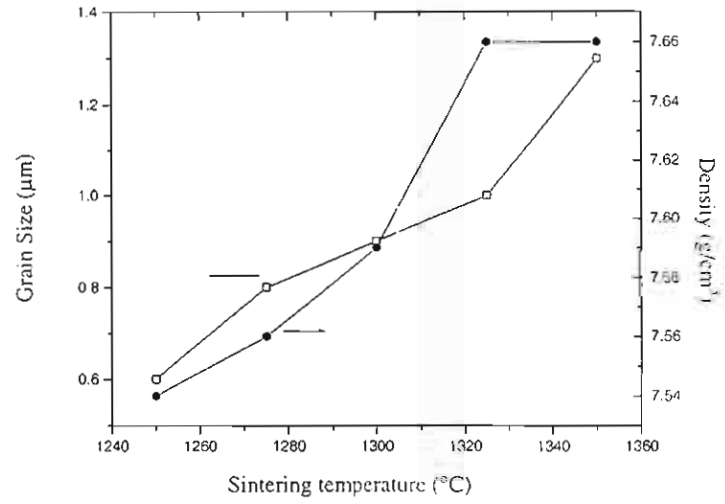

Figure 5. Grain size and density of PBZ10 ceramics at various sintering temperatures: (□) grain size and (●) density.

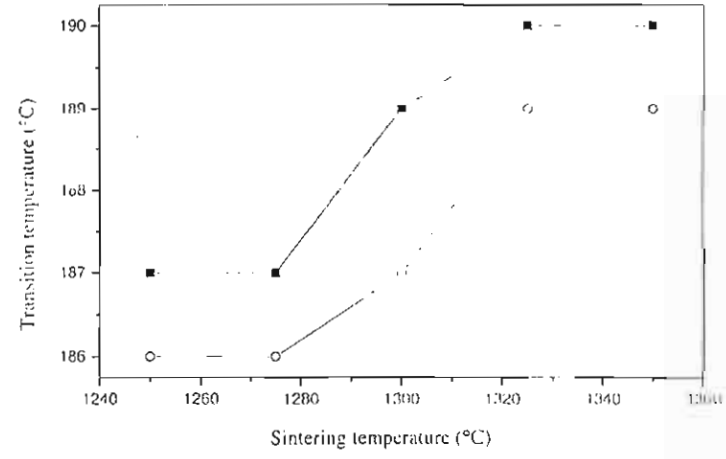

Figure 6. Transition temperature vs sintering temperature of PBZ10 ceramics. (■) FE-to-PE phase transition and (○) PE-to-FE phase transition.

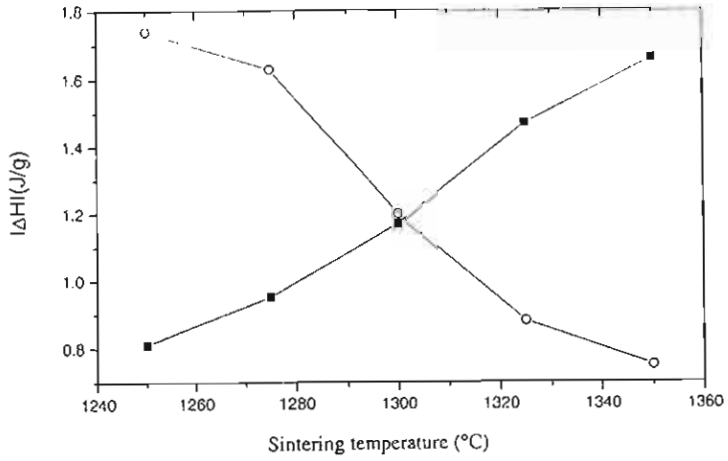

Figure 7. |ΔH| of PBZ10 ceramics as a function of sintering temperature: (■) FE-to-PE phase transition and (○) PE-to-FE phase transition.

shown in Table I. The d_{33} values are found in the range of 19–27 pC/N, while the k_p of the samples is about 0.3 for all samples. Roberts reported that the d_{33} value of $(Pb_{0.7}Ba_{0.3})ZrO_3$ (PBZ30) was about 65 pC/N, and it is 10^{-1} pC/N for PZ. Because the PBZ30 is a ferroelectric material at room temperature, the d_{33} value reported by Roberts was then higher than our results as well as that obtained from PZ.

CONCLUSIONS

In the present work, the PBZ10 was prepared by a solid state reaction method. We investigated the phase transition and piezoelectric properties at various heat treatment processes. The AFE phase was found in the samples calcined at 850°C and sintered at 1325 and 1350°C. The transition temperatures from the AFE phase to the FE phase in the samples were 157 and 161°C respectively. We also found that the transition temperature from the FE phase to the PE phase slightly increased as the sintering temperature increased.

For the FE-to-PE transition, the enthalpy change as a function of sintering temperature was observed. The values of ΔH increased at a higher sintering temperature. Furthermore, the values of d_{33} and k_p of the samples were measured to be in the range of 19–27 pC/N and about 0.3, respectively.

ACKNOWLEDGMENTS

This work was supported by The Thailand Research Fund, Graduate School of Chiang Mai University, and Ministry of University Affairs. We acknowledge the Department of Physics, Srinakharinwirot University for the use of x-ray diffraction facilities. Acknowledgements are also to Miss P. Komprapan for her help in operating DSC and Dr. L.D. Yu for his helpful comments and correction on the manuscript.

REFERENCES

[1] B. Jaffe, W. R. Cook, and H. Jaffe, *Piezoelectric ceramics* (R.A.N. Publishers, 1971), pp. 123–131.
[2] E. Sawaguchi, H. Maniwa, and S. Hoshino, *Phys. Rev.* 83, 1078 (1951).
[3] F. Jona, G. Shirane, F. Mazzi, and R. Pepinsky, *Phys. Rev.* 105(3), 849 (1957).
[4] M. T. Lanagan, J. H. Kim, S. J. Jang, and R. E. Newnham, *J. Am. Ceram. Soc.* 71(4), 311 (1988).
[5] W. N. Lawless, *Phys. Rev.* B 30(11), 6555 (1984).
[6] J. F. Li, D. D. Viehland, T. Tani, C. D. E. Lakeman, and D. A. Payne, *J. Appl. Phys.* 75(1), 442 (1994).
[7] E. Cockayne and K. M. Rabe, *J. Phys. Chem. Sol.* 61, 305 (2000).
[8] E. E. Oren, E. Taspinar, and A. C. Tas, *J. Am. Ceram. Soc.* 80(10), 2714 (1997).
[9] G. Shirane, *Phys. Rev.* 86(2), 219 (1952).
[10] B. P. Pokharel, M. K. Datta, and D. Pandey, *J. Mater. Sci.* 34, 691 (1999).
[11] B. P. Pokharel and D. Pandey, *J. Appl. Phys.* 88(9), 5364 (2000).
[12] K. H. Yoon and S. C. Hwang, *J. Mater. Sci.* 32, 17 (1997).
[13] B. P. Pokharel and D. Pandey, *J. Appl. Phys.* 86(6), 3327 (1999).
[14] B. P. Pokharel and D. Pandey, *J. Appl. Phys.* 90(6), 2985 (2001).
[15] Z. Ujima, J. Handerek, M. Pawelczyk, and D. Dmytrow, *Ferroelectrics* 129, 127 (1992).
[16] C. Heremans and H. L. Tuller, *J. Eur. Ceram. Soc.* 19, 1133 (1999).
[17] G. Zhilun, L. Longtu, G. Suhua, and Z. Xiaowen, *J. Am. Ceram. Soc.* 72(3), 486 (1989).
[18] X. Li and W. H. Shih, *J. Am. Ceram. Soc.* 80(11), 2844 (1997).

เอกสารหมายเลข 1.4

INSTITUTE OF PHYSICS PUBLISHING SMART MATERIALS AND STRUCTURES
Smart Mater. Struct. 12 (2003) 656–659 PII: S0964-1726(03)64639-2

Homogeneous precipitation synthesis and characterization of $BaTi_5O_{11}$ powders

S Tangjuank, L D Yu and T Tunkasiri

Department of Physics, Faculty of Science, Chiang Mai University, Chiang Mai 50200, Thailand

E-mail: tawee@chiangmai.ac.th

Received 8 November 2002, in final form 19 May 2003
Published 23 July 2003
Online at stacks.iop.org/SMS/12/656

Abstract

$BaTi_5O_{11}$ powders with microwave dielectric application potentials were synthesized using the homogeneous precipitation method and characterized. The precursor of the powders was prepared by co-precipitation of a solution of barium and titanium species with oxalic acid at a temperature of 80 °C and subsequent calcination at different temperatures. The phase evolution and characteristics of the samples were studied using differential thermal analysis, Fourier transform infrared spectroscopy, x-ray diffractometry, and transmission electron diffraction. The results show that formation of $BaTi_5O_{11}$ starts around 700 °C and continues until 1100 °C in air, and in this calcination temperature range all powders appear to be single-phase, monoclinic $BaTi_5O_{11}$. Scanning electron microscopy and transmission electron microscopy observations reveal that the sizes of the particles, nearly round in shape, formed due to agglomeration, are about 100 nm at a calcination temperature of 700 °C, and 600 nm at 1100 °C.

1. Introduction

Nowadays, microwave communication systems such as personal communication systems, global positioning systems, and cellular systems are widely used. There is great interest in developing dielectric resonator ceramics for these applications due to their high dielectric constants, high quality factors, low dielectric loss, and near-zero temperature coefficients of the resonant frequency [1]. $BaTi_5O_{11}$ is one of the most important titania-rich compounds in the $BaO–TiO_2$ system, which is of considerable interest for microwave dielectric applications. Since Ritter *et al* [2] concluded from O'Bryan's data [3] that single-phase $BaTi_5O_{11}$ might have superior microwave properties, relevant work has been carried out aimed at producing single-phase $BaTi_5O_{11}$ powder. According to O'Bryan [4], it was shown that the conventional solid-state reaction could not yield single-phase $BaTi_5O_{11}$. Chemical processes were then employed in an attempt to obtain single-phase $BaTi_5O_{11}$. Fukui *et al* [5] and Ritter *et al* [2] showed that $BaTi_5O_{11}$ powder could be produced by annealing alkoxide-derived powder at 700–1100 °C, but for a prolonged heating time (48 h) at 1200 °C, $BaTi_5O_{11}$ would be decomposed. Javadpour and Eror [6] and Lu *et al* [7] employed a liquid-mix technique and a new sol–gel process, respectively, to prepare $BaTi_5O_{11}$ powder and obtained single-phase $BaTi_5O_{11}$ powder at 700–1100 °C. Nevertheless, new chemical preparation methods for obtaining single-phase $BaTi_5O_{11}$ were still searched for. It had been thought that the homogeneous precipitation method [8] could also have potential for yielding single-phase $BaTi_5O_{11}$, since it was successfully employed to prepare single-phase $BaTiO_3$ powder [8–10] and lead zirconate titanate (PZT) [11]. This method has the additional merit of being able to produce fine particles with high purity. Therefore, the homogeneous precipitation method was employed in this work.

2. Experimental details

The preparation of $BaTi_5O_{11}$ is similar to that described by Tunkasiri and Rujijanagul [8]. Barium chloride ($BaCl_2·H_2O$) (>99% purity, Carlo Erba), titanium tetrachloride ($TiCl_4$) (>98% purity, Carlo Erba), hydrochloric acid (HCl), and oxalic acid were used as the starting materials. These materials were mixed and treated in the following steps to produce the targeted $BaTi_5O_{11}$. The solution of barium

0964-1726/03/040656+04$30.00

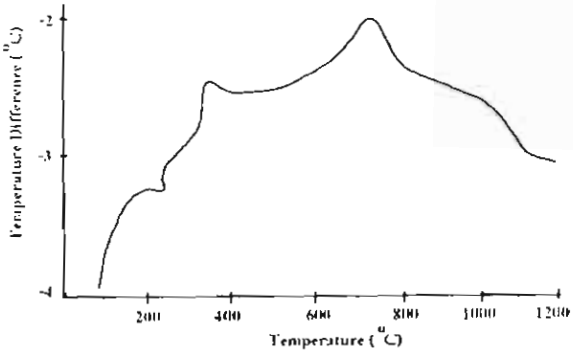

Figure 1. A DTA thermogram of the precipitated precursor of $BaTi_5O_{11}$.

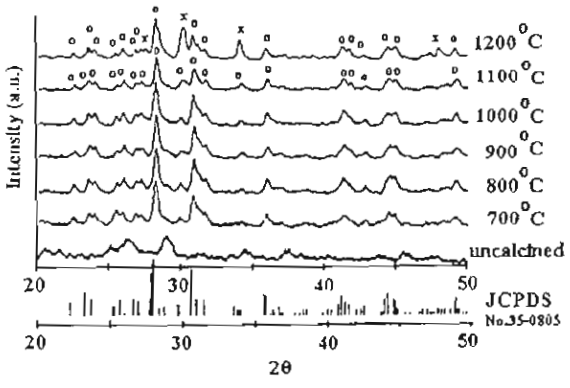

Figure 2. XRD powder patterns of the precipitated precursor of $BaTi_5O_{11}$ calcined at various temperatures for 4 h (o = $BaTi_5O_{11}$ and x = $BaTi_4O_9$).

chloride was prepared by dissolving $BaCl_2 \cdot H_2O$ in distilled water. The solution was then slowly added to a solution of titanium tetrachloride in 1N HCl (i.e. 36.5 gm HCl/l of water) at 4 °C to reach the stoichiometric $BaTi_5O_{11}$ composition. After vigorous stirring, this mixture was slowly added to aqueous oxalic acid (30% in excess over the stoichiometric amount required for precipitation) and heated up to 80 °C for about 1 h. After barium titanyl oxalate tetrahydrate ($BaTiO(C_2O_4)_2 \cdot 4H_2O$) precipitated [8], the precipitate was filtered and washed with distilled water three times, dried, and then heated to yield $BaTi_5O_{11}$. The heating was carried out for 4 h at each of the temperatures ranging from 700 to 1200 °C with a separation of 100 °C. The phase development of the dried powders was analysed by differential thermal analysis (DTA), which was performed up to the temperature of 1200 °C at a heating rate of 20 °C min^{-1}. The calcined powders were characterized by x-ray diffraction (XRD) (Cu Kα radiation), scanning electron microscopy (SEM), transmission electron microscopy (TEM), and transmission electron diffraction (TED). The reaction features in the calcination processes were studied using Fourier transform infrared spectroscopy (FTIR) at room temperature using the KBr plate method [12].

Table 1. Results of the phase analysis at various calcination temperatures.

Calcination temperature (°C)	Phases present		
	This work	Reference [7]	Reference [6]
700	$BaTi_5O_{11}$	$BaTi_5O_{11}$	$BaTi_5O_{11}$
800	$BaTi_5O_{11}$	—	—
850	—	$BaTi_5O_{11}$	$BaTi_5O_{11}$
900	$BaTi_5O_{11}$	—	—
1000	$BaTi_5O_{11}$	$BaTi_5O_{11}$	$BaTi_5O_{11}$
1100	$BaTi_5O_{11}$	$BaTi_5O_{11}$	$BaTi_5O_{11}$
1200	$BaTi_5O_{11}$ + $BaTi_4O_9$	—	$BaTi_5O_{11}$ + $BaTi_4O_9$

3. Results and discussion

Figure 1 shows the DTA thermogram obtained from the dried precipitates of barium titanyl oxalate tetrahydrate, up to 1200 °C. It can be seen that evaporation of water and crystal water occurred at below 250 °C, there is a loss of remnant organics indicated by the broad peak at about 370 °C, and decomposition of barium carbonate and titanium oxide and the reaction between fresh nuclei to form single-phase $BaTi_5O_{11}$ occur at about 700 °C. The formation of the final phase has been noted to be related to the ratio between the main components, such as Ba and Ti, in the precursor. With the same precursor, when the ratio of Ba and Ti was 1:1, the formation of $BaTiO_3$ could occur [8], whereas the present Ba–Ti ratio of 1:5 resulted in the formation of $BaTi_5O_{11}$. The formation of the $BaTi_5O_{11}$ single phase is confirmed by the XRD characterization. Figure 2 shows a series of x-ray diffractograms for the as-mixed powder and those calcined at various temperatures. The XRD patterns were analysed on the basis of the Joint Committee on Powder Diffraction Standard (JCPDS), card No 35-0805. Every peak in the patterns at the temperatures from 700 to 1100 °C can be attributed to $BaTi_5O_{11}$. This indicates that the powder is single-phase monoclinic $BaTi_5O_{11}$, which starts to form from about 700 °C. However, the $BaTi_5O_{11}$ phase decomposes into a mixture of $BaTi_5O_{11}$ and $BaTi_4O_9$ when heated up to 1200 °C as demonstrated by the increasing height of the $BaTi_5O_{11}$ peaks that overlap the $BaTi_4O_9$ peaks. The formation and decomposition of $BaTi_5O_{11}$ in relation to temperature obtained from our XRD results agree with those obtained by Ritter *et al* [2], Lu *et al* [7], Fukui *et al* [5], and Javadpour and Eror [6], as shown in table 1. Figure 3 shows the FTIR spectra of the $BaTi_5O_{11}$ powders calcined at various temperatures. The absorption peaks for the dried precipitates (110 °C) appear at 1686, 1420, 1354, 1306, 808, and 535 cm^{-1}, which correspond to the modes of vibration of the oxalate group [13], resembling those reported by Potdar *et al* [10] and Cernea *et al* [14] for $BaTiO_3$ and $BaTi_4O_9$ respectively. At 700–1100 °C, the same infrared (IR) peaks appear at 844 and 743 cm^{-1}, whereas the peaks at 1686, 1420, 1354, 1306, 808, and 535 cm^{-1} disappear. This indicates that a reaction between barium carbonate and titanium oxide took place and resulted in formation of the $BaTi_5O_{11}$ powder. Electron diffraction experiments were carried out on one sample, calcined at 800 °C. The diffraction rings confirmed a crystalline phase (figure 4), corresponding

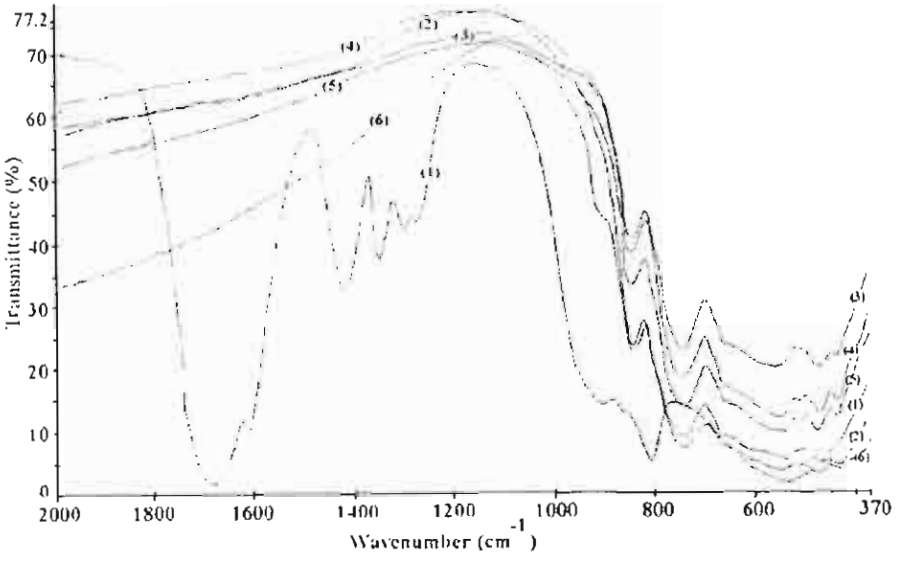

Figure 3. FTIR spectra of the precipitated precursor of $BaTi_5O_{11}$ calcined at different temperatures: 110 °C (spectrum 1), 700 °C (spectrum 2), 800 °C (spectrum 3), 900 °C (spectrum 4), 1000 °C (spectrum 5), 1100 °C (spectrum 6).

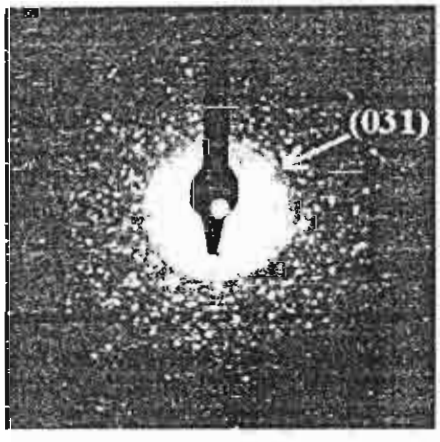

Figure 4. A TED pattern of the $BaTi_5O_{11}$ powder calcined at 800 °C.
(This figure is in colour only in the electronic version)

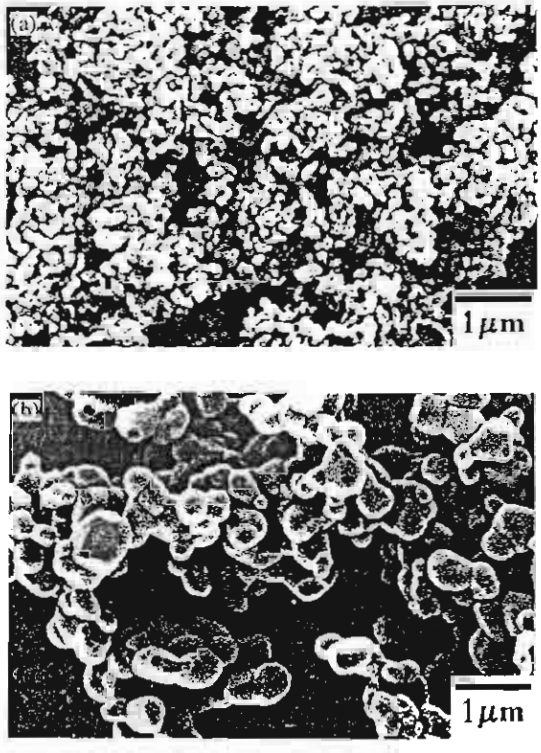

Figure 5. Scanning electron micrographs of $BaTi_5O_{11}$ powders calcined at: (a) 800 °C; and (b) 1100 °C.

to JCPDS card No 35-0805, of $BaTi_5O_{11}$ with planes (*hkl*) of (031), (040), (041), (221), ($\bar{2}$41), ($\bar{3}$41), and (361). Figure 5 shows some of the scanning electron micrographs of the calcined $BaTi_5O_{11}$ powders at 800 and 1100 °C, and figure 6 shows a TEM micrograph for the powder calcined at 800 °C. It can be seen that the $BaTi_5O_{11}$ powders consist of weakly aggregated fine particles almost round in shape; these are expected grow larger at higher temperatures. The particle sizes are estimated to be 100 nm at a calcination temperature of 700 °C, and 600 nm at 1100 °C.

4. Conclusions

$BaTi_5O_{11}$ powders were prepared using the homogeneous precipitation method in which the $BaTi_5O_{11}$ precursor was calcined at temperatures from 700 to 1100 °C for 4 h. DTA, FTIR, XRD, and TED analyses show that the powders formed exhibit a stable single phase of $BaTi_5O_{11}$ in this temperature range, whereas the phase dissociates into $BaTi_5O_{11}$ and $BaTi_4O_9$ when the calcination temperature is as high as 1200 °C. The microstructure analyses reveal that the $BaTi_5O_{11}$ powders consist of weakly aggregated fine particles almost

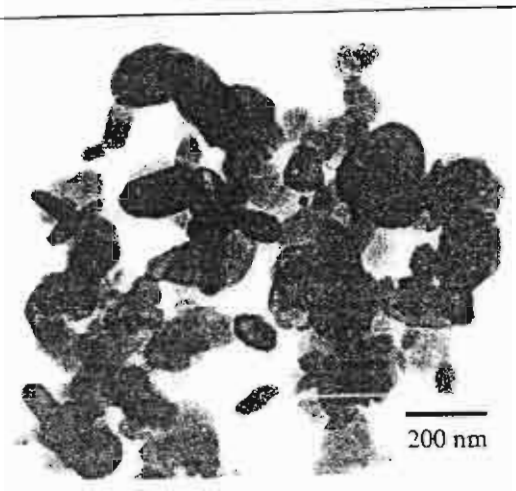

Figure 6. A TEM micrograph of the $BaTi_5O_{11}$ powder calcined at 800 °C.

round in shape. The particle sizes are estimated to be 100 nm at a calcination temperature of 700 °C, and 600 nm at 1100 °C.

Acknowledgments

The authors would like to express their sincere thanks to the Thailand Research Fund for financial support and to Dr S J Milne from Leeds University, UK, for his helpful comments.

References

[1] Plourde K and Ren C L 1981 Application of dielectric resonators in microwave components *IEEE. Trans. Microw. Theory Tech.* 29 754–70

[2] Ritter J J, Roth R S and Blendell J E 1986 Alkoxide precursor synthesis and characterization of phases in the barium–titanium oxide system *J. Am. Ceram. Soc.* 69 155–61

[3] O'Bryan H M, Plourde J K, Thomson J and Linn D F 1974 A new $BaO–TiO_2$ compound with temperature-stable high permittivity and low microwave loss *J. Am. Ceram. Soc.* 57 450–3

[4] O'Bryan H M and Thomson J 1975 Preparation of $BaTi_5O_{11}$ by solid state reaction *J. Am. Ceram. Soc.* 58 454

[5] Fukui T, Sakurai C and Okuyama M 1992 Effects of heating rate on sintering of alkoxide-derived $BaTi_5O_{11}$ powder *J. Mater. Res.* 7 192–6

[6] Javadpour J and Eror N G 1988 Raman spectroscopy of higher titanate phases in the $BaTiO_3$–TiO_2 system *J. Am. Ceram. Soc.* 71 206–13

[7] Lu H N, Burkhart L E and Schrader G L 1991 Sol–gel process for the preparation of $Ba_2Ti_9O_{20}$ and $BaTi_5O_{11}$ *J. Am. Ceram. Soc.* 74 968–72

[8] Tunkasiri T and Rujijanagul G 1994 Characterization of barium titanate prepared by precipitation technique *J. Mater. Sci. Lett.* 13 165–169

[9] Seungwon K, Moonhee L, Taeyong N and Chul I. 1996 Preparation of barium titanate by homogeneous precipitation *J. Mater. Sci.* 31 3643–5

[10] Potdar H S, Deshpade S B, Deshpande A S, Khollam Y B, Patil A J, Pradhan S D and Date S K 2001 Simplified chemical route for the synthesis of barium titanyl oxalate (BTO) *Int. J. Inorg. Mater.* 3 613–23

[11] Cuneyt Tas A 1999 Preparation of lead zirconate titanate $Pb(Zr_{0.52}Ti_{0.48})O_3$ by homogeneous precipitation and calcination *J. Am. Ceram. Soc.* 82 1582–4

[12] William K 1980 *Organic Spectroscopy* 2nd edn (London: Macmillan Educational) p 38

[13] Nakamoto K 1997 *Infrared and Raman Spectra of Inorganic and Coordination Compounds* 5th edn (New York: Wiley) p 75

[14] Cernea M, Chirtop E, Neacsu D, Pasuk I and Iordanescu S 2002 Preparation of $BaTi_4O_9$ from oxalates *J. Am. Ceram. Soc.* 85 499–503

Effects of $Ba(Mg_{1/3}Nb_{2/3})O_3$ on microstructure and dielectric properties of barium titanate ceramics

A. MUNPAKDEE, J. TONTRAGOON, K. SIRIWITAYAKORN, T. TUNKASIRI
Department of Physics, Faculty of Science, Chiang Mai University, Chiang Mai 50200, Thailand
E-mail: tawee@chiangmai.ac.th

The current trends in the electronic apparatus require small sized electronic components with high volumetric efficiency, high reliability and low cost. Ceramic capacitive components must have high permittivity for volumetric efficiency and low temperature coefficient of capacitance for reliable circuit performance. These capacitors are based primarily on ferroelectric compounds such as barium titanate ($BaTiO_3$; BT), lead magnesium niobate ($PbMgNbO_3$; PMN) and lead zirconate niobate ($PbZrNbO_3$; PZN) [1].

Due to environmental concerns, specific work has been devoted to lead free compounds over the last few years. Some promising compounds are modified $BaTiO_3$ ceramics. $BaTiO_3$ exhibits a high dielectric constant about 5000–18 000 below its Curie temperature (~130 °C) [2] but rather narrow dielectric constant peak which makes it not suitable for high performance capacitors in a wide temperature range. The idea of incorporating ions to this material in order to adjust or change its properties has been suggested and realized many years ago. Various modifications have been considered and prepared to cause homovalent or heterovalent substitution on the Ba or the Ti-site, especially on the Ti-site which yields more interesting result [3]. In order to obtain the required dielectric properties of modified BT ceramics, oxides or complex compounds such as zirconium oxide (ZrO_2) [4, 5], niobium oxide (Nb_2O_5) [6], strontium titanate ($SrTiO_3$) [6, 7], lead titanate ($PbTiO_3$) [7] and barium magnesium niobate ($Ba(Mg_{1/3}Nb_{2/3})O_3$, BMN) [8] were employed for substitutions. Weill *et al.* [9] obtained very high dielectric constant (ε_r) by adding BMN onto BT ceramics. However, the behavior of ε_r over wide range of temperature and evolution of the microstructure of the modified BT ceramics are not fully understood. Furthermore, the starting powders prepared by Weill *et al.* [9] were carried out via a chemical route which would rather be costly on the manufacturing scale. The purpose of this work is therefore to examine the effects of small additions of BMN on the microstructure and dielectric properties of $BaTiO_3$ ceramics by synthesizing all compounds via mixed oxide route.

The raw materials used in this work were all reagent grade chemicals such as barium carbonate ($BaCO_3$), magnesium oxide (MgO), niobium oxide (Nb_2O_5) and titanium oxide (TiO_2). They were weighed in appropriate proportionality on the basis of the formula $(1-x)$ $BaTiO_{3+x}$, $Ba(Mg_{1/3}Nb_{2/3})O_3$ (where $0 \leq x \leq 0.06$), the mixed chemical powders were then ball milled with zirconia balls in ethyl alcohol for 24 h and dried in an oven (at about 100 °C). The samples were calcined at 1200 °C for 2 h in air. The calcined powders were ball milled again in PVA 2 wt% solution for 2 h and dried. Disc shaped, green compact samples were produced by uniaxially cold pressing the powder at 60 MPa. The green compact samples were sintered at various temperatures for 2 h in air. They were heated by controlling the furnace temperature at the rate of 5 °C/min. The bulk densities of the sintered samples were determined by the Archimedes method. The sintered samples were analyzed by scanning electron microscopy (SEM) and X-ray diffractometry (XRD). Silver paste was applied on both faces of the sample discs for electrical measurements. Evolution of the dielectric constant against the temperature was measured at various ambient temperatures ranging from room temperature to 200 °C, using an LCZ meter (Hewlett Packard 4276A) operated at 1 kHz.

Fig. 1 shows the XRD patterns of the BMN doped BT and the pure BT powders. Various amounts of BMN were used for doping. All the peaks can be attributed to cubic phase BT. The analysis was carried out based on the Joint Committee on Powder Diffraction Standard (JCPDS) [10, 11]. No trace of BMN was observed.

The X-ray diffractograms of the BMN doped BT ceramics are also shown in Fig. 2 after sintering at 1400 °C. It was found that tetragonal BT structure [10] became cubic [11] at room temperature when more than 4 mol% of BMN was added to BT. This is quite agreeable with Weill *et al.* [9] who found that tetragonal-cubic transformation for BMN doped BT ceramics occurred when the doping ratio was higher than 5 mol% though employing chemical route in preparation.

Fig. 3 reveals the observation of chemically etched polished ceramic surfaces of undoped and doped BT. The grain size grew bigger as $X = 0.01$ to 0.03 mol (Fig. 3b) with reasonably homogeneous shape of about 50 μm. Discontinuous growth showed up when $X = 0.04$. (Fig. 3c). This is in accordance with the obtained XRD data (Fig. 2) which indicates that the tetragonal—cubic transformation occurs at $X = 0.04$. However, continuous growth of the grain size, of about less than 50 μm, appeared at higher doping ratio ($X = 0.06$). These results are agreeable with the report made by Weill *et al.* [8], who found that the grain size was less than 50 μm for $X < 0.06$ and decreased as X was increased.

0261–8028

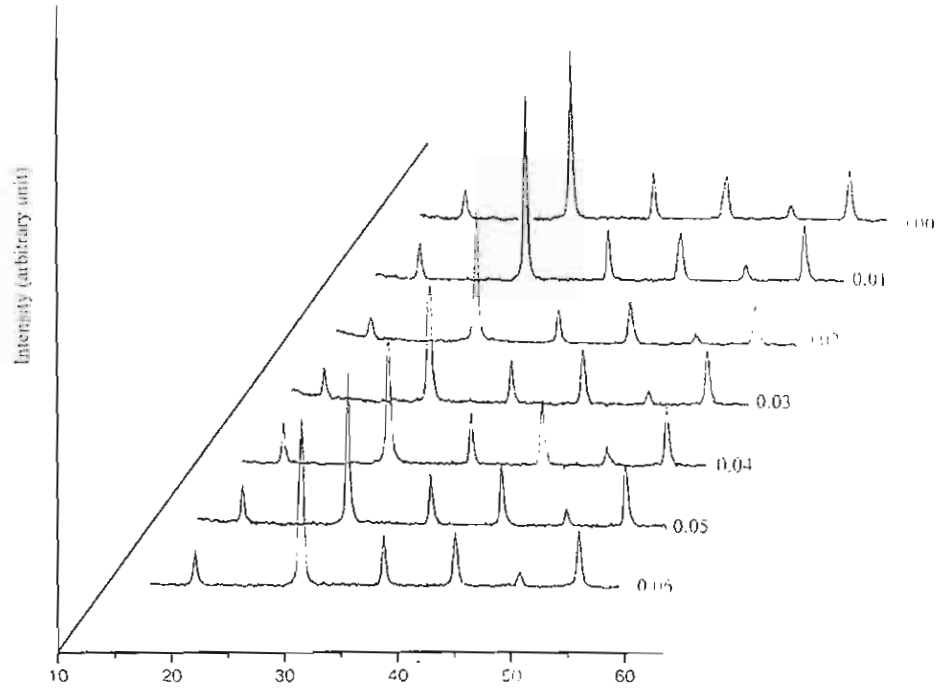

Figure 1 X-ray diffractograms of $(1-x)$BT + xBMN powders when x varies from 0.00 to 0.06.

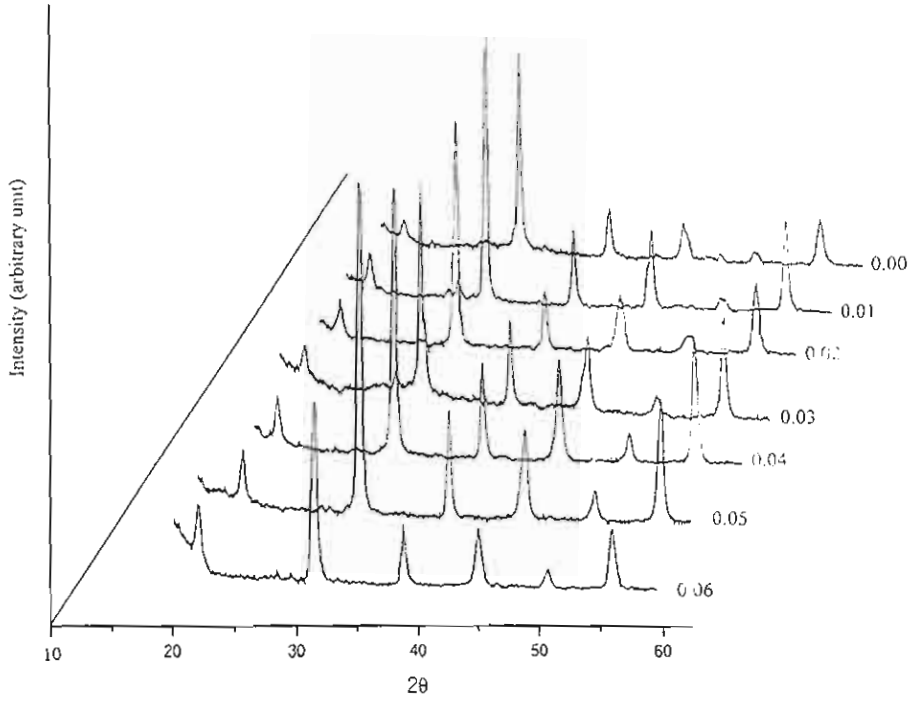

Figure 2 X-ray diffractograms of $(1-x)$BT + xBMN ceramics when x varies from 0.00 to 0.06 (sintered at 1400 °C).

Changes of dielectric constant of the sample sintered at 3 different sintering temperatures (T_s) and dissipation factor ($\tan\delta$) of the sample sintered at 1350 °C, against temperature were plotted in Fig. 4. The doping rate of 2% was selected due to its highest value of ε_r. It can be concluded that a very small variation of ε_r with temperature occurs in the range of 20 °C to 80 °C which is the normal operating temperature range of most capacitors. The sample sintered at 1300 °C was found to have the highest ε_r of 43 000. The dissipation factor ($\tan\delta$) slightly increased after 50 °C while the highest $\tan\delta$ was 0.04 which is generally acceptable.

Physical property data such as density and dielectric constant (ε_r) of the BMN doped BT ceramics at different sintering temperatures are tabulated in Table I. It can be concluded that the Curie temperature (T_C) tends to decrease from around 120 °C to 30 °C as x increases. Shrinkage of the ceramics was found to increase with increasing T_s. The sintering temperature has the tendency to increase as the dopant increases. At the doping rate of 4% where the abnormal grain growth occurred the density decreased and became reasonably constant at higher doping rate. The highest ε_r value was about 43 000 for the BT ceramic containing

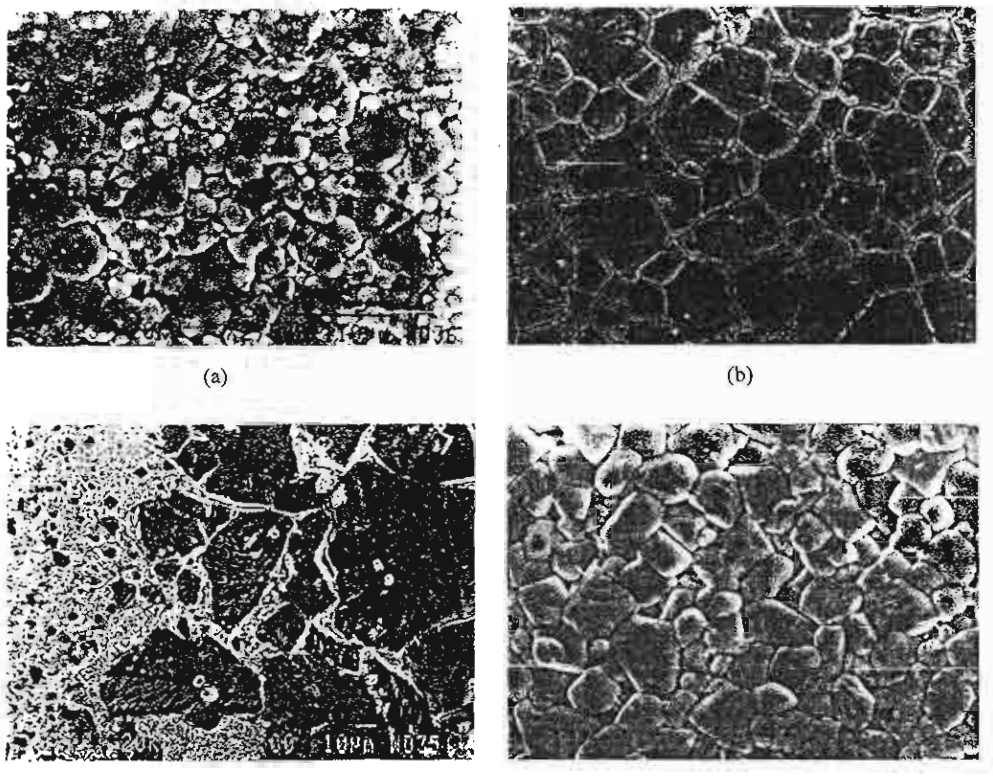

Figure 3 Evolution of grain size against the doping ratio of $(1 - x)BaTiO_3 + xBaMg_{1/3}Nb_{2/3}O_3$: (a) $X = 0$, (b) $X = 0.02$, (c) $X = 0.04$, and (d) $X = 0.06$ (All the samples were sintered at 1400 °C).

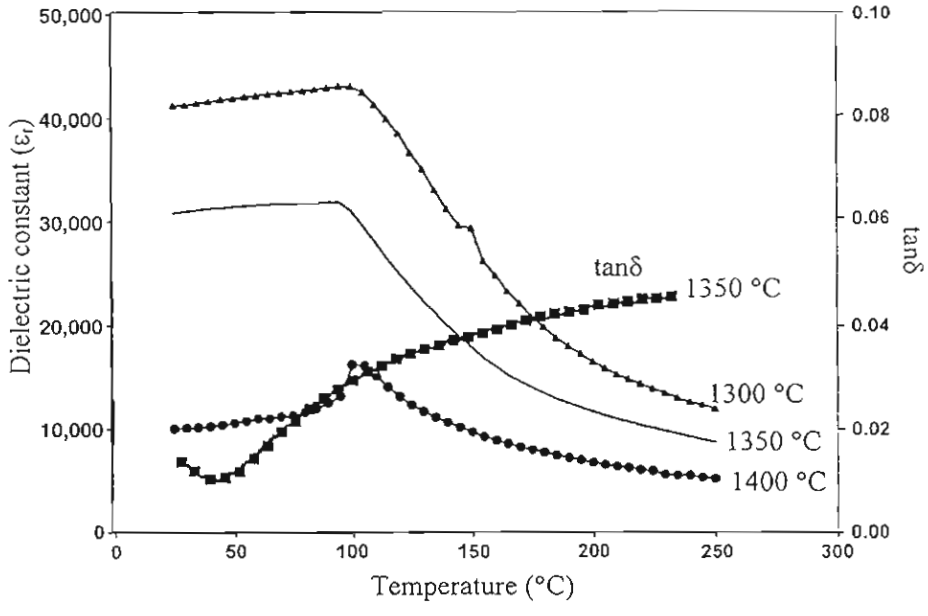

Figure 4 Changes of dielectric constant (at 1 kHz) and dissipation factor (tan δ) against temperature of 2 mol% BMN doped BT ceramics at various sintering temperatures.

2 mol% BMN sintered at 1300 °C, which is lower than that obtained by Weill *et al.* [9]. This may be due to different methods of preparation, i.e., we sintered via mixed oxide route while Weill *et al.* employed the chemical method. Consequently, the starting powders of our method are considerably bigger which may result in lower ε_r value. This reasoning in accordance with the result obtained by Enomoto and Yamaji [12] who found that the dielectric constant of $BaTiO_3$ ceramic depends markedly on its particle size prior to sintering.

In conclusion, the effects of BMN on microstructure and dielectric properties of BT ceramics were studied. Various amounts of BMN were used for doping corresponding to the general formula $(1 - x)BT + xBMN$ where x varies from 0.01 to 0.06. The sintering temperature was varied from 1300 °C to 1450 °C. Results showed that higher T_s was required for higher amount of

TABLE I Physical properties of BMN doped BT ceramics

Sintering temperature T_s (°C)	Shrinkage (%)	Density (g/cm^3)	x	Dielectric constant (ε_r)	T_C (°C)
1300	13.71	5.84	0.01	9600	126
1350	13.47	5.84		10000	119
1400	13.65	5.86		8500	120
1300	15.81	5.85	0.02	43000	98
1350	15.72	5.81		32000	95
1400	15.93	5.80		16000	103
1400	15.60	5.80	0.03	9500	74
1450	15.46	5.84		10000	73
1400	15.95	5.61	0.04	12000	54
1450	15.90	5.76		14300	54
1400	15.68	5.81	0.05	21000	~30
1450	15.62	5.82		15000	~30
1400	16.27	5.80	0.06	15000	~30
1450	16.90	5.76		9300	~30

T_C = Curie temperature.

dopant. The grain size became bigger and more homogeneous at higher T_s. The XRD data confirmed the ferroelectric phase of the ceramics at the low doping ratios ($x = 0.01$–0.03). The transformation from ferroelectric to paraelectric phase occurred when $x \geq 0.04$. The microstructure also showed discontinuous grain growth at $x = 0.04$ but homogeneous grain shape pronounced at $x > 0.04$. The dielectric constant of the doped samples was found to be considerably higher than that of the undoped ones.

Acknowledgment

The authors would like to express their sincere thanks to the Thailand Research Fund for the financial support.

References

1. T. S. SHROUT and A. HALLIYAL, *Ceram. Bull.* **66** (1987) 707.
2. D. W. RICHERSON, "Modern Ceramics Engineering" (Marcel Dekker Inc, N.Y., 1992) p. 263.
3. A. J. MOULSON and J. M. HERBERT, "Electroceramics: Materials, Properties and Applications" (Chapman and Hall, London, 1990) p. 245.
4. S. M. NEIRMAN, *J. Mater. Sci.* **23** (1988) 3973.
5. H. Y. LU, J. S. BOW and W. H. DENG, *J. Amer. Ceram. Soc.* **73** (1990) 3562.
6. I. BURN, *J. Mater. Sci.* **17** (1982) 1398.
7. Y. ITO, S. SHIMADA and M. INAGAKI, *J. Amer. Ceram. Soc.* **78** (1995) 2695.
8. F. WEILL, J. L. REHSPRINGER, P. POIX, C. KIPELEN and J. C. BERNIER, *J. Mater. Sci.* **27** (1992) 2316.
9. F. WEILL, J. L. REHSPRINGER, P. POIX and J. C. BERNIER, *J. Mater. Sci.* **27** (1992) 2321.
10. Powder Diffraction File, Card No 5-626, Joint Committee on Powder Diffraction Standards (International Centre for Diffraction Data, Swarthmore, P.A., 2000).
11. Powder Diffraction File, Card No 31-174, Joint Committee on Powder Diffraction Standards (International Centre for Diffraction Data, Swarthmore, P.A., 2000).
12. Y. ENOMOTO and A. YAMAJI, *Ceram. Bull.* **60** (1981) 566.

Received 7 May
and accepted 30 May 2003

เอกสารหมายเลข 1.6

Perovskite phase formation and ferroelectric properties of the lead nickel niobate–lead zinc niobate–lead zirconate titanate ternary system

Naratip Vittayakorn, Gobwute Rujijanagul, and Tawee Tunkasiri
Department of Physics, Faculty of Science, Chiang Mai University, Chiang Mai 50200 Thailand
Xiaoli Tan and David P. Cann
Materials Science and Engineering Department, Iowa State University, Ames, Iowa 50011

(Received 23 June 2003; accepted 24 September 2003)

The ternary system of lead nickel niobate $Pb(Ni_{1/3}Nb_{2/3})O_3$ (PNN), lead zinc niobate $Pb(Zn_{1/3}Nb_{2/3})O_3$ (PZN), and lead zirconate titanate $Pb(Zr_{1/2}Ti_{1/2})O_3$ (PZT) was investigated to determine the influence of different solid state processing conditions on dielectric and ferroelectric properties. The ceramic materials were characterized using x-ray diffraction, dielectric measurements, and hysteresis measurements. To stabilize the perovskite phase, the columbite route was utilized with a double crucible technique and excess PbO. The phase-pure perovskite phase of PNN–PZN–PZT ceramics was obtained over a wide compositional range. It was observed that for the ternary system $0.5PNN–(0.5 - x)PZN–xPZT$, the change in the transition temperature (T_m) is approximately linear with respect to the PZT content in the range $x = 0$ to 0.5. With an increase in x, T_m shifts up to high temperatures. Examination of the remanent polarization (P_r) revealed a significant increase with increasing x. In addition, the relative permittivity (ϵ_r) increased as a function of x. The highest permittivities ($\epsilon_r = 22{,}000$) and the highest remanent polarization ($P_r = 25\ \mu C/cm^2$) were recorded for the binary composition $0.5Pb(Ni_{1/3}Nb_{2/3})O_3–0.5Pb(Zr_{1/2}Ti_{1/2})O_3$.

I. INTRODUCTION

Lead-based complex perovskites, such as $Pb(Zn_{1/3}Nb_{2/3})O_3$ (PZN) and $Pb(Ni_{1/3}Nb_{2/3})O_3$ (PNN), having the general formula $Pb(B'B'')O_3$ have received significant attention since the 1970s because of their peculiar dielectric and piezoelectric behavior. These materials have been applied in many areas such as electrostrictive actuators, transducers, and multilayer ceramic capacitors.[1–6]

Lead zinc niobate, PZN, was first synthesized in the 1960s.[7] Its permittivity versus temperature curve displayed a broad peak around 140 °C (T_m) with a strong frequency dependence. Extremely high relative permittivities have been measured in the vicinity of the peak with a $\epsilon_r \sim 60{,}000$ reported for single crystals.[4,8–11] Nanometer-level chemical heterogeneity in the form of short range order of Zn^{2+} and Nb^{5+} at B-sites was proposed to account for the observed diffuse phase transition.[12,13] The crystal structure of PZN is rhombohedral ($R3m$) at room temperature and transforms to cubic ($Pm3m$) at high temperatures.

Unfortunately, phase-pure perovskite PZN polycrystalline ceramics have not been synthesized by conventional solid-reaction methods because of a steric and an electrostatic interaction between high polarization of the Pb^{2+} cation and the Zn^{2+} cation, which favors the formation of the pyrochlore phase instead of the perovskite phase.[14] Moreover, the low tolerance factor and small electronegativity difference[2] makes the perovskite phase unstable, requiring the addition of normal ferroelectric compounds such as $BaTiO_3$[15] and $PbTiO_3$[16] to stabilize the perovskite phase. Recently, Fan *et al.*[17,18] mixed $Pb(Zr_{0.47}Ti_{0.53})O_3$ with PZN by a conventional solid-state reaction method and successfully stabilized perovskite PZN. A morphotropic phase boundary (MPB) between the PZN-rich rhombohedral phase and the PZT-rich tetragonal phase was reported at PZN:PZT47/53 = 1:1. At this composition, a high electromechanical coupling factor of $k_p = 0.67$ was measured.

Lead nickel niobate (PNN) exhibits a diffuse phase transition around −120 °C with a much lower peak permittivity of about 4000.[19] The crystal structure of PNN at room temperature is cubic ($Pm3m$) with a lattice parameter of 4.03 Å.[19] Phase-pure perovskite PNN can be prepared via the columbite method.[2,20] Luff *et al.*[21] investigated solid solutions in the $PNN–PbTiO_3–PbZrO_3$ system and identified the composition of 0.5PNN–0.35PT–0.15PZ with optimal piezoelectric properties. Detailed reaction kinetics during solid state processing of

PNN–PZT was recently investigated by Babushkin and several pyrochlore phases have been detected.[22] The piezoelectric PNN–PZT ceramics have found wide applications and are now commercially available.

The investigation of the ferroelectric properties of the PNN–PZN–PZT ternary system is of interest for a number of reasons. Both PNN and PZN have distinct transition temperatures, and the transition temperature for the solid solution of PNN–PZN should lie in the ambient temperature range. This implies that the ultrahigh permittivity values can be realized at room temperature. As demonstrated in the binary PZN–PZT and PNN–PZT systems, the addition of PZT imparts superior piezoelectric properties to the solid solutions. Therefore, there is great potential for excellent dielectric and piezoelectric properties within the ternary system PNN–PZN–PZT.

Information in the literature on the PNN–PZN–PZT ternary system is extremely limited. Lee *et al.*[23] tried to fabricate phase-pure perovskite PNN–PZN–PZT ceramics with a Zr/Ti ratio in PZT of 1.0. In their study, powders of PZT, PZN, and PNN were prepared separately and then mixed and calcined again to form perovskite PNN–PZN–PZT. The highest amount of perovskite phase in their work was found to be 92%. The Curie temperature was found to vary from 50 to 250 °C, depending on the mol fraction of PZT. The best piezoelectric properties at room temperature, k_p= 0.63, were found in the composition 0.5PNN–0.3PZN–0.2PZT.

The presence of pyrochlore phase is extremely detrimental to the dielectric and piezoelectric properties in most perovskite ceramics. The process of prereacting the B-site cations to form a columbite phase $B'B''_2O_6$ prior to the addition of PbO has been successfully applied to many systems to suppress pyrochlore phase formation.[2,20,24,25] However, this technique has been largely unsuccessful for PZN and fabrication of phase-pure PZN-containing solid solutions remains a challenging issue. In this work, a processing route different from that used previously by Lee *et al.* [23] was used to successfully prepare phase-pure perovskite PNN–PZN–PZT ceramics. The use of the double crucible technique, using excess PbO, and maintaining a fast heating rate were all found to be essential factors in perovskite phase development. Dielectric and ferroelectric properties of single-phase perovskite ceramics are reported in the present article and piezoelectric characterization is underway and will be published in a separate paper.

II. EXPERIMENTAL

In this method, the columbite precursors $ZnNb_2O_6$ and $NiNb_2O_6$ were prepared from the reaction between ZnO (99.9%) and Nb_2O_5 (99.9%) at 975 °C for 4 h and between NiO (99.9%) and Nb_2O_5 (99.9%) for 4 h at 1100 °C, respectively.[24,25] The wolframite phase $ZrTiO_4$ was formed by reacting ZrO_2 (99.9%) with TiO_2(99.9%) at 1400 °C for 4 h.[26] The powders of $ZnNb_2O_6$, $NiNb_2O_6$, and $ZrTiO_4$ were mixed in the required stoichiometric amounts with PbO (99.9%) with an excess of 2 mol% of PbO added. The compositions synthesized in this study were x = 0, 0.1, 0.3, and 0.5 in the ternary system 0.5PNN–(0.5 – x)PZN–xPZT. The milling process was carried out for 24 h in isopropyl alcohol. After drying at 120 °C, the powders were calcined at 900–950 °C for 4 h in a double crucible configuration with a heating rate of 20 °C/min. After grinding and sieving, 5 wt.% of polyvinyl alcohol binder was added. Disks with a diameter of 1.5 cm were prepared by cold uniaxial pressing at a pressure of 150 MPa. Binder burnout occurred by slow heating to 500 °C and holding for 2 h. To investigate the sintering behavior, the disks were sintered in a sealed alumina crucible at temperatures ranging from 950 to 1250 °C using a heating rate of 5 °C/min and a dwell time of 2 h. To prevent PbO volatilization from the disks, a PbO atmosphere was maintained by placing $PbZrO_3$ powders in the crucible. Phase formation and crystal structure of the calcined powders and sintered discs were examined by x-ray diffraction (XRD). Data collection was performed in the 2θ range of 20–60° using step scanning with a step size of 0.02° and counting time of 2 s/step. The relative amounts of perovskite and pyrochlore phase were determined by measuring the primary x-ray peak intensities of the perovskite and pyrochlore phase. The percentage of perovskite phase was estimated by the following equation:

$$\% \text{ perovskite phase} = \left(\frac{I_{perov}}{I_{perov} + I_{pyro} + I_{PbO}} \right) \times 100 \quad , \tag{1}$$

where I_{perov}, I_{pyro}, and I_{PbO} refer to the intensity of the (110) perovskite peak, and the intensity of the (220) pyrochlore and PbO peaks, respectively. The pellets were polished and electroded via gold sputtering, over which a layer of air-dried silver paint was applied. The relative permittivity (ϵ_r) and dissipation factor (tan δ) of the pellets sample were measured at various temperatures ranging from −100 to 180 °C with a heating and cooling rate of 3 °C/min over the frequency range between 100 Hz and 100 kHz using an LCR meter (HP 4284A, Tokyo, Japan) in conjunction with a Delta Design 9023 (San Diego, CA) temperature chamber. The remanent polarization P_r was determined from a P-E hysteresis loop measurements using a Sawyer–Tower circuit at temperatures between −66 and 60 °C.

III. RESULTS AND DISCUSSION

A. Perovskite phase development

The perovskite and pyrochlore phase formation at different calcination temperatures in 0.5PNN–(0.5 – x) PZN–xPZT powders with x = 0.1 to 0.5 were studied

and analyzed by XRD. XRD patterns from this system are given in Fig. 1. The cubic pyrochlore-type structure of $Pb_{1.83}(Nb_{1.71}Zn_{0.29})O_{6.39}$[27] was identified in the x = 0.0, 0.1, and 0.3 compositions at the 900 °C calcination temperature. The pyrochlore formation reaction from PbO and the columbite precursors is an extremely fast process, which is completed within 2–3 min at temperatures as low as 750 °C.[28] With increased calcination temperatures the amount of perovskite phase increased sharply. In our work, it was observed that the primary phase in all of the compositions at 950 °C was well-crystallized perovskite. Within the detection limits of the XRD technique, the samples were essentially 100% perovskite and free of pyrochlore. The heat treatment and percent perovskite phase for all the compositions are listed in Table I. The first two rows listed are for the calcined powders, and the remaining data are derived from sintered samples using powders calcined at 950 °C.

In this study, the combination of using a double crucible, excess PbO (2 mol%), and a fast heating/cooling rate (20 °C/min) were shown to be effective in reducing the total amount of pyrochlore phase during calcination at 950 °C. The 2 mol% excess PbO was chosen because there were observations reported that compositions with excess PbO additions greater than 2.8 mol% resulted in degraded electrical properties. This was attributed to the presence of an excess PbO layer at the grain boundary.[29,30]

XRD patterns from a set of samples prepared at various sintering temperatures are given in Fig. 2. In this study, for the x = 0 composition single-phase perovskite was obtained for sintering temperatures below 1150 °C. Above 1150 °C, the cubic pyrochlore phase $Pb_{1.83}(Nb_{1.71}Zn_{0.29})O_{6.39}$[27] formed and the percentage of pyrochlore phase increased as the sintering temperature increased, as shown in Table I. This behavior also appeared in the x = 0.1 composition at sintering temperatures above 1200 °C. The behavior is believed to be due to the volatilization of PbO at high temperatures. Nevertheless, the XRD patterns for the x = 0.3 and 0.5 compositions do not show the formation of the

TABLE I. Perovskite phase development during calcinations and sintering process of 0.5PNN–(0.5 – x)PZN–xPZT system. (The first two rows indicate the data in calcined powders and the rest of the rows are data from sintering of powders calcined at 950 °C.)

Temperature (°C)	Perovskite phase (%)			
	x = 0.0	x = 0.1	x = 0.3	x = 0.5
900[a]	91.53	92.67	92.5	100
950[a]	100	100	100	100
1000	100	100	...	...
1050	100	100	100	...
1100	100	100	100	...
1150	100	100	100	100
1200	84.468	100	100	100
1225	76.249	76.79	100	100
1250	...	...	100	100
1275	...	...	100	100

[a]Calcination temperatures.

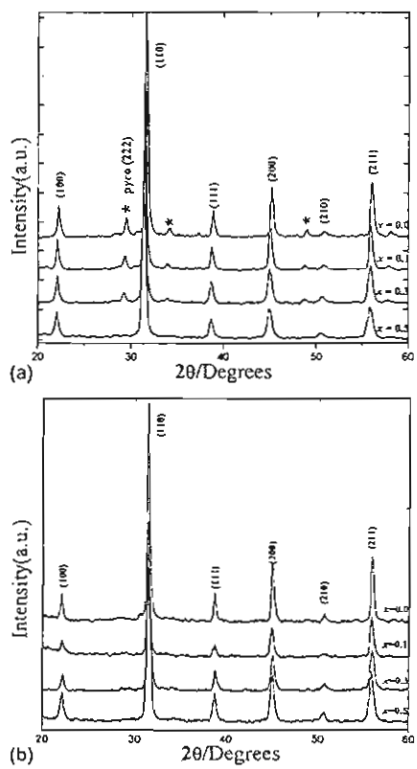

FIG. 1. Powder XRD patterns of a stoichiometric composition of 0.5PNN–(0.5 – x)PZN–xPZT ceramics: (a) calcined at 900 °C for 4 h with 20 °C/min heating rate, (b) calcined at 950 °C for 2 h with 20 °C/min heating rate; pyrochlore phase indicated with (*).

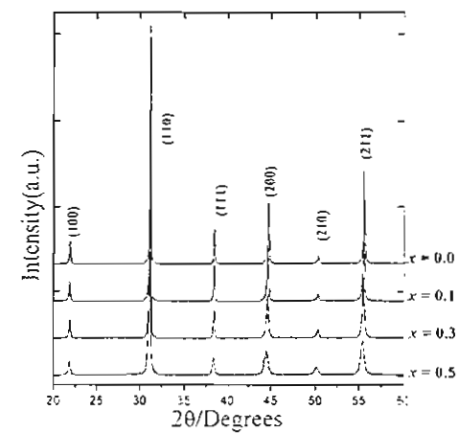

FIG. 2. XRD patterns of 0.5PNN–(0.5 – x)PZN–xPZT ceramics at the optimum sintering conditions.

pyrochlore phase. It is interesting to note that the intensity of (100) perovskite peak decreased at high temperatures for the $0.1 \leq x \leq 0.5$ composition.

In the PNN–PZN–PZT system, the A-site is occupied by Pb^{2+} (1.630 Å) ions, and the Ni^{2+}, Nb^{5+}, Zn^{2+}, Zr^{4+}, and Ti^{4+} ions occupy the B site of the ABO_3 perovskite crystal structure. The average ionic radius of B-site ions in the composition $0.5Pb(Ni_{1/3}Nb_{2/3})O_3$–$(0.5 - x)Pb(Zn_{1/3}Nb_{2/3})O_3$–$xPb(Zr_{1/2}Ti_{1/2})O_3$ can be calculated from the following equation:

$$r_{B\text{-site}} = 0.5\left[\tfrac{1}{3}r_{Ni^{2+}} + \tfrac{2}{3}r_{Nb^{5+}}\right] + (0.5 - x)\left[\tfrac{1}{3}r_{Zn^{2+}} + \tfrac{2}{3}r_{Nb^{5+}}\right] + x\left[\tfrac{1}{2}r_{Zr^{4+}} + \tfrac{1}{2}r_{Ti^{4+}}\right] \quad (2)$$

where the ionic radii of Ni^{2+}, Nb^{5+}, Zn^{2+}, Zr^{4+}, and Ti^{4+} are 0.830, 0.780, 0.880, 0.860 and 0.745 Å, respectively.[31] A simple description of the geometric packing within perovskite structure can be characterized by tolerance factor t, which is defined by the following equation:[5,8,13,32]

$$t = \frac{(r_A + r_O)}{\sqrt{2}(r_B + r_O)}, \quad (3)$$

where r_A, r_B, and r_O are the ionic radii of the A, B and O ions, respectively. The calculated average B-site ionic radii and tolerance factor of the PNN–PZN–PZT system is presented in Table II using 1.260 Å for the radius of O^{2-}.[31] The effective size of the B-site ion decreases with an increasing mol faction of PZT primarily due to the smaller ionic radii of Ti^{4+}. This results in a slight increase in the tolerance factor as it approaches 1.0. However, the lattice parameter is found to increase as the mol faction of PZT increases, and the symmetry changes from pseudocubic to rhombohedral.

The crystal symmetry of PNN at room temperature was determined to be pseudo-cubic perovskite with a cell parameter $a = 4.0308$ Å. The PZN composition at room temperature was determined to be the rhombohedral space group $R3m$. According to the $PbZrO_3$–$PbTiO_3$ phase diagram, at room temperature $Pb(Zr_{1/2}Ti_{1/2})O_3$ is within the tetragonal phase field near the MPB region.[33] In this work, the crystal structure and lattice parameters of the PNN–PZN–PZT compositions were determined through room temperature diffraction experiments. The indexing procedure of the perovskite phase in the $x = 0.0$ and $x = 0.1$ samples was performed based on cubic symmetry. For the $x = 0.3$ and 0.5 samples, however, no splitting of 002 and 200 peak was observed with increased PZT concentration, as shown in Fig. 2. However, the superposition was clearly observed for the (220) peak as shown in Fig. 3. This result indicates that the crystal structure was rhombohedral. In addition, from the data listed in Table II, it is evident that the lattice parameter a increased with increasing concentration of PZT due to the increase in B-site radius.

B. Dielectric properties

The permittivity at 1 kHz as a function of temperature for 0.5PNN–(0.5 – x)PZN–xPZT ceramics under different sintering conditions is shown in Fig. 4. The sintering temperature was found to have a significant effect on the

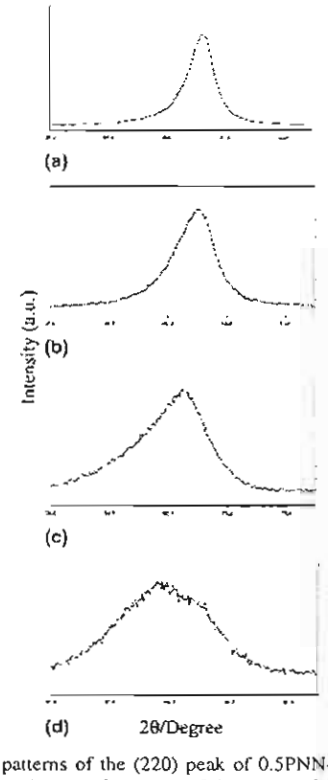

FIG. 3. XRD patterns of the (220) peak of 0.5PNN–(0.5 – x)PZN–xPZT ceramics: (a) $x = 0$, (b) $x = 0.1$, (c) $x = 0.3$, (d) $x = 0.5$.

TABLE II. Comparison of the calculated average B-site ionic radii, the crystal structure, and lattice parameters derived from XRD data.

Composition 0.5PNN–(0.5 – x)PZN–xPZT	Average B-site ionic radii (Å)	Tolerance factor, t	Lattice parameter, a (Å)	Crystal structure	Distortion angle, α
$x = 0.0$	0.8050	0.9896	4.049	Cubic	90.0
$x = 0.1$	0.8039	0.9901	4.054	Cubic	90.0
$x = 0.3$	0.8018	0.9912	4.057	Rhombohedral	89.88
$x = 0.5$	0.7996	0.9922	4.060	Rhombohedral	89.89

permittivity. All compositions exhibited an increase in the permittivity with increased sintering temperatures. However, at the highest sintering temperature the permittivity decreased due to the formation of a pyrochlore phase. The $x = 0$ composition showed an increase in permittivity up to a maximum of 10,000 at a sintering temperature of 1150 °C. At higher sintering temperatures there is both a decrease in permittivity and a shift in the temperature at which the permittivity is maximum (T_m) from −20 to −50 °C. This shift in T_m is likely to be the result of a change in the stoichiometry of the perovskite phase due to the effects of Zn volatilization and the formation of the pyrochlore phase $Pb_{1.83}(Nb_{1.71}Zn_{0.29})O_{6.39}$. This shifted the overall perovskite composition closer to PNN, with a lower T_m of −120 °C. In addition, the decrease in permittivity that was observed was the result of the low permittivity of $Pb_{1.83}(Nb_{1.71}Zn_{0.29})O_{6.39}$ ($\epsilon_r \sim 100$).

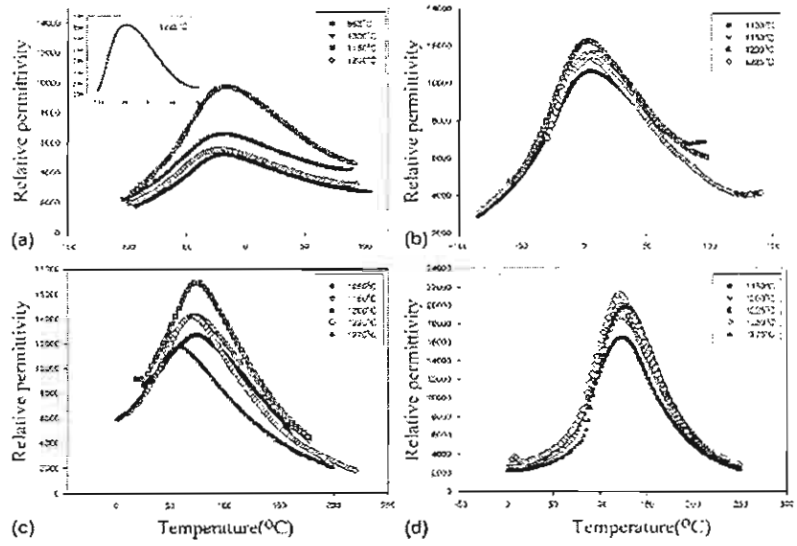

FIG. 4. Relative permittivity and dissipation factor at 1kHz for 0.5PNN–(0.5 − x)PZN –xPZT: (a) $x = 0$, (b) $x = 0.1$, (c) $x = 0.3$, (d) $x = 0.5$. Dielectric data for different sintering temperatures is shown.

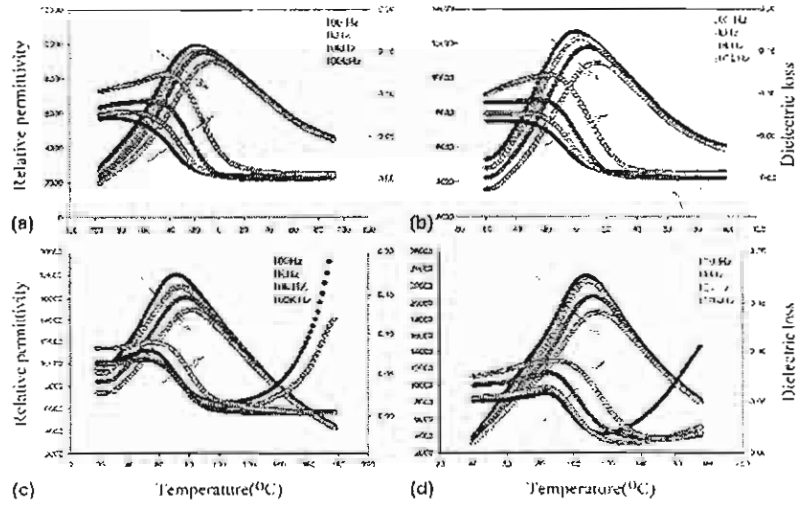

FIG. 5. Relative permittivity and dissipation factor of 0.5PNN–(0.5 − x)PZN–xPZT ceramics prepared at the optimum sintering conditions. (a) $x = 0$, ceramics sintered at 1150 °C for 2 h; (b) $x = 0.1$, ceramics sintered at 1200 °C for 2 h; (c) $x = 0.3$, ceramics sintered at 1200 °C for 2 h; (d) $x = 0.5$, ceramics sintered at 1250 °C for 2 h.

The $x = 0.1$ composition exhibited a maximum permittivity of approximately 12,000 with a $T_m \sim 0$ °C at a sintering temperature of 1200 °C. Higher sintering temperatures resulted in a decrease in the permittivity. Likewise the $x = 0.3$ composition exhibited a maximum permittivity of 17,000 at $T_m = 70$ °C at a sintering temperature of 1200 °C. Consistent with the other compositions, increased sintering temperatures resulted in a decrease in permittivity and a shift in T_m. Finally, the highest permittivities in this study were recorded for the $x = 0.5$ composition at a sintering temperature of 1250 °C with $\epsilon_{r,max} = 22{,}000$ at $T_m \sim 120$ °C. This is significantly larger than the previous value reported in the literature.[23]

In this work, the dielectric experiments showed that the optimum sintering conditions for 0.5PNN–(0.5 – x) PZN–xPZT were for 2 h at 1150, 1200, 1200, and 1250 °C, for the $x = 0$, $x = 0.1$, $x = 0.3$, and $x = 0.5$ compositions, respectively. Ceramics sintered under these conditions were used in the determination of the crystal structure and lattice parameters, which had been shown in Figs. 2 and 3, and Table II. The following characterization of the dielectric and ferroelectric properties of each composition was also carried out in sample sintered at their optimum conditions.

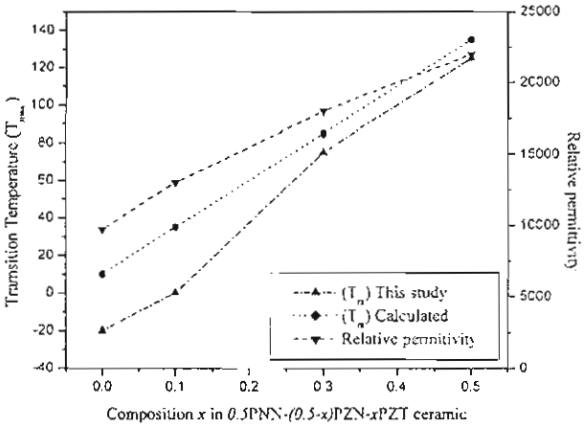

FIG. 6. T_m, calculated T_m, and maximum relative permittivity as a function of composition x at 1 kHz.

Figure 5 shows the dielectric properties for each composition at the optimum sintering conditions. All of compositions showed a broadening of the permittivity maxima and the T_m increased with increasing measurement frequency, as expected. Experimental results indicate that all of compositions show a diffuse phase transition with the strong frequency dispersion, which is characteristic of relaxor ferroelectrics.[1,3,12,34] From this result, it is clear from the sharpness of the permittivity peak that the compositions gradually approached normal ferroelectric behavior as the mol fraction of PZT increased. As x approached 0, the behavior was strongly relaxor in nature. This may be a function of the degree of B-site cation ordering or the influence of the macro-domains.

In general, the sintering temperature of this system increased with increased mol percent of PZT. Both the maximum permittivity, $\epsilon_{r,max}$ and T_m increased quasi-linearly as the molar fraction of PZT increased. The T_m of the constituent compounds PNN, PZN, and PZT are −120, 140, and 390 °C, respectively,[10,19,33] which can be used to calculate an empirical estimate of T_m via the equation:

$$T_m = 0.5 \times (-120\ °C) + (0.5 - x) \times (140\ °C) + x \times (390\ °C) \quad . \tag{4}$$

The variation of the measured T_m, the calculated T_m, and the measured $\epsilon_{r,max}$ with composition x is shown in Fig. 6. It is evident that Eq. (4) gives a reasonable indication of the transition temperature T_m. A summary of the dielectric properties for each of the compositions is shown in Table III. As Table III illustrates, the PNN–PZN–PZT ceramics in this study resulted in significantly higher permittivities than in previous studies. Through controlling PbO loss and preventing pyrochlore phase formation, single-phase perovskite ceramics can be processed with excellent electrical properties.

TABLE III. Comparisons of dielectric properties of ceramics in the 0.5PNN–(0.5 – x) PZN–xPZT system at the optimum sintering conditions.

	Composition 0.5PNN–(0.5 – x)PZN–xPZT	Percent perovskite	T_m (°C)	Relative permittivity (at 25 °C) at 1 kHz	Relative permittivity (at T_m) at 1 kHz	Dielectric loss (at 25 °C) at 1 kHz
Lee *et al.*[23]	$x = 0.0$	85	55	4000	6000	···
	$x = 0.1$	87	80	4700	8000	···
	$x = 0.3$	92	140	5500	13000	···
	$x = 0.5$	78	225	2500	7000	···
Vierheilig *et al.*[37]	$x = 0.0$	100	−10	6077	6980	0.010
This work	$x = 0.0$	100	−20	8500	9700	0.011
	$x = 0.1$	100	0	11500	13000	0.032
	$x = 0.3$	100	70	9000	18000	0.050
	$x = 0.5$	100	125	4000	22000	0.048

C. Ferroelectric properties

Polarization hysteresis measurements at room temperature were performed using a modified Sawyer–Tower circuit. The hysteresis loops as a function of x are shown in Fig 7. The $x = 0$ and $x = 0.1$ compositions exhibited slim loops characteristic of relaxor ferroelectrics. The saturation polarization P_s, remanent polarization P_r, and coercive field E_c were increased with increased mol percent of PZT as illustrated in Table IV. The loop area values were calculated by integrating the polarization with respect to the electric field. The maximum remanent polarization was observed for the $x = 0.5$ composition. The values of P_s, P_r, and E_c for the $x = 0.5$ composition are 31.9 $\mu C/cm^2$, 25.2 $\mu C/cm^2$, and 4.0 kV/cm, respectively.

These hysteresis data are consistent with the dielectric results in illustrating the gradual trend from relaxor to normal ferroelectric as the mol fraction of PZT is increased.[1,35,36] The hysteresis loops for the compositions $x = 0$ and $x = 0.3$ at various temperatures are shown in Fig. 8. The coercive field values for each composition were found to exhibit an increase with decreased temperature. This is due to the influence of the metastable macro-domain structure and the immobilizations of the domain walls.[1,35,36]

The $x = 0.3$ and 0.5 compositions exhibited square loop behavior at −66 °C. However, as the temperature increased the square loops transformed to slim loops and the remanent polarization and coercive filed values decreased significantly. The $x = 0$ and $x = 0.1$ compositions exhibited slim loop behavior near room temperature. All of compositions displayed a clear transition from square-loop behavior to slim-loop behavior in

TABLE IV. Polarization hysteresis data as a function of x in the 0.5PNN–(0.5 – x)PZN–xPZT system.

Composition	P_s ($\mu C/cm^2$)	P_r ($\mu C/cm^2$)	E_c (kV/cm)	Loop area (mC/cm^2)
$x = 0.0$	22.5	0.9	0.008	49.88
$x = 0.1$	23.8	1.8	0.010	72.81
$x = 0.3$	28.1	8.5	1.221	255.12
$x = 0.5$	31.9	25.2	4.024	628.47

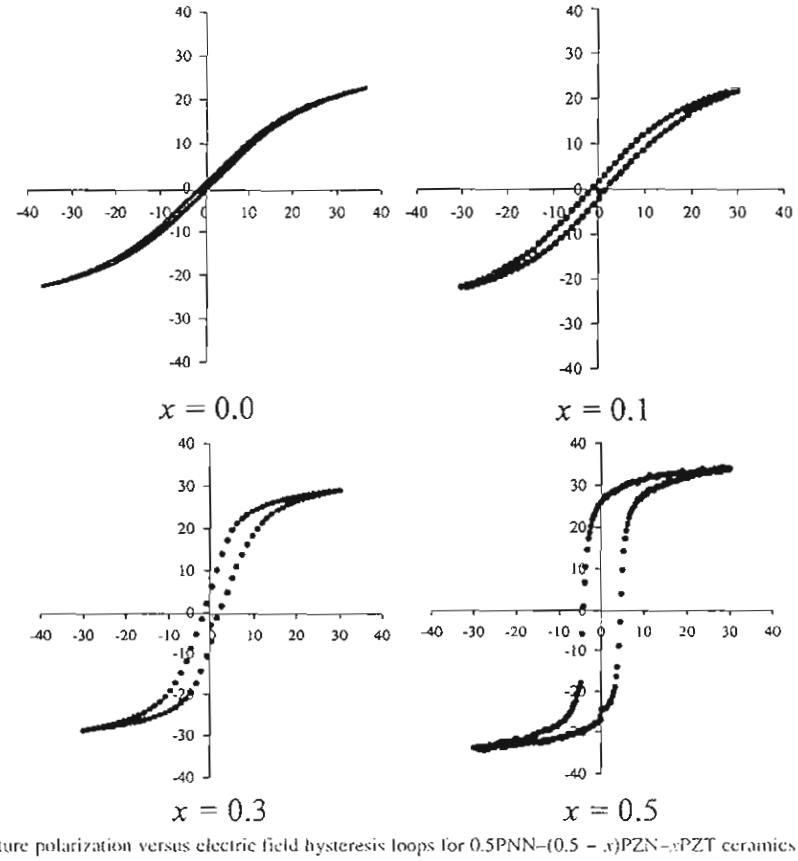

FIG. 7. Room-temperature polarization versus electric field hysteresis loops for 0.5PNN–(0.5 – x)PZN–xPZT ceramics at the optimum sintering conditions.

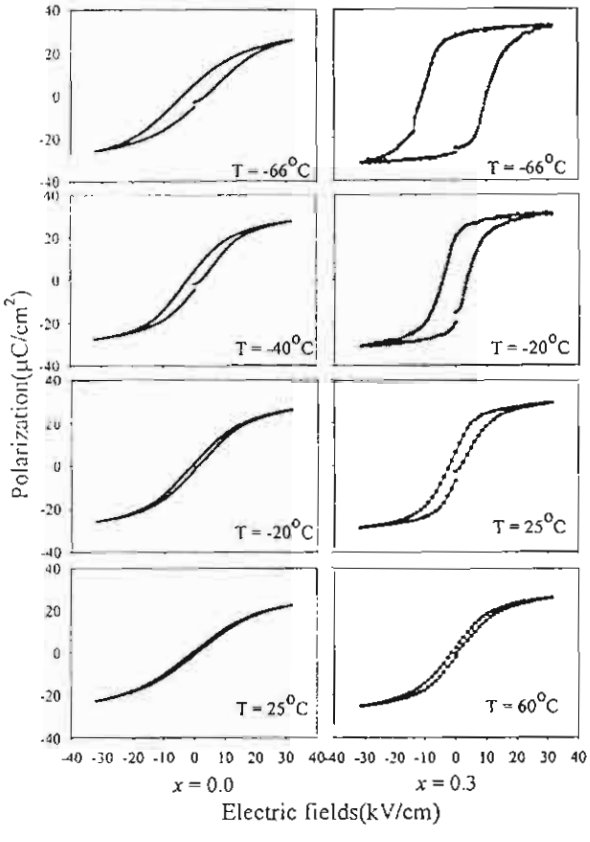

FIG. 8. Temperature dependence of the *P–E* hysteresis of 0.5PNN–(0.5 – *x*)PZN–*x*PZT ceramics at optimum sintering conditions, compositions $x = 0$ and $x = 0.3$ are shown

the vicinity of T_m. In addition, the hysteresis loops showed that the remanent polarization is nonzero at T_m but decays to zero at temperatures above T_m.

IV. CONCLUSIONS

In this work, it was shown that by controlling PbO loss and preventing pyrochlore formation high permittivity ceramics in the PNN–PZN–PZT system can be processed through high-temperature calcination. This can be accomplished by utilizing a double crucible during calcination, adding excess PbO (2mol%), and maintaining a fast heating/cooling rate (20 °C/min). The dielectric properties and the T_m of 0.5PNN–(0.5 – *x*)PZN–*x*PZT was found to increase with increasing PZT concentration. Furthermore, the transition from the normal ferroelectric to the relaxor ferroelectric state was clearly observed as the mol fraction of PZT decreased. The optimum dielectric properties were observed for the $x = 0.5$ composition with a permittivity of 22,000 and P_s, P_r and E_c values of 31.9 μC/cm², 25.2μC/cm², and 4.0 kV/cm, respectively.

ACKNOWLEDGMENTS

The authors are grateful to the Thailand Research Fund, Graduate School Chiang Mai University and Ministry of University Affairs for financial support.

REFERENCES

1. L.E. Cross, Ferroelectrics **76**, 241 (1987).
2. T.R. Shrout and A. Halliyal, Am. Ceram. Soc. Bull. **66**, 704 (1987).
3. K. Uchino, Ferroelectrics **151**, 321 (1994).
4. K. Uchino, Solid State Ionics **108**, 43 (1998).
5. K. Uchino, *Ferroelectric Devices* (Marcel Dekker, New York, 2000).
6. K. Uchino, *Piezoelectric Actuators and Ultrasonic Motors* (Kluwer Academic Publishers, Boston, MA, 1996).
7. V.A. Bokov and I.E. Mylnikova, Sov. Phys-Solid State **2**, 2428 (1960).
8. J. Kuwata, K. Uchino, and S. Nomura, Ferroelectrics **37**, 579 (1981).
9. K. Uchino, Ceram. Int. **21**, 309 (1995).
10. S.E. Park and T.R. Shrout, IEEE Tr. UFFC. **44**, 1140 (1997).
11. M.L. Mulvihill, L.E. Cross, W. Cao, and K. Uchino, J. Am. Ceram. Soc. **80**, 1462 (1997).
12. C.A. Randall and A.S. Bhalla, Jpn. J. Appl. Phys. **29**, 327 (1990).
13. A.S. Bhalla, R. Guo, and R. Roy, Mat. Res. Innovat. **4**, 3 (2000).
14. N. Mizutani, N. Wakiya, K. Shinozaki, and N. Ishizawa, Mater. Res. Bull. **30**, 1121 (1995).
15. A. Halliyal, U. Kumar, R.E. Newham, and L.E. Cross, Am. Ceram. Soc. Bull. **66**, 671 (1987).
16. J.R. Belsick, A. Halliyal, U. Kumar, and R.E. Newnham, Am. Ceram. Soc. Bull. **66**, 664 (1987).
17. H.Q. Fan and H.E. Kim, J. Appl. Phys. **91**, 317 (2002).
18. H.Q. Fan and H.E. Kim, J. Mater. Res. **17**, 180 (2002).
19. V.A. Bokov and I.E. Myl'nikova, Sov. Phys. Solid State **3**, 631 (1961).
20. L. Veitch, Thesis, Pennsylvania State University (1982).
21. D. Luff, R. Lane, K.R. Brown, and H.J. Marshallsay, Trans. J. Brit. Ceram. Soc. **73**, 251 (1974).
22. O. Babushkin, T. Lindback, J.C. Luc, and J. Leblais, J. Eur. Ceram. Soc. **18**, 737 (1998).
23. S.H. Lee, H.G. Kim, H.I. Choi, and G. Sa-Gong, IEEE Int. Conf. Prop. Appl. Dielectric Mater. **2**, 1062 (1997).
24. S.L. Swartz and T.R. Shrout, Mater. Res. Bull. **17**, 1245 (1982).
25. G. Robert, M.D. Maeder, D. Damjanovic, and N. Setter, J. Am. Ceram. Soc. **84**, 2869 (2001).
26. S. Ananta, R. Tipakontitikul, and T. Tunkasiri, Mater. Lett. **4214**, 1 (2002).
27. JCPDS No. 25-0446 (International Center for Diffraction Data, Newton Square, PA, 2000).
28. H.M. Jang, S.R. Cho, and K.M. Lee, J. Am. Ceram. Soc. **78**, 297 (1995).
29. F. Xia and X. Yao, J. Mater. Sci. **36**, 247 (2001).
30. S.L. Swartz, T.R. Shrout, W.A. Schulze, and L. E. Cross, J. Am. Ceram. Soc. **67**, 311 (1984).
31. R.D. Shannon, Acta. Crystallogr. A **32**, 751 (1976).
32. T.R. Shrout, R. Eitel, and C.A. Randall, IEEE Tr. UFFC. **44**, 1140 (2002).
33. A.J. Moulson and J.M. Herbert, *Electroceramics: Materials, Properties, Applications* (Chapman and Hall, New York, 1990).
34. L.E. Cross, Ferroelectrics **151**, 305 (1994).
35. H. Fan, L. Zhang, L. Zhang, and X. Yao, J. Phys. Condens. Matter **12**, 4381 (2000).
36. D. Pandey, Key Eng. Mater. **101–102**, 177 (1995).
37. A. Vierheilig, A. Safari, and A. Halliyal, Ceram. Trans. **8**, 75 (1990).

เอกสารหมายเลข 1.7

Available online at www.sciencedirect.com
SCIENCE DIRECT®
Current Applied Physics 4 (2004) 179–181
Current Applied Physics
Physics, Chemistry and Materials Science
www.elsevier.com/locate/cap

Effect of sintering temperatures on phase transition of lead zirconate ceramics

C. Puchmark *, S. Jiansirisomboon, G. Rujijanagul, T. Tunkasiri

Department of Physics, Faculty of Science, Chiang Mai University, Chiang Mai 50200, Thailand

Abstract

In this report, effect of sintering temperature on the phase transition temperature from antiferroelectric phase to paraelectric phase of $PbZrO_3$ is presented. $PbZrO_3$ ceramics were prepared via the solid state reaction route. Calcination and sintering were done at 750 °C for 2 h and 1150–1250 °C for 2 h respectively. The transition temperature increased with increasing sintering temperature up to 1200 °C then decreased with the temperature.

PACS: 77.80.–e
Keywords: Antiferroelectrics; Lead zirconate; Ceramics

1. Introduction

Lead zirconate ($PbZrO_3$) is an antiferroelectric ceramic. It is reported that $PbZrO_3$ has an orthorhombic crystal structure at room temperature with lattice parameters of $a = 5.87$ Å, $b = 11.74$ Å, $c = 8.20$ Å. The dielectric constant of $PbZrO_3$ shows a sharp maximum at the phase transition from orthorhombic to cubic at the Curie point near 230 °C [1]. It is reported that antiferroelectric to ferroelectric transition (under the application of a strong electric field to the ceramics in the antiferroelectric phase) leads to significant energy storage [2]. Thus, $PbZrO_3$ is a candidate material for energy storage applications. It is reported that the properties of $PbZrO_3$ can be improved by adding Ba ions into the Pb sites of $PbZrO_3$ [3–6]. The important modified $PbZrO_3$ compound is $(Pb_{1-x}Ba_x)ZrO_3$. Many authors have reported that as the Ba ions in $(Pb_{1-x}Ba_x)ZrO_3$ increase, the Curie temperature of the $(Pb_{1-x}Ba_x)ZrO_3$ shifts to a lower temperature [3,7]. However there is no report about effect of sintering temperature on the phase transition of $PbZrO_3$. In the present paper, experimental results of the preparation of $PbZrO_3$ by solid state reaction are presented. The effect of the sintering temperature on the phase transition was studied.

2. Experiment

In the present study, $PbZrO_3$ powders were prepared by the mixed-oxide method. Reagent-grade PbO and ZrO_2 powders were used as the starting materials. The starting powders were ball milled in ethyl alcohol for 24 h using zirconia balls as the grinding media. After mixing, the slurry was dried and the powder ground into a fine powder using an agate mortar and pestle. The mixed powder was calcined at various temperatures ranging from 500 to 900 °C for 3 h at a heating rate of 5 °C/min. In order to study the phase formation of the calcined powders, X-ray diffraction analysis (XRD) was performed using a diffractometer with Cu K_α radiation. It was found that powders calcined at ≥775 °C provide a single phase of $PbZrO_3$. To improve compaction, 0.3 wt% of PVA binder was blended with the powder before pressing at 40 MPa into cylindrical pellets 15 mm in diameter and 2 mm in thickness. The pellets were then sintered at 1100–1300 °C for 2 h at a heating rate of 5 °C/min. The density of the sintered samples was measured by the Archimedes method with distilled water as the fluid medium. (The phases present in the sintered samples after various sintering temperatures

* Corresponding author.
E-mail address: kungmic2002@yahoo.com (C. Puchmark).

1567-1739/$ - see front matter © 2003 Elsevier B.V. All rights reserved.
doi:10.1016/j.cap.2003.11.003

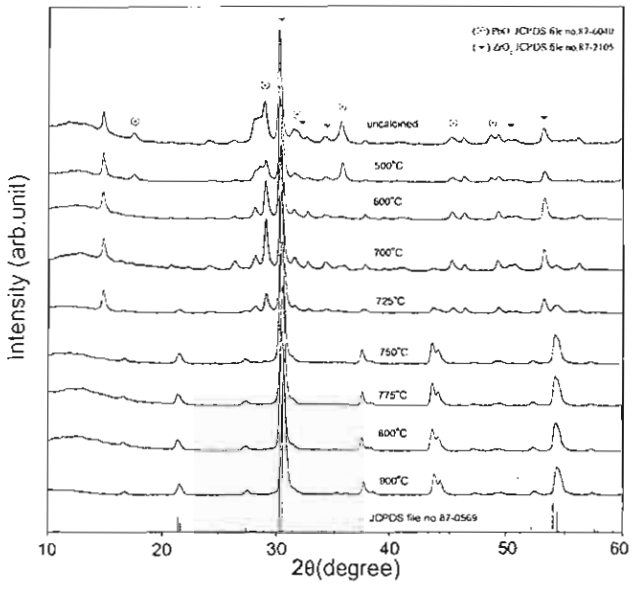

Fig. 1. X-ray diffraction patterns of $PbZrO_3$ calcined at different temperatures.

was investigated by XRD.) Microstructural evolution of the sintered samples was examined by using scanning electron microscopy (SEM). For dielectric measure-

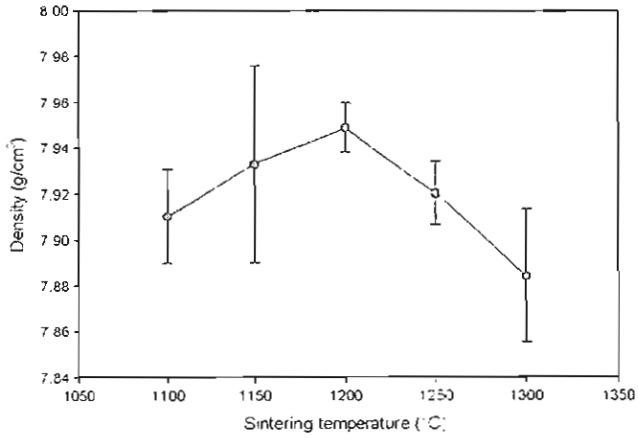

Fig. 2. Plot of density as a function of sintering temperature of $PbZrO_3$ ceramics.

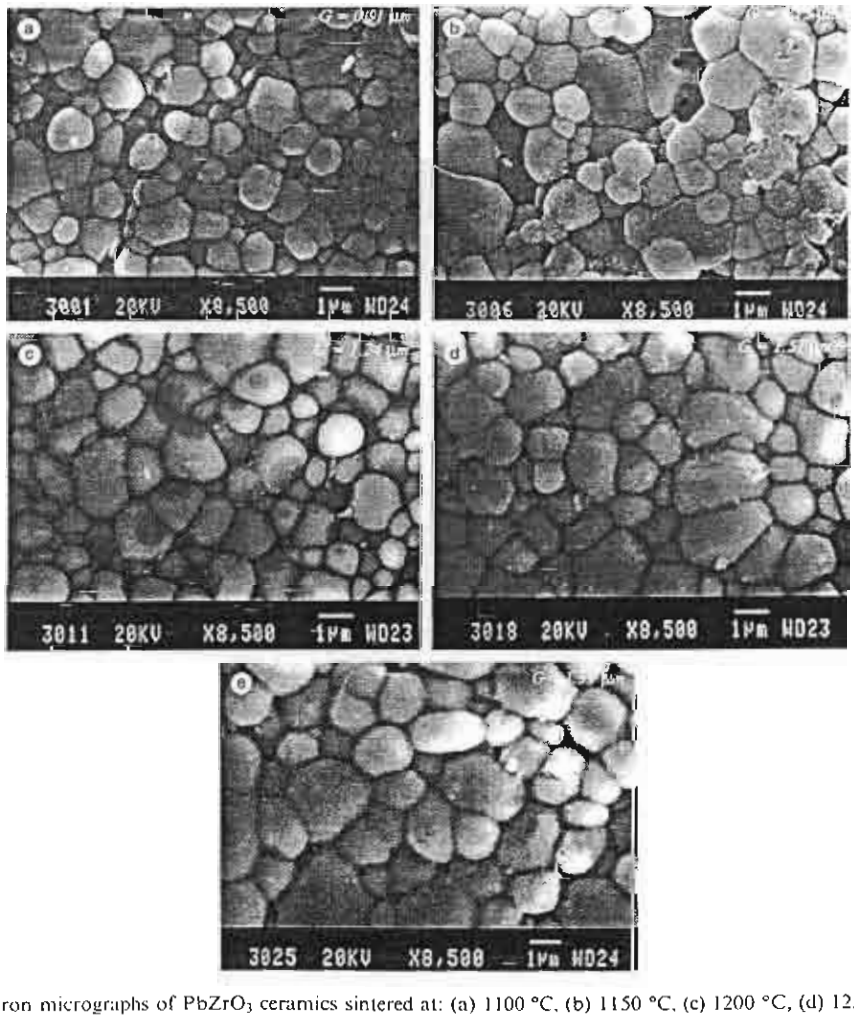

Fig. 3. Scanning electron micrographs of $PbZrO_3$ ceramics sintered at: (a) 1100 °C, (b) 1150 °C, (c) 1200 °C, (d) 1250 °C and (e) 1300 °C.

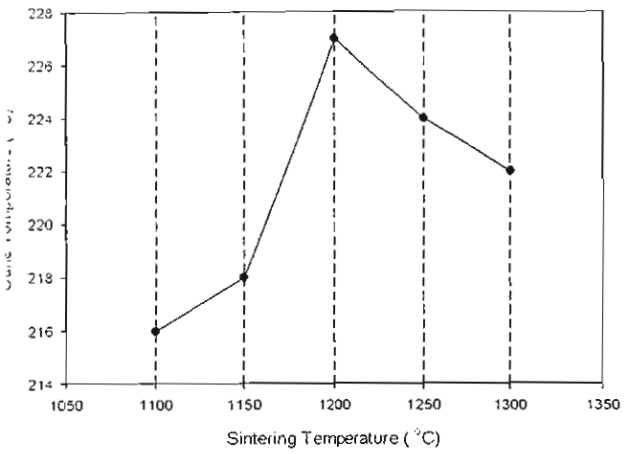

ig. 4. Plot of Curie-temperature as a function of sintering temperature f $PbZrO_3$ ceramics sintered at different temperatures.

ients. gold electrodes were sputtered on the samples hich were then subjected to an automated dielectric ystem measurement controlled by a computer. An mpedance analyzer was also used to measure the ielectric constant and dissipation factor. The dielectric onstant and dissipation factors were measured at kHz. as the samples were heated in the range of 5–250 °C at a rate of 3 °C/min. The phase transition of he samples was studied by measuring the dielectric– emperature curve.

3. Results and discussion

From the XRD pattern (Fig. 1), the second phase was bserved at calcination temperatures below 775 °C. The nalysis was carried out based on the Joint Committee n Powder Diffraction Standard (JCPDS) [8]. A plot of lensity as a function of calcination temperature is hown in Fig. 2. The density increases with increasing he calcination temperature up to 1200 °C and decreases vith further increase of the calcination temperature. Fig. shows SEM micrographs of the $PbZrO_3$ ceramics intered at various temperatures. The grain size increases slightly with increasing sintering temperature. ully dense grain packing was found in samples sintered t higher sintering temperatures.

The dielectric constants of $PbZrO_3$ at temperature bove the phase transition may be expressed by an approximation to the Curie–Weiss law. In the present work, the Curie temperature of the samples was normally obtained from the plot of ε_r^{-1} as a function of temperature. The variation of Curie temperature with sintering temperature is shown in Fig. 4. Many authors have reported that as the Ba ions added to $PbZrO_3$ increased, the Curie temperature of the materials is shifted to a lower temperature [3,7]. In this work, the Curie temperature increases with sintering temperature up to 1200 °C, then decreases with further increase of the sintering temperature. It can be noted that the dielectric results corresponded well with the density results.

4. Conclusion

In the present work, $PbZrO_3$ was prepared via the mixed oxide method. The single phase of $PbZrO_3$ was found in samples calcined at temperatures $\geqslant$ 775 °C. The sintering temperature affects the density, microstructure and phase transition.

Acknowledgements

We would like to thank the Thailand Research Fund, Graduate School, Chiang Mai University, Faculty of Science Chiang Mai University and Ministry of University Affairs for financial support throughout the project.

References

[1] B. Jaffe, W.R. Cook, H. Jaffe, Piezoelectric Ceramics, RAN Publishers, 1971, pp. 123–131.
[2] E.E. Oren, E. Taspinar, A.C. Tas, J. Am. Ceram. Soc. 80 (10) (1997) 2714.
[3] G. Shirane, Phys. Rev. 86 (2) (1952) 219.
[4] B.P. Pokharel, M.K. Datta, D. Pandey, J. Mater. Sci. 34 (1999) 691.
[5] B.P. Pokharel, D. Pandey, J. Appl. Phys. 88 (9) (2000) 5364.
[6] K.H. Yoon, S.C. Hwang, J. Mater. Sci. 32 (1997) 17.
[7] S. Roberts, J. Am. Ceram. Soc. 33 (2) (1950) 63, 64 (9) (1981) 533–538.
[8] Powder Diffraction File, Card No.80-0569. Joint Committee on Powder Diffraction Standards, Swarthmore, PA.

เอกสารหมายเลข 1.8

Ferroelectric Letters, 31:1–13, 2004

ISSN: 0731-5171 print / 1543-5288 online
DOI: 10.1080/07315170490449763

Taylor & Francis
Taylor & Francis Group

Effect of Sintering Temperature on Phase Transition and Mechanical Properties of Lead Zirconate Ceramics

C. PUCHMARK, G. RUJIJANAGUL, S. JIANSIRISOMBOON, and T. TUNKASIRI

Department of Physics, Faculty of Science, Chiang Mai University, Chiang Mai, Thailand 50200

Communicated by George W. Taylor

(Received July 1, 2003)

Phase transition and mechanical properties of $PbZrO_3$ (PZ) at different sintering temperatures were studied. The Curie temperature depends on the sintering temperature. Hardness and fracture toughness of the PZ were measured using Vickers and Knoop microhardness testers. The lower density at the higher sintering temperature resulting from the loss of lead oxide (PbO) causes the lower value of the Curie temperature, hardness and fracture toughness. The results were well corresponding to the microstructure of the PZ ceramics.

Keywords: lead zirconate ceramics; $PbZrO_3$; phase transition; mechanical properties

INTRODUCTION

$PbZrO_3$ (PZ) is an antiferroelectric material, which is reported to have an orthorhombic crystal structure at room temperature with lattice parameters of $a = 8.23$ Å, $b = 11.77$ Å, $c = 5.81$ Å [1]. The dielectric constant of PZ ceramic shows a sharp maximum at the phase transition from orthorhombic to cubic at the Curie point near 230°C [2]. Previous author reported that antiferroelectric to ferroelectric transition (under the application of a strong electric field to the ceramics in the antiferroelectric phase) leads to significant energy storage [3]. Then PZ is a candidate material for energy storage applications. PZ was also searched for its microwave dielectric properties because its dielectric relaxation is near microwave frequencies [3, 4]. The dielectric properties of PZ can be improved by incorporation of Ba ions into the Pb sites of PZ [5–8]. Therefore, the important modification of PZ becomes $(Pb_{1-x}Ba_x)$

ZrO_3 (PBZ). Many authors found that as the number of Ba ions in PBZ is increased, the Curie temperature of the PBZ is shifted to a lower temperature [5, 9]. Because of a large volume change in the phase transition, the PBZ is selected as a candidate material for energy conversion [8]. For the past decade, the electrical properties of PZ were widely studied, however, its mechanical properties have not been well researched. In this paper, the experimental results of the preparation of PZ by solid state reaction method are presented. Effect of sintering temperature on phase transition, electrical properties, and mechanical properties were also studied.

EXPERIMENT

In the present study, PZ powders were prepared by the mixed-oxide method. Reagent-grade of lead oxide (PbO) and zirconium dioxide (ZrO_2) powders were used as the starting materials. The starting powders were ball milling in ethanol for 24 h using zirconia balls as a grinding media. After mixing, the slurry were dried, the powder was then ground using an agate mortar and pestle into a fine powder. The mixed powder was calcined at various temperatures ranging from 500 to 900°C for 3 h with a heating rate of 5°C/min. To study the phase formation of the calcined powders, x-ray diffraction analysis (XRD) of the powders was performed using a diffractrometer with CuK_α radiation. To improve the powder compaction, 0.3 wt% of PVA binder was blended with the powder before pressing at 40 MPa into cylindrical pellets with 15 mm in diameter and 2 mm in thickness. The pellets were then sintered at 1100–1300°C for 2 h with a heating rate of 5°C/min. Density of the sintered samples was measured by Archimedes method with distilled water as the fluid medium. The phase of the sintered samples at various sintering temperatures was investigated by XRD. The microstructural evolution of the sintered samples was examined by scanning electron microscopy (SEM). For dielectric measurement, gold electrodes were sputtered on the samples and then subjected to an automated dielectric system measurement controlled by a computer. An impedance analyzer was also used to measure the dielectric constant and dissipation factor. The dielectric constant and dissipation factors were measured at 1 kHz, as the samples were heated in the range of 25–250°C at a rate of 3°C/min. Phase transition of the samples was studied by measuring the dielectric-temperature curve. The dielectric constants of the PZ at temperature above the phase transition may be expressed to an approximation by the Curie-Weiss law. The Curie temperature of the samples can be normally obtained from the plot of ε_r^{-1} as a function of temperature.

Effect of sintering temperatures on the mechanical properties of the ceramics was studied by Vickers and Knoop microhardness testers. Indentations were applied on the polished surfaces of PZ ceramics. Applied loads were in the range of 200–1000 g with an indentation period of 15 s. Indentation crack length (c) and indentation diagonal (d) was measured, and then used to calculate Vickers hardness, Knoop hardness and fracture toughness by the following equations:

$$H_V = 1854.4\left(\frac{P}{d_V^2}\right) \tag{1}$$

where H_V is a Vickers hardness (in GPa), d_V (in μm) and P is an applied load (in N).

$$H_K = 1.451\left(\frac{P}{d_K^2}\right) \tag{2}$$

where H_K is a Knoop hardness (in kg/mm^2), d_K is a longer diagonal length of a Knoop indentation (in mm) and P is an applied load (in N).

$$K_{IC} = \xi\left(\frac{E}{H_V}\right)^{1/2}\left(\frac{P}{c^{3/2}}\right) \tag{3}$$

where K_{IC} is a fracture toughness (in MPa·m$^{1/2}$), H_V is a Vickers hardness (in GPa), P is an applied load (in N), E is Young's modulus (in GPa) and c is the radial length measured from the centre of indentation impression (in m) [10, 11]. ξ is a material independent, dimensionless calibration constant which characterizes the geometry of the deformation filed. Studies on many ceramics led to an average value of $\xi = 0.016 \pm 0.004$ [12]. After indentation, the samples were etched by 10% HCl + 1 drop HF. Microstructure of the etched samples was again studied by SEM.

RESULTS AND DISCUSSION

Effect of calcination temperatures on the phase formation of the PZ powder was shown by XRD patterns in Fig. 1. At the calcination temperatures starting from 775°C, a single phase of PZ was detected. The phase analysis was carried out based on the Joint Committee on Powder Diffraction Standard (JCPDS) [1]. The density and Curie temperature of PZ ceramics were plotted as a function of sintering temperature are shown in Fig. 2. The value of density is in the range of 7.88–7.95 g/cm^3 or 97.68–98.48% of the PZ theoretical

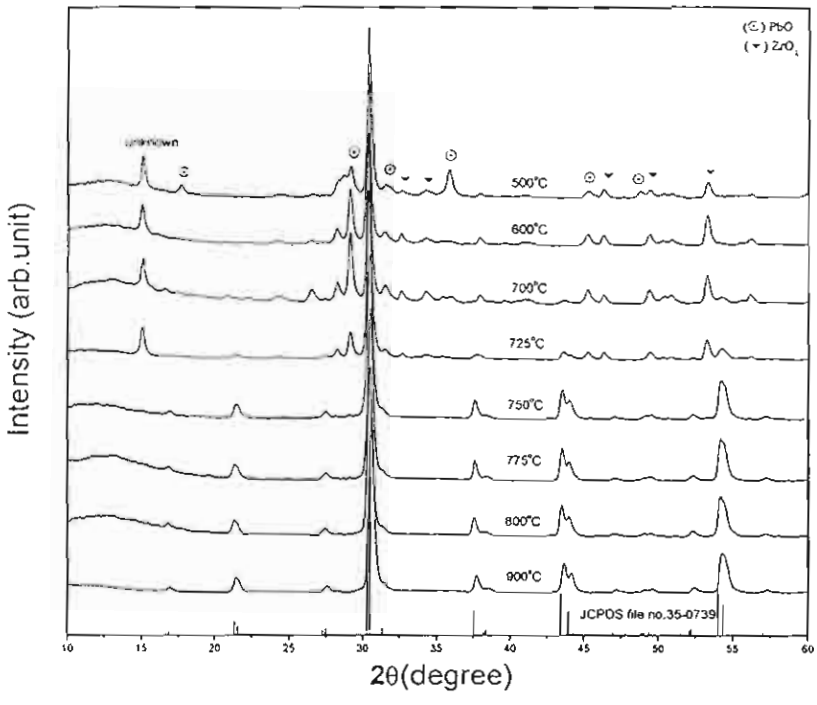

Figure 1. X-ray diffraction patterns of $PbZrO_3$ calcined at different temperatures.

density. The density increases with increasing the sintering temperature up to 1200°C and decreases with further increasing the sintering temperature. The maximum value of density is 98.48% of the theoretical density, observed in the ceramic sintered at 1200°C. Decreasing of the density is likely due to a vaporization of PbO at the temperatures above 1200°C [14]. Figure 3 shows the plot of grain size and porosity as a function of sintering temperature. Grain size of the samples is in the range of 0.9 to 1.5 μm and found to slightly increase with the increasing of the sintering temperature. Weight loss of the PZ ceramics as a function of sintering temperature is shown in Fig. 4. The weight loss increased with increasing the sintering temperature as expected.

The temperature dependences of dielectric constant and dissipation factor at various sintering temperatures were studied and as shown in Table I and plotted in Fig. 5. The measurement of dielectric constant at room temperature is in the range of 157 to 170, while the dissipation factor (tan δ) is in the range of 0.0042 to 0.0205. The highest dielectric constant at room

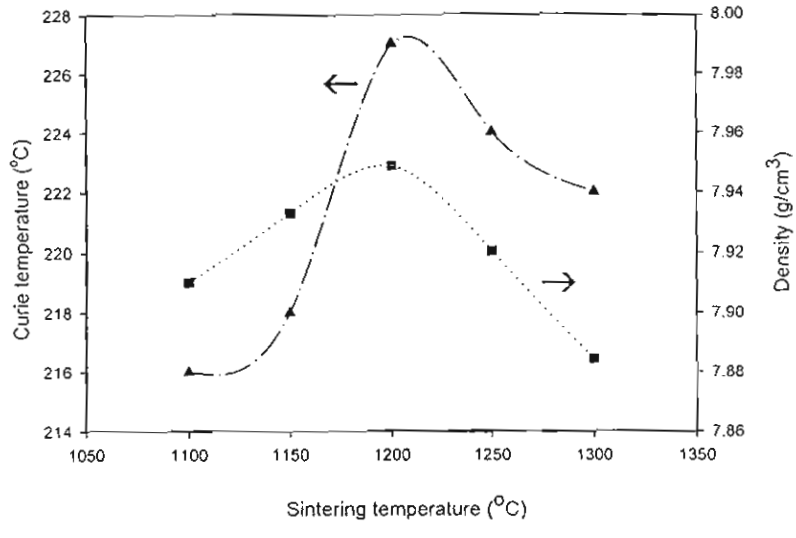

Figure 2. (▲) Curie temperature and (■) density of the sintered PZ ceramics with sintering temperature.

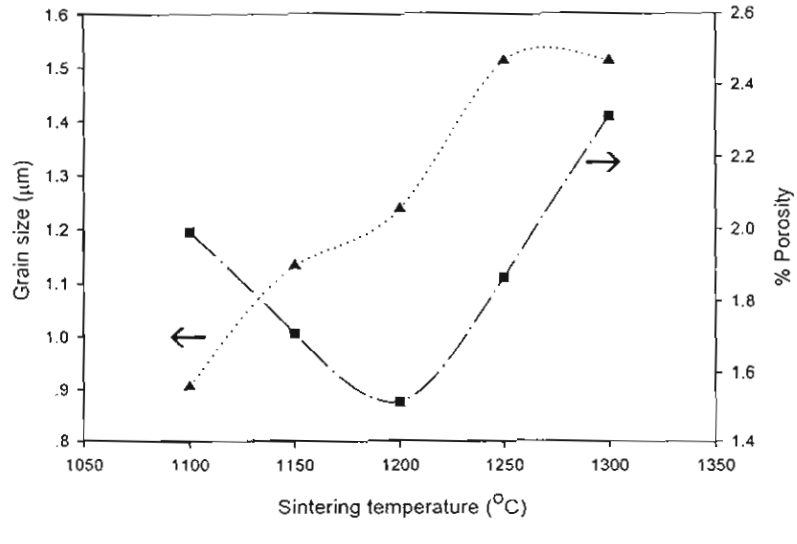

Figure 3. (▲) Grain size and (■) porosity as a function of sintering temperature.

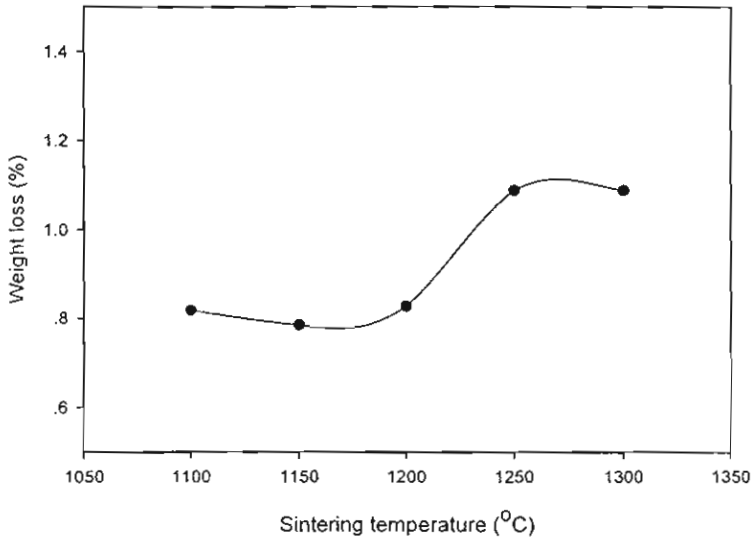

Figure 4. Weight loss of PZ ceramics at various sintering temperatures.

temperature is 170, observed in the PZ ceramic sintered at 1200°C with the grain size of 1 μm. Kong *et al.* prepared PZ ceramics from high-energy ball-milling method and found that the dielectric constant of their PZ ceramic decreases at the higher sintering which is caused by the loss of PbO [13]. The highest dielectric constant in their work is about 218 for the sample sintered at 1200°C with grain size of 8 μm. However, the highest value of the dielectric constant ($\varepsilon_r = 170$) at room temperature in our work for the ceramics with 1 μm grain size is close to the value found in their work.

TABLE I Dielectric properties of $PbZrO_3$ ceramics sintered at different temperatures

Sintering temperature (°C)	Dielectric constant at 27°C	Dissipation factor at 27°C	Curie temperature (°C)
1100	163	0.0042	227
1150	157	0.0147	228
1200	170	0.0205	232
1250	155	0.0230	231
1300	164	0.0229	230

The variation of Curie temperature as a function of the sintering temperature is also shown in Fig. 5. The maximum dielectric constants at the phase transition temperature are between 6750 and 7762, while Robert [9] and Shirane [5] reported the maximum values of dielectric constant at the phase

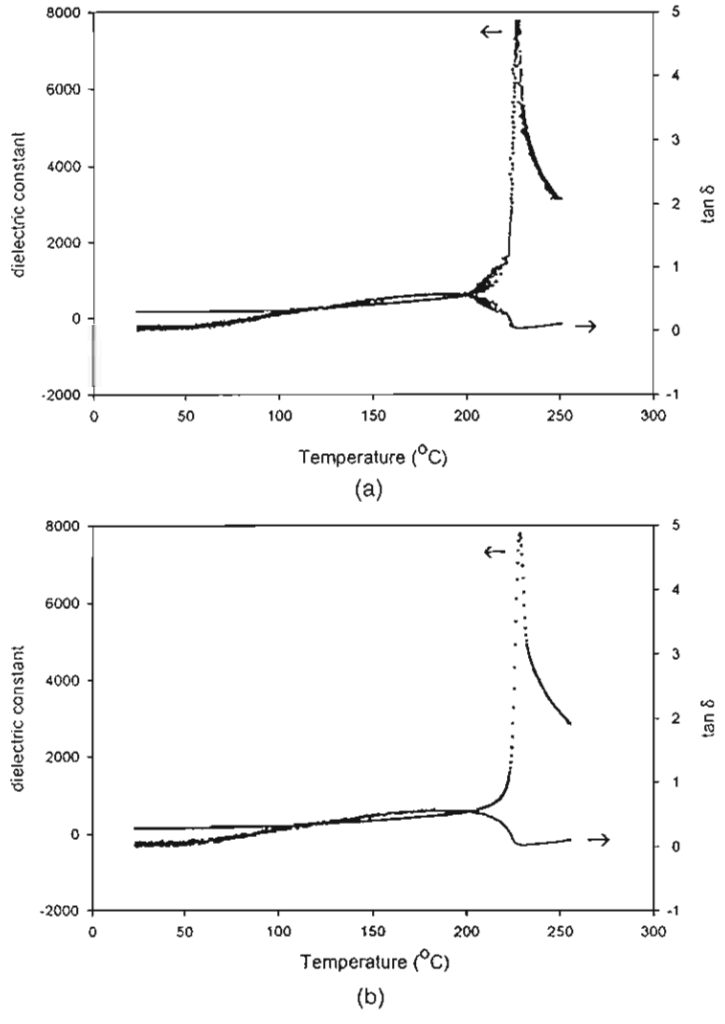

Figure 5. Temperature dependence of the dielectric constant and dissipation factor of PZ sintered at: (a) 1100°C, (b) 1150°C, (c) 1200°C, (d) 1250°C, and (e) 1300°C. *(Continued)*

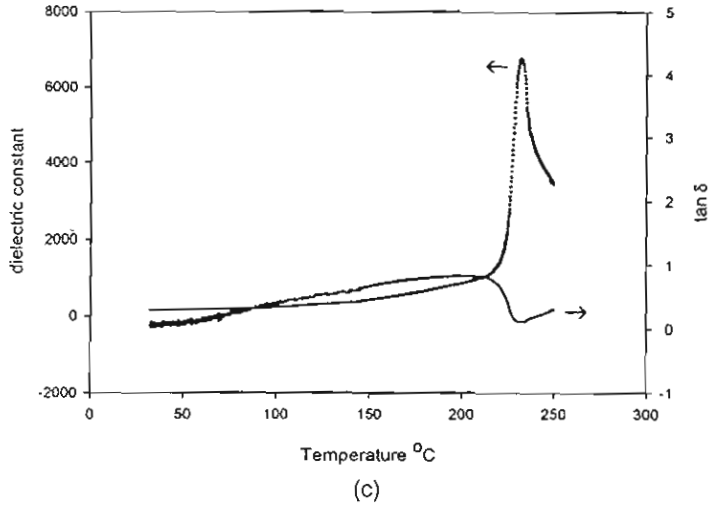

(c)

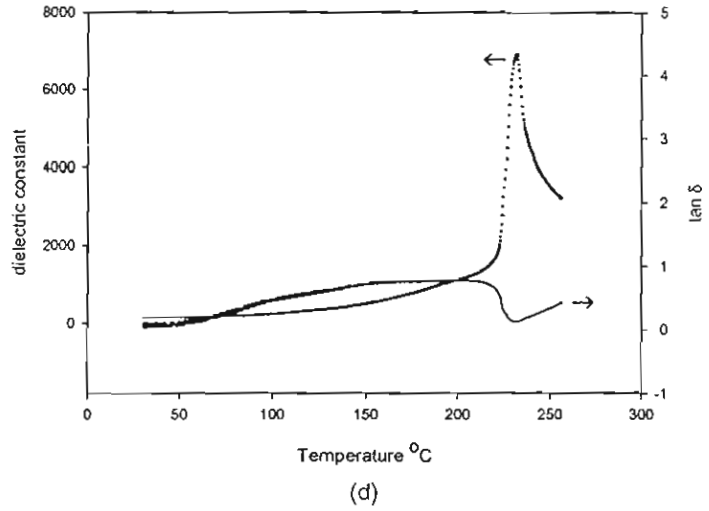

(d)

Figure 5. (Continued)

transition temperature are approximately 3260 and 2300, respectively. In the present work, the Curie temperature increases with the sintering temperature up to 1200°C and then decreases with further increasing the temperature. It can be noted that the Curie temperature results are well corresponded to the density results. This is well corresponded with the work done on a

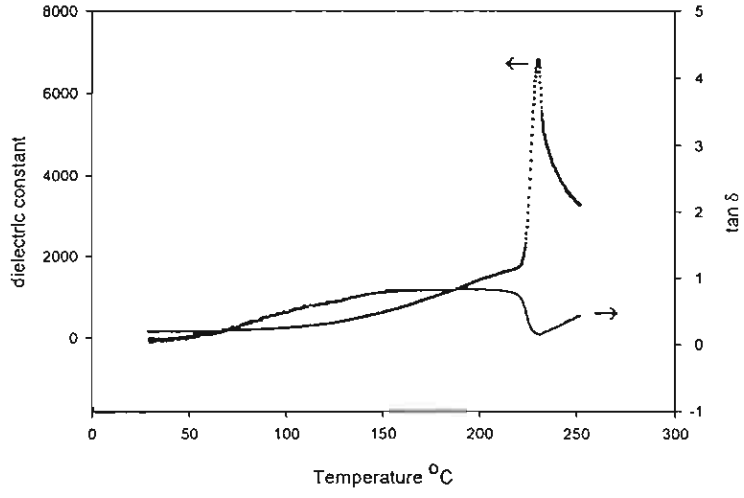

(e)

Figure 5. (Continued)

ferroelectric materials, i.e., $BaTiO_3$ by Fang *et al.*, where the Curie temperature increased with increasing the density of $BaTiO_3$ which is a ferroelectric materials [14].

The effect of sintering temperature on the mechanical properties of the samples was studied by using Vickers and Knoop microhardness testers. The values of Vickers hardness, Knoop hardness, and fracture toughness are listed in Table II, and the plot of these values as a function of sintering temperature are shown in Fig. 6. The hardness values trend to decrease as increasing the sintering temperatures. This result would be well corresponding

TABLE II Mechanical properties of $PbZrO_3$ ceramics sintered at different temperatures

Sintering temperature (°C)	Vickers hardness (GPa)	Knoop hardness (GPa)	Fracture toughness (MPa·m$^{1/2}$)
1100	5.37	4.42	1.38
1150	4.85	4.54	2.91
1200	4.77	4.49	2.91
1250	4.50	4.46	1.97
1300	4.65	3.94	1.12

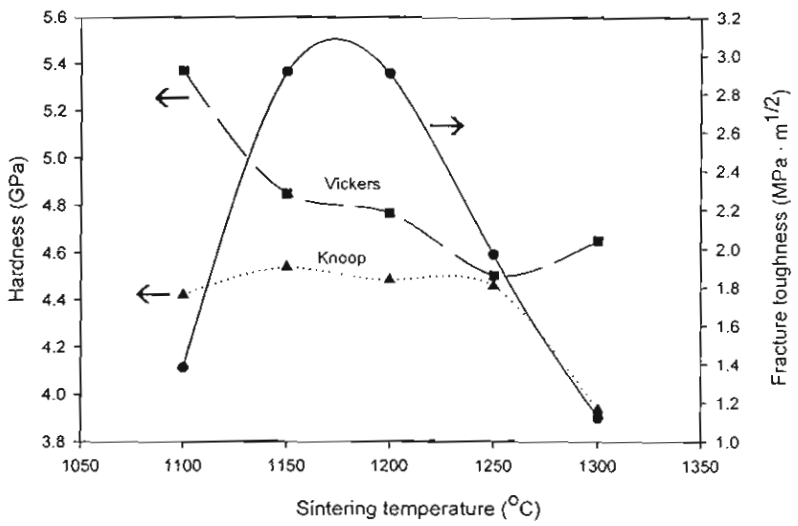

Figure 6. (▲,■) Hardness and (●) fracture toughness of the PZ ceramics plotted as a function of sintering temperatures.

with the density (Fig. 2.) and porosity (Fig. 3.) results, where they are significantly changed due to the loss of PbO at the temperature above 1200°C. For the fracture toughness values which were calculated mainly from the hardness and crack extension from the Vickers indentation impressions, seem to depend significantly on the density and porosity as well. The fracture toughness dramatically increases with the sintering temperature up to 1150°C and then decreases with further increasing the temperature. Figure 7(a) and (b) are SEM micrographs of Vickers and Knoop indentations performed on polished PZ samples sintered at 1200°C. The examples of crack characteristic extended from the Vickers indentation impressions are shown in Fig. 7(c) and 7(d). The cracks of PZ sintered at 1150°C are followed the grain boundaries, so called intergranular crack (Fig. 7(c)), while those cracks found in the sample sintered at 1300°C are rather straight through the grains indicating transgranular fracture (Fig. 7(d)). According to the Table II, the fracture toughness value of PZ sintered at 1150°C ($K_{IC} = 2.91$ MPa·m$^{1/2}$) is higher than that of PZ sintered at 1300°C ($K_{IC} = 1.12$ MPa·m$^{1/2}$). This result is well corresponding to the microstructure; the higher the fracture toughness, the harder the crack cut through the grains and vice versa. Generally, the

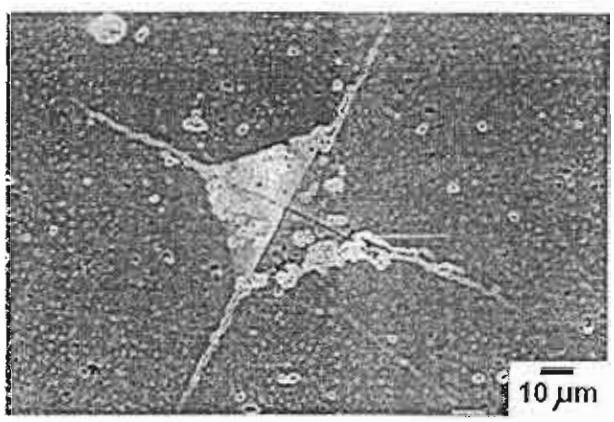

(a)

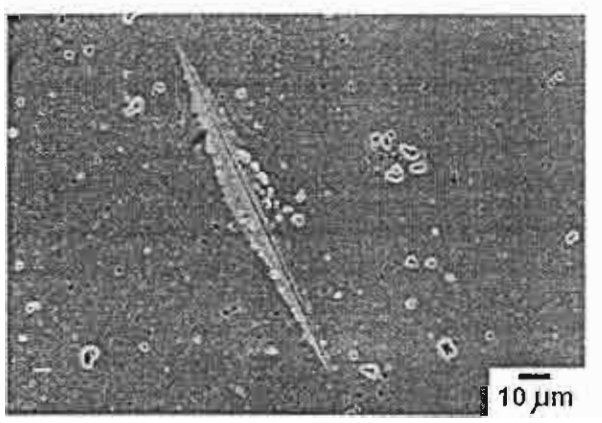

(b)

Figure 7. SEM micrographs of (a) Vickers indentation on surface of PZ sintered at 1200°C, (b) Knoop indentation on surface of PZ sintered at 1200°C, (c) indentation crack of PZ sintered at 1150°C, and (d) indentation crack of PZ sintered at 1300°C. *(Continued)*

hardness and fracture toughness of lead base ceramics depends on many factors such as grain size and porosity [15, 16]. In the present work, the reduction of hardness and fracture toughness at higher sintering temperature is likely to cause by the loss of PbO during sintering which form the lower density and imperfect ceramics [13].

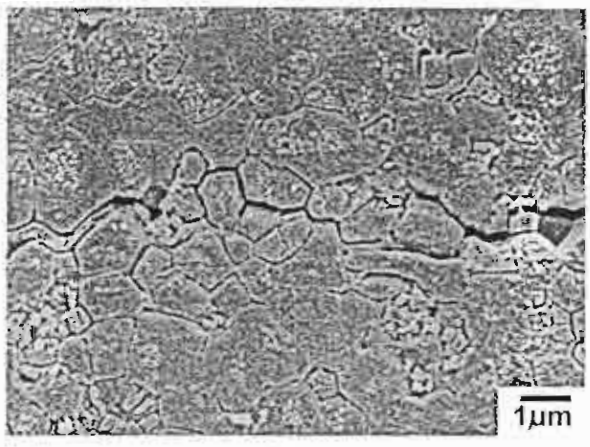

(c)

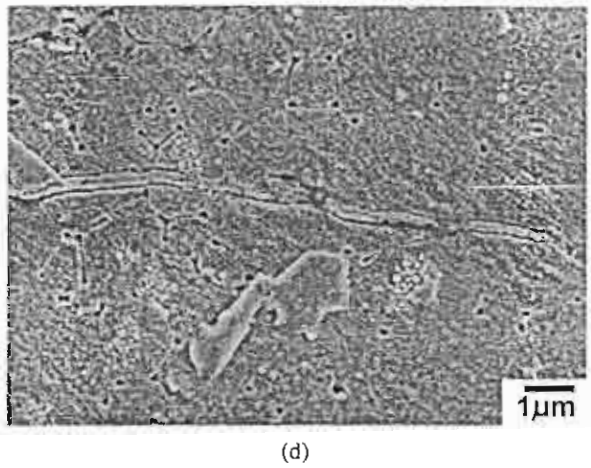

(d)

Figure 7. (Continued)

CONCLUSIONS

In the present work, the $PbZrO_3$ (PZ) was prepared via the mixed oxide method. The single phase of PZ was found in the powders calcined at the temperature $\geq$775°C. The sintering temperature has effects on phase transition behavior and mechanical properties of the PZ. Curie temperature and density of the PZ ceramics increased with increasing sintering temperature

up to 1200°C. However, they decreased for higher sintering temperature. The lower density is likely to cause by the loss of PbO during sintering above 1200°C which then result to the reduction of density, Curie temperature, hardness, and fracture toughness values.

ACKNOWLEDGMENTS

We would like to thank the Thailand Research Fund, Graduate School, Chiang Mai University, Faculty of Science Chiang Mai University, and Ministry of University Affairs for financial support throughout the project.

REFERENCES

[1] Powder Diffraction File, Card No. 35-0739. Joint Committee on Powder Diffraction Standards (JCPDS) PDF-4. Internation Centre for Diffraction Data (ICDD), 2000.
[2] B. Jaffe, W. R. Cook, and H. Jaffe, *Piezoelectric ceramics* (R.A.N. Publishers, 1971), pp.123–131.
[3] E. E. Oren, E. Taspinar, and A. C. Tas, *J. Am. Ceram. Soc.* **80**(10), 2714 (1997).
[4] M. T. Lanagan, J. H. Kim, S. Jang, and R. E. Newnham, *J. Am. Ceram. Soc.* **71**(4), 311 (1988).
[5] G. Shirane, *Phys. Rev.* 86(2), 219 (1952).
[6] B. P. Pokharel, M. K. Datta, and D. Pandey, *J. Mater. Sci.* **34**, 691 (1999).
[7] B. P. Pokharel and D. Pandey, *J. Appl. Phys.* **88**(9), 5364 (2000).
[8] K. H. Yoon, S. C. Hwang, and D. H. Kang, *J. Mater. Sci.* **32**, 17 (1997).
[9] S. Roberts, *J. Am. Ceram. Soc.* **33**(2), 63 (1950).
[10] D. B. Marshall and B. R. Lawn, *J. Mat. Sci.* **14**, 2001 (1979).
[11] B. R. Lawn, A. G. Evans, and D. B. Marshall, *J. Am. Ceram. Soc.* **63**, 574 (1980).
[12] G. R. Anstis, P. Chuntikul, B. R. Lawn, and D. B. Marshall, *J. Am. Ceram. Soc.* 64(9), 533 (1981).
[13] L. B. Kong, J. Ma, W. Zhu, and O. K. Tan, *Mater. Lett.* **49**, 96 (2001).
[14] T. Fang, H. Hsieh, and F. Shiau, *J. Am. Ceram. Soc.* **76**(5), 1205 (1993).
[15] K. Uchino, *Piezoelectric Actuators and Ultrasonic Motors* (Kluwer Academic Publishers, 1997), pp. 113–114.
[16] D. R. Biswas and R. M. Fulrath, *Trans. J. Brit. Cer. Soc.* **79**, 1 (1980).

เอกสารหมายเลข 1.9

ELSEVIER

Materials Science and Engineering B 108 (2004) 258–265

MATERIALS SCIENCE & ENGINEERING B

www.elsevier.com/locate/mseb

Influence of processing conditions on the phase transition and ferroelectric properties of $Pb(Zn_{1/3}Nb_{2/3})O_3$–$Pb(Zr_{1/2}Ti_{1/2})O_3$ ceramics

Naratip Vittayakorn [a,*], Gobwute Rujijanagul [a], Tawee Tunkasiri [a], Xiaoli Tan [b], David P. Cann [b]

[a] *Department of Physics, Faculty of Science, Chiang Mai University, Chiang Mai 50200, Thailand*
[b] *Materials Science and Engineering Department, Iowa State University, Ames, IA 50011 USA*

Received 23 July 2003; accepted 12 January 2004

Abstract

Ceramics solid solutions within the binary system of $xPb(Zn_{1/3}Nb_{2/3})O_3-(1-x)Pb(Zr_{1/2}Ti_{1/2})O_3$ with $x = 0.1$–0.5 were synthesized via the mixed oxide method and the columbite method. Phase development of calcined powders and the crystal structure of sintered ceramics were analyzed by X-ray diffraction. Ferroelectric properties were measured to elucidate the phase transformation and identify the impact of the processing conditions. It is shown that there was no significant difference in P_r across the composition range. However, the coercive field E_c was shown to exhibit a strong compositional dependence. Compared with ceramics prepared by the columbite method, ceramics prepared by the mixed oxide method showed a lower remanent polarization P_r and a higher coercive field E_c. In addition, both X-ray diffraction and ferroelectric measurements indicated a phase transformation from a tetragonal to a pseudo-cubic rhombohedral phase when the fraction of $Pb(Zn_{1/3}Nb_{2/3})O_3$ (PZN) was increased. The morphotropic phase boundary (MPB) is located between $x = 0.2$ and 0.3 according to observations made on ceramics prepared with the columbite method. However, this transformation was obscured in the ceramics prepared with the mixed oxide method. It is proposed that compositional heterogeneities were responsible for these experimental investigations.

Keywords: Phase transition; Ferroelectric properties; Ceramics

1. Introduction

Ferroelectric materials are widely used for various devices, including multilayer capacitors, sensors, and actuators. By the 1950s, the piezoelectric solid solution $Pb(Zr_{1-x}Ti_x)O_3$ (PZT) was found to host exceptionally high dielectric and piezoelectric properties for compositions close to the morphotropic phase boundary (MPB). This MPB is located around $PbTiO_3$:$PbZrO_3$ ~1:1 and separates the Ti-rich tetragonal phase from the Zr-rich rhombohedral phase [1]. Most commercial PZT ceramics are thus designed in the vicinity of the MPB with various dopings in order to achieve high properties.

$Pb(Zn_{1/3}Nb_{2/3})O_3$ (PZN) is an important relaxor ferroelectric material with the rhombohedral structure at room temperature. A diffuse phase transition from the paraelectric state to a ferroelectric polar state occurs at 140 °C [2]. Extensive research has been carried on PZN single crystals because of their excellent dielectric, electrostrictive, and optical properties [2,3]. Although single crystals of PZN can routinely be grown by the flux method, [4] it is known that perovskite PZN ceramics cannot be synthesized by the conventional mixed-oxide method without doping. This is because PZN has a low tolerance factor and small electronegativity difference between the cations and the pyrochlore phase appears to be more thermodynamically stable than the perovskite phase [5]. Attempts to synthesize perovskite PZN ceramics invariably results in the formation of pyrochlore phase with inferior dielectric and piezoelectric properties. The columbite method, as suggested by Schwartz and Shrout [6] for the prepa-

* Corresponding author. Tel.: +1-515-294-3801; fax: +1-515-294-5444.
E-mail address: naratip@iastate.edu (N. Vittayakorn).

0921-5107/$ – see front matter © 2004 Elsevier B.V. All rights reserved.
doi:10.1016/j.mseb.2004.01.006

ration of perovskite $Pb(Mg_{1/3}Nb_{2/3})O_3$ (PMN) ceramic, is not effective in suppressing pyrochlore phase formation in PZN ceramics [5]. Hot isostatic pressing was reported to be able to produce phase-pure perovskite PZN ceramics [7]. However, relatively poor piezoelectric properties were measured in the as-pressed ceramic. Various chemical additives, such as $Ba(Zn_{1/3}Nb_{2/3})O_3$, $BaTiO_3$, and $SrTiO_3$ have thus been explored in an attempt to stabilize the perovskite PZN ceramic and retain the excellent piezoelectric properties. Halliyal et al. [8] prepared $BaTiO_3$-stabilized PZN ceramics using $BaCO_3$, PbO, ZnO, Nb_2O_5, and TiO_2 as the starting materials. Villlegas et al. [9] incorporated $BaTiO_3$ and $Pb(Zr_{0.4}Ti_{0.6})O_3$ into PZN to produce the ternary system with the perovskite structure from $ZnNb_2O_6$ powder. However, a trade-off was made with these additives which yielded reduced dielectric constants and piezoelectric coefficients. Therefore, there is significant interest in finding a method to stabilize the perovskite phase in PZN without sacrificing the excellent dielectric and piezoelectric properties.

Since both PZT and PZN have perovskite structure and are known to have excellent dielectric and piezoelectric properties, it is suggested to alloy PZN with PZT to stabilize and optimize the PZN ceramics. Recent work by Fan and Kim [10] has shown promise in producing phase-pure perovskite PZN–PZT ceramics with the conventional mixed-oxide method. The present work aims to provide a comprehensive study on the process-property relationships in the binary system of PZN–PZT with a wide composition range. Both the conventional mixed-oxide method and the columbite precursor method have been used in synthesizing the PZN–PZT ceramics. The conventional method utilized a one-step reaction with all of starting materials whereas the columbite method was used an initial step of preparing columbite precursor ($ZnNb_2O_6$) and wolframite precursor ($ZrTiO_4$) followed by a reaction with PbO to form the PZN–PZT ceramics. Finally, a comparison of the important ferroelectric properties was made to identify the optimum processing conditions.

2. Experimental procedure

For the conventional method, regent grade oxides of PbO, ZnO, ZrO_2, TiO_2 and Nb_2O_5 were mixed in the required stoichiometric ratios for the general composition xPZN–$(1-x)$PZT where x = 0.1, 0.2, 0.3, 0.4, and 0.5. After ball milling for 24 h and drying at 120 °C, the mixture was calcined at temperatures between 750 and 950 °C for 4 h in a double crucible configuration [11]. A heating rate of 20 °C/min was selected for all of the compositions in this system [11]. For the columbite method, the columbite precursor $ZnNb_2O_6$ was prepared from the reaction between ZnO (99.9%) and Nb_2O_5 (99.9%) at 975 °C for 4 h. The wolframite precursor $ZrTiO_4$ was formed by reacting ZrO_2 (99.9%) with TiO_2 (99.9%) at 1400 °C for 4 h. The precursors $ZnNb_2O_6$, $ZrTiO_4$ were then subsequently mixed with PbO (99.9%) (with 2 mol% excess PbO) [11] and milled, dried, and calcined under the same conditions as the powder prepared by conventional method. The calcined powders of both methods were cold isostatically pressed into pellets at a pressure of 150 MPa. Five sintering conditions were selected to be used with both methods ranging 1175, 1200, 1225, 1250, and 1275 °C dwell 2 h. To prevent PbO volatilization from the pellets, a PbO atmosphere was controlled with a bed of $PbZrO_3$ powder placed in the vicinity of the pellets. The calcined powder and sintered pellets were checked for perovskite phase formation by X-ray diffraction (XRD). Data collection was performed in the 2θ range of 20°–60° with a step scan with a step size of 0.02° and counting time of 2 s per step. For profile fitting, a step scan

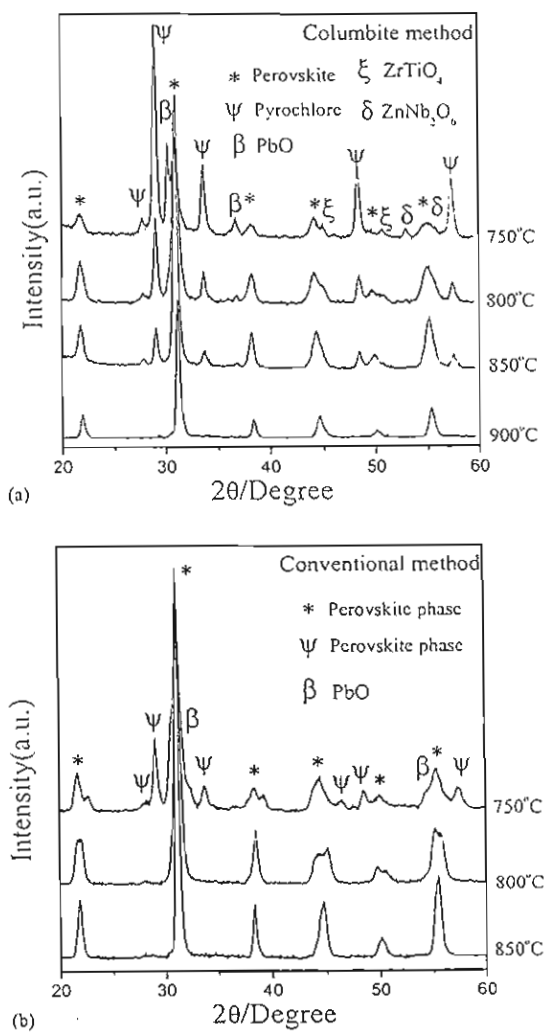

Fig. 1. XRD patterns for 0.3PZN–0.7PZT ceramics calcined at varies temperature for 4 h. (a) Columbite method; (b) conventional method.

with step size of 0.004° was used with a counting time of 5 s per step and peak deconvolution was done with JADE v.6.

The relative amounts of perovskite and pyrochlore phases were approximated by calculating the ratio of the major XRD peak intensities of the perovskite and pyrochlore phase via the following equation:

$$\text{Perovskite intensity (\%)} = \left(\frac{I_{\text{perov}}}{I_{\text{perov}} + I_{\text{pyro}} + I_{\text{PbO}}}\right) \times 100$$

where I_{perov}, I_{pyro}, and I_{PbO} refer to the intensity of the (1 1 0) perovskite peak, (2 2 2) pyrochlore peak, and the intensity of the highest lead oxide peak, respectively.

To investigate the influence of post-sintering heat treatments, specimens from both methods which had been sintered at 1175 °C were annealed at 1250 °C for a dwell time of 6 h in a closed Al_2O_3 crucible with PbO-rich atmosphere. The specimens were polished and electroded via gold sputtering, over which a layer of air-dry silver paint was applied to enhance the electrical contact. The ferroelectric polarization versus electric field (P–E) measurements was made using an RT66A standard ferroelectric test system.

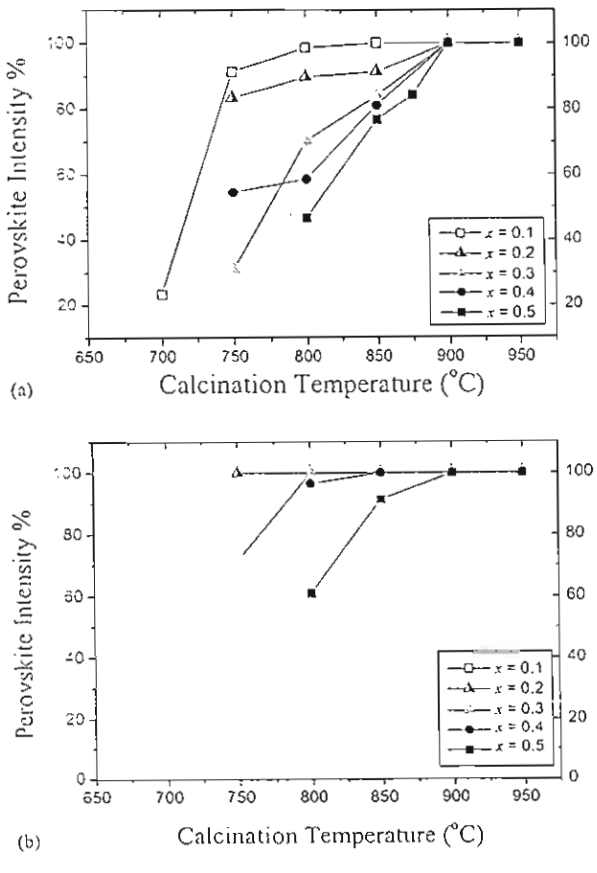

Fig. 2. Percentage of perovskite phase as a function of calcination temperature for xPZN–$(1-x)$PZT ceramics: (a) columbite method; (b) conventional method.

3. Results and discussion

3.1. Perovskite phase formation and the MPB

Powder XRD patterns of the calcined 0.3PZN–0.7PZT powders at different calcination temperatures for both methods are shown in Fig. 1(a) and (b). The XRD results show that the pyrochlore phase $Pb_{1.88}(Zn_{0.3}Nb_{1.25})O_{5.305}$ (JCPDS No. 25-0446) was dominant at calcination temperatures below 750 °C for all of the columbite-derived powders. The precursor phases PbO, $ZrTiO_4$, $ZnNb_2O_6$ were also detected by XRD at below 800 °C. No evidence of the precursor phase ZrO_2, TiO_2, Nb_2O_5 or ZnO was detected by XRD for conventional preparation. Moreover, the pyrochlore phase was only observed in the conventional method-derived powders for compositions with a high concentration of lead zinc niobate. It is assumed that the columbite phase $ZnNb_2O_6$

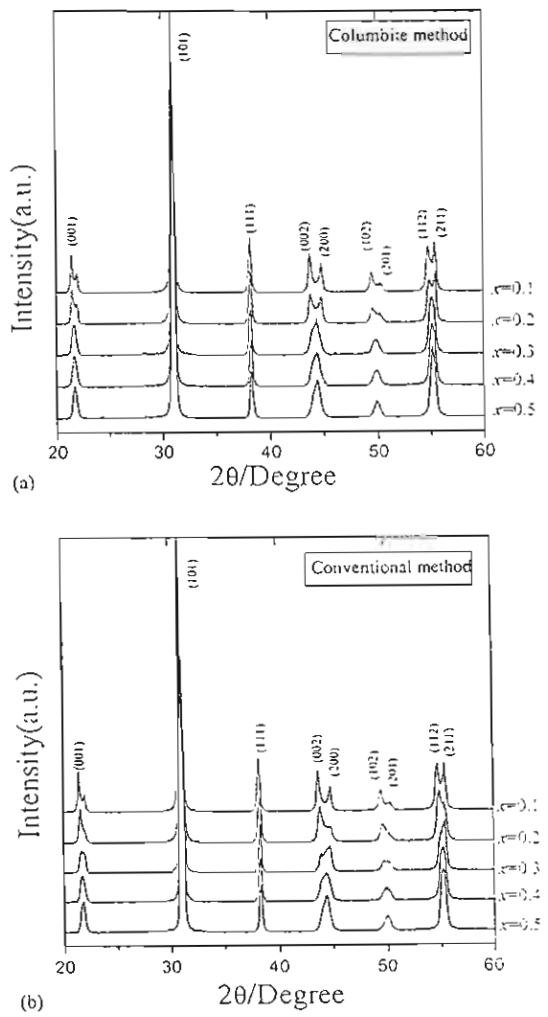

Fig. 3. XRD patterns for xPZN–$(1-x)$PZT ceramics sintered at 1250 °C for 2 h: (a) columbite method; (b) conventional method.

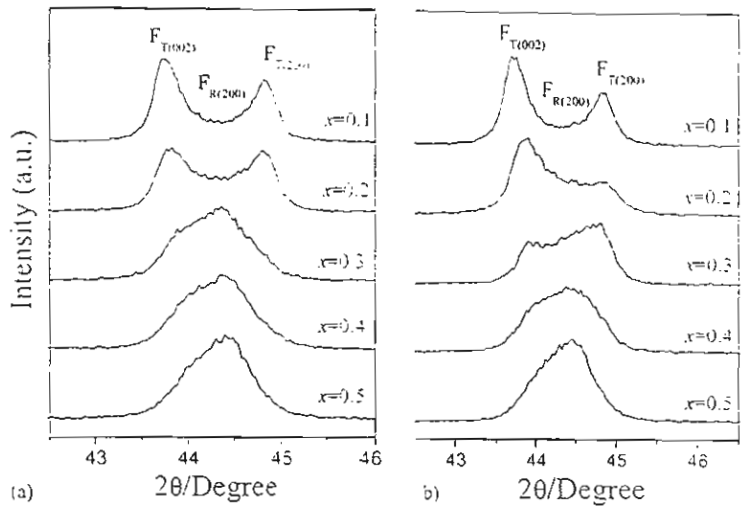

Fig. 4. Close examination of the (0 0 2) peaks shown in Fig. 2. (a) Columbite method; (b) conventional method.

decomposed via reaction with PbO at low temperatures to form the pyrochlore phase $Pb_{1.88}(Zn_{0.3}Nb_{1.25})O_{5.305}$. For the conventional method, $Pb_xNb_yO_z$ pyrochlore phases were found at calcination temperatures below 800 °C for $x > 0.3$. In the work by Chen et. al. [12] it was reported that in the lead-niobium pyrochlore system the cubic $Pb_3Nb_4O_{13}$, pyrochlore phase (JCPDS No. 25–443) forms first around 580 °C. At higher temperatures, it transforms to $Pb_2Nb_2O_7$, (JCPDS No. 40–828) and finally to $Pb_3Nb_2O_8$, (JCPDS No. 30–712) with increased calcination temperatures. At

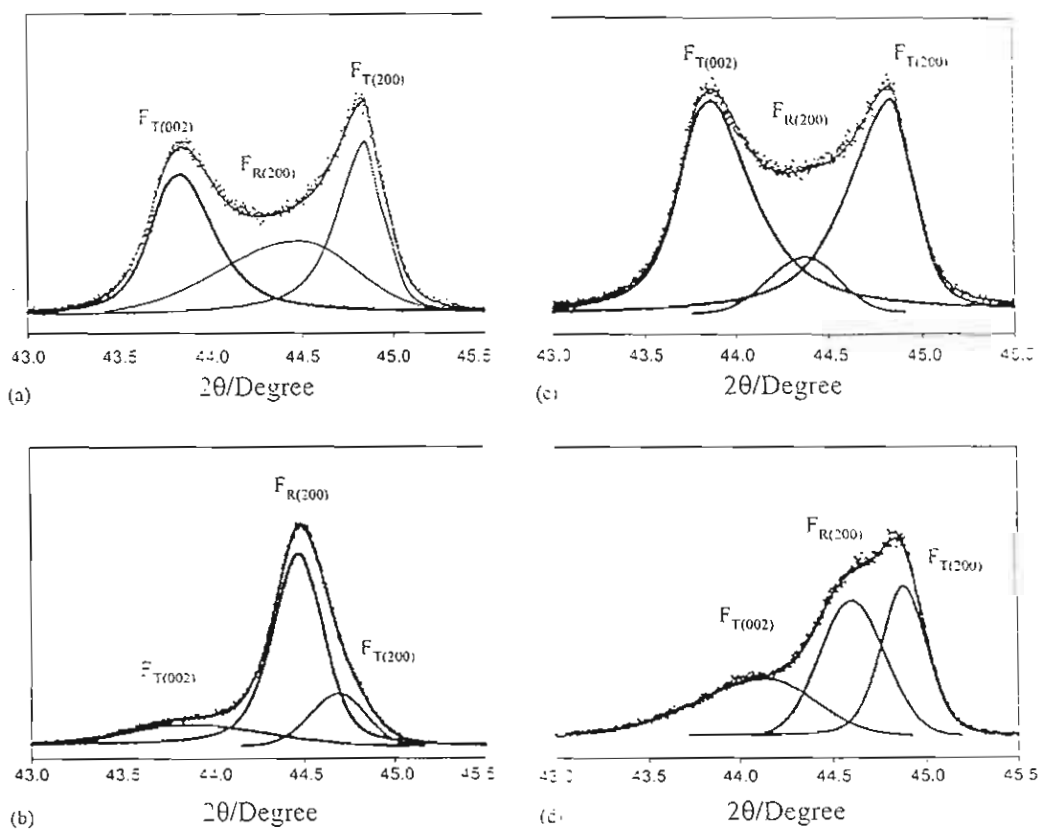

Fig. 5. Individual X-ray diffraction (0 0 2) peak for the tetragonal ($F_{T(002)}$, $F_{T(200)}$) and rhombohedral($F_{R(200)}$) phase for difference methods, (a) 0.2PZN–0.8PZT prepared by columbite method, (b) 0.3PZN–0.7PZT prepared by columbite method, (c) 0.2PZN–0.8PZT prepared by conventional method, (d) 0.3PZN–0.7PZT prepared by conventional method.

800 °C, the pyrochlore phase began to decrease and disappeared completely at 850 °C for powder prepared by conventional method and at 900 °C for the columbite method. The optimum calcination temperature for the formation of phase pure perovskite was found to be about 850 °C for the conventional method and 900 °C for the columbite method.

The perovskite phase formation for both processing methods at various calcination temperatures is shown in Fig. 2(a) and (b), respectively. All the compositions from both methods in the present work showed pyrochlore-free XRD scans at calcination temperatures at above 900 °C. These experiments indicate that for both methods as the concentration of the PZN phase increased the calcination temperature must be increased in order to obtain phase-pure perovskite. Most processing procedures for PZN-based ceramics make use of calcination temperatures in excess of 900 °C. The experiments in this study suggest that the conventional method helps to stabilize the perovskite phase compared with the columbite method. Moreover the perovskite formation temperature for the conventional method was significantly lower than that of the columbite method. The difference in the formation temperatures was presumably due to a different reaction path to the formation of the perovskite phase for the two methods.

Fig. 3 shows the XRD patterns of xPZN–$(1-x)$PZT ceramics sintered at 1200 °C for 2 h to illustrate the change in crystal structure as a function of composition for both processing methods. The results indicate that, for the same composition, different processing methods may develop a perovskite structure with different symmetries. Fig. 4 shows the evolution of the (2 0 0) peak as a function of composition and processing method. The $PbZrO_3$–$PbTiO_3$ phase diagram predicts that at room temperature $Pb(Zr_{1/2}Ti_{1/2})O_3$ falls within the tetragonal phase field near the MPB. The XRD patterns with low PZN concentration show strong (2 0 0) peak splitting which is indicative of the tetragonal phase. As the PZN concentration increased, for both processing methods the (2 0 0) transformed to a single peak which suggests rhombohedral symmetry.

Fig. 5(a–d) show the XRD patterns for both processing methods in the vicinity of the MPB at $x = 0.2$ and 0.3 over the range $2\theta = 43$–45.5. The data shows the appearance of a triplet peak due to the superposition of the tetragonal and rhombohedral (2 0 0) peaks. The columbite prepared samples show a relatively sharp transition between the tetragonal phase at $x = 0.2$ to the rhombohedral phase at $x = 0.3$. In the conventional prepared samples, while the $x = 0.2$ samples shows the presence of the tetragonal phase there is a strong co-existence of both phases for the $x = 0.3$ pattern.

While Fan and Kim report a phase boundary in the same PZN–PZT system at the composition $x = 0.5$, [13] there are no prior reports of the phase boundary observed in this work between $x = 0.2$ and 0.3.

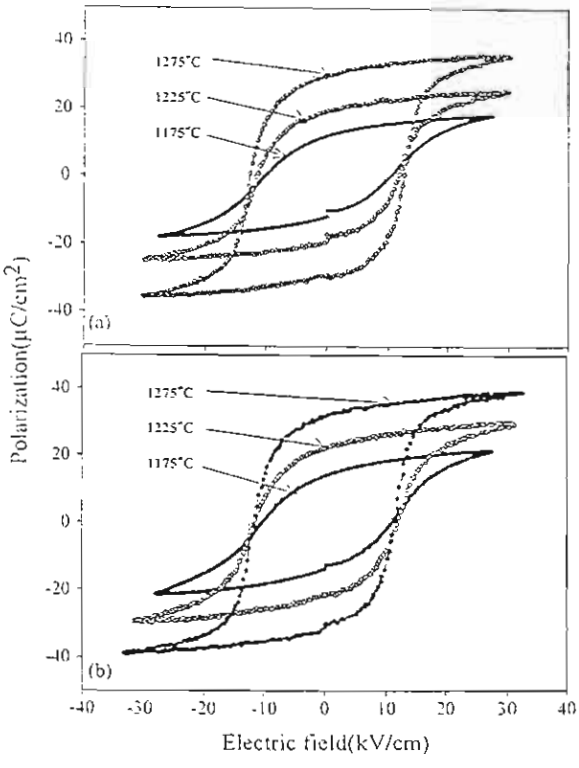

Fig. 6. Room temperature P–E hysteresis as a function of sintering temperature for 0.2PZN—0.8PZT: (a) columbite method; (b) conventional method.

3.2. Effect of sintering temperature and post-sinter annealing

The effect of sintering temperature on the properties was assessed by the polarization–field (P–E) measurements. Fig. 6 shows the results for the composition of $x = 0.2$ for both methods at different sintering temperatures. Ceramics from both methods showed normal ferroelectric behavior with a rectangular loop. The remanent polarization, P_r, was observed to increase with increasing sintering temperature. This is probably due to the smaller grain size at low sintering temperature. This may result in a smaller domain size, and furthermore domain wall motion in smaller grains is subject to stricter constraints [1]. Strong internal stresses are expected in fine-grained specimens and polarization switching is thus greatly suppressed. This was accompanied by the decrease in the coercive field with increasing sintering temperature [14].

For compositions with $x > 0.3$, the P_r decreased at high sintering temperatures. For the composition of $x = 0.1$, rectangular hysteresis loops were not observed even at a sintering temperature of 1250 °C, as shown in Fig. 7. It has been reported that post-sinter annealing is effective in improving the dielectric and ferroelectric properties of lead-based ceramics [15]. Specimens for each composition sintered at the lowest temperature (1175 °C) were annealed at 1250 °C for 6 h. Indeed, significant improvements of

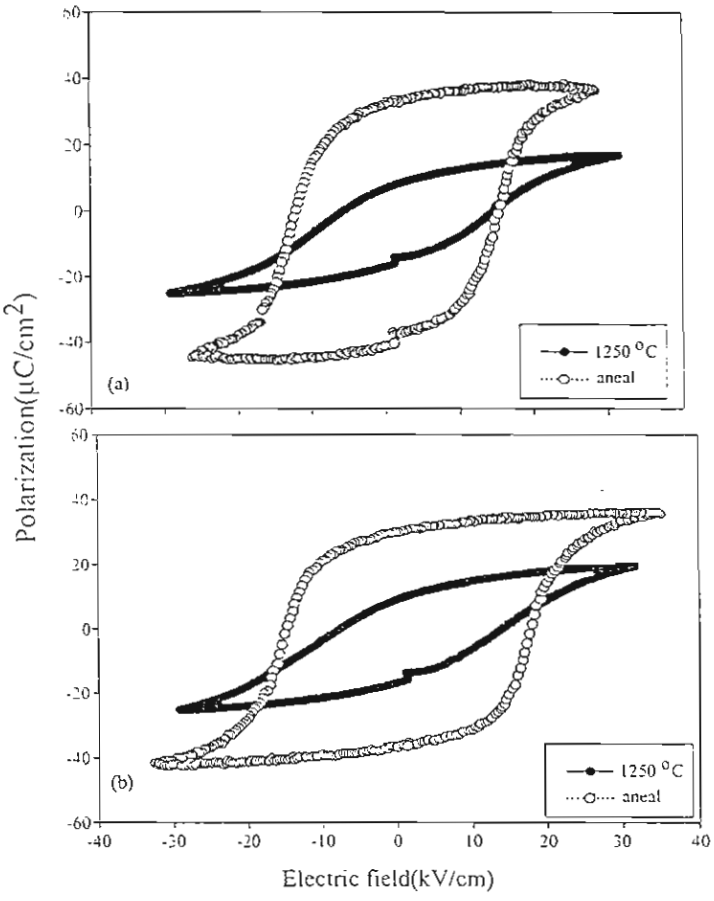

Fig. 7. Effect of post-sinter annealing on the P–E hysteresis for 0.1PZN–0.9PZT ceramics: (●) sintered at 1250 °C, (○) sintered at 1175 °C and annealed at 1250 °C for 6 h: (a) columbite method, (b) conventional method.

the ferroelectric properties were demonstrated (see Fig. 7 for the 0.1PZN–0.9PZT). The results on other compositions are listed Table 1. Very limited improvements were observed for the $x = 0.5$ composition because the higher PZN content required lower sintering temperatures, thus limiting the efficacy of the annealing step. It has been suggested that PZT ceramics should be sintered at temperatures above 1200 °C [8,9,16] and PZN-based ceramics should be sintered below this temperature [17] to achieve the best combination of density and properties. This explains the results in our present study where increasing molar fraction of PZN directly led to a lower sintering temperature. Therefore, post-sinter heat treatment is not necessary for ceramics with high PZN content.

Based on these ferroelectric measurements, the optimum sintering conditions for compositions of $x = 0.3$, 0.4, and

Table 1
Post-sinter annealing effects on the remanent polarization P_r and saturation polarization P_s in xPZN–$(1-x)$PZT ceramics sintered at 1175 °C for 2 h and annealed at 1250 °C for 6 h

x	xPZN–$(1-x)$PZT							
	Columbite method				Conventional method			
	P_r		P_s		P_r		P_s	
	Sintered	Annealed	Sintered	Annealed	Sintered	Annealed	Sintered	Annealed
0.1	7.6	37.1	15.8	42.9	9.4	34	19.0	39.2
0.2	14.6	36.1	20.6	38.9	13.8	31.5	21.4	35.0
0.3	31.9	30.4	37.2	33.5	23.8	20.0	27.9	23.2
0.4	32.3	30.6	35.8	34.5	30.5	23.2	35.0	28.7
0.5	35.6	36.4	40.4	42.1	29.4	29.5	34.5	34.9

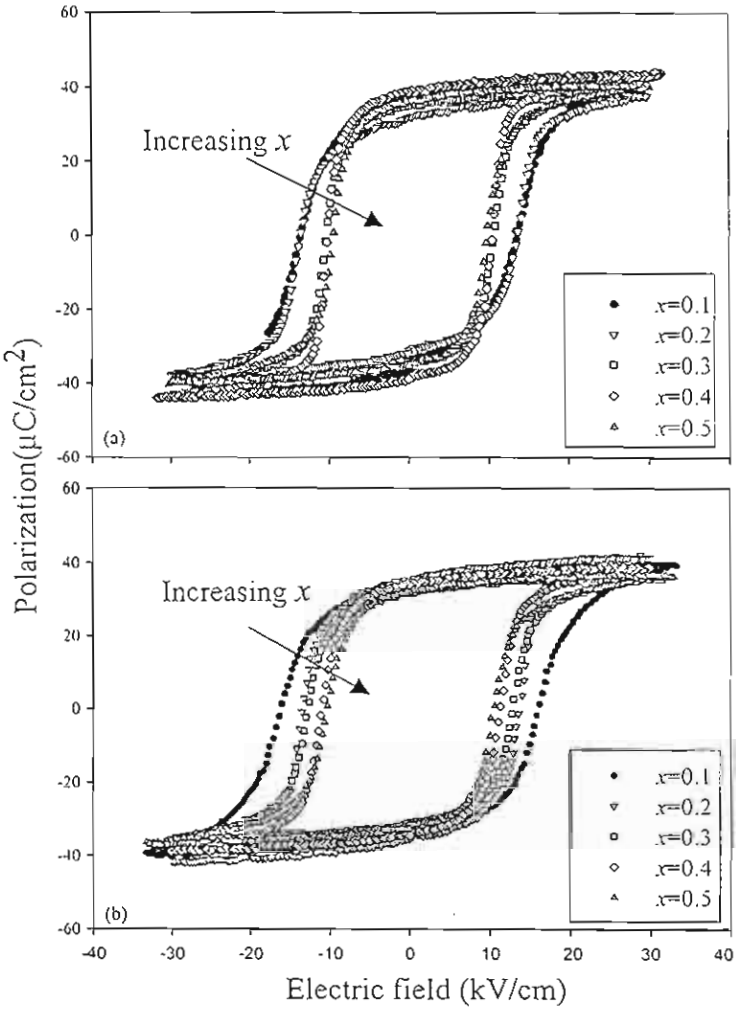

Fig. 8. Effect of composition (x) on the P–E hysteresis loops for xPZN–$(1-x)$PZT processed at the optimum processing conditions: (a) columbite method; (b) conventional method.

0.5 is 1200 °C for 2 h. The sintering process was not completed at these sintering conditions for compositions of $x = 0.1$ and 0.2 and therefore post-sinter annealing at 1250 °C for 6 h is necessary for improvement of ferroelectric properties. Further characterization techniques and comparisons, which are described in the following section, were made on these as-sintered specimens (for $x = 0.3$, 0.4, 0.5) and annealed specimens (for $x = 0.1$, 0.2) because they were found to have the optimum ferroelectric properties.

3.3. Effect of processing method on the phase transformation

The P–E ferroelectric property measurements for the specimens processed at optimum conditions are summarized in Fig. 8. It is shown that there is no significant difference in P_r across the composition range. However, the coercive field E_c is well dispersed over the compositions. This is further illustrated in Fig. 9. Compared to the conventional method, columbite method produces a slightly higher remanent polarization P_r as well as a lower coercive field E_c. Both methods show a considerable decrease in E_c with increasing molar fraction of PZN. However, the variation in ceramics prepared by conventional method is gradual and continuous, while an abrupt change in E_c occurs in ceramics processed by the columbite method, as indicated in Fig. 9(b). Combined with the XRD examination described in Section 3.1, the change in E_c clearly indicates a phase transformation over that compositional range. Therefore, an MPB separating the tetragonal phase (PZT-rich) from the pseudo-cubic rhombohedral phase (PZN-rich) exists between $x = 0.2$ and 0.3. Also consistent with the XRD data, the phase transformation in ceramics prepared by the conventional method is smeared out due probably to the chemical heterogeneities. These results lead to the conclusion that the columbite method produces ceramics with bet-

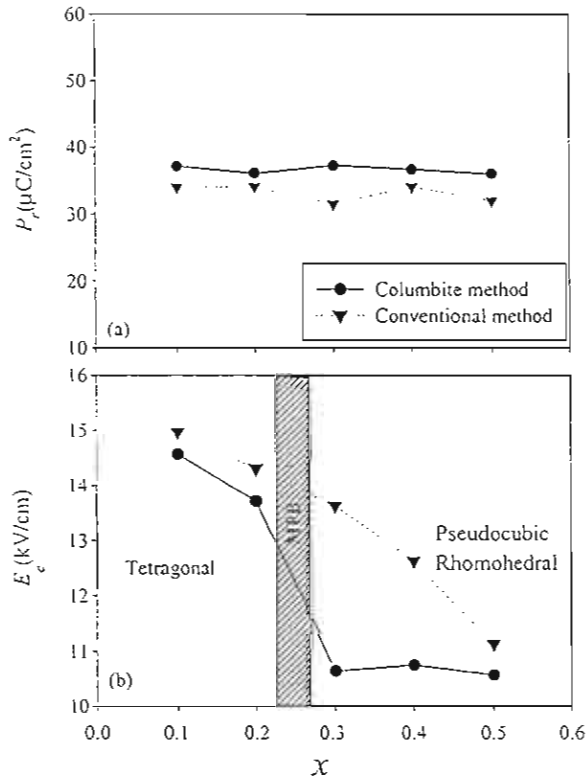

Fig. 9. Variation of remanent polarization P_r and coercive field E_c with composition for xPZN–(1 − x)PZT ceramics: (a) remanent polarization; (b) coercive field.

ter ferroelectric properties even though this method seems initially be prone to form pyrochlore phase. These results underscore the important role that B-site ordering plays in determining the thermodynamic stability and electrical properties of perovskite ferroelectrics.

4. Conclusion

A comparison between the conventional method and the columbite method was made in the preparation of ceramics within the solid solution of xPZN–(1 − x)PZT over a wide range in composition (x = 0.1–0.5). The optimum processing conditions for excellent ferroelectric properties were identified. Based on the X-ray structural analysis and ferroelectric property measurements, the following conclusions can be drawn:

1. Compared to the columbite method, the conventional method requires lower calcination temperature to eliminate the pyrochlore phase formation. Increasing in the molar fraction of PZN requires increased calcination temperatures in order to achieve phase-pure perovskite. At 900 °C, all the compositions for both methods can be converted to single-phase perovskite.
2. In ceramics sintered from columbite method prepared powders, a sharp transition from tetragonal to pseudo-cubic rhombohedral phase was evidenced by the XRD analysis. Thus, an MPB exists between x = 0.2 and 0.3. However, such a phase transformation is diffuse in ceramics prepared by the conventional method.
3. The results from XRD analysis are consistent with the ferroelectric property measurements. An abrupt change in coercive field, E_c, was observed in ceramics prepared by the columbite method at the same composition range of x = 0.2–0.3. In contrast, gradual change was found in ceramics prepared by the conventional method.
4. Lower sintering temperatures were required for compositions with an increasing molar fraction of PZN. For the x = 0.1 and 0.2 compositions, sintering at 1250 °C for 2 h was observed to produce inferior ferroelectric properties and post-sinter annealing was required to achieve excellent ferroelectric properties.
5. For both methods, no considerable variation of the remanent polarization with compositions was observed. However, the coercive field was observed to decrease with increasing amount of PZN. The columbite method was found to produce ceramics with better ferroelectric properties with higher remanent polarization and lower coercive field.

Acknowledgements

The authors are grateful to The Thailand Research Fund, Graduate School of Chiang Mai University, and the Ministry of University Affairs for financial support.

References

[1] A.J. Moulson, J.M. Herbert, Electroceramics: Materials, Properties, Applications, Chapman and Hall, New York, 1990.
[2] K. Uchino, Solid State Ionics 108 (1998) 43.
[3] K. Uchino, Ferroelectrics 151 (1994) 321.
[4] V.A. Bokov, I.E. Mylnikova, Sov. Phys-Solid state 2 (1960) 2428.
[5] T.R. Shrout, A. Halliyal, Am. Ceram. Soc. Bull. 66 (1987) 704–711.
[6] S.L. Swartz, T.R. Shrout, Mater. Res. Bull. 17 (1982) 1245–1250.
[7] Y. Matsuo, H. Sasaki, S. Hayakawa, F. Kanamaru, M. Koizumi, J. Am. Ceram. Soc. 52 (1969) 516–517.
[8] A. Halliyal, U. Kumar, R.E. Newham, L.E. Cross, Am. Ceram. Soc. Bull. 66 (1987) 671–676.
[9] M. Villegas, A.C. Caballero, C. Moure, R.E. Newham, J. Am. Ceram. Soc. 83 (2000) 141.
[10] H. Fan, H.-E. Kim, J. Mater. Res. 17 (2002) 180.
[11] N. Vittayakorn, G. Rujijanagul, T. Tunkasiri, X. Tan, D.P. Cann, J. Mater. Res. 18 (2003) 2882–2889.
[12] S.-Y. Chen, C.-M. Wang, S.-Y. Cheng, Mater. Chem. Phys. 49 (1997) 70–77.
[13] H. Fan, H.-E. Kim, J. Appl. Phys. 91 (2002) 317.
[14] U. Kenji, Ferroelectric Devices, Marcel Dekker Inc., 2000.
[15] F. Xia, X. Yao, J. Mater. Sci. 36 (2001) 247.
[16] J.R. Belsick, A. Halliyal, U. Kumar, R.E. Newnham, Am. Ceram. Soc. Bull. 66 (1987) 664.
[17] A. Halliyal, A. Safari, Ferroelectrics 158 (1994) 295–300.

เอกสารหมายเลข 1.10

ELSEVIER

Materials Science and Engineering B 108 (2004) 223–226

MATERIALS SCIENCE & ENGINEERING B

www.elsevier.com/locate/mseb

Effects of heat treatment on structural evolution and morphology of $BaTi_5O_{11}$ powder synthesized by the sol–gel method

S. Tangjuank, T. Tunkasiri*

Department of Physics, Faculty of Science, Chiang Mai University, Chiang Mai 50200, Thailand

Received 17 November 2003; accepted 26 November 2003

Abstract

$BaTi_5O_{11}$ powder was successfully prepared and characterized by the sol–gel method. The mechanisms of $BaTi_5O_{11}$ formation were studied by the fourier transform infrared spectroscopy (FTIR). The IR absorption peaks confirm the existence of a substitution reaction with the chelating reagent corresponding to different modes of vibration characteristic of the acetate group. The X-ray diffraction (XRD) results showed that the formation of single-phase monoclinic $BaTi_5O_{11}$ began at 700 °C and were stable up to 1100 °C in air. The particle sizes observed from scanning electron microscopy (SEM) are about 100 nm for a calcination temperature at 700 °C and 600 nm at 1100 °C.

Keywords: $BaTi_5O_{11}$ powder; Sol–gel method; FTIR; Calcination temperature

1. Introduction

Now a days, microwave communication systems have a great need for wireless communication such as personal communication, global positioning systems, etc. Dielectric resonator ceramics have been widely exploited in these systems because of their high dielectric constants, high quality factors, low dielectric loss, and near-zero temperature coefficients of resonant frequency [1]. $BaTi_5O_{11}$ has recently received much attention after Ritter et al. [2] used O'Bryan's et al's. [3] data to point out that single-phase $BaTi_5O_{11}$ ceramic might have superior properties suitable for microwave applications. A number of researchers tried to produce single-phase $BaTi_5O_{11}$ powder using several methods. O'Bryan and Thomson [4] prepared $BaTi_5O_{11}$ using solid state reaction but the technique could not yield single-phase material. Chemical processes were however successfully employed to obtain single-phase $BaTi_5O_{11}$. Fukui et al. [5] and Ritter et al. [2] reported that $BaTi_5O_{11}$ powder could be obtained by preparing via the alkoxide method at the calcination temperatures between 700 and 1100 °C. Other chemical preparation methods are still being searched in order to obtain single-phase and fine powder of $BaTi_5O_{11}$. Since these methods were successfully employed to prepare single-phase barium titanate ($BaTiO_3$) powder [6–8] and barium tetratitanate ($BaTi_4O_9$) powder [9]. Javadpour and Eror [10] prepared $BaTi_5O_{11}$ by liquid-mix technique of barium carbonate with tetraisopropyl titanate in an ethylene glycolcitric acid solution, while Lu et al. [7] used sol–gel process of barium granules with titanium ethoxide in nitric acid solution. Single-phase $BaTi_5O_{11}$ were obtained at 700–1100 °C in both cases. However, the reaction mechanisms, structural evolution and morphology of $BaTi_5O_{11}$ powder due to heat treatment are still not clearly understood. In this work, the sol–gel process was employed to prepare $BaTi_5O_{11}$ powder using barium oxide and titanium(IV) isopropoxide in acetic acid solution. Various techniques were used to characterize the synthesized powder.

2. Experimental

Barium oxide (BaO), titanium(IV) isopropoxide ($C_{12}H_{28}O_4Ti$), concentrated acetic acid ($C_2H_4O_2$), methanol (CH_3OH), and dried *n*-butanol ($CH_3(CH_2)_3OH$) were used as starting compounds. To form barium methoxide, BaO (0.1 mol) was dissolved in 30 cm^3 acetic acid and methanol (50 cm^3) was used as a solvent. Dried *n*-butanol (80 cm^3) was added to 50 cm^3 titanium(IV) isopropoxide to obtain a

* Corresponding author. Tel.: +66-53-943376; fax: +66-53-357512.
E-mail address: tawee@chiangmai.ac.th (T. Tunkasiri).

stable Ti-solution. The mixed solution of barium and titanium was heated at 80 °C on a hot plate with continuous stirring for 1 h. After that, 20 cm^3 of distilled water was added to the solution to form gel. The gel was dried in an oven at 110 °C for 24 h during which the white powder precursor was formed. The dried precursor was ground and heated in air at temperatures ranging from 500 to 1200 °C in steps of 100 °C. The annealing time at each temperature was 4 h to completely yield $BaTi_5O_{11}$ phase. The differential scanning calorimetry (DSC) and the thermogravimetic analysis (TGA) were used for the analysis of phase transformations of dried powders. In these analytical techniques, the samples were heated up to 1000 °C with a heating rate of 5 °C/min. Phase evolution of the calcined powders was carried out by X-ray diffraction (XRD). The morphology of the calcined powders was studied using scanning electron microscopy (SEM). The reaction mechanisms related to the calcination processes were studied using the fourier transform infrared spectroscopy (FTIR) at room temperature in the KBr plate method. [11].

3. Results and discussion

The DSC and TGA data are shown in Fig. 1. The results suggested that the decomposition occurred in three different weight loss steps. The first endothermic peak in the DSC curve was due to the vaporization of water at the temperatures below 100 °C and crystal water at below 300 °C, and

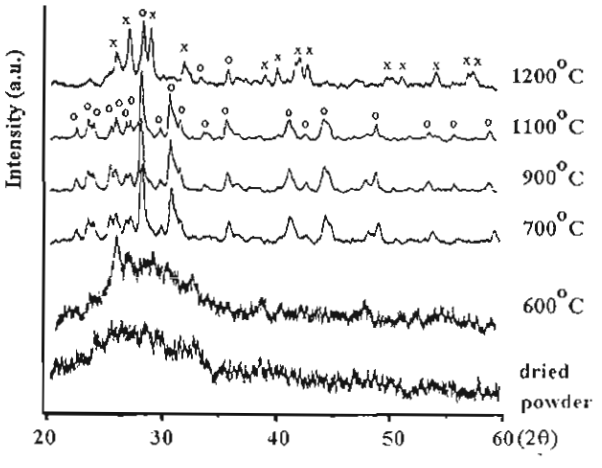

Fig. 2. XRD powder patterns of the dried precursor of $BaTi_5O_{11}$ calcined at various temperatures for 4 h (o: $BaTi_5O_{11}$ and x: $Ba_2Ti_9O_{20}$).

corresponded to 12% weight loss in the TGA curve. The second peak, corresponding to an endothermic peak accompanied by weight loss of 20.5%, was observed from 250 to 600 °C. This is related to the decomposition of the acetate groups and organic derivatives into carbonate which barium carbonate took place. Finally, the exothermic peak between 600 and 750 °C was probably due to the beginning of $BaTi_5O_{11}$ formation which can occur by the decomposition of the intermediate carbonate phase without any weight change. X-ray diffraction analysis (Fig. 2) showed that the dried powder and powders heated below 700 °C

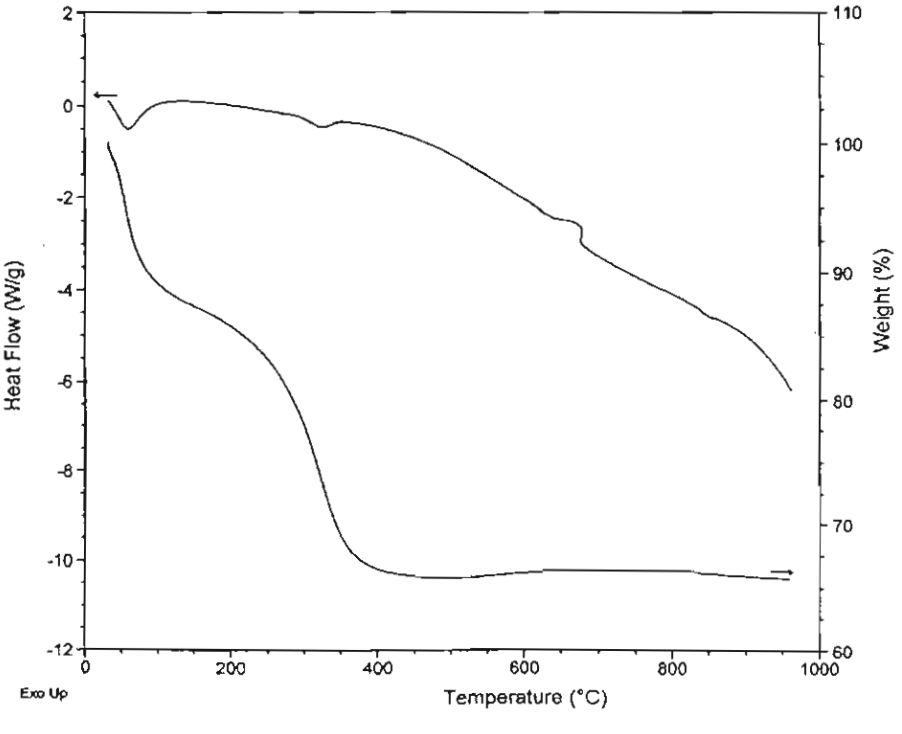

Fig. 1. DSC and TGA thermograms of the dried precursor of $BaTi_5O_{11}$.

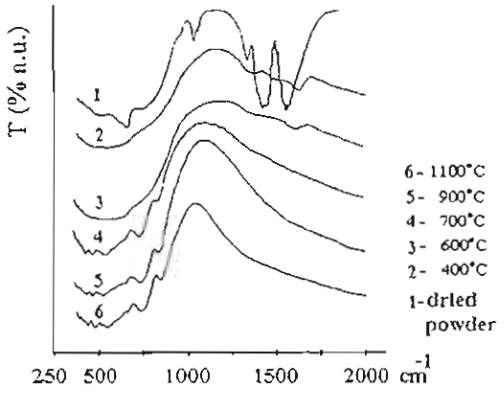

Fig. 3. FTIR spectra of the dried precursor of $BaTi_5O_{11}$ calcined at different temperatures: 110 °C (spectrum 1); 400 °C (spectrum 2); 600 °C (spectrum 3); 700 °C (spectrum 4). 900 °C (spectrum 5); 1100 °C (spectrum 6).

were amorphous. This amorphous phase was converted to single-phase crystalline $BaTi_5O_{11}$ only after heat treatment at 700 °C until 1100 °C. The phase analysis was based on the available data from joint committee on powders diffraction standard (JCPDS), card no. 35-0805. Heat treatment at 1200 °C for 4 h resulted in the crystallization of $BaTi_5O_{11}$ and $Ba_2Ti_9O_{20}$ phases. The results agree with those obtained by Lu et al. [7] and Javadpour and Eror [10]. However, the samples calcined at 1200 °C, Javadpour and Eror [10] obtained $BaTi_5O_{11}$ and $BaTi_4O_9$ (Table 1). Some FTIR spectra of the $BaTi_5O_{11}$ powders calcined at various temperatures are shown in Fig. 3. The absorption peaks located at 1552, 1414, 1323, 1020, and 645 cm^{-1} for the dried precursor (110 °C) corresponded to the vibration modes of the acetate group [12]. This agrees well with the reports of Woei-Kwo and Yong-Chien [13] and Xionghui et al. [14] for $BaTiO_3$ and $PbTiO_3$, respectively. Both groups employed acetate route. At 400–600 °C, the similar spectra showed up at 1342 and 1610 cm^{-1} whereas the peaks at 1552, 1414, 1323, 1020, and 645 cm^{-1} disappeared. This may be due to decomposition of the acetate group and can be attributed to the vibration modes of the ionic carbonate [12]. At 700–1100 °C, the peaks of 1342 and 1610 cm^{-1} disappeared and the infrared (IR) peaks were found at 835 and 729 cm^{-1}. This indicates that the carbonate group decomposed and the reaction occurred between barium carbonate and titanium oxide to form $BaTi_5O_{11}$ powder. The results are confirmed by DSC, TGA, and XRD characterizations as described earlier. Fig. 4 shows the particle morphology of $BaTi_5O_{11}$ powder after calcination at 800 and 1100 °C. The calcined powders

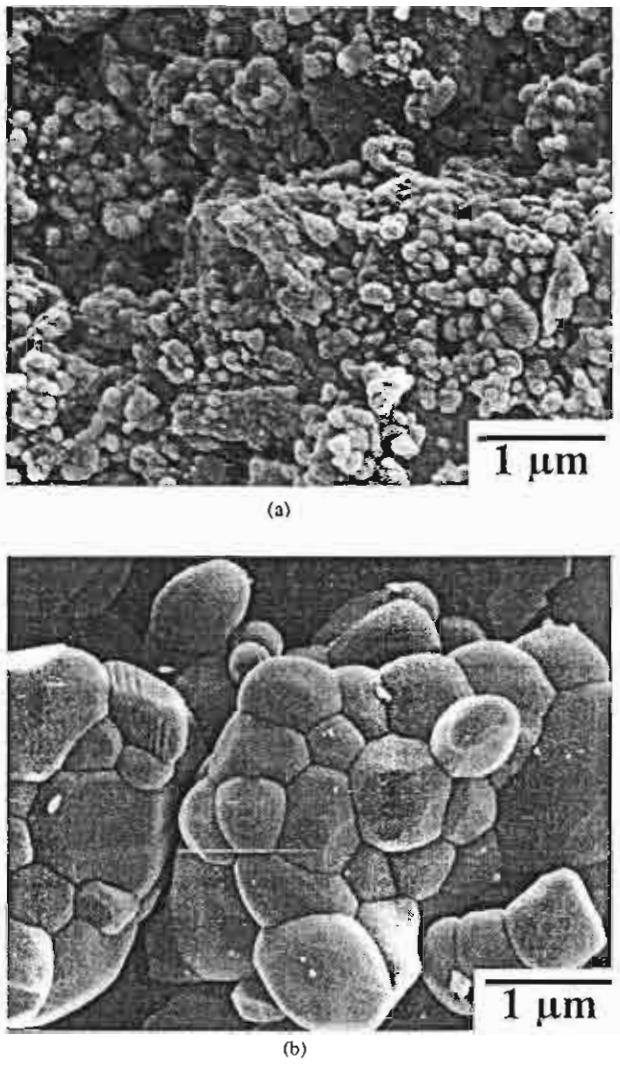

Fig. 4. The scanning electron micrographs of $BaTi_5O_{11}$ powders calcined at (a) 800 °C and (b) 1100 °C.

Table 1
Results of phases analysis of Ba:Ti = 1:5 at various calcination temperatures

Calcination temperature (°C)	Phases present		
	This work	Lu et al. [7]	Javadpour and Eror [10]
700	$BaTi_5O_{11}$	$BaTi_5O_{11}$	$BaTi_5O_{11}$
800	$BaTi_5O_{11}$	–	–
850	–	$BaTi_5O_{11}$	$BaTi_5O_{11}$
900	$BaTi_5O_{11}$	–	–
1000	$BaTi_5O_{11}$	$BaTi_5O_{11}$	$BaTi_5O_{11}$
1100	$BaTi_5O_{11}$	$BaTi_5O_{11}$	$BaTi_5O_{11}$
1200	$BaTi_5O_{11}$ + $Ba_2Ti_9O_{20}$	$BaTi_5O_{11}$ + $Ba_2Ti_9O_{20}$	$BaTi_5O_{11}$ + $BaTi_4O_9$

consisted of fine particles and the agglomerates were almost round in shape and were slightly bigger for higher calcination temperatures. With increasing the calcination temperature, the amount of agglomeration also increased. The occurring of aggregated particles during heat treatment resulted from a dense and rigid resin intermediate of acetic acid. The particle sizes were estimated to be in the range of 100–600 nm for the calcination temperatures from 700 to 1100 °C.

4. Conclusion

$BaTi_5O_{11}$ powder could be synthesized using the sol–gel method. Analysis by DSC, TGA, and XRD confirmed that the stable single-phase of $BaTi_5O_{11}$ occurred at the calcination temperatures ranging from 700 to 1100 °C, whereas at 1200 °C, the $BaTi_5O_{11}$ phase converted into a mixture of $BaTi_5O_{11}$ and $Ba_2Ti_9O_{20}$. The IR absorption peaks confirmed the existence of a substitution reaction with the chelating reagent, corresponding to different modes of vibration characteristic of the acetate group. The morphology of the $BaTi_5O_{11}$ powder indicated hard aggregates of fine particles which were almost round in shape. The particle sizes were estimated to be in the range of 100–600 nm and was found to increase with increasing calcination temperature.

Acknowledgements

The authors would like to express their sincere thanks to the Thailand Research Fund for the financial support.

References

[1] K. Plourde, C.L. Ren, IEEE Trans. Microwave Theory Tech. 29 (1981) 754.
[2] J.J. Ritter, R.S. Roth, J.E. Blendell, J. Am. Ceram. Soc. 69 (1986) 155.
[3] H.M. O'Bryan, J.K. Plourde, J. Thomson, D.F. Linn, J. Am. Ceram. Soc. 57 (1974) 450.
[4] H.M. O'Bryan, J. Thomson, J. Am. Ceram. Soc. 58 (1975) 454.
[5] T. Fukui, C. Sakurai, M. Okuyama, J. Mater. Res. 7 (1992) 192.
[6] T. Tunkasiri, G. Rujijanagul, J. Mater. Sci. Lett. 13 (1994) 165.
[7] H.C. Lu, L.E. Burkhart, G.L. Schrader, J. Am. Ceram. Soc. 76 (1991) 968.
[8] H.S. Potdar, S.B. Deshpade, A.S. Deshpande, Y.B. Khollam, A.J. Patil, S.D. Pradhan, S.K. Date, Int. J. Inorg. Mater. 3 (2001) 613.
[9] A. Cuneyt Tas, J. Am. Ceram. Soc. 82 (1999) 1582.
[10] J. Javadpour, N.G. Eror, J. Am. Ceram. Soc. 71 (1988) 206.
[11] K. William, Organic Spectroscopy, second ed., Macmillam Education Ltd., London, 1980, p. 38.
[12] K. Nakamoto, Infrared and Raman Spectra of Inorganic and Coordination Compounds, fifth ed., Wiley, New York, 1997, p. 75.
[13] K. Woei-Kwo, L. Yong-Chien, J. Mater. Lett. 29 (1994) 5625.
[14] Z. Xionghui, L. Yayan, W. Xiugan, Y. Wenchun, W. Lan, G. Hongxia, Mater. Chem. Phys. 77 (2002) 209.

เอกสารหมายเลข 1.11

JOURNAL OF MATERIALS SCIENCE 39 (2004) 1831–1835

Microstructures and positive temperature coefficient resistivity (PTCR) characteristics of high silicon addition barium-strontium titanate ceramics

P. BOMLAI, N. SIRIKULRAT, T. TUNKASIRI
Department of Physics, Faculty of Science, Chiang Mai University 50200, Thailand
E-mail: scphi003@chiangmai.ac.th

Ferroelectric barium titanate ($BaTiO_3$) shows a high intrinsic resistivity of more than 10^{10} Ω-cm when prepared in an oxidizing atmosphere [1, 2]. When polycrystalline $BaTiO_3$ ceramics are doped with higher valence cations such as La^{3+}, Y^{3+}, Nb^{5+} or Ta^{5+}, semiconducting properties and the positive temperature coefficient of resistivity (PTCR) effect can be obtained [1–5]. These effects involve a nonlinear change in the resistivity with temperature occurring around 120–130 °C which is known as the Curie temperature (T_C) [6, 7]. The T_C of $BaTiO_3$ can be shifted to lower temperatures by substituting barium with strontium [8–10]. The solid solution of $(Ba,Sr)TiO_3$ materials has, therefore, been widely used for fabrication of positive temperature coefficient (PTC) thermistors with various Curie temperatures [8]. The most acceptable model to explain the temperature dependent conduction mechanism in the PTCR barium titanate ceramics was proposed by Heywang and Jonker [7, 8, 11–13]. Above the Curie temperature, Heywang suggested that the formation of a Schottky barrier is caused by the presence of electron traps. Below the Curie temperature, Jonker proposed that the highly conductive semiconductor results from the charge compensation due to the polarized charges at the grain boundaries [11, 13].

In recent PTCR processing, excess titanium and silicon are commonly used to create a liquid phase and reduce the sintering temperature [14]. The eutectic temperature resulting from excess titanium is around 1320 °C. After addition of silicon, this temperature decreases to approximately 1260 °C [15]. Cheng *et al.* [11] prepared $Ba_{0.8}Sr_{0.2}TiO_3$ ceramics by adding 12.5 mole percent aluminum, silicon, and titanium (so called AST) with a ratio of 4:9:3. After sintering at 1350 °C for 1.5 h, a uniformly small granular structure was obtained with an increase in resistivity of 5 orders of magnitude (from 10^3 to 10^8 Ω-cm) at the Curie temperature. Many investigations have been

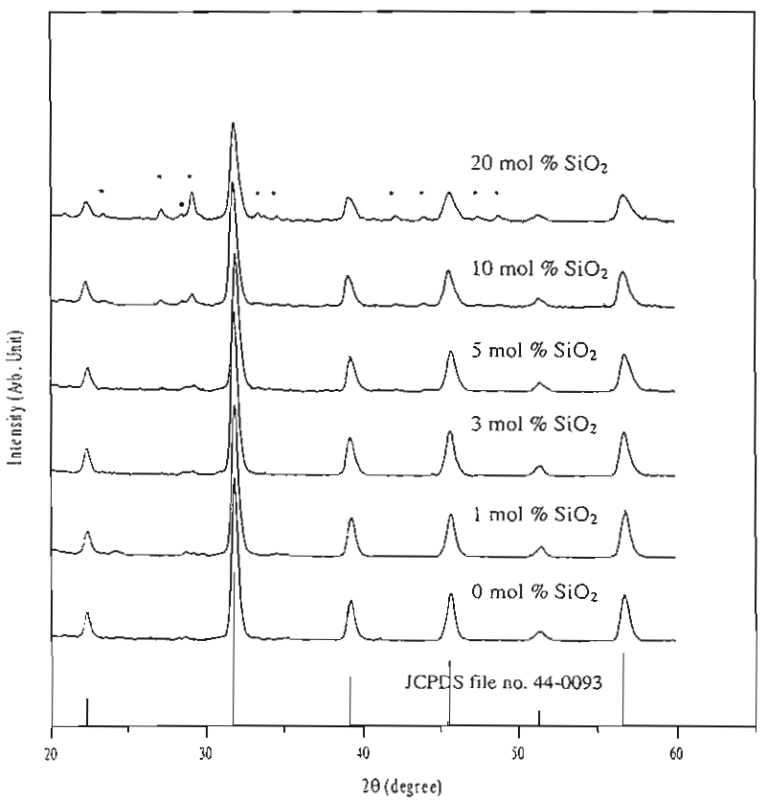

Figure 1 X-ray diffractograms of powders with various silicon content when calcined at 1100 °C. * = $Ba_2TiSi_2O_8$; · = $Ba_6Ti_{17}O_{40}$.

0022–2461

undertaken to study the effects of silicon additions to the PTCR ceramics [2, 14, 16]. However, the microstructures were found to be inhomogeneous due to the considerable difference in the densities of barium titanate and silicon [16]. Most of the investigations were performed with small (1–4 mol%) silicon additions [2, 14, 16]. The microstructural evolution might be significantly different when the liquid phase is incorporated in a larger proportion. The aim of the present investigation is, therefore, focused on studying the sintering behavior, microstructures and PTCR characteristics of antimony-doped $Ba_{0.8}Sr_{0.2}TiO_3$ materials with high levels of silicon addition.

Ceramic specimens in this work were prepared by the conventional mixed oxide process. The starting materials ($BaCO_3$, TiO_2, $SrCO_3$, Sb_2O_3, SiO_2, Aldrich Chemical Company, Inc.) were weighed according to the composition $Ba_{0.8}Sr_{0.2}TiO_3 + 0.15$ mol% $Sb_2O_3 + 1$ mol% $TiO_2 + xSiO_2$ where x varied from 0 to 20 mole percent. Antimony was used in order to form an n-type semiconductor and the amount of 0.15 mole percent was found to be optimum in these experiments. The excess of TiO_2 (1 mole percent) was added as a sintering aid to create a liquid phase during sintering so as to reduce the sintering temperature. The mixed powders were ball milled for 24 h and calcined at 1100 °C for 2 h in an alumina crucible using heating and cooling rates of 10 °C/min. In order to obtain compact pellets, the calcined powder was mixed with a small amount of polyvinyl alcohol (PVA) before being pressed into pellets and the specimens were sintered in air at 1275, 1285, 1300, 1350, 1400 and 1450 °C, for 2 h using heating and cooling rates of 5 °C/min. X-ray diffraction (Siemens D500) was employed to characterize the samples. The microstructures of the as-sintered surface were observed by scanning electron microscopy (Jeol JSM-840A). The resistivity change of the specimens as a function of temperature from room temperature to about 285 °C was measured using a digital multimeter (Agilent 34401A) and a D.C. power supply, after both sides of specimens were painted with silver paste.

Fig. 1 shows the X-ray diffractograms of the specimens with various silicon contents. Traces of fresnoite ($Ba_2TiSi_2O_8$) and $Ba_6Ti_{17}O_{40}$ are found, in addition to the major tetragonal barium-strontium titanate ($Ba_{0.77}Sr_{0.23}TiO_3$) phase. Peaks were identified on the basis of Joint Committee on Powder Diffraction Standards (JCPDS) data (card number 44-0093, 84-0924, 35-0817). Furthermore, it was found that the amount of the $Ba_2TiSi_2O_8$ increased with increasing silicon content. The presence of $Ba_2TiSi_2O_8$ and $Ba_6Ti_{17}O_{40}$ in these results is in agreement with those obtained by Abicht *et al.* [16] and Felgner *et al.* [17].

The developments of the microstructures of the specimens with various amounts of silicon are shown in Figs 2 and 3. It is obvious that the specimens show an abnormal grain growth and the size of the abnormally growing grains decreases with increasing sintering temperature as shown in Fig. 2. The grain structures of all the specimens when sintered above 1300 °C become rather uniform with sizes of 3–12 μm. The grain structures in the specimens with various amounts of silicon are shown in Fig. 3. It can be concluded that the grain size tends to decrease with increasing silicon contents, although the grain size of the sample with 5 mole percent of silicon (Fig. 2c) is slightly larger than that of the sample with 3 mole percent of silicon (Fig. 3b). In the specimen without silicon, the grains are irregularly sized and roughly equiaxed. However, in the specimens with higher silicon content (up to 20 mole percent) they

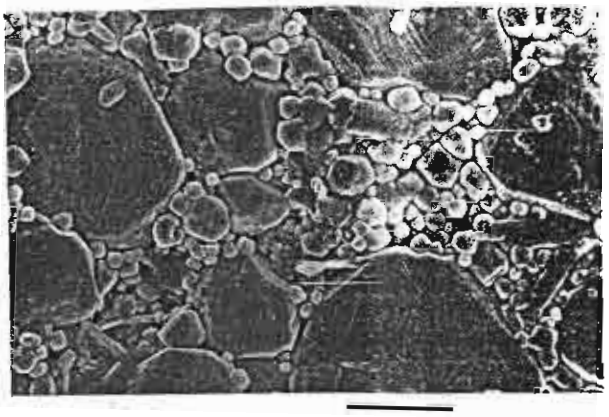

(a)

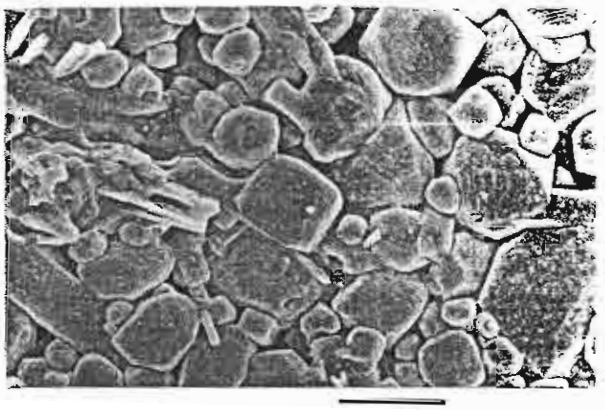

(b)

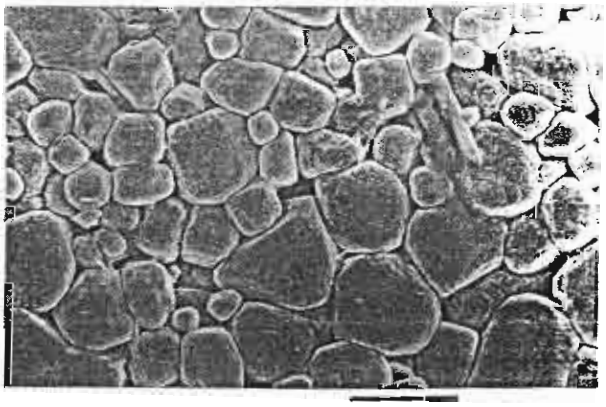

(c)

Figure 2 Microstructures of the specimens containing 5 mole percent of SiO_2 after sintering at various temperatures: (a) 1285 °C, (b) 1300 °C, and (c) 1350 °C.

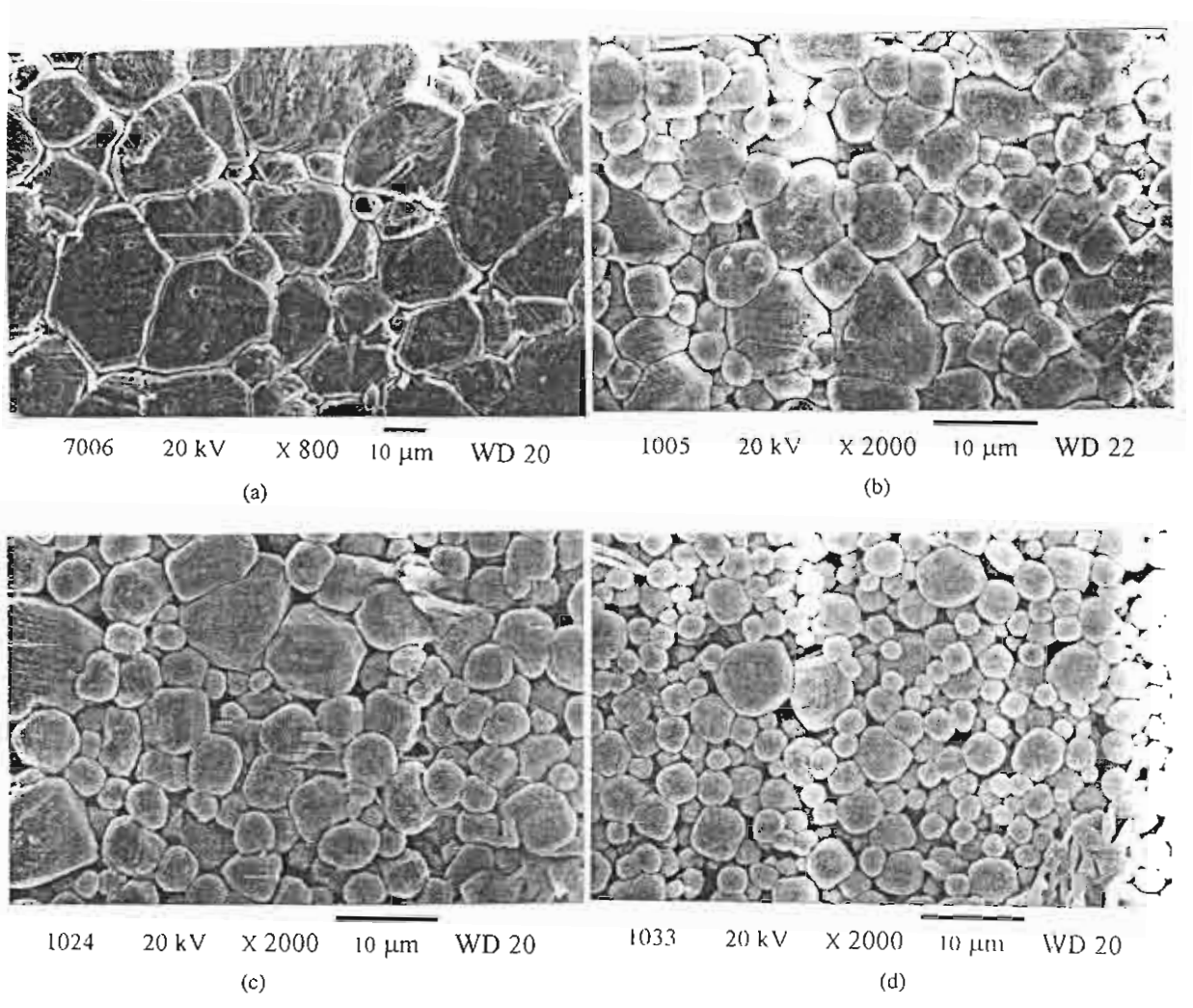

Figure 3 Microstructures of the specimens with various SiO_2 contents sintered at 1350 °C: (a) 0 mole percent SiO_2, (b) 3 mole percent SiO_2, (c) 10 mole percent SiO_2, and (d) 20 mole percent SiO_2.

become rounder and smaller with a grain size of about 2–5 μm as shown in Fig. 3d. The decrease in grain size with increasing silicon content is most probably caused by the large amount of liquid phase formed during sintering. Subsequently, the solid grains dissolve and become rounder in shape and smaller.

Porosity of the samples was also measured. It is found that porosity increases with decreasing sintering temperature but increases with increasing silicon content (Tables I and II).

The resistivity-temperature characteristics of the specimens prepared at various sintering temperatures and silicon contents are shown in Fig. 4. The Curie temperatures of these specimens are around 60 °C. It is also found that the room temperature resistivity (ρ_{RT}) varies as a function of silicon content and sintering temperature. The specimens without silicon cannot be sintered at temperatures lower than 1350 °C. The specimens sintered at 1350 °C show high resistivity. According to Liu and Roseman [14], however, low resistivity can be achieved by the addition of silicon to $Ba_{0.8}Sr_{0.2}TiO_3$. The resistivity at room temperature decreases to 10^1–10^4 Ω-cm in the specimens containing 1–20 mole percent silicon. The lowest room-temperature resistivity of about 25 Ω-cm can be obtained in the specimens containing 3 mole percent silicon when sintered at 1300 °C (see Fig. 5). The change in ρ_{RT} to higher values with decreasing sintering temperature is due to the coexistence of very large and very fine grains, as seen in Fig. 2a, As the silicon content increases so does the amount of $Ba_2TiSi_2O_8$ second phase (see Fig. 1). Consequently ρ_{RT} increases and there is a decrease in the magnitude of the PTCR characteristics (see Fig. 4d). Abicht *et al.* [16] found that the silicon containing second phases affect the electrical properties in an indirect manner. The resistivity changed over five orders of magnitude for the samples with 8–13% porosity (samples with 5–10 mole percent of silicon content, sintered at 1300 °C). Change of resistivity reduced to 2–3 orders

TABLE I Porosity, grain size and magnitude of PTCR effect in the specimens containing 5 mole percent SiO_2 sintered at various temperatures

Sintering temperature (°C)	% Porosity	Grain size (μm)	Order of magnitude of change in resistivity
1285	10.3	3.0–29.0	2.8
1300	8.6	3.5–12.0	4.7
1350	7.6	4.0–11.0	4.5

TABLE II Porosity, grain size and magnitude of PTCR effect in the specimens with various SiO_2 contents sintered at 1300 and 1350 °C

SiO_2 contents (mole %)	% Porosity		Grain size (μm)		Order of magnitude change in resistivity	
	1300 °C	1350 °C	1300 °C	1350 °C	1300 °C	1350 °C
0	–	5.2	–	10.0–30.0	–	–
3	8.4	5.8	3.0–11.0	3.1–10.0	3.8	3.3
10	13.2	11.1	3.2–10.0	3.6–7.0	5.0	3.1
20	20.8	16.9	2.7–5.5	2.3–5.5	3.2	2.0

if the porosity was less than 8%. It can be noted that the appropriate silicon addition brought a considerable enhancement of the PTCR characteristics. However, grain size, sintering temperature, porosity, and other second phases still affect the PTCR properties.

In conclusion, antimony-doped $Ba_{0.8}Sr_{0.2}TiO_3$ positive temperature coefficient resistors can be prepared below 1300-°C by the conventional mixed oxide process using silicon addition. The grains of the specimens sintered with a large addition of SiO_2 become rounder and smaller. However, $Ba_2TiSi_2O_8$ appeared as a second phase resulting in a decline in the electrical properties. The lowest room temperature resistivity of about 25 Ω-cm was obtained in the specimens containing 3 mole percent silicon, sintered at 1300 °C and the highest magnitude change in PTCR characteristics of

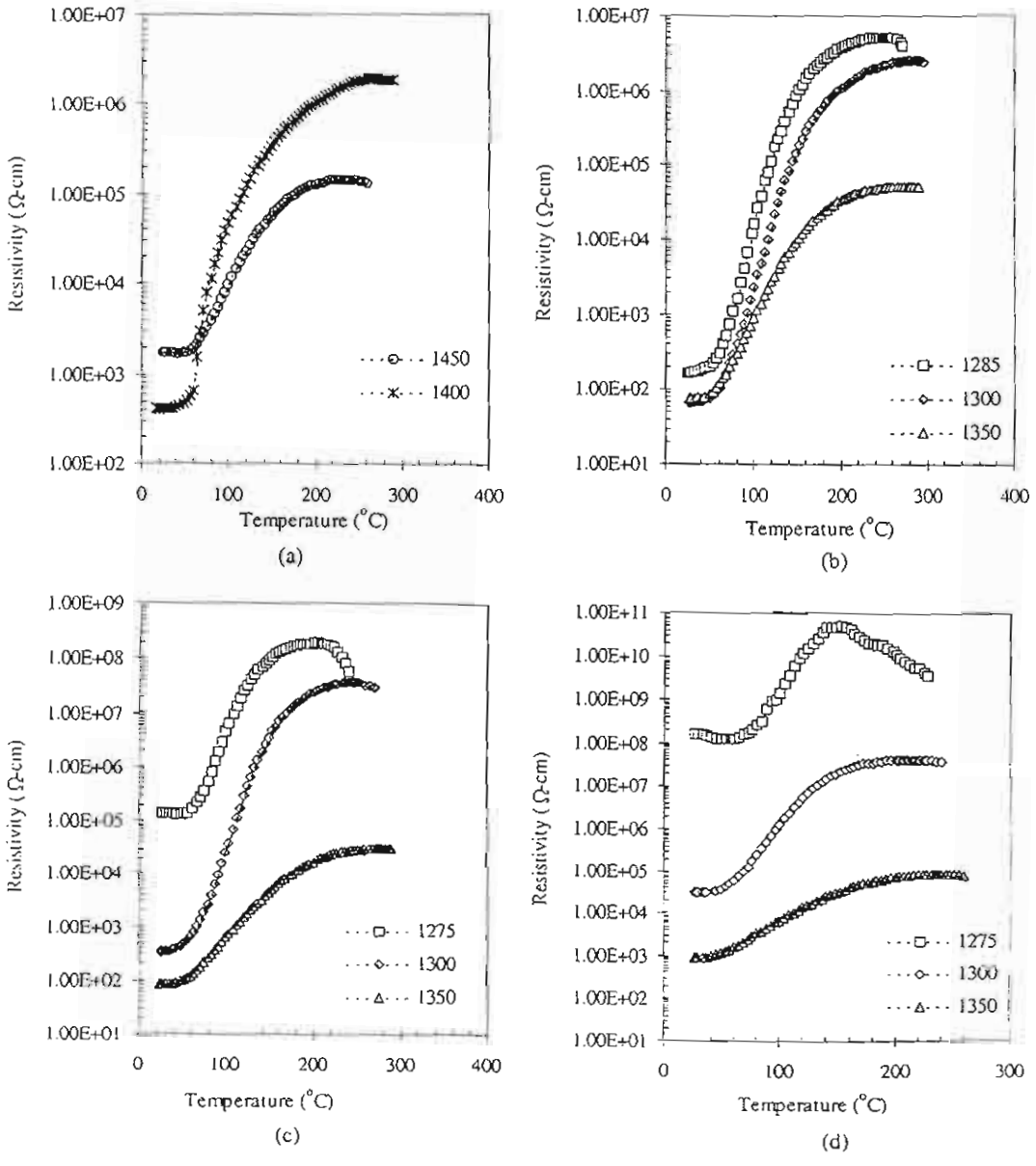

Figure 4 The resistivity-temperature (ρ-T) characteristics of the specimens with various sintering temperatures and SiO_2 contents: (a) 0 mole percent SiO_2, (b) 5 mole percent SiO_2, (c) 10 mole percent SiO_2, and (d) 20 mole percent SiO_2.

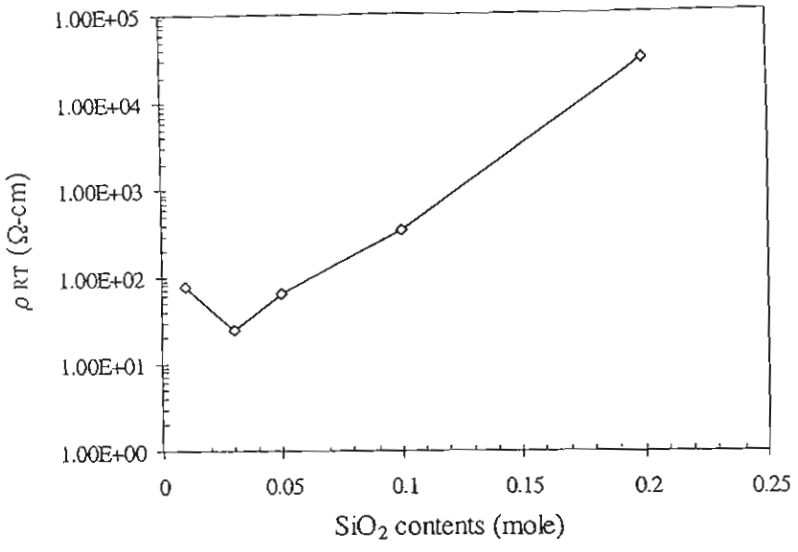

Figure 5 The room temperature resistivity of specimens with various amounts of SiO_2 sintered 1300 °C.

about 5 orders of magnitude was found in the specimens containing 5–10 mole percent silicon.

Acknowledgments

The authors would like to express their sincere thanks to the Thailand Research Fund, the National Metal and Materials Technology Center (MTEC) and the scholarship under the Ministry Staff Development Project of the Ministry of University Affairs, Thailand for the financial support. The authors would also like to thank Dr. L.D. Yu for his useful comments and correction on the manuscript.

References

1. R. D. ROSEMAN, J. KIM and R. C. BUCHANAN, in Proceeding of the 8th IEEE International Symposium on Application of Ferroelectrics (ISAF-92), 1992, edited by B. M. Kulwiki, A. Amin and A. Safari (IEEE, Piscataway, NJ, 1992) p. 185.
2. H. F. CHENG, *J. Appl. Phys.* **66** (1989) 1382.
3. B. HUYBRECHTS, K. ISHIZAKI and M. TAKATA, *J. Mater. Sci.* **30** (1995) 2643.
4. J. QI, Z. GUI, Y. WANG, Q. ZHU, Y. WU and L. LI, *Ceram. Intern.* **28** (2002) 141.
5. J. G. KIM, W. S. CHO and K. PARK, *Mater. Sci. Eng.* B **83** (2001) 123.
6. D. C. HILL and H. L. TULLER, in "Ceramic Materials for Electronics," edited by R. C. BUCHANAN (Marcel Dekker, New York, 1991) p. 249.
7. A. J. MOULSON and J. M. HERBERT, in "Electroceramics: Materials, Properties and Application" (Chapman & Hall, London, 1995) p. 147.
8. J. ZHAO, L. LI and Z. GUI, *Sens. Actuators* A **95** (2001) 46.
9. M. VIVIANI, P. NANNI, M. T. BUSCAGLIA, M. LEONI and V. BUSCAGLIA, *J. Eur. Ceram. Soc.* **19** (1999) 781.
10. D. KOLAR, M. TRONTELJ and Z. STADLER, *J. Amer. Ceram. Soc.* **65** (1982) 470.
11. H. F. CHENG, T. F. LIN, C. T. HU and I. N. LIN, *ibid.* **76** (1993) 827.
12. B. HUYBRECHTS, K. ISHIZAKI and M. TAKATA, *ibid.* **75** (1992) 722.
13. *Idem.*, *ibid.* **77** (1994) 286.
14. G. LIU and R. D. ROSEMAN, *J. Mater. Sci.* **34** (1999) 4439.
15. H. M. AL-ALLAK, T. V. PARRY, G. J. RUSSELL and J. WOODS, *ibid.* **23** (1988) 1083.
16. H. P. ABICHT, H. T. LANGGHAMMER and K. H. FELGNER, *ibid.* 26 (1991) 2337.
17. K. H. FELGNER, T. MÜLLER, H. T. LANGHAMMER and H. P. ABICHT, *J. Eur. Ceram. Soc.* **21** (2001) 1657.

Received 15 May
and accepted 1 October 2003

เอกสารหมายเลข 1.12

Ferroelectric Letters, 31:79–85, 2004

ISSN: 0731-5171 print / 1543-5288 online
DOI: 10.1080/07315170490480975

Taylor & Francis
Taylor & Francis Group

Analysis of X-Ray Diffraction Line Profiles of Lead Zirconate Titanate Using the Fourier Method

W. THAMJAREE, W. NHUAPENG, and T. TUNKASIRI

Department of Physics, Faculty of Science, Chiangmai University, Chiangmai 50200, Thailand

Communicated by Dr. George W. Taylor

(Received November 3, 2003)

Lead zirconate titanate (PZT) powder was prepared by a solid state reaction. The X-ray line broadening produced in PZT powder was analyzed by the Fourier method to estimate particle size and microstrain. It was found that an increase of the annealing temperature caused the microstrain to decrease owing to an increase in particle size. The Scherrer formula used to calculate the particle size yielded considerably smaller values.

Keywords: PZT; particle; Fourier method

INTRODUCTION

In the world of modern electronic ceramics, lead zirconate titanate (PZT) ceramics have become most widely employed as transducer materials. This is due to its high electromechanical coupling coefficients, enabling them to yield a high degree of mechano-electrical conversion [1]. As a result, PZT ceramics are being widely employed in hydrophones [2], ignitors, actuators for fine movement control [3] and many other applications.

Properties of fine ceramics such as PZT or barium titanate ($BaTiO_3$) depend greatly on the particle size of the starting materials [4]. Various techniques have been employed to measure the particle size of the starting powder prior to sintering, such as sedimentation, laser diffraction techniques [5], or scanning electron microscopy (SEM) [6].

X-ray diffraction profiles are also widely used to estimate the particle size and microstrain of materials. Uchino et al. [7], and Tornoda et al. [8] used the Scherrer formula to estimate the particle sizes of $BaTiO_3$ and lead

titanate (PT) powders, respectively. Tunkasiri and Rujijanagul [9] employed the integral breadth method of Halder and Wagner [10] to estimate the particle size and microstrain of $BaTiO_3$ powders. X-ray line broadening can also be analyzed employing the Fourier method of Warren and Averbach [11]. According to Lewis and Northwood [12], the particle sizes of filed lithium fluoride estimated by the Fourier method as well as by electron microscopy were of the same order of magnitude. The main purpose of this paper is the estimation of the particle size and the microstrain of PZT powder using both the Fourier method and the Scherrer formula.

EXPERIMENTAL PROCEDURE

PZT powder was prepared by the mixed oxides route. Lead oxide (PbO), zirconium oxide (ZrO_2) and titanium oxide (TiO_2), (mole ratio of 1:0.52:0.48), were mixed and milled in a zirconia pot with zirconia balls for 24 hours. The product was heated for 1 hour at temperatures ranging from 400°C to 1300°C in steps of 100°C. X-ray diffractometry was employed to study the sample obtained from each annealing step.

The X-ray diffraction profiles were scanned using a Jeol diffractometer with Ni filtered CuK_α radiation, at the speed of 1/8 degree per minute in 2θ. The (111) interplanar spacing was selected to estimate the particle size and microstrain. Rachinger's method [13] was used to resolve the $K_{\alpha 1}$ and $K_{\alpha 2}$ lines. Indexing of the samples was carried out according to the Joint Committee on Powder Diffraction Standards [14]. The measured line profiles were corrected for the instrumental broadening by the deconvolution of Fourier method of Stokes [15]. The sample annealed at 1300°C was used as the standard to estimate the contribution of the instrument broadening. The Fourier coefficients were determined using a computer programme, and analyzed by the procedure of Warren and Averbach [11]. For comparison, Scherrer's formula was also employed to estimate the particle sizes of the samples at each annealing step. The Scherrer method was performed in the way described by Klug and Alexander [16]. Both correction and without correction for instrumental broadening on the line profiles were carried out in the particle size estimation. Correction of the instrumental response was done according to the method described by Li and Shih [17].

RESULTS AND DISCUSSION

Figure 1 shows the variation of the Fourier coefficients (A_n) of some samples as a function of the harmonic number n, where n is the particular Fourier

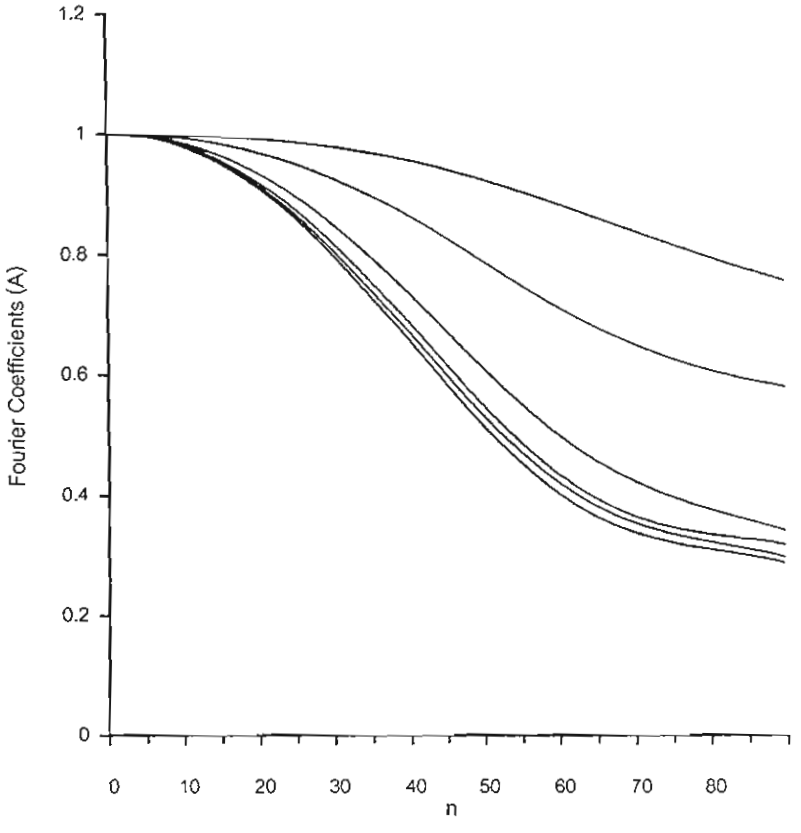

Figure 1. Variation of the Fourier coefficients A_n with n. From the bottom: ball milled sample at 25°C, and samples annealed at 500, 700, 900, 1000 and 1100°C, respectively.

series under consideration. The particle sizes and microstrains were calculated for each annealing step and plotted in Fig. 2. The microstrain decreased slowly with temperature up to about 900°C with little increase in particle size. At annealing temperatures above 900°C, the microstrain showed rapid decrease while the particle size increased by a factor of four. Beyond an annealing temperature of 1100°C both the change in microstrain and particle size slowed down. In Fig. 2 the particle sizes obtained from Scherrer's formula are presented together with other results from the literature [6, 18, 19]. The particle size obtained by Wu et al. [18] is rather close to those reported here, though their samples were prepared by the solgel technique and the average

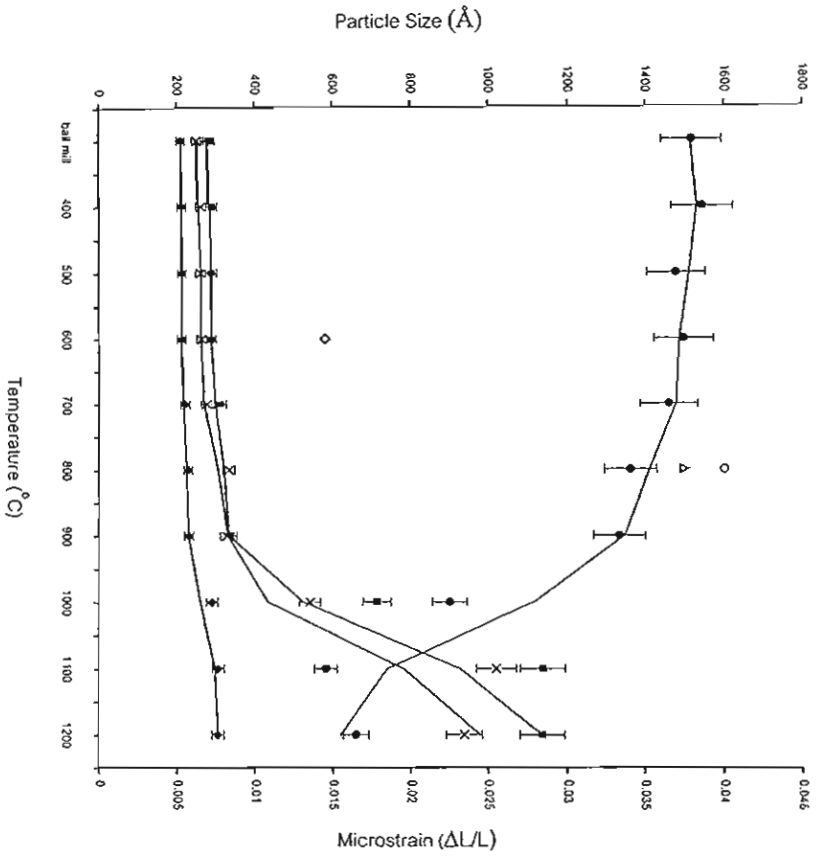

Figure 2. Particle size (Å) and microstrain of PZT powders as a function of the annealing temperature. Our data: × Fourier method [11]; ■ Scherrer formula with correction for instrument broadening [17]; υ Scherrer formula with out correction for instrument broadening [16]; ● Microstrain [11]. Reference data: ○ Chakrabarti and Maiti [19]; ◇ Wu et al. [18]; △ Yamamura et al. [6].

particle size were estimated using scanning electron micrographs. On the other hand, the results presented by Yamamura et al. [6] and Chakrabarti and Maiti [19] show much larger particle sizes. This may be due to the method of preparation and estimation since Yamamura et al. [6] Chakrabarti and Maiti [19] prepared the samples by co-precipitation and auto-combustion of citratenitrate gel methods, and particle size estimation were carried out from scanning electron micrographs and selected surface area respectively.

X-ray diffractograms indicated that the sample consist of PZT with trace of PbO. The line splitting of (100) and (001) PZT peaks showed that the tetragonal phase appear between 1100°C–1200°C, whereas the cubic phase exists at lower temperatures. Annealing at 1100, 1125, 1150, 1175 and 1200°C were carried out and the samples were re-examined. Some of the diffractograms are shown in Fig. 3. It may be concluded that transformation

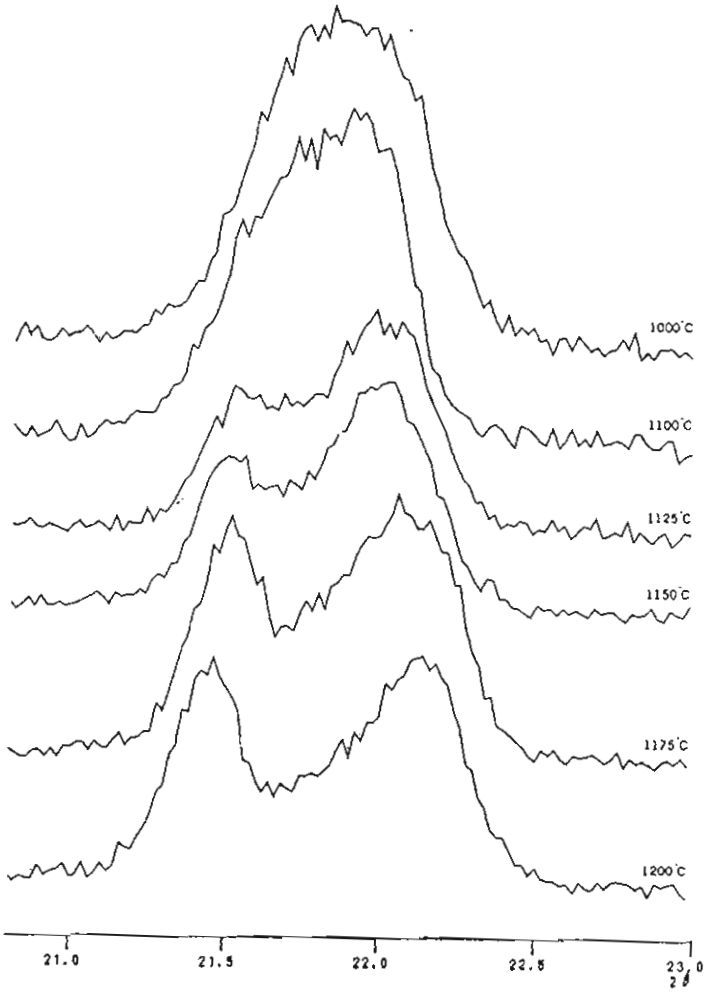

Figure 3. XRD pattern of the (100) and (001) peaks of PZT powder annealed at different temperatures.

of the cubic to the tetragonal phase starts at 1125°C, and is essentially completed at 1200°C. Tetragonality (c/a) was also calculated using Cohen's method [20] to be 1.011, 1.012, 1.013 and 1.015 for annealing temperatures of 1125, 1150, 1175, and 1200°C, respectively.

CONCLUSIONS

In conclusion, X-ray line broadening produced in PZT powder by ball milling is mainly due to the decrease in particle size. The Fourier analysis of Warren and Averbach can be used as a suitable method to analyze the microstructural changes introduced into the powder as a result of annealing. As the annealing temperature increases, an increase in particle size and a subsequent decrease in the intra-particle microstrain are observed. X-ray diffraction technique confirmed that the cubic to tetragonal phase started at 1125°C and was essentially completed at 1200°C.

ACKNOWLEDGEMENTS

The authors express their grateful thanks to the Thailand Research Fund (TRF) and the National Metal and Materials Technology Center (MTEC) of Thailand for the funding of this project. Thanks are aslso extened to Prof. Dr. Robert B. Heimann, Freiberg University of Mining and Technology, Germany for his fruitful and productive comments.

REFERENCES

[1] R. C. Buchanan, *Ceramic Materials for Electronics, Processing, Properties and Applications* (Marcel Dekker, New York, 1986), p. 164.
[2] Y. Kurihara, K. Mizumusa, and H. Ohashi, *Japan. J. Appl. Phys.* **31**, 3067 (1992).
[3] J. Randeraat and R. E. Setterington, *Piezoelectric Ceramics* (Mullard, London, 1974) p. 23.
[4] K. Kinorhita and A. Yamaji, *J. Appl. Phys.* **47**, 371 (1976).
[5] J. S. Reed, *Introduction to the Principles of Ceramic Processing* (John Wiley & Sons Inc., New York, 1988), p. 87.
[6] H. Yamamura, S. Kuramoto, H. Haneda, A. Watanbe, and S. Shirasaki, *Yogyo-Kyokai-Shi (Japan)* **94**, 545 (1986).
[7] K. Uchino, E. Sadanga, and T. Hirose, *J. Am. Ceram. Soc.* **72**, 1555 (1989).
[8] W. Tornoda, N. Okada. K. Yoshikawa, E. Anno, and K.Ishikawa, *Bull. Res. Inst. Electron. Shizuoka Univ. (Japan)* **23**, 11 (1988).
[9] T. Tunkasiri and G. Rujijanagul, *J. Mats. Sci. Lett.* **13**, 165 (1994).

[10] N. C. Halder and C. N. J. Wagner, *Acta Crystallogr.* **20**, 312 (1966).
[11] B. E. Warren and B. L. Averbach, *J. Appl. Phys.* **21**, 595 (1950).
[12] D. Lewis and D. A. Northwood, *Brit J. Appl. Phys.* **2**, 21 (1969).
[13] W. A. Rachinger, *J. Sci. Inst.* **25**, 254 (1948).
[14] Powder Diffraction File, Card No. 33-784, Joint Committee on Powder iffraction Standards, Swarthmore, PA.
[15] A. R. Stokes, *Proc. Phys. Soc.* **61**, 382 (1948).
[16] H. P. Klug and L. E. Alexander, X-ray diffraction procedures for polycrystalline and amorphous materials (Wiley, New York, 1974), p. 618.
[17] X. Li and W. Shih, *J. Am. Ceram. Soc.* 80, 2844 (1997).
[18] A. Wu, I. M. M. Salvado, P. M. Vilarinho, and J. L. Baptista, *J. Am. Ceram. Soc.* 81, 2640 (1998).
[19] N. Chakrabarti and H. S. Maiti, *Mater. Lett. (Netherlands)* 30, 169 (1997).
[20] B. D. Cullity, *Elements of X-ray diffraction* (Addison-Wesley, Reading, MA, 1987), p. 102.

เอกสารหมายเลข 1.13

2004 14th IEEE International Symposium on Applications of Ferroelectrics--ISAF-04

Influence of Processing Conditions on the Morphotropic Phase Boundaries and Ferroelectric Properties of $Pb(Zn_{1/3}Nb_{2/3})O_3$-$Pb(Ni_{1/3}Nb_{2/3})O_3$-$Pb(Zr_{1/2}Ti_{1/2})O_3$ Solid Solutions

David P. Cann, Xiaoli Tan
Materials Science and Engineering
Iowa State University
Ames, IA 50011 USA
$BaTiO_3$@iastate.edu

Naratip Vittayakorn, Gobwute Rujijanagul, and Tawee Tunkasiri
Department of Physics, Faculty of Science
Chiang Mai University
Chiang Mai, 50200 Thailand

Abstract— Ceramic solid solutions within the ternary system of $Pb(Zn_{1/3}Nb_{2/3})O_3$ - $Pb(Ni_{1/3}Nb_{2/3})O_3$ - $Pb(Zr_{1/2}Ti_{1/2})O_3$ (PZN-PNN-PZT) were synthesized via two methods: the mixed oxide method and the columbite method. Phase development of the calcined powders and the crystal structure of sintered ceramics were analyzed by x-ray diffraction. The ferroelectric properties of the ceramics were characterized by a combination of dielectric and hysteresis measurements. It was observed that for the binary systems PZN-PZT and PNN-PZT, the change in the transition temperature (T_m) is nearly linear with respect to the PZT content. Ferroelectric properties were analyzed to elucidate the nature of the phase transformation and identify the impact of the processing conditions. With these data, ferroelectric phase diagrams were derived showing the transition between the pseudo-cubic relaxor behavior of PZN and PNN to the tetragonal normal ferroelectric behavior of PZT. This transition was also correlated to changes in the diffuseness parameter δ_γ. When comparing ceramics prepared by the columbite method and the mixed oxide route, ceramics prepared by the mixed oxide method showed a lower remanent polarization P_r and a higher coercive field E_c. Additionally, ceramics prepared by the columbite method displayed sharp transitions in ferroelectric properties across the MPB composition, whereas these transitions were obscured in ceramics prepared by the mixed oxide method. It is proposed that the different reaction paths influenced the degree of compositional heterogeneity in these complex perovskite solid solutions, which was clearly reflected in the nature of the phase transition.

Keywords: morpotropic phase boundary, columbite method, perovskite, phase transition

I. INTRODUCTION

Ferroelectric materials based on Pb-perovskites have found use in countless applications including piezoelectric sensors and actuators, capacitors, pyroelectric and electro-optic devices, and ferroelectric memories [1,2]. In many instances, compositions near a morphotropic phase boundary (MPB) between ferroelectric phases of different symmetry have advantageous dielectric and piezoelectric performance characteristics [1,3]. There have been a number of MPB's identified in Pb-based systems including the most widely exploited system $PbZrO_3$-$PbTiO_3$ (PZT) [3]. Other MPB systems include $Pb(Mg_{1/3}Nb_{2/3})O_3$-$PbTiO_3$ (PMN-PT) [4], $Pb(Zn_{1/3}Nb_{2/3})O_3$-$PbTiO_3$ (PZN-PT) [5], $Pb(Sc_{1/2}Nb_{1/2})O_3$-$PbTiO_3$ (PSN-PT) [6], and many others.

This work will focus on perovskite solid solutions in two quasi-binary systems within the overall ternary system $Pb(Zr_{1/2}Ti_{1/2})O_3$- $Pb(Zn_{1/3}Nb_{2/3})O_3$- $Pb(Ni_{1/3}Nb_{2/3})O_3$: specifically $Pb(Zn_{1/3}Nb_{2/3})O_3$-$Pb(Zr_{1/2}Ti_{1/2})O_3$ (PZN-PZT) and $Pb(Ni_{1/3}Nb_{2/3})O_3$-$Pb(Zr_{1/2}Ti_{1/2})O_3$ (PNN-PZT). Polycrystalline ceramics based on Pb-perovskites are typically synthesized through high temperature solid state processes. A number of processing methods have been proposed to ensure phase pure perovskite. In this work, two common processing methods will be contrasted with the aim of understanding the influence of processing conditions on the phase equilibria and ferroelectric properties. The conventional mixed oxide method involves simply reacting all of the binary oxides (e.g. PbO, TiO_2, ZrO_2, etc.) in a single calcination step to form the desired perovskite phase. In the columbite method, first proposed by Swartz and Shrout [7], the B-site oxides are first pre-reacted to form intermediate phases such as $ZnNb_2O_6$, $ZrTiO_4$, $NiNb_2O_6$, etc. These intermediate phases are then reacted with PbO to form the desired perovskite phase.

Given that the PZN-PNN-PZT phases are all perovskite solid solutions, it is likely that the different reaction paths may lead to distinct differences in the homogeneity of the B-cation distributions. In this study, a combination of x-ray diffraction (XRD), dielectric measurements, and Raman spectroscopy will be employed to probe the influence of the different processing methods on such parameters as the perovskite phase distributions, remanent polarization (P_r), coercive field (E_C), diffuseness parameter (δ_γ), and others. With this information, it will be possible to optimize the processing conditions for solid solutions near MPBs.

0-7803-8410-5/04/$20.00 (c)2004 IEEE.

II. EXPERIMENTAL

The columbite precursors $ZnNb_2O_6$ and $NiNb_2O_6$ were prepared from the reaction between ZnO (99.9%) and Nb_2O_5 (99.9%) at 975°C for 4h and between NiO (99.9%) and Nb_2O_5 (99.9%) for 4h at 1100°C, respectively. The wolframite phase $ZrTiO_4$ was formed by reacting ZrO_2 (99.9%) with TiO_2(99.9%) at 1400°C for 4h. The powders of $ZnNb_2O_6$, $NiNb_2O_6$, and $ZrTiO_4$ were mixed in the required stoichiometric amounts with PbO (99.9%) with an excess of 2 mol% of PbO added. The milling process was carried out for 24 hours in isopropyl alcohol. The powders were calcined at 900°C-950°C for 4 h in a double crucible configuration with a heating rate of 20°C/min. After grinding and sieving, 5 wt% of polyvinyl alcohol (PVA) binder was added. Discs with a diameter of 12.5 mm were prepared by cold uniaxial pressing at a pressure of 150MPa. Binder burnout occurred by slow heating to 500°C and holding for 2h. The discs were sintered in a sealed alumina crucible at temperatures ranging from 950°C-1250°C using a heating rate of 5°C/min and a dwell time of 2 h. To prevent PbO volatilization from the discs, a PbO atmosphere was maintained by placing a bed of $PbZrO_3$ powder in the crucible.

Phase formation and crystal structure of the calcined powders and sintered discs were examined by x-ray diffraction (XRD). The pellets were polished and electroded via gold sputtering, over which a layer of air-dried silver paint was applied. The relative permittivity (ε') and dissipation factor (tan δ) of the pellets sample were measured at various temperatures over the frequency range between 100 and 100KHz using an LCR meter (HP 4284A). The remanent polarization P_r was determined from a P-E hysteresis loop measurements using a Sawyer-Tower circuit at temperatures between -66°C and 60°C.

III. RESULTS

Single phase perovskite was obtained for the pseudo-binary systems over the composition ranges *(1-x)*PZN-*x*PZT at $0.5 \leq x \leq 0.9$ and for *(1-x)*PNN-*x*PZT at $0.4 \leq x \leq 0.9$. For the 0.6PZN-0.4PZT composition a small amount of pyrochlore phase was noted. The results of the XRD, dielectric, and Raman measurements and the influence that can be attributed to processing conditions are summarized for each pseudo-binary system in the following sections.

A. PZN-PZT System

In the PZN-PZT system, phase pure perovskite was obtained at lower calcination temperatures using the conventional method compared to the columbite method. As shown in Fig. 1, the columbite method required calcination temperatures as much as 150°C higher for some PZN-PZT compositions. This effect was especially prevalent at high mole fractions of PZT. In analyzing the phase evolution at low temperatures, a high volume fraction of a pyrochlore phase was observed in the XRD data for the columbite derived powders. In the conventionally prepared powders the perovskite phase was the dominant phase even at 750°C. This suggests that each processing route followed a different reaction path in eventually forming the perovskite phase.

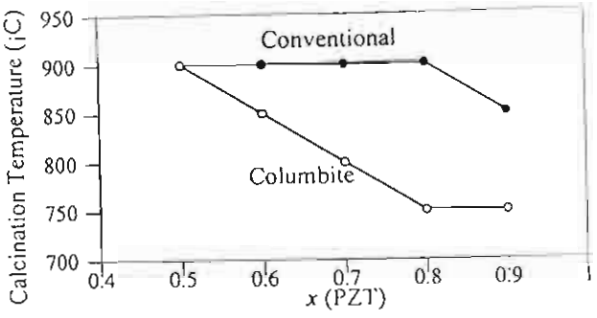

Figure 1. Calcination temperature at which phase pure perovskite is obtained for both the conventional and columbite methods.

The symmetry of the resultant perovskite phases obtained through XRD allows a pseudo-binary phase diagram to be derived (Fig. 2). Compositions close to PZT are tetragonal at room temperature, with a transition to rhombohedral symmetry for compositions at $x \leq 0.7$. Inspection of the XRD patterns of compositions close to the MPB at $x \approx 0.7$ revealed that the processing method had an influence on the phase distribution (Fig. 3). In columbite derived powders, only the rhombohedral perovskite phase was observed. However, in conventionally prepared powders a mixture of the rhombohedral and tetragonal phases were observed. This is strong evidence that the conventional method produces non-uniform mixing of the B-site cations as compared to the columbite method.

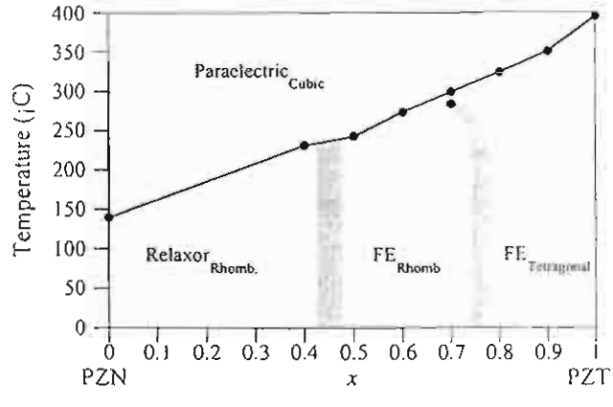

Figure 2. PZN-PZT phase diagram obtained through room temperature XRD and dielectric measurements.

Further evidence is seen in the dielectric data presented in Fig. 4. For compositions near the MPB at $x = 0.7$, a phase transition was clearly seen in the columbite derived ceramics at 284°C. As indicated in the phase diagram (Fig. 2), this corresponds to a transition from rhombohedral to tetragonal symmetry. The conventionally prepared ceramics at $x = 0.7$ did not show any anomalies within that temperature range.

Comparisons of the dielectric data for PZN-PZT ceramics prepared by the two methods are presented in Table I. These data show that ceramics prepared via the columbite method exhibit a significantly higher room temperature permittivity, higher permittivity at T_{max}, and a higher remanent polarization (P_r) determined from hysteresis measurements.

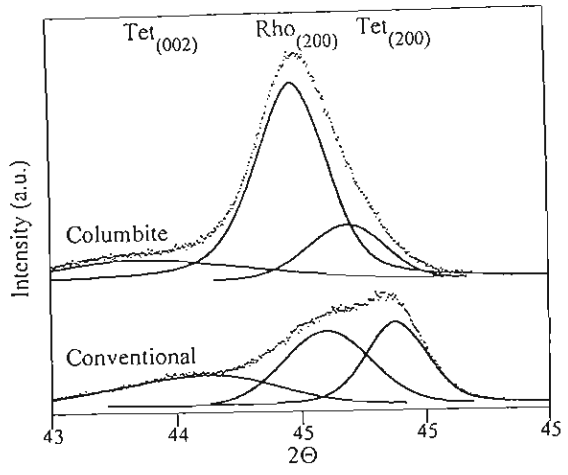

Figure 3. XRD patterns for the (002) peak for conventional and columbite prepared ceramics. Deconvolution of the data shows that relative proportions of the rhombohedral and tetragonal phases.

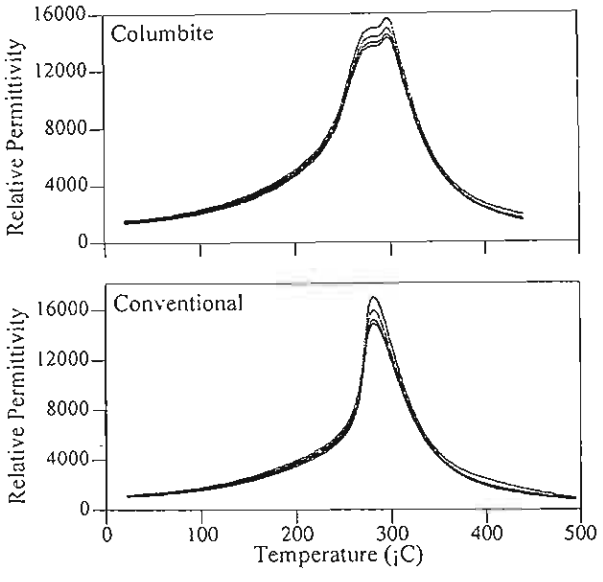

Figure 4. Relative permittivity versus temperature for a 0.3PZN-0.7PZT ceramic at measurement frequencies of 0.1, 1, 10, and 100 KHz.

It is important to note that there were no significant differences in the density or grain size when comparing the two processing methods. All samples in this study were of high density ($\rho_{Theoretical}$ > 96%) with grain sizes close to 5 μm. Therefore, it is possible to exclude the influence of density or grain size effects from these results.

In Fig. 5, the coercive field (E_C) as a function of x exhibits very different trends comparing the conventional and columbite prepared ceramics. The columbite ceramics exhibited a sharp transition in E_C at the MPB, whereas the conventionally prepared ceramic displayed a gradual transition.

TABLE I. PZN-PZT DIELECTRIC DATA

x	K at 25°C		K at T_{max}		P_r	
	Conv.	Col.	Conv.	Col.	Conv.	Col.
0.4	1,230	1,440	11,400	13,200		
0.5	1,220	1,430	20,800	21,200	29.5	36.4
0.6	1,230	1,440	17,000	20,800	23.2	30.6
0.7	980	1,580	14,300	15,700	20.0	30.4
0.8	1,230	1,550	25,000	25,800	31.5	36.1
0.9	810	1,590	13,300	21,200	34.0	37.1

Taking all of these results into account, PZN-PZT ceramics prepared by the columbite method exhibited more clearly defined phase transitions and MPBs compared to conventionally processed ceramics. Rhombohedral distortions in perovskites are linked to the geometric tolerance factor (t). In the PZN-PZT system, the magnitude of t is determined by the average B-cation radius. In the conventionally prepared ceramics, the coexistence of the tetragonal and rhombohedral phases near the MPB are indicative of a significant degree of variation in the composition of the B-site. Regions which were rich in smaller cations would favor tetragonal distortions, whereas regions rich in larger cations would favor rhombohedral distortions. The formation of columbite oxides prior to perovskite formation assures intimate mixing of the B-site cations. This ultimately leads to a more homogeneous distribution of B-site cations.

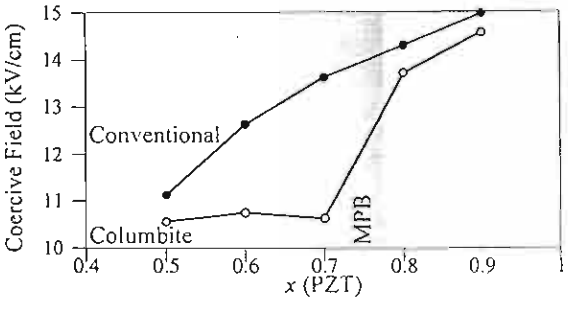

Figure 5. Coercive field as a function of composition x for columbite and conventionally prepared ceramics.

B. PNN-PZT System

In the PNN-PZT system, the columbite method was utilized to prepare phase-pure perovskite ceramics. Based on room temperature XRD and measurements of the relative permittivity versus temperature a phase diagram for PNN-PZT was derived (Fig. 6). At x = 0.8, an MPB region separates a tetragonal normal ferroelectric phase field from a rhombohedral relaxor ferroelectric phase field. XRD data within the MPB region featured splitting of both (200) and (111) peaks. This is indicative of the coexistence of both rhombohedral and tetragonal phases. Alternatively, as has been demonstrated in PZT the multiple peak splitting could be indicative of another lower symmetry phase (e.g. monoclinic) [8].

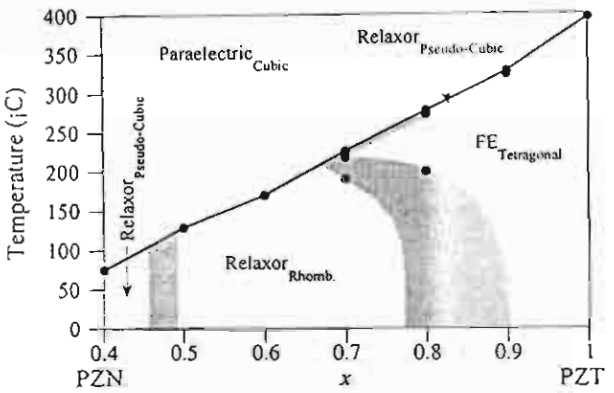

Figure 6. PNN-PZT phase diagram obtained through room temperature XRD and dielectric measurements.

Table II summarizes the results of the dielectric measurements on the PNN-PZT ceramics. As expected, the relative permittivity peaked at the MPB composition (x = 0.8) at a value of 36,000. A general transition from normal ferroelectric to relaxor ferroelectric behavior was observed as the mole fraction of PNN increased. Fig. 7 illustrates the relative permittivity versus temperature for $0.4 \le x \le 0.9$. The transition from normal ferroelectric behavior to relaxor ferroelectric behavior was clearly observed from the dispersion in the vicinity of T_{max}.

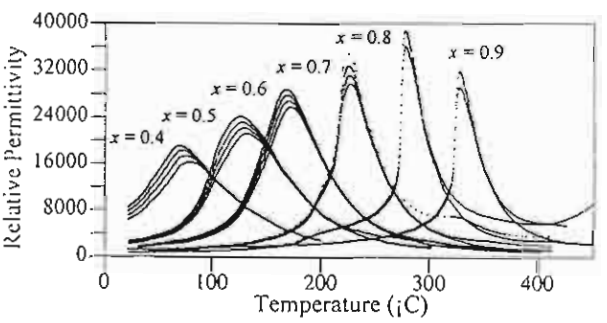

Figure 7. Relative permittivity versus temperature for *(1-x)*PNN-*x*PZT ceramics.

TABLE II. PNN-PZT DIELECTRIC DATA

x	T_{max} (°C)	K at 25°C	tan δ at 25°C	K at T_{max}	δ_γ
0.4	75.4	7,500	0.062	17,500	29.5
0.5	128.9	2,500	0.042	22,000	24.4
0.6	169.7	1,600	0.042	27,000	22.4
0.7	225.5	1,060	0.029	31,200	14.0
0.8	277.4	835	0.011	36,000	10.2
0.9	326.7	950	0.005	32,000	8.6

The parameter δ_γ can be used to quantify the diffuseness of the ferroelectric transition through the equation [9]:

$$\frac{K_{max}}{K(f,T)} = 1 + \frac{\left[T - T_{max}(f)\right]^{\gamma}}{2\delta_{\gamma}^{2}} \qquad (1)$$

where $\gamma = 1$ for Curie-Weiss behavior and $\gamma = 2$ for pure relaxor character. As shown in Table II, the δ_γ parameter increased linearly with increased PNN content.

IV. CONCLUSIONS

In this work, the ferroelectric phases within the pseudo-binary systems PZN-PZT and PNN-PZT were characterized. For the PZN-PZT compositions, MPBs were noted at $x \approx 0.75$ and $x \approx 0.45$. It was observed pre-reacting the B-site cations via the columbite method had significant effects on the perovskite phase stability and dielectric properties. These effects were most pronounced in the vicinity of the MPB, located near $x \approx 0.75$. It is likely that the columbite method produced a more homogeneous distribution of the B-site cations compared to the mixed oxide prepared ceramics. These compositional variations could be inferred from the observation of multiple phases near the MPB and poorly defined phase transitions.

In the PNN-PZT compositions, two MPBs were noted at $x \approx 0.8$ and $x \approx 0.45$. Even with columbite prepared ceramics, rhombohedral and tetragonal phases were found to coexist at the MPB at $x \approx 0.8$. It is interesting to note that in PNN the transition from the tetragonal PZT phase to the relaxor rhombohedral phase is more gradual than in PZN. This is likely due to the much closer B-cation radii match between $Zr_{0.5}Ti_{0.5}$ (0.803 Å) and $Ni_{1/3}Nb_{2/3}$ (0.797 Å), as compared to $Zn_{1/3}Nb_{2/3}$ (0.813 Å).

ACKNOWLEDGMENT

The authors are grateful to the Thailand Research Fund, Graduate School at Chiang Mai University and Ministry of University Affairs in Thailand for financial support.

REFERENCES

[1] A. J. Moulson and J. M. Herbert, Electroceramics: Materials, Properties, Applications. New York: Chapman and Hall, 1990.

[2] K. Uchino, Ferroelectric Devices. New York: Marcel Dekker, Inc., 2000.

[3] B. Jaffe and W. R. Cook, Piezoelectric ceramics. R.A.N., 1971

[4] S. W. Choi, T. R. Shrout, S. J. Jang, and A. S. Bhalla, "Dielectric and pyroelectric properties in the $Pb(Mg_{1/3}Nb_{2/3})O_3$-$PbTiO_3$ system," Ferroelectrics, vol. 100, 1989.

[5] J.Kuwata, K.Uchino, and S.Nomura, "Dielectric and piezoelectric properties of $0.91Pn(Zn_{1/3}Nb_{2/3})O_3$-$0.09PbTiO_3$ single crystals.," Jpn. J. Appl. Phys., vol. 21, pp. 1298-1302, 1982.

[6] V. J. Tennery, K. W. Hang, and R.E.Novak, "Ferroelectric and structure properties of $Pb(Sc_{1/2}Nb_{1/2})_{1-x}Ti_xO_3$ system," J. Am. Ceram. Soc., vol. 51, pp. 671-674, 1968.

[7] S. L. Swartz and T. R. Shrout, "Fabrication of perovskite lead magnesium niobate," Mater. Res Bull., vol. 17, pp. 1245, 1982.

[8] B. Noheda, D.E. Cox, G. Shirane, J.A. Gonzalo, L.E. Cross, and S-E. Park, "A monoclinic ferroelectric phase in the $Pb(Zr_{1-x}Ti_x)O_3$ solid solution," Appl. Phys. Lett. Vol. 74, pp. 2059 (1999).

[9] K.Uchino and S.Nomura, "Critical exponents of the dielectric constants in diffused phase transition crystals," Ferroelectrics Letters, vol. 44, pp. 55, 1982.

เอกสารหมายเลข 1.14

Appl. Phys. A (2004)
DOI: 10.1007/s00339-004-3136-6

Applied Physics A
Materials Science & Processing

W. THAMJAREE
W. NHUAPENG✉
A. CHAIPANICH
T. TUNKASIRI

Fabrication of combined 0–3 and 1–3 connectivities PZT/epoxy resin composites

Department of Physics, Faculty of Sciences, Chiang Mai University, Chiang Mai 50200, Thailand

Received: 20 October 2004/Accepted: 25 October 2004
Published online: 21 December 2004 • © Springer-Verlag 2004

ABSTRACT PZT/epoxy resin composites of combined 0–3 and 1–3 connectivities were fabricated, for the first time, using suction, dice and fill techniques. Two types of composites (PZT(m)/epoxy resin and PZT(sp)/epoxy resin) were produced using PZT powders prepared by mixed oxide and spray-drying methods. Physical, mechanical, dielectric and piezoelectric properties of the composites were examined. Generally, overall results between the two composites were found to be very similar (volumetric changes ~ 34%–37%, $d_{33} \sim 20.2$–25.3 pC/N, $K_p \sim 0.54$–0.61). Higher density was found in PZT(sp)/epoxy resin, however, due to better packing of particles. Moreover, both PZT/epoxy resin composites exhibited very low acoustic impedance ($Z \sim 4.12$–4.84 Mrayls), which is very close to that of human tissue and water. Therefore, these new composites may be suitable for use in medical applications.

PACS 81.05.Qk; 81.05.Zx; 77.87.-s

1 Introduction

Piezoelectric ceramics, such as lead zirconate titanate ($Pb(Zr_xTi_{1-x})O_3$ or PZT), have been employed as sensors, actuators and transducers due to their high piezoelectric coefficient (d_{33}) and dielectric constant (ε_r) [1, 2]. Nevertheless, their transverse charge coefficient (d_h), the hydrostatic voltage coefficient (g_h) and the hydrophone figure of merit ($d_h g_h$) are low. Furthermore, PZT ceramics are hard and brittle in nature and may not be flexible enough to suit a curved surface. They also exhibit high acoustic impedance, causing great acoustical mismatching between ceramics and the transmitting medium, like water or human tissue [3, 4]. In order to obtain low acoustic impedance for matching these media, piezocomposites which employed an active piezoelectric material in conjunction with an active or passive polymer phase have been suggested with different connectivity patterns [5].

Early reports revealed that the connectivity of 1–3 ceramic/polymer composites, which comprise an active piezoceramic rod embedded with a passive polymer, possessed excellent overall piezoelectric properties when used in hydrophone and medical-imaging applications [3, 6–8]. Schwarzer and Roosen [1] fabricated 1–3 PZT/polymer composites by dice and fill, tape-casting and injection-molding methods. These composites were found to exhibit good piezoelectric and dielectric properties ($d_{33} = 466$ pC/N and $\varepsilon_r = 1146$). Janas et al. [3] produced 1–3 piezocomposites by tape casting, honeycomb dicing and ceramic fiber weaving, obtaining $d_{33} = 370$ pC/N and $\varepsilon_r = 300$. Taunaumang et al. [7] also fabricated 1–3 piezocomposites by the dice and fill method; the obtained d_{33} and K_p for the composites were 746 pC/N and 0.64, respectively. Furthermore, other techniques which may be regarded as novel in producing 1–3 piezocomposites have been developed by weaving PZT fiber bundles through a honeycomb support [6], lost mold [8] and laser cutting [9].

On the other hand, the 0–3 connectivity of piezoceramic polymer is considered to be less complicated in terms of fabrication and appropriate to be molded to any designed surface due to its high flexibility. In this type of composite, the ceramic powder has no physical particle–particle contact while the polymer phase has a three-dimensional connection. One of the methods used to prepare the 0–3 ceramic/polymer was the centrifuge method by Nhuapeng and Tunkasiri [10]. However, the acoustic impedance (Z) obtained from their results was about 6 Mrayls (at a volumetric percentage of ceramic phase of 30%), which is still high in comparison to that of human tissue or water (1.6 Mrayls [11]). In order to obtain a reasonably low acoustic impedance compared to that of water and a considerably high piezoelectricity of piezocomposites, we have attempted to fabricate piezocomposites with a combination of 0–3 and 1–3 connectivities. In this work, the samples were fabricated based on the dice and fill techniques. The physical, mechanical and electrical properties of composite samples were investigated. The microstructure of piezocomposites was also studied with the use of scanning electron microscopy (SEM).

2 Experimental details

Combinations of 0–3 and 1–3 connectivities composites were produced based on the dice and fill method [7]. Firstly, PZT powders obtained from the mixed-oxide method (particle size ~ 4 μm) and the spray-drying technique (particle size ~ 1 μm) were used as active phase and epoxy resin (Epofix, Strurer) was employed as passive polymer phase.

✉ Fax: +66-5335-7512, E-mail: nhuapeng@yahoo.com

Thereafter, 0–3 PZT/epoxy resin composites were fabricated by the suction technique. Details of the suction technique are described in Fig. 1. PZT powders were put in a plastic syringe with a filter paper (Whatman) placed underneath. Epoxy resin was then poured into the syringe with PZT powders and the resin was plugged in a flask partly filled with water, as shown in Fig. 1; suction was carried out using an air pump for enhancing the flow of the resin through the PZT powders. A filter (no. 42) was used to prevent the powders flowing into the suction system. The samples were left for two days at room temperature, allowing them to settle. The sample in the syringe is now a 0–3 piezoceramic/epoxy resin composite, about 1-cm thick and 1.5 cm in diameter. The sample was then diced using a diamond saw (series 15HC Diamond, Buehler) into squares of $0.35 \times 0.35\ mm^2$ to create a 1–3 connectivity pattern. Epoxy resin was then poured in again to fill up the spaces. The samples were left for two days to settle. These new samples are now a combined 0–3 and 1–3 ceramic/epoxy resin composite where each column (0–3 ceramic/epoxy resin) formed a 1–3 connectivity with the resin in the spaces. The composite sample was then taken out from the syringe and cut into disks with a thickness of 1 mm (Fig. 1b). The density of the samples was measured by the conventional Archimedes' method.

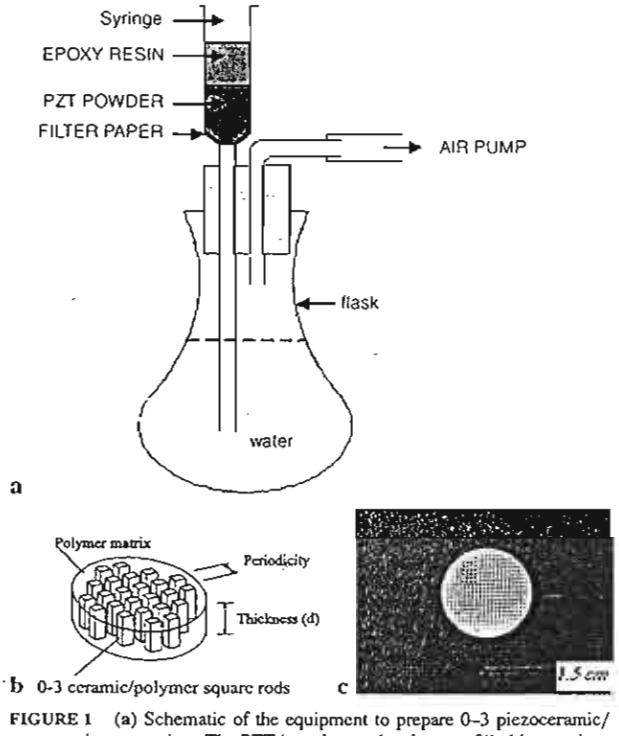

FIGURE 1 (a) Schematic of the equipment to prepare 0–3 piezoceramic/epoxy resin composites. The PZT/powders and resin were filled in a syringe with a filter underneath. The syringe was plugged in a flask partly filled with water. Suction was carried out through an air pump. (b) Schematic of photograph of (0–3) and (1–3) combined piezocomposite sample where polymer matrix = epoxy resin filled in the spaces to form the 1–3 connectivity with 0–3 ceramic/polymer rods (0.35×0.35 mm). Thickness (d) = 1 mm, periodicity = 0.7 mm. (picture based on [7]) (c) Top view photograph of the composite

Disks of the composite samples were electroded by silver paste (Electrodrag 1415M, Acheson) to the top and bottom surfaces and left to dry at room temperature. Dielectric properties were measured using a LCZ meter (model 4276, Hewlett-Packard). Poling was done in silicone oil at 80 °C with a poling field of 8 kV/mm for 30 min. The piezoelectric coefficient (d_{33}) of the samples was measured using a piezo d_{33} meter, while the echo-shift method [12] was used for the acoustic impedance measurements. Distributions of PZT powder phase in the composites were investigated using SEM.

3 Results and discussion

Figure 2 shows a typical SEM micrograph of the top view of the composite (combined 0–3 and 1–3 connectivities). Particles obtained from both preparation techniques were found to have similar morphology. The dark area belongs to the resin while the brighter squares belong to the 0–3 composites. Enlarged pictures of some squares are shown in Fig. 3. It can be concluded that the average size of the powders obtained from the mixed-oxide route is bigger ($\sim 4\ \mu m$) than that obtained from the spray-drying technique ($\sim 1\ \mu m$). This is confirmed by the cross-section micrographs (Fig. 4). However, in Fig. 3 the PZT phase shows agglomeration of the particles produced from the spray-drying technique. The composites fabricated by the suction, dice and fill method have a very low acoustic impedance (4–5 Mrayls).

Table 1 illustrates the volumetric percentage of density (ϱ) and acoustic impedance (Z) of the composites, compared with those obtained by others [10, 13–15].

PZT/epoxy produced from PZT powder of smaller particle size (PZT(sp)/epoxy resin) yields higher volumetric percentage (37%) and possesses higher ϱ ($2119.6\ kg/m^3$) and Z

composites	vol(%)	density (kg/m^3)	Z (Mrayls)
PZT(m)/epoxy resin	34	1878.6	4.12
PZT(sp)/epoxy resin	37	2119.6	4.84
Nhuapeng and Tunkasiri [10]	60	5026	11.41
Sripada et al. [13]	-	4225.4	13.94
Grewe et al. [14]	40	-	7.50
Slayton and Setty [15]	70	-	8.00

TABLE 1 Physical and mechanical properties of the PZT/polymer composites PZT(m), PZT(sp) = powders obtained from mixed oxide method and spray drying techniques, respectively

composites	d_{33} (pC/N)	K_p	ε_r	tanδ
PZT(m)/epoxy resin	25.3	0.61	14	0.026
PZT(sp)/epoxy resin	20.2	0.54	15	0.05
Schwarzer and Roosen [1]	466	0.58	1146	0.028
Janas et al. [3]	370	-	300	0.029
McNulty et al. [6]	230	-	130	-
Taunaumang et al. [7]	29.6	-	-	-
Nhuapeng and Tunkasiri [16]	26	-	84	0.0141
Sripada et al. [13]	-	0.4	-	-
Shrout et al. [16]	270	-	480	0.017
Ohara et al. [17]	274	-	536	-

TABLE 2 Dielectric and piezoelectric properties of the PZT/polymer composites compared with those of previous work

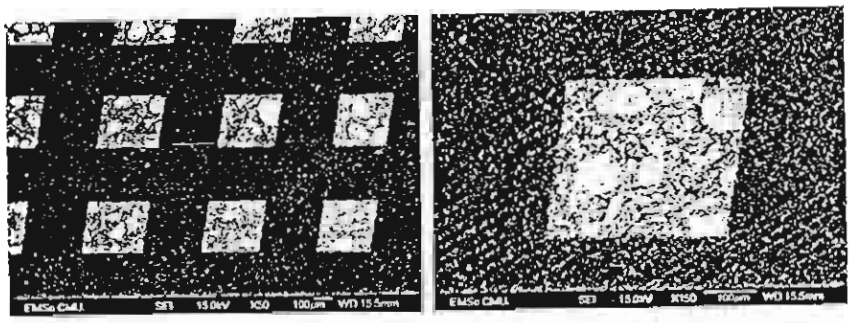

FIGURE 2 The typical SEM micrographs of top view of PZT/epoxy resin composites

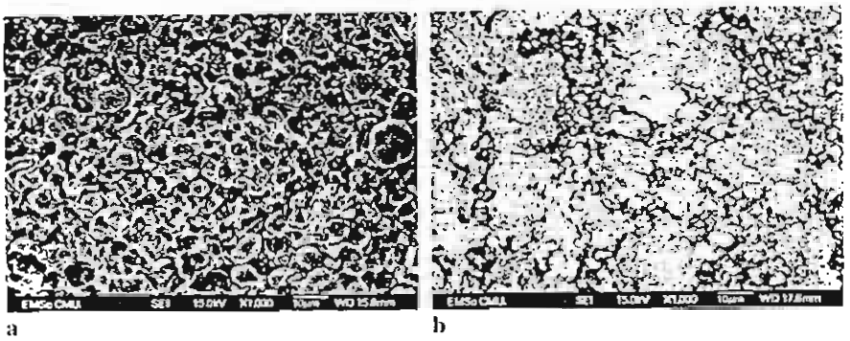

FIGURE 3 SEM micrographs of PZT/epoxy resin which PZT composites employing powders prepared from mixed oxide route (a) and spray dry techniques (b)

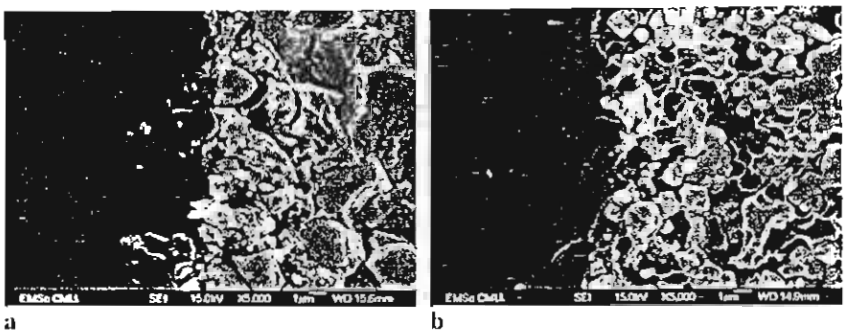

FIGURE 4 SEM micrographs of cross section of PZT/epoxy resin composites employing powders PZT powder prepared from mixed oxide route (a) and spray dry techniques (b). Dark and brighter areas correspond to the resin and the PZT powders, respectively

(4.84 Mrayls) values as compared to the PZT(m)/epoxy resin composite with corresponding values of 34%, 1878.6 kg/m^3 and 4.12 Mrayls, respectively. Both composites fabricated by our methods (combination of suction, dice and fill) were noted to have very low acoustic impedance (4.12 and 4.84 Mrayls). These values are lower than those previously reported by Nhuapeng and Tunkasiri [10], Sripada et al. [13], Grewe et al. [14] and Slayton and Setty [15]. This is due to the different fabrication routes and different volumetric percentages.

Furthermore, our Z values were found to be comparable to that of water (1.6 Mrayls). Therefore, this fabrication method could be seen as suitable in preparing low acoustic impedance PZT/epoxy resin composites for biomedical applications. Table 2 shows dielectric properties (ε_r and tanδ) and piezoelectric properties (d_{33} and K_p) of the composites, together with those of Schwarzer and Roosen [1], Janas et al. [3], McNulty et al. [6], Taunaumang et al. [7], Nhuapeng and Tunkasiri [10], Sripada et al. [13], Shrout et al. [16] and Ohara et al. [17].

The d_{33} and K_p values obtained from PZT(m)/epoxy composite are 25.3 pC/N and 0.61, respectively, while the d_{33} and K_p values of PZT(sp)/epoxy composite are 20.2 pC/N and 0.54, respectively. It can be seen that the d_{33} values for both composites are very close to the value reported by Nhuapeng and Tunkasiri [10], who fabricated the 0–3 PZT/polymer composites by the centrifuge method. The ε_r values obtained from this work are quite low (14–20), which may be due to the effect of quantity of PZT particles in the composites.

4 Conclusions

Through a combination of suction, dice and fill techniques, a new type of PZT/epoxy resin composites combining 0–3 and 1–3 connectivities was fabricated. The measured piezoelectric coefficient (d_{33}) and coupling factor (K_p) were 25.3 pC/N and 0.61 for PZT(m)/epoxy resin, respectively, while the values for PZT (sp)/epoxy resin were 20.2 pC/N (d_{33}) and 0.54 (K_p).

The most interesting finding in this investigation, however, is the very low acoustic impedance obtained for both PZT/epoxy resin composites (4.12 Mrayls for PZT(m)/epoxy resin and 4.84 Mrayls for PZT (sp)/epoxy resin). There is, therefore, a potential for these composites to be used

in biomedical applications since these acoustic impedance values are very close to those of human tissue and water.

Furthermore, from SEM, the particles from the spray-drying technique were shown to be better packed together, resulting in the composite being denser than the one prepared from the mixed-oxide method.

ACKNOWLEDGEMENTS The authors would like to express their sincere thanks to the Thailand Research Fund and the Graduate School of Chiang Mai University for financial support.

REFERENCES

1 S. Schwarzer, A. Roosen: J. Eur. Ceram. Soc. **19**, 1007 (1999)
2 S.T. Lau, K.W. Kwok, H.L.W. Chan, C.L. Choy: Sens. Actuators A **96**, 14 (2002)
3 V.F. Janas, T.F. McNulty, F.R. Walker, R.P. Schaeffer, A. Safari: J. Am. Ceram. Soc. **78**, 2425 (1995)
4 R.P. Tandon, D.R. Chaubey, R. Singh, N.C. Soni: J. Mater. Sci. Lett. **12**, 1182 (1993)
5 S.S. Livneh, F.V. Janas, A. Safari: J. Am. Ceram. Soc. **78**, 1900 (1995)
6 T.F. McNulty, V.F. Janas, A. Safari: J. Am. Ceram. Soc. **78**, 2913 (1995)
7 H. Taunaumang, I.L. Guy, H.L.W. Chan: J. Appl. Phys. **76**, 484 (1994)
8 R.K. Panda, V.F. Janas, A. Safari: in *Proc. 10th IEEE Int. Symp. Applications of Ferroelectrics, 1996*, Vol. 2, p. 551
9 K. Li, D.W. Zeng, K.C. Yung, H.L.W. Chan, C.L. Choy: Mater. Chem. Phys. **75**, 147 (2002)
10 W. Nhuapeng, T. Tunkasiri: J. Am. Ceram. Soc. **85**, 2 (2002)
11 T.R. Gururaja, W.A. Schulze, L.E. Cross, R.E. Newnham, B.A. Auld, Y.J. Wang: Trans. Son. Ultrason. **32**, 481 (1985)
12 T. Bui, H.L.W.C.J. Unsworth: J. Acoust. Soc. Am. **83**, 2416 (1988)
13 S. Sripada, J. Unsworth, M. Krishnamurty, Y.S. Ng: Mater. Res. Bull. **31**, 731 (1996)
14 M.G. Grewe, T.R. Gururaja, R.E. Newnham, T.R. Shrout: in *IEEE Ultrasonics Symp., 1989*, p. 713
15 M.H. Slayton, H.S.N. Setty: in *IEEE Int. Symp. Applications of Ferroelectrics, 1990*, p. 90
16 T.R. Shrout, L.J. Bowen, W.A. Schulze: Mater. Res. Bull. **15**, 1371 (1980)
17 Y. Ohara, M. Shiwa, H. Yanagida, T. Kishi: J. Ceram. Soc. Jpn. **102**, 368 (1994)

เอกสารหมายเลข 2

เอกสารหมายเลข 2.1

Materials Research Centre
Indian Institute of Science
BANGALORE - 560012

Prof. S.B. Krupanidhi

16th July, 2004.

Dear Author,

We sincerely thank you for participating in the recent AMF-4 meeting at Bangalore, India. Your manuscript has been reviewed and the reviewer's evaluation sheet is enclosed herewith. Following is the recommendations of the referee for your paper.

- ☐ Accepted in its present form. Please send the soft copy on a floppy or e-mail us as an attachment file if you have not given it to us already during the conference.
- ☑ Revise and send two copies of revised manuscript, along with the soft copy on a floppy or e-mail us as an attachment file
- ☐ Rejected

Your response should reach us not later than August 20, 2004, so that it can be included in the conference proceedings as the special issues of either "Ferroelectrics" or "Integrated Ferroelectrics".

Looking forward to hearing soon from you.

Thanking you,

Sincerely,

(S.B. KRUPANIDHI)
Chairman, AMF-4, Guest Editor
Ferroelectrics, Integrated Ferroelectrics
Phone: ++91-80-23601330; FAX: ++91-80-23600683; E.Mail: sbk@mrc.iisc.ernet.in

Prof. S.B. Krupanidhi
Conference Chair, AMF-4
Materiel Research Centre
Indian Institute of Science
BANGALORE - 560 012, INDIA

PIEZOCERAMIC-POLYMER COMPOSITES FOR DETECTOR APPLICATIONS

PREUKSA AUISUI[a], SUPASAROTE MUENSIT[a], IAN L. GUY [b],
GOBWUTE RUJIJANAGUL[c], AND TAWEE TUNKASIRI[c]

[a] Materials Physics Research Unit, Department of Physics,
Prince of Songkla University, Hatyai, 90112, Thailand;

[b] Department of Physics, Macquarie University, NSW 2109, Australia;

[c] Electroceramics Laboratory, Department of Physics,
Chiangmai University, Chiangmai, 50200, Thailand.

ABSTRACT

Ferroelectric powders of $PbTiO_3$ were fabricated and sintered at low-temperatures. . The ceramic pores were filled with an epoxy using a vacuum impregnation technique. SEM analysis showed a composite with 3-3 connectivity. The piezoelectric coefficient of the composite was evaluated as $(6.0 \pm 1.0)x10^{-12}$ m/V by an interferometric technique. The pyroelectric coefficient was 23 $\mu C/m^{2\circ}C$. The pyroelectric detector properties and figures-of-merit of the composite are reported.

Keywords composite; piezoelectric; pyroelectric, interferometric; IR detector, thermal detector.

INTRODUCTION

Piezoceramic-polymer composites with various connectivity patterns[1] are now an alternative to conventional piezoelectric materials. Owing to the advantages over other materials in terms of cost and ease of manufacture, epoxy-based composites were of interest in this work. Fine grained ceramic of Lead Titanate ($PbTiO_3$:PT) was fabricated to produce a porous PT the pores of which were impregnated with an epoxy. The PT-epoxy composites were tested as materials for pyroelectric long wavelength infrared (IR) radiation detectors.[2] The important parameters investigated were the strain piezoelectric coefficient, the pyroelectric coefficient. the thermal

diffusivity, the voltage responsivity, the specific detectivity, and the three figures-of-merit.

MATERIALS AND METHODS

Sample Preparation

In order to prepare PT powders, commercial powders of lead oxide (PbO) and titanium oxide (TiO_2) supplied by Fluka Ltd. were mixed and wet-ball milled for 24 h. The mixture was dried before sieving, then calcined at 750°°C for 2 h. The X-ray diffraction pattern analysed by a PHILIPS X'Pert MPD diffractometer confirmed the tetragonal phase of the calcined powders. The calcined powders were crushed and sieved into an alumina crucible for sintering at 1150°C to produce a porous-structure ceramic. The ceramic voids were filled with an epoxy by a vacuum impregnation technique at room temperature. The PT-epoxy composite was cut into disk samples and surface finished by grinding and polishing. The density of the sample was found to be 4.4 x 10^3 kg/m^3 so the volume fractions of ceramic : epoxy was determined to be 50:50. .

The microstructure morphology of the composite was studied using a JEOL JSM-5200 scanning electron microscope (SEM). In order that the SEM micrographs would show the regions of the PT ceramic and epoxy more clearly, the micrographs were made on the polished surface before and after the epoxy was etched with acetone. As seen in FIGURE 1, each phase was almost completely interconnected. Therefore, this composite had a 3-3 connectivity.

The composite samples were electroded with silver paint and subjected to a ferroelectric hysteresis measurement at room temperature and the coercive field E_c of 4.5 MV/m was observed. The samples were poled with a DC electric field of 6 MV/m for 30 min at room temperature.

Experimental procedure

A single-beam interferometer of a Michelson type as developed by the PennState group[3] has been successfully used for determining the d_{33} piezoelectric coefficient of the 1-3 PZT-epoxy composites. [4] A similar technique was used to find a value for the poled PT-epoxy composite.

The pyroelectric coefficient was measured by detecting the charges generated for a known temperature change[5]. To minimize the humidity in the surrounding environment and avoid the softening temperature of the polymer, the measurements were made below room temperature and at a reduced pressure of 10^{-3} Pa.

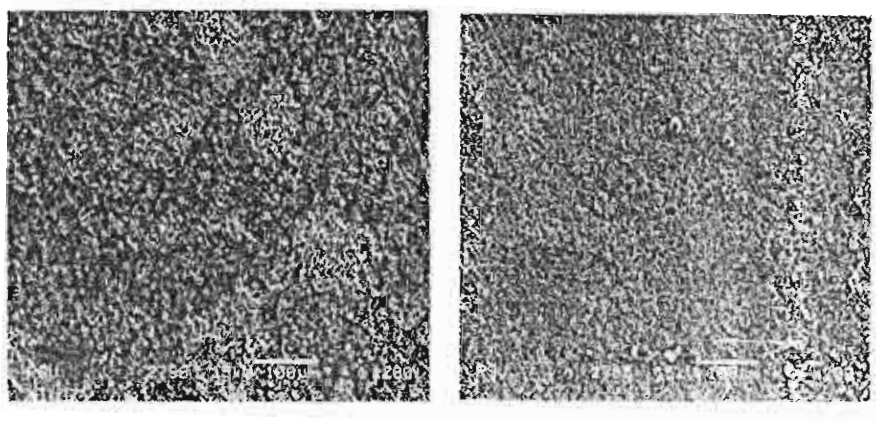

(a)

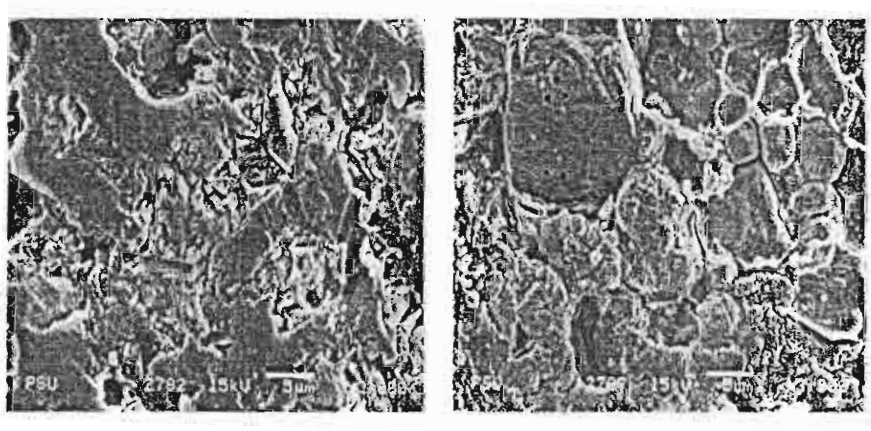

(b)

FIGURE 1 SEM micrographs of polished (left) and polished-etched (right) surface of PT-epoxy at (a) x 200 and (b) x 3000

Thermal diffusivity measurements [6] were made on the composite using a commercial $LiTaO_3$ wafer as a pyroelectric detector. A sinusoidally modulated laser

beam from a Lasiris diode laser (Edmund Scientific Co.) was incident on the sample surface so that the heat diffused through the sample to the $LiTaO_3$ detector. The heat capacity of the sample was measured using a Differential Scanning Calorimeter (Perkin Elmer, DSC7).The unknown thermal diffusivity of the composite was analysed from the dimensions, density, heat capacity and the measured phase lag vs modulation frequency. Similar measurements were made on a glass sample with the PT-epoxy composite acting as a detector in order to determine the thermal diffusivity of the glass.

In the responsivity measurements, the modulated laser beam was incident on the electroded surface of a free-standing sample of the composite. The pyroelectric voltage was measured at different modulation frequencies. The voltage responsivity, R_V, was the voltage divided by the absorbed laser power. The voltage (F_V), current (F_I) and noise (F_D) figures-of-merit and the specific detectivity (D^*) of the composite were calculated at the frequency of the maximum responsivity of the composite. The following equations were used in the calculations: [7] :

$$R_V(\max) = \eta p A[R_G/G_T(\tau_E+\tau_T)] \quad (1)$$

$$F_V = p/c'\varepsilon_r\varepsilon_0 \quad 2)$$

$$F_I = p/c' \quad (3)$$

$$F_D = p/c'(\varepsilon_r\varepsilon_0\tan\delta)^{1/2} \quad (4)$$

$$D^* = A^{1/2}/\mathrm{NEP} \quad (5)$$

The composite element had an area A, emissivity η, pyroelectric coefficient p, and volumetric heat capacity c'. G_T is the thermal conductance to the surroundings which gave the thermal time constant τ_T. R_G is the input resistance of the lock-in amplifier, giving the electrical time constant τ_E. ε_r and $\tan\delta$ are the relative permittivity and loss tangent of the composite, respectively. ε_0 is the permittivity of free space. NEP is the noise-equivalent power which depends upon the Johnson noise voltage and R_V.

RESULTS AND DISCUSSIONS

During the interferometric measurements, the composite was rigidly glued on the substrate and only a surface of the composite was monitored. The measured d_{33} value

was corrected for substrate clamping [8] and the value obtained was $(6.0 \pm 1.0)\times10^{-12}$ m/V. FIGURE 2 shows a linear piezoelectric response observed from the 1.3 mm PT-epoxy composite.

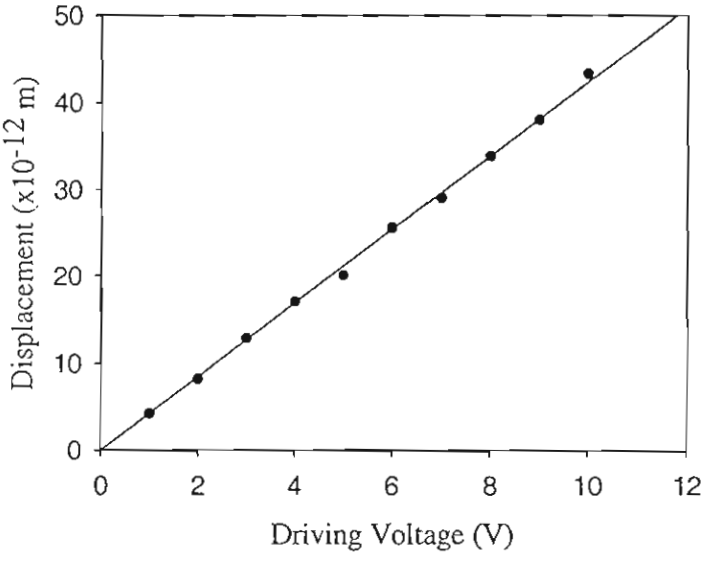

FIGURE 2 Piezoelectric responses at 1 kHz for PT-epoxy composite.

The pyroelectric coefficient of the composite was found to be 23 $\mu C/m^2$ °C. The low piezoelectric and pyroelectric activities were due both to incomplete poling and to porosity in the composite. At room temperature and 1 kHz , the composite had a high dielectric constant of 96 and low loss tangent of 0.03.

Using a $LiTaO_3$ detector, the thermal diffusivity of PT-epoxy composite was found to be 2.2×10^{-7} m^2/s. A value of 5.1×10^{-8} m^2/s was found for a glass microscope slide using the PT-epoxy composite as a thermal detector.

For the IR detector data, FIGURE 3 shows the R_v vs frequency curve. F_V, F_I, F_D and D* were found to be 0.031 m^2/C, 26×10^{-12} m/V, 5.2×10^{-6} $Pa^{-1/2}$ and 1.4×10^6 $cmHz^{1/2}/W$, respectively.

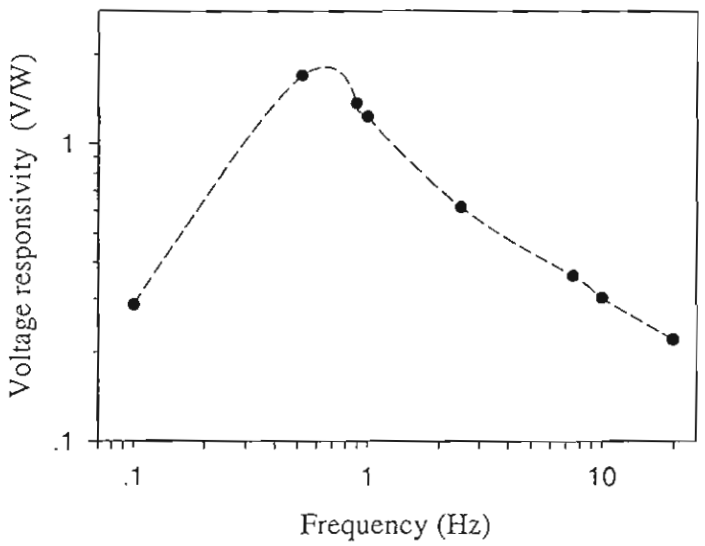

FIGURE 3 The voltage responsivity as a function of modulation frequency obtained from the PT-epoxy composite acting as an IR detector.

SUMMARY

A first attempt to produce a piezoceramic-polymer composite was described in this work. SEM investigations showed a composite with 3-3 connectivity. TABLE 1 presents the measured physical properties of the composite. A comparison with other ceramic and polymeric materials is listed in TABLE 2. As seen from the tables, after further development, the PT-epoxy composite will have a good potential for various ferroelectric devices.

TABLE 1 Measured physical properties of PT-epoxy composite.

Volume fract.	Density (10^3 kg/m^3)	Heat Capacity (J/kg °C)	Dielectric const.	tanδ	Thermal diffusivity (10^{-7} m^2/s)
50-50	4.4	200	96	0.03	2.2

TABLE 2 Detector properties of PT-epoxy composite compared with those of other materials.

Parameter	PT-Epoxy	50/50 P(VDF/TrFE)[9]	PT[10]	PZT[11]	$LiTaO_3$[11]
d_{33} (10^{-12} m/V)	6.0	25	56	374	9.2
p ($\mu C/m^2$ °C)	23	40	250	380	180
F_V (m^2/C)	0.031	0.11	0.046	0.059	0.14
F_I (10^{-12}m/V)	26	17	78	152	56
F_D (10^{-6}m/$Pa^{-1/2}$)	5.2	7.4	25	55	39
D* (10^6 cm$Hz^{1/2}$/W)	1.4	-	-	-	-

The relatively high detector parameters of the PT-epoxy composite showed that it could be used as an IR detector or a thermal detector in applications such as thermal diffusivity measurements. In order to make a real detector[12], the fabrication processing and various parameters of the composite will be optimized before the material is fabricated into its final form.

ACKNOWLEDGEMENT

This work is gratefully supported by Thailand Research Fund (TRF).

REFERENCES

[1] R.E. Newnham, D.P. Skinner, L.E. Cross, Mater Res. Bull. **13** (1978).

[2] S.B. Lang and D.K. Das-Gupta, Ferroelectrics. Rev. **2**:3-4 (2000).

[3] Q.M. Zhang, W.Y.Pan and L.E.Cross, J.Appl.Phys. **63**: 8 (1988).

[4] Y.Phermpornsagul, S. Muensit and I.L. Guy, IEEE Trans. Dielec. Electr. Insul. (in press).

[5] W.Y. Ng, B. Ploss, H.L.W. Chan, F.G. Shin and C.L. Choy IEEE Int. Symp. **2** (2001).

[6] S. Muensit and S.B. Lang, Ferroelectrics. **293.** 341 (2003).

[7] R.W. Whatmore, Rep. Prog. Phys. **49** (1986).

[8] D. Royer and V. Kmetik, Electron. Lett. **28** (1992).

[9] N. Neumann, R. Kohler, R. Gottfried-Gottfried, and N. HeB, Integr. Ferroelectr. **11** (1995).

[10] R. Takayama, Y. Tomita, K. Iijima and I. Ueda, Ferroelectrics **118** (1991).

[11] B. Ploss and S. Bauer, Sens. Actuators A **25-27** (1991).

[12] http://www.boselec.com.

เอกสารหมายเลข 2.2

Subject: Manuscript for MRI
From: "Meredith Weber" <maw9@psu.edu>
Date: Tue, November 2, 2004 9:32 am
To: tawee@chiangmai.ac.th
Priority: Normal
Options: View Full Header | View Printable Version | View Message details

Dear Dr. Tunkasiri,

Thank you for your inquiry about your submission to Materials Research Innovations, Ref. No. 03-072, and for your patience. Your manuscript is scheduled to be published in Vol. 8, issue 6 of the journal. We look forward to seeing your paper online and the Executive Summary in the new print format.

Sincerely,

Meredith Weber

Meredith Anne Weber

Managing Editor

Materials Research Innovations

The Pennsylvania State University

103 Materials Research Laboratory

University Park, PA 16802

P: 814-865-2610

F: 814-863-7040

Preparation and Characterization of High-Purity PZT Powders and Ceramics Made by Modified Spray Drying Techniques

W. Thamjaree, L.D. Yu, K. Pengpat and T. Tunkasiri

Department of Physics, Faculty of Science, Chiang Mai University, Chiang Mai, THAILAND

Abstract

A modified chemical method in which considerably low-purity and low-price chemicals were employed to produce fine and homogeneous PZT powders in the composition of $Pb(Zr_{0.52}Ti_{0.48})O_3$ by spray drying and calcining techniques was developed. Phase evolution, thermal properties and microstructure of the spray dried granules were studied using X–ray diffractometry (XRD), Differential thermal analysis (DTA) & Thermogravimetric analysis (TG) and Scanning electron microscopy (SEM) techniques respectively. The results showed that the high-purity PZT phase started to appear at 500°C and become increasingly pronounced as temperature rose. No impurity was detected as can be confirmed by transmission electron diffraction (TED) analysis and energy dispersive spectroscopy (EDS). The corresponding ceramics were sintered between 900 °C and 1250 °C. The planar coupling coefficient (K_p), piezoelectric constant (d_{33}), loss angle ($\tan\delta$), density and dielectric constant (ε), as well as grain size of the ceramics were measured. The highly dense ceramics with the relative density of 97 % to the theoretical value could be obtained at the sintering temperature of 1000 °C. All the values obtained in this work were among those of the ceramics produced from high-purity chemicals in previous work.

Keywords : Piezoelectric and dielectric properties; PZT; Spray drying

Introduction

Lead zirconate titanate (PZT) ceramics have been widely studied due to their very high electromechanical coupling coefficient. As a result they have been employed in many applications such as hydrophones [1], igniters, fine movement controllers, etc. [2] Earlier studies [3-5] revealed that the PZT properties are affected by their microstructures which partly depend on size and homogeneity of the starting powders. Generally, those conventional methods [6] using ball milling of the constituent oxides have the difficulty in controlling the powder size, particle size distribution and homogeneity of the PZT powders. However, fine, homogeneous PZT particles can be obtained via chemical processes [7,8,9,10]. Ceramics produced from these powders often yield encouraging piezoelectric and dielectric properties. The PZT ceramics produced via the chemical processes usually require very high purity (> 99.9 %) and high cost chemicals which are not appropriate for large scale production.

The spray drying technique was of particular interest because the quality powders may be produced in a large quantity. Lal *et al.* [11] and Uematsu *et al.*[12] revealed that fine and very homogeneous particles of strontium-doped PZT and silicon nitride (Si_2N_4) respectively could be produced via this technique. Both of them used the reagent grade of high cost chemicals as starting materials. However, the problem arises as the powders produced via spray drying technique using starting chemical of reasonably lower purity (<99.9 wt%) often yield unexpected secondary phase particles.

In this work, the attempts have been made in order to develop a modified chemical method via the spray drying technique followed by calcining process using low purity grade (< 99 wt %) and comparatively low price chemicals to produce PZT powders, which have comparable properties with those produced via the previously

described processes. The pH of the mixed nitrate solution of the constituents was carefully controlled and the spray drying process was carried out. The characteristic of the spray-dried PZT powders was investigated. The piezoelectricity, dielectricity and densities of the corresponding ceramics were also studied.

Experimental procedure

The low-price chemicals used in this work are solutions of lead nitrate ($Pb(NO_3)_2$, 99 % by weight), zirconyl nitrate hydrate ($Zr(NO_3)_4.6H_2O$, ~27 % of Zr by weight and tetraisopropyl orthotitanate ($C_{12}H_{28}O_4Ti$, ~99 % by weight). The molar ratio of those solutions was kept at 1:0.52:0.48 which is corresponding to the crystal phase of $Pb(Zr_{0.52}Ti_{0.48})O_3$. By following the work done by Tunkasiri [7], the aqueous solutions of $Pb(NO_3)_2$ and $(Zr(NO_3)_4.6H_2O$ were firstly mixed. Then the mixture of the $C_{12}H_{28}O_4Ti$ solution and strong nitric acid (HNO_3, pH ~ 1) was gradually added into the previously mixed solution. In order to stabilize the metals in the solution, the hydrogen peroxide (H_2O_2) was added. Aqueous ammonium solution was then slowly added to control the pH of the mixture solution. In order to obtain manganese-doped PZT ceramics for reducing the loss angles and increasing the resistivity [13], a solution of manganese chloride ($MnCl_2$) was admixed. The solution was then fed into the nozzle of a spray dryer at an operating temperature of 130 °C to obtain fine granules. The granules were subsequently calcined at 500, 600, 700, 800 and 850 °C for 1 hour. An X-ray diffractometer (XRD, Siemens) was employed to study the phase evolution. The microstructures of the powders and ceramics were investigated using SEM. The purity of the PZT particles was observed using TED and EDS. The thermal characteristics of PZT powders were studied using DTA and TG.

In order to obtain Mn-doped PZT ceramics, the powder that was calcined at 700 °C for 2 hours was pressed (3500 psi) into circular disks with approximately 2.5 cm in diameter and 1 mm in thickness. Polyvinyl alcohol (PVA) was used as a binder. The samples were sintered at 900, 1000, 1100, 1200 and 1250 °C for 1 hour respectively, with the heating rate of 100°C/h. Then the samples were held at 500°C for 30 mins for binder removal before heating up to their sintering temperatures. The XRD was used to study the phase formation and SEM was used to observe the surface microstructure of the sintered ceramics.

Silver paste was applied to the samples for electrical contact. Poling was carried out at 130 °C in a stirred silicone oil bath using a field of 18 kV cm^{-1} for about 5 min. The dielectric constant (ε_r), loss factor (tanδ) and planar coupling coefficient (K_p) were measured using an impedance/gain-phase analyzer (LCZ) (Model 4276, Hewlett Packard). The piezoelectric coefficient (d_{33}) was measured using a piezo-d_{33} meter (Model CADT Berlincourt). Relative densities of the prepared ceramics were also measured using Archimedes' principle. X-ray diffraction and electron microscopy were employed to analyse the ceramic samples.

Results and Discussion

Fig.1(a) shows X-ray diffractograms of the prepared samples after the calcination, at different calcination temperatures, indicating the phase evolution of the spray dried granules. It can be seen that the PZT phase began to appear at 500 °C and became even more pronounced at 850 °C. Every peak can be attributed to PZT [14]. No impurities or secondary phases were detected using this XRD method. The formation of the perovskite PZT phase is agreeable to that formed in other methods,

such as the coprecipitation method [9] and the mechanochemical method. [15] The X-ray diffractograms of the PZT ceramics sintered at different sintering temperatures are also shown in Fig.1(b). It can be seen that transformation of the cubic to tetragonal phase occurred at 1100 °C onward.

The thermograms of DTA and TG indicating the phase tranformation and weight loss, respectively, of the spray dried granules at various temperatures are shown in Fig. 2. The first weight loss accompanied by an endothermic peak is around 100 °C. This is due to the evaporation of water and volatile residues that generally exist in the powder. The endothermic peak at about 400 °C may be attributed to the evolution of gases as indicated by Wang *et al.* [8] and Das *et al.*[10], which can be confirmed by the weight loss in TG trace from about 80 wt% down to 60 wt%. The noticeable exothermic peak at around 530 °C is possibly due to the crystallization of PZT phase. [9] This is consistent with the XRD result in Fig 1(a), which shows the growth of PZT cubic phase starting at 500°C.

The microstructure and morphology of the as-sprayed and calcined PZT powders obtained by the spray drying technique are shown in the SEM micrographs (Fig.3). It can be seen that the size of the as-sprayed granules is about 1-2 μm and the shape is almost spherical but with dimples (Fig.3a). The granules grew bigger at the higher calcining temperature (Fig.3b) as generally expected. The same shape was also observed in the spray-dried granules produced by Uematsu *et al.* [12]

In order to confirm the purity of the PZT particles, the EDS and TED analyses were employed. A typical EDS spectrum was illustrated in (Fig.3c), showing no sign of impurity excepting gold particles which were sputtered on the sample. The transmission electron diffraction (TED) patterns of selected area were studied. The

typical TED and its corresponding TEM were shown in Fig 4. By using the method from Andrews *et al.* [16], the TED spots (Fig. 4a) were analysed. It was found that all TED spots are corresponding to the PZT phase [14]. This confirmed the high-purity of the PZT powders. Its corresponding transmission electron micrograph (Fig. 4b) shows thin layers of PZT locating on top of each other which is contributed to the spots and rings in the TED.

For the correspondingly produced PZT ceramics, the XRD study of the phase evolution indicated that the transformation of the cubic to tetragonal phase occurred at the sintering temperature of 1100°C, as shown in Fig. 1b. The SEM micrographs in Fig.5 show that the grain grew from 0.5 μm (sintered at 1000 °C) to 2.5 μm (sintered at 1250 °C) on an average. This result is closed to that obtained from Lal *et al.* [11], who prepared ceramics from spray-dried granules using high purity chemicals.

In Table 1, the dielectric, piezoelectric and physical properties of the prepared ceramics are compared with those of Tunkasiri [7], Lal *et al.* [11] and Zhilun *et al.* [17]. It can be seen that the ceramic sintered at 1000 °C has the highest density (about 7.82 g/cm^3 or 97 % of theoretical density) which is closed to that of Tunkasiri [7], who however used the high-quality and high-cost chemicals. The density of the ceramics is noticed to increase as the temperature rises up to 1000 °C and gradually decrease as further increasing of temperature. This is probably owing to the lead loss that normally occurs at the high sintering temperature thus resulting in shrinkage and subsequent porosities in the ceramics. The values of the dielectric constant, with the maximum of 780 obtained from the ceramics sintered at 1100 °C, are pretty well between those of the previous work [7,11,17]. The tanδ, d_{33} and K_p values of our

results are in the ranges of 0.004 to 0.02, 130 to 168 pC/N and 0.52 to 0.60 respectively. These are comparable to those obtained by Lal *et al.* [11], Tunkasiri [7] and Zhilun *et al.* [17], though the former two used the high purity chemicals for their preparations and the latter employed mixed oxide route plus low melting frit.

Conclusions

A modified chemical method using spray drying technique followed by calcinations using low-purity and low-cost chemicals has been developed to produce fine, homogenous and high-purity PZT powders. The round-shape particles of PZT phase started to form at 500 °C and the complete crystallization occured at about 850 °C. The particles grew accordingly as temperature rose. No impurity was detected. The values of the grain size, piezoelectricity, dielectricity and densities of the ceramics sintered from the spray-dried PZT powders were among those of the ceramics produced from high purity chemicals.

Acknowledgements

The authors would like to express their sincere thanks to the Thailand Research Fund for the financial support.

References

1. Y. Kurihara, K. Mizumusa, H. Ohashi, Transmitter properties of porous $Pb(Zr,Ti)O_3$ transducer, Jpn, J.App.Phys, **31** (1992) 3067-3069.
2. J.V. Randeraat, R.E Setterington, Piezoelectric Ceramic, Mullard, London, (1974) 23-44.
3. S.S Chiang, M. Nishioka, R.M Fulrath, J.A Pask, Effects of processing on microstructure and properties of PZT ceramics, Am.Ceram.Soc.Bull, **51** (1972) 484-489.
4. D.A Buckner, P.D Wilcox, Effects of calcining on sintering of lead zirconate-titanate ceramics, Am.Ceram.Soc.Bull, **51** (1972) 218-222.
5. C.K. Liang, L. Wu, Microstructure and properties of Cr_2O_3-doped ternary lead zirconate titanate ceramics, J.Am.Ceram.Soc., **76(8)** (1994) 2023-2026.
6. D.E Wittmer, R.C Buchanan, Low temperature densification of lead zirconate titanate with vanadium pentoxide additive, J.Am.Ceram.Soc, **64(8)** (1981) 485-490.
7. T. Tunkasiri, Properties of PZT ceramics prepared from aqueous solutions, Smart Mater.Struct., **3** (1994) 243-247.
8. W.W. Wang, D.A. Hall, F.R. Sale, Phase homogeneity and segregation in PZT powders prepared by thermal decomposition of Metal-EDTA complexes derived from nitrate and chloride solutions, J.Am.Ceram.Soc, **75(1)** (1992) 124-130.
9. B.A. Menegazzo, J.A. Eiras. Preparation of coprecipitation ferroelectric ceramic powders by two stage calcination, J.Am.Ceram.Soc, **76(11)** (1993) 2734-2736.

10. R.N. Das, A. Pathak, P. Pramanik, Low-temperature preparation of nanocrystalline lead zirconate titanate and lead lanthanium zirconate titanate powders using triethanolamine, J.Am.Ceram.Soc, **81(12)** (1998) 3357-3360.

11. R. Lal, N.M. Gokhale, R. Krishnan, P. Ramakrishnan, Effect of sintering parameters on the microstructure and properties of strontium modified PZT ceramics prepared using spray-dried powders, J.Mater.Sci., **24** (1989) 2911-2916.

12. K. Uematsu, N. Uchida, Z. Kato, S. Tanaka, T. Hotta, M. Naito, Infrared microscopy for examination of structure in spray-dried granules and compacts, J.Am.Cer.Soc., **84(1)** (2001) 254-256.

13. R. C Buchanan, Ceramic Materials for Electronics: Processing, Properties and Applications, Marcel Dekker, New York, (1986) 110.

14. Powder Diffraction File, Card No.33-784 (2000). (Swarthmore , P.A. Joint Committee on Powder Diffraction Standards, International Centre for Diffraction Data).

15. J. Xue, D. Wan, S.E. Lee, J. Wang, Mechanical synthesis of lead zirconates titante from mixed oxides, J.Am.Ceram.Soc., **82(7)** (1999) 1687-1692.

16. K.W. Andrews, D.J. Dyson and S.R. Keown "Interpretation of Electron Diffraction Patterns", (Plenum press, New York) (1971), 149.

17. G. Zhilun, L. Longtu, G. Sahuo, Z. Xiaowen, Low-temperature sintering of lead-based piezoelectric ceramics, J. Am. Ceram. Soc., **72(3)** (1989) 486-491.

Table 1. Piezoelectric, dielectric and physical properties of the PZT ceramics produced from the spray dried granules.

Sintering temperature (C^o)	**Density (gm/cc)**	**Dielectric constant (ε_r)**	**Loss angle ($\tan\delta$)**	**K_p**	**d_{33} (pC/N)**
900	7.65	675	0.02	0.54	136
960 [16]	7.56	1100	0.008	0.57	250
1000	7.82	690	0.001	0.60	168
1050 [7]	7.94	490	0.001	0.44	-
1100	7.80	780	0.002	0.52	130
1200	7.75	675	0.004	0.60	156
1200 [11]	7.61	1180	0.007	0.45	230
1250	7.66	630	0.002	0.58	153

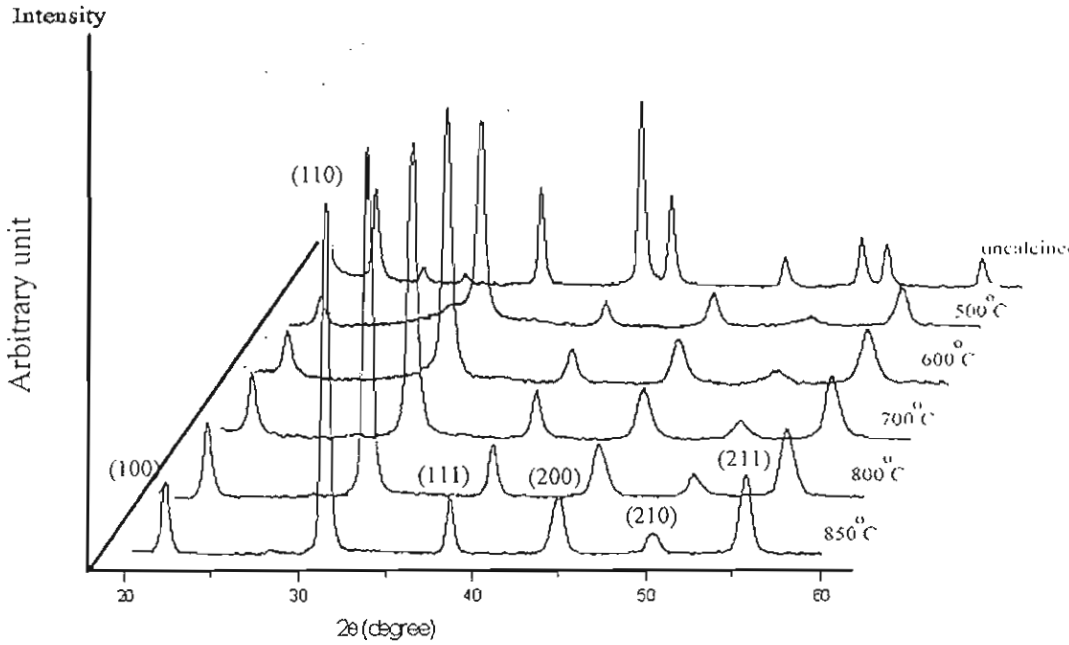

(a)

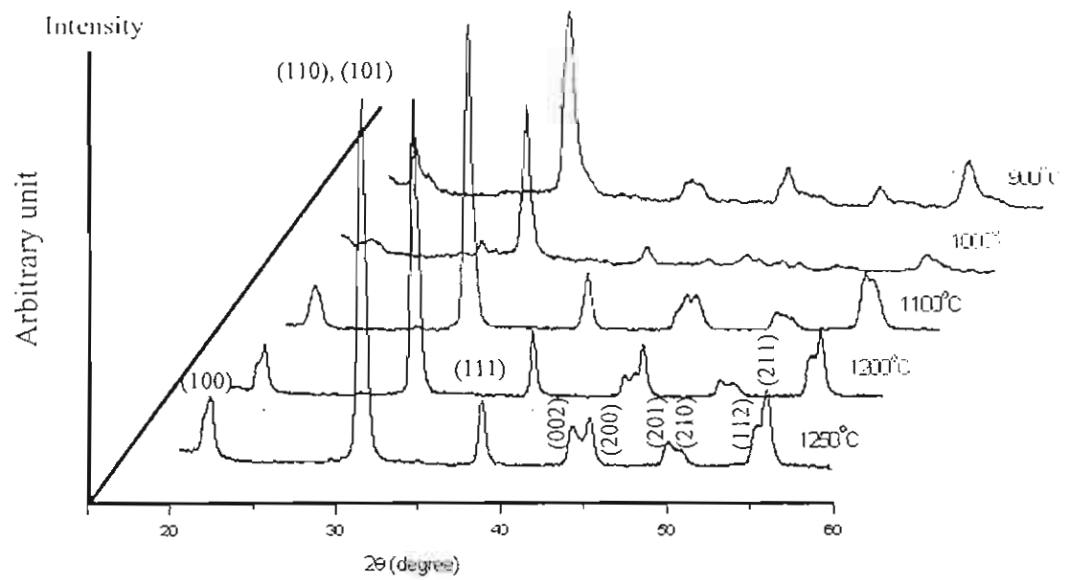

(b)

Figure 1. X-ray diffractograms of the spray dried granules and ceramics after calcining (a) and sintering (b), respectively, at various temperatures.

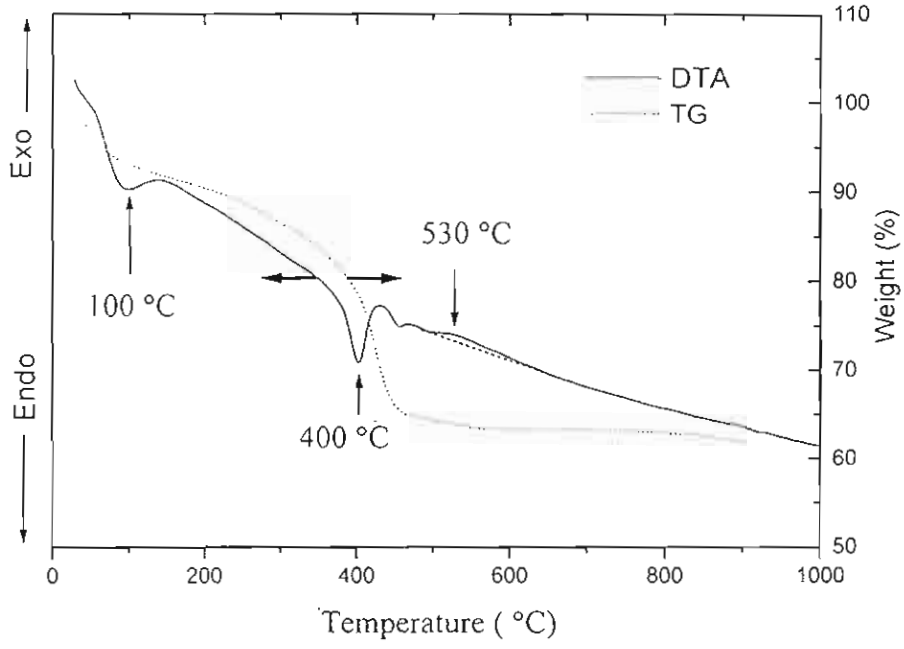

Figure 2. DTA and TG thermograms of the spray dried granules.

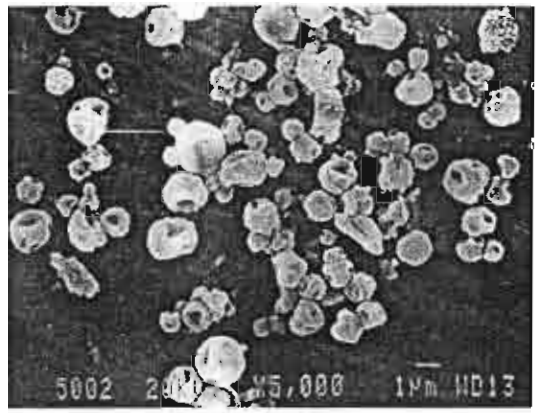

(a)

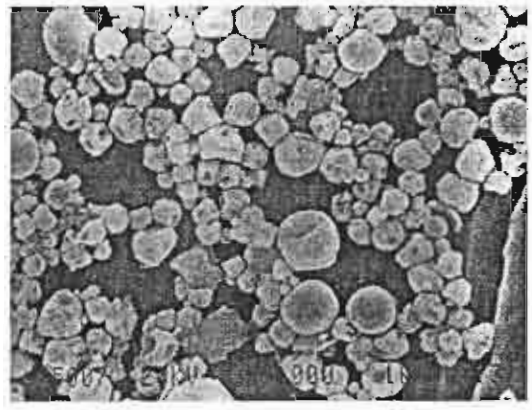

(b)

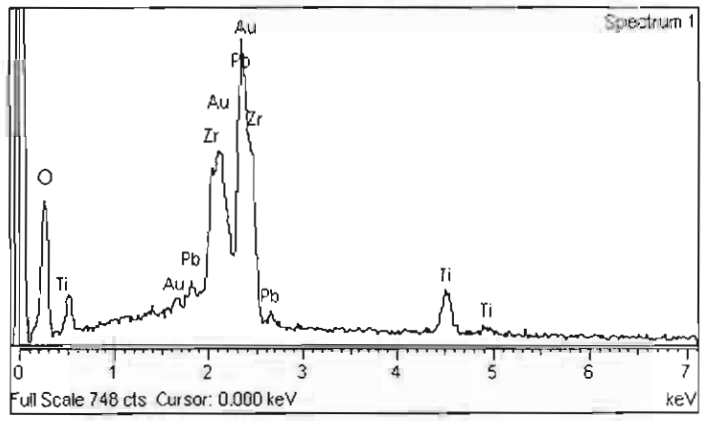

(c)

Figure 3. Scanning electron micrographs of the (a) as-sprayed and (b) heat treated (at 700 °C) particles and (c) EDS spectrum of corresponding PZT powders.

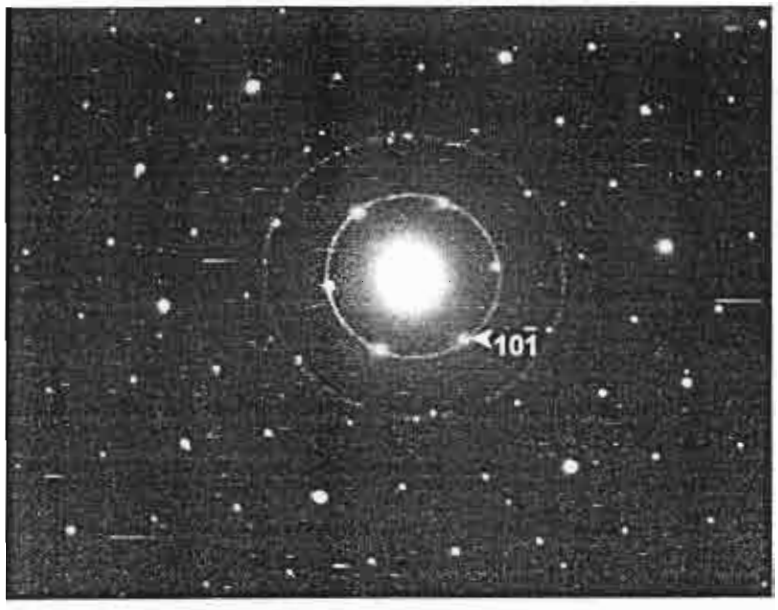

(a)

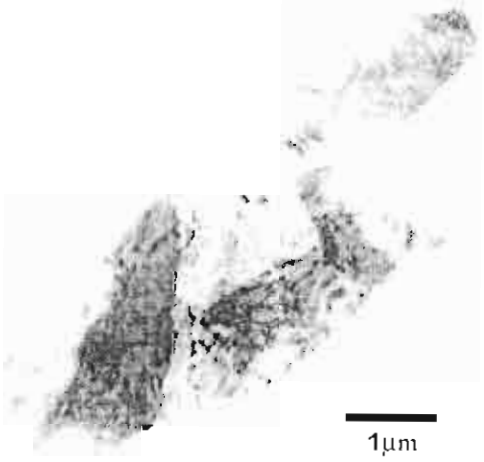

(b)

Figure 4. TED (a) and TEM (b) micrographs of selected area of PZT powder.

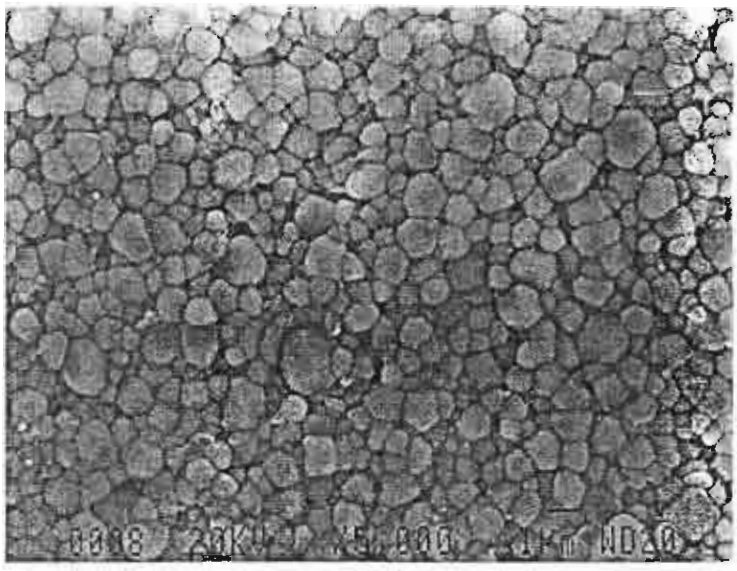

(a)

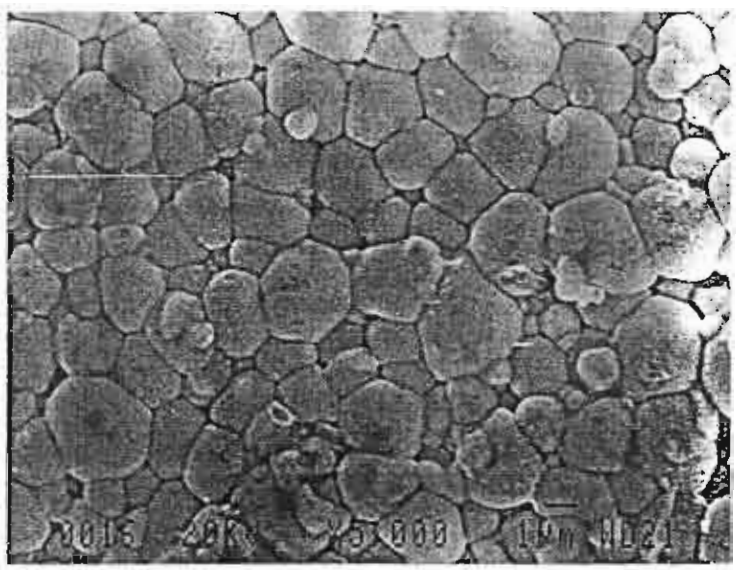

(b)

Figure 5. Scanning electron micrographs of the microstructure of the PZT ceramics sintered at 1000 °C (a) and 1250 °C (b).

List of Table

List of Figures

N.B.

Figure 1. should appear after the first paragraph page 5

Figure 2. should appear after the second paragraph page 5

Figure 3. and 4. should appear after the first paragraph page 6

Figure 5. should appear after the second paragraph page 6

Table 1 should appear after the first paragraph page 7

เอกสารหมายเลข 2.3

Your paper submitted to Applied Physics A: # 5998

Dear Dr. Tangjuank,

Your paper "Sol-gel synthesis and characterization of BaTi2O5 powders" by S. Tangjuank and T. Tunkasiri has been accepted for publication in Applied Physics A on June 15, 2004. Please inform your co-author, thank you.

If not already done so, please send the electronic version of your paper and a signed copyright transfer statement together with the list of up to five PACS numbers to:

Mrs.
Friedhilde Meyer
Applied Physics A
Springer Verlag
Tiergartenstr. 17
D-69121 Heidelberg

friedhilde.meyer@springer.de

You will receive within the next couple of weeks the galley proofs of your paper directly from the printing office. Please do check them carefully for any misprints or small errors.

We look forward to receiving also your excellent future papers for publication in
Applied Physics A
Materials: Science & Processing.

With best regards

Prof. Dr. Michael Stuke
Editor-in-Chief
Applied Physics A

Uncorrected paper

Sol – gel synthesis and characterization of $BaTi_2O_5$ powders

S. Tangjuank* and T. Tunkasiri**

* Department of Physics, Faculty of science, Uttaradit Rajabhat University, Uttaradit 53000, Thailand

**Department of Physics, Faculty of Science, Chiang Mai University, Chiang Mai 50200, Thailand

e-mail : singhadej@mail.riu.ac.th e-mail : tawee@chiangmai.ac.th

Abstract

$BaTi_2O_5$ powders was synthesized using the sol – gel method and characterized. Phase evolution and characteristics of the samples were studied using the differential scanning caloriemetry (DSC), the thermogravimetic analysis (TGA) and X-ray diffractometry (XRD). The results show that the formation of $BaTi_2O_5$ starts around 800°C and continues until 1200°C in air and in this calcination temperature range all powders appear to be single-phase monoclinic $BaTi_2O_5$. The mechanism of $BaTi_2O_5$ formation was studied by Fourier transform infrared spectroscopy (FTIR). The IR absorption peaks confirm the existence of a substitution reaction with the chelating reagent corresponding to different modes of vibration characteristic of the acetate group. Scanning electron microscopy (SEM) observations reveal that the size of the particles in nearly round shape formed due to agglomeration is about 0.1–1.5 μm and increases with calcination temperature.

1. Introduction

The compounds in the $BaO – TiO_2$ system about their properties are widely used in electronic ceramic because of having high dielectric constant and lead-free. $BaTi_2O_5$ is

one of the most important compounds of the titania-rich compounds in this system which is of considerable interest for electronic dielectric applications. In recently, Yukikuni *et al*, [1] reported that the $BaTi_2O_5$ showed a large dielectric constant of 30,000 at a curie temperature of T_c = 430 °C. $BaTi_2O_5$ was first studied by Rase and Roy [2], they suggested that $BaTi_2O_5$ prepared by solid state reaction was not stable below 1200°C. By this method, several researchers [3-6] concluded that $BaTi_2O_5$ could be obtained above the solidus temperature (1300°C) or from melt but was not stable below this temperature. Therefore, the newly evolving wet chemical techniques have been considered. Ritter *et al*., [7] Paff[8] and Javadpour *et al*.[9] employed liquid mix technique, peroxide method and Pechini method, repectively. They reported that $BaTi_2O_5$ started to form at about 700°C to 1150°C, but at higher temperature about 1200°C $BaTi_2O_5$ decomposed into $BaTiO_3$ and $Ba_6Ti_{17}O_{40}$. Xu *et al*.[10] also prepared $BaTi_2O_5$ by sol – gel method using ethylenediammetetraacetic acid (EDTA) as a chelating agent. They found that $BaTi_2O_5$ formed at 800 – 1200°C for 2 h. Nevertheless, new chemical preparation methods have still been researched in order to obtain single-phase $BaTi_2O_5$. Therefore in this paper, we prepare $BaTi_2O_5$ by a sol – gel method using acetic acid as a chelating agent, since it was successfully employed to prepare single-phase $BaTiO_3$ powder [11-12] and has an additional merit of achieving fine particles with high purity and use of low – temperature synthesis techniques. In addition, we investigate the phase and morphology evolution of $BaTi_2O_5$ powders after various firing conditions with attention paid on the correlation between the effects of calcination, phase formation and morphology development.

2. Experiment details

Barium oxide, titanium (IV) isopropoxide, conc. acetic acid, methanol and dried n-butanol were used as the starting compounds. To form a barium methoxide, BaO (5.2 g)

was dissolved in 30 cc acetic acid and methanol (50 cc) was used as solvent. For Ti/Ba = 2, dried n-butanol (50 cc) was added to 20 cc titanium (IV) isopropoxide to obtain the stable Ti- solution. The mixed solution of barium and Titanium was heated at 80 °C on a hot plate with continuous stirring for 1 h. After that 20 cc of distilled water was added to the solution to form a gel. The gel was dried in an oven at 110 °C for 24 h, the white powder precursor was form. The dry precursor was ground and then heated in air at the temperature which ranged from 400 to 1250°C for 4 h to yield $BaTi_2O_5$. Phase transformations of the dried powders were analyzed by differential scanning caloriemetry (DSC) and thermogravimetic analysis (TGA), which was preformed up to a temperature of 1200°C with a heating rate of 10°C/min. Phase evolution of the calcined powders was characterized by X-ray diffraction (XRD) (CuK_α radiation). The morphology of the calcined powders was studied using scanning electron microscopy (SEM). The reaction mechanism related to the calcination processes was studied using Fourier transform infrared spectroscopy (FTIR) at room temperature in the KBr plate method. [13]

3. Results and discussion

Fig. 1 shows the DSC/TGA thermogram obtained from the dried precursors of $BaTi_2O_5$ to 1000°C. It can be seen that evaporation of water occurred at below 250°C, corresponding to endothermic peak with 12.5% weight loss, losing of remnant organics or decomposition of acetate group to form barium carbonate accompanied by the endothermic peak at about 370°C with 19% weight loss located at 250°C to 450°C, and the decomposition of barium carbonate and titanium oxide and the reaction between fresh nuclei to form single-phase $BaTi_2O_5$ observed in exothermic peak at about 750°C to 900°C with no weight change. Fig. 2 shows a series of the X-ray diffractograms from the as-

mixed powder and those calcined at various temperatures. The XRD patterns were analyzed based on the Joint Committee on Powders Diffraction Standard (JCPDS), card No.70-1188. They showed that the powder heated at below 700°C are amorphous. Every peak in the patterns at the temperatures from 800°C to 1200°C can be attributed to $BaTi_2O_5$. This indicates that the powder is single-phase monoclinic $BaTi_2O_5$, which starts to form from about 800°C. However, the $BaTi_2O_5$ phase decomposes into $BaTiO_3$ and $Ba_6Ti_{17}O_{40}$ when heated over 1200°C. The formation and decomposition of $BaTi_2O_5$ in relation to temperature between 800 to 1200°C obtained from our XRD results are agreeable to those obtained by Ritter *et al.*,[7] Paff[8] and Javadpour *et al.*[9] But at the samples calcined at 1200°C appeared to be somewhat different where their results of $BaTi_2O_5$ decomposed into $BaTiO_3$ and $Ba_6Ti_{17}O_{40}$ while our result also showed $BaTi_2O_5$ and was consistent with the results of Xu *et al*[10]. Fig. 3 shows the IR spectra of dried precursor powders calcined at various temperatures i.e., 400, 500, 600, 700, 800, 900, 1000, 1100 and 1200°C. The IR peaks of dried precursors appeared at 1555, 1411, 1325, 1045, 1022, 934, 783 and 650 cm^{-1}. These IR data are consistent with the modes of vibration of acetate groups[14]. Peak at 1022 is assigned to Ti-O-C vibration and peaks at 1325 and 1411 are ascribed to the symmetric COO vibration. While peak at 1555 cm^{-1} is ascribed to the asymmetric COO vibration. So we conclude that acetate groups existed in gel network by ionic form. For the powders calcined at 400 to 600°C, the similar spectrums show bands at 1607, 1419 and 1386 cm^{-1} whereas the peaks at 1555, 1411, 1325, 1045, 1022, 934, 783 and 650 cm^{-1} disappear. This implies that acetate group decomposed and can be attributed to the vibration modes of the ionic carbonate. But these peaks disappear at 700°C and peaks of 896, 891, 755, 663, 656 and 503 cm^{-1} are observed. This indicates that the carbonate group decomposed and occurs reaction between barium carbonate and titanium oxide and resulted in formation of the unknown phase. While the formation of $BaTi_2O_5$ powders occurs

completely at 800 to 1200°C with the similar spectrums at 845, 756, 549 and 451 cm^{-1}. These results were confirmed by XRD patterns (Fig.2). Fig. 4 shows some of the scanning electron micrographs of the calcined $BaTi_2O_5$ powders at 800°C and 1200°C. It can be seen that the $BaTi_2O_5$ powders consist of hard aggregated fine particles in almost round shape and slightly grow at higher temperatures. The particle sizes are estimated to be in the range of 0.1 – 1.5 μm for the calcination temperatures from 800°C to 1200°C.

4. Conclusion

Single – phase $BaTi_2O_5$ powder could be prepared using sol - gel method with calcining the $BaTi_2O_5$ precursor at temperatures from 800°C to 1200°C for 4 h. XRD analyses of $BaTi_2O_5$ powders show that the formed powders have the stable single phase of $BaTi_2O_5$ in this temperature range, whereas the phase dissociates into $BaTiO_3$ and $Ba_6Ti_{17}O_{40}$ when sample is heated up to 1250°C. The IR absorption peaks confirm the existence of a substitution reaction with the chelating reagent corresponding to different modes of vibration characteristic of the acetate group. The microstructure of $BaTi_2O_5$ powders consist of weakly aggregated fine particles in almost round shape. The particle size is estimated to be in the range of 0.1– 1.5 μm and increases with temperature.

Acknowledgement

The authors would like to express their sincere thanks to the Thailand Research Fund for the financial support.

References

1. A. Yukikuni, F. Katsuhiro, S. Hirotake: Jpn. J. Appl. Phys. **42**, L946 (2003)
2. D. E. Rase, R. Roy: J. Am. Ceram. Soc. **38**, 33 (1955)
3. H. M. O'Bryan, J. Thomson: J. Am. Ceram. Soc. **57**, 522 (1974)
4. T. Negas, R. S. Roth, H. S. Pakker, D. Minor: J. Solid. State. Chem. **9**, 297 (1974)
5. K. W. Kirby, B. A. Wechsler: J. Am. Ceram. Soc. **74**, 1841 (1991)
6. J. P. Guha: J. Am. Ceram. Soc. **60**, 246 (1997)
7. J.J. Ritter, R.S. Roth, J.E. Blendell: J. Am. Ceram. Soc. **69**, 155 (1986)
8. G. pfaff: J. Mater. Sci. Lett. **9**, 1145 (1990)
9. J. Javadpour, N.G. Eror: J. Am. Ceram. Soc. **71**, 206 (1988)
10. Y. Xu, G. Huang, H. Long: Mater. Letts. **22**, 3570 (2003)
11. A. Cuneyt Tas: J. Am. Ceram. Soc. **82**, 1582 (1999)
12. L. Christine, G. Bernard, J. L. Andre: J. Appl. Phy. 175, 1 (1994)
13. K. William: Organic Spectroscopy, 2nd (Macmillam Education Ltd., London 1980)
14. K. Nakamoto: Infrared and Ramann Spectra of Inorganic and Coordination Compounds., 5th edition (John Wiley & Sons Inc., New York 1997)

เอกสารหมายเลข 2.4

Springer

Journals
Editorial Office

101 Philip Drive | Assinippi Park
Norwell | MA 02061 | USA
www.springeronline.com

tel +1 781 871 6600
fax +1 781 878 0449

Prof. T. Tunkasiri
Chiang Mai University
Department Of Physics
Faculty Of Science
Materials Science Research Lab.
Chiang Mai
50200 Thailand

Date: 04 January 2005

Our ref.: JMSL10387-04 J3AUT1 76558
Properties of CdS:Ni Films Prepared by Chemical Bath Deposition Method
EITSSAYEAM/INTATHA/PENGPAT/TUNKASIRI

Dear Prof. Tunkasiri:

I am pleased to inform you that your manuscript has been accepted for publication and will appear in one of the next issues of the JOURNAL OF MATERIALS SCIENCE LETTERS

Any queries concerning the production of your manuscript should be sent to:

Mrs. Angela DePina
Springer
JMSL
101 Philip Drive
Assinippi Park
Norwell, MA 02061 U.S.A.
Email address: angela.depina@springer-sbm.com

Please remember to quote the manuscript number JMSL10387-04 at all times. Thank you.

It would be greatly appreciated if you could provide us with an electronic version of your paper (please see the enclosed instructions). Thank you.

Sincerely yours,
Springer

Betty Pinney & Amiee DeSouza
Editorial Office JMSL
Email address: jms@springer-sbm.com

P.S.: If you would like to submit your accepted paper to the Open Choice program, please access the following URL: http://www.springeronline.com/openchoice

Properties of CdS:Ni films prepared by Chemical bath deposition method

S. Eitssayeam, U. Intatha, K. Pengpat and T. Tunkasiri

Department of Physics, Faculty of Science, Chiang Mai University,

Chiang Mai 50200, Thailand

Cadmium sulphide (CdS) is one of the well known II-VI compounds, which has gained considerable attention as a promising candidate for photodetector application. It has a wide range of applications in the technology of optical detectors, field-effect transistors and optoelectronic devices [1, 2, 3]. CdS thin films are also widely used as n-type window layers in thin film solar cells. There are many methods to fabricate CdS thin films, such as vaccum evaporation (VE), hot-wall vacuum evaporation (HWVE), close-spaced vapor transport (CSVT), spray pyrolysis (SP), chemical vapor deposition (CVD), screen printing (ScP), electrodeposition (ED), sputtering (ST) and chemical bath deposition (CBD) [4]. Among them, the chemical bath deposition (CBD) was the most suitable method to produce CdS thin films for n-CdS/p-CdTe solar cells applications because it has 15.8% cell efficiency, cost-effective and large-scale method [4,5]. In the CBD, CdS films were formed by precipitation from solution that containing cadmium ions and thiourea molecules in ammonia solutions. In order to improve the efficiency

of the CdS films, many works have been attempted to mix or dope other materials into the films. For examples, Atay et. al [6] prepared CdS:NiS films which prepared by spray pyrolysis, as nickel sulphide (NiS) is an interesting compound, it has a good electronic conductivity and an energy band gap of 0.35 eV [7]

In this work, we have synthesized thin films of CdS:NiS by CBD method. Various quantities of Ni were used for mixing. Surface characterization, structure, microstructure and morphology of the films due to heat treatment as well as their resistivities have been studied.

The CdS and CdS:Ni films, at the Ni mole percentages of 10 to 40, were deposited by chemical bath deposited method on 2.5x7 cm^2 commercial glass substrates. The starting solutions containing 0.05 M $CdCl_2$ (cadmium chloride), 0.01 $SC(NH_2)_2$ (thiourea), ammonia solution (NH_4OH 25%) was added to maintain the pH value of the solution at 11. The $CdCl_2$, $NiCl_2$ solutions were mixed together at room temperature with continuous stirring, afterthat, the NH_4OH solution was added until a colorless solution was obtained. Then the $SC(NH_2)_2$ solution was added. The mixed solution was maintained at 80^oC. The clean glass substrates were immersed vertically in the bath. The solution was continuosly stirred during 30 min of film deposition to keep a homogeneous distribution of chemical components. Finally, after

deposition, the glass substrates were removed from the chemical bath, and cleaned for several times with de-ionized water, then dried in air atmoshere. The experimental setup is shown in Fig.1.

The structural properties of the films were studied by an x-ray diffractometer with CuK_{α} radiation (Jeol model JDX-8030). Microstructure and surface characterization of the films were investigated using the scanning electron microscopy (Jeol SEM 6335F) and the atomic force microscopy (Seiko model SPI 3800 N), respectively. The compositions of the films were determined by the energy dispersive X-ray spectroscopy (EDS) and the resistivity of films (both dark and light conditions) were determined by the two-probe technique, using Fluke digital multimeter model 111. Various intensities of light were used for the light conditions employing a 40 W Phiplip superlux lamp. Intensities of light were detected using Foot Candle/Lux meter (EXTECH INSTRUMENTS : model 407000).

The plots of resistivities against the light intensities of CdS and CdS:Ni films at various ratios of Ni, were presented in Fig. 2. The plot of CdS:Ni, 7:3 was omitted since it is almost similar to the graph of ratio 6:4. It was seen that the resistivities of the films decreased sharply at high light intensities. However, the drop of resistivities becomes constant at 10830 Lux (40% of

light source). This may be due to the fact that the light energy raises the electrons across the energy band gaps of CdS and NiS. The higher light intensities the more electrons jump pass the gaps. Subsequently their mobility increases and hence reduces their resistivities. The dark and light resistivity values of CdS and CdS:Ni films were tabulated in the Table 1. It can be seen that all the films are photoconductive materials and that the resistivity of the film decreases as the Ni concentration increases both dark and light conditions. The values obtained in our work are in the same order as that obtained by Atay et. al [6], though they employed spray pyrolysis for preparing. Eventually at Ni concentration of 40%, both dark and light resistivities are equal.

Fig. 3. shows the x-ray diffractograms of the CdS and CdS:Ni films. It can be seen that the as-deposited CdS films appear to be in cubic form which is in agreement with that obtained by Oliva et. al [8] who used the same method for preparing. In contrast to the films prepared by Atay et. al [6], which were in hexagonal phase. This may due to the occurrence of heat during spraying process. However, after heat treatment at 300^{o}C onward the cubic CdS films in our work transformed into hexagonal phase. The undoped cubic structure CdS films gradually distorted as the Ni concentration increased. Eventually the hexagonal nickel sulphide (NiS) film appeared to mix with the CdS film. Furthermore, the more Ni concentrations were mixed in the

films, the broader peaks of CdS were detected, indicating of the smaller particle size we obtained. The same trend was also obtained by Atay et al. [6]. Analysis of the XRD peaks was carried out based on the Joint Committee Powder Diffraction Standard (JCPDS) file No. 75-1546 [9] and No.50-1791 [10] respectively.

From the AFM observation of the CdS films, it was found that the Ni concentration affects the thickness and rounghness of CdS films. These values are tabulated in Table 2. The thickness and rounghness of the films were found to vary as the Ni concentration. This may be due to the fact that the ionic radius of Ni (0.720 A°) is smaller compared to that of Cd (0.976 A°). Therefore, the roughness increases as the Ni concentration increase. The reason for thickness increasing can be attributed to the strong ionic bonding between Ni and S which may reduce the rate of evaporation of S, which, in turn, increase the thickness of the films with increasing Ni concentration. Our results on thickness agree well with that obtained by Atay et al. [6].

The elements on the films were analysed by the energy dispersive X-ray spectroscopy (EDS). The results are shown in Fig. 4. EDS analysis results show that the films contain O, Na, Mg, Al, Si, S, Ca, Ni, Cd and Au elements. The Cd, Ni and S elements were found as expected.

The other elements such as O, Na, Mg, Al, Si and Ca are the composition of glass substrates and Au element resulted from the Au coating for SEM observation.

The surface morphology of the films were investigated by scanning electron microscopy (SEM) and atomic force microscopy (AFM). SEM micrographs of the films are shown in Fig. 5. and AFM micrographs of the films are shown in Fig. 6. It was seen that the CdS films have different sizes of spherical particles stacking on glass substrate which high porosity. In the CdS:Ni films with different concentrations showed hard aggomerate of spherical particles.

In conclusion, CdS and CdS:Ni films were prepared by chemical bath deposition technique (CBD). Effects of the Ni concentration on the structural, morphological properties as well as the resistivities both dark and light conditions were investigated. The as-depositied CdS films were found to be in cubic form which transform into hexagonal after annealing at over 300^{o}C. Incorporation of Ni concentration causes some damage regarding the crystallinity of CdS films. The hexagonal NiS appeared to mix with the CdS in the CdS:Ni films. Roughness and thickness increased with increasing of Ni concentration. Spherical particles of 200-400 nm in diameter were found to pack into thin CdS sheets with high porosity while hard aggomeration of

the spherical particles appeared on CdS:Ni films. Resistivities of CdS and CdS:Ni films decreases with increasing of light intensities and decrease with Ni concentrations.

Reference

1. K. V. Zinoviev and O. Zelaya-Angel, Materials Chemistry and Physics, 70 (2001) 100.

2. H. Zhang, X. Ma and D. Yang, Materials Letters, 58 (2004) 5.

3. K. H. Jurgen Buschow, R. W. Cahn, M. C. Flemings, B. Ilschner, E. J. Kramer and S. Mahajan, in "Encyclopedia of Materials: Science and Technology Vol 2" (Elsevier, 2001) p. 873.

4. M. Rami, E. Benamar, M. Fahoume, F. Chraibi and A. Ennaoui, Solid State Sciences, 1 (1999) 179.

5. Y. Hashimoto, N. Kohara, N. Nishitani and T. Wada, Solar Energy Materials and Solar Cells, 50 (1998) 71.

6. F. Atay, S. Kose, V. Bilgin and I. Akyuz, Materials Letters, 4366 (2003) 1-12.

7. S. Han, H. Kim, M. Song, P. Lee, J. Lee and H. Ahn, J. Alloys and Compounds, 349 (2003 290.

8. A. I. Oliva, R. Castro-Rodriguez, O. Solis-Canto, Víctor Sosa, P. Quintana and J. L. Peña, *Applied Surface Science*, 205 (2003) 56.

9. The Joint Committee Powder Diffraction Standard (JCPDS) file No. 75-1546.

10. The Joint Committee Powder Diffraction Standard (JCPDS) file No. 50-1791.

List of Figures

List of Tables

N.B.

Fig. 1. should appear after the first paragraph of page 3.

Fig. 2. should appear after the first paragraph of page 4.

Fig. 3. should appear after the first paragraph of page 5.

Fig. 4. should appear after the first paragraph of page 6.

Fig. 5. should appear after the second paragraph of page 6.

Fig. 6. should appear after the second paragraph of page 6.

Table 1. should appear after the first paragraph of page 4.

Table 2. should appear after the second paragraph of page 5.

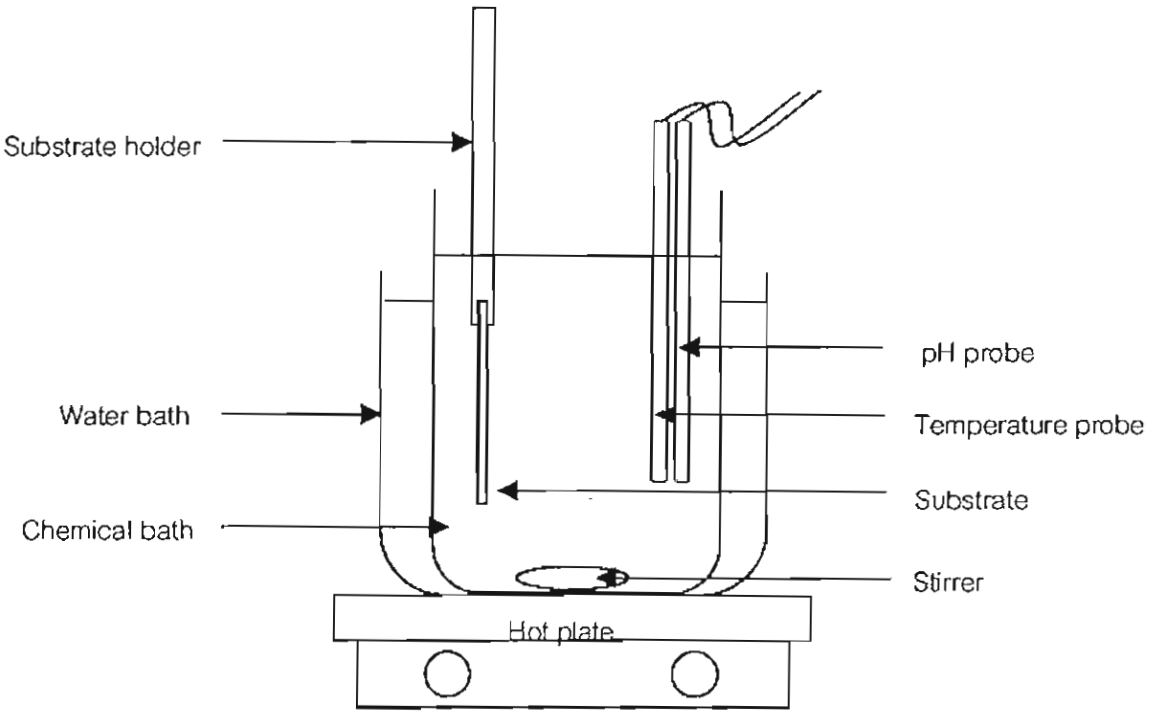

Fig. 1. Experimental setup for preparation of chemical bath deposited CdS and CdS:Ni.

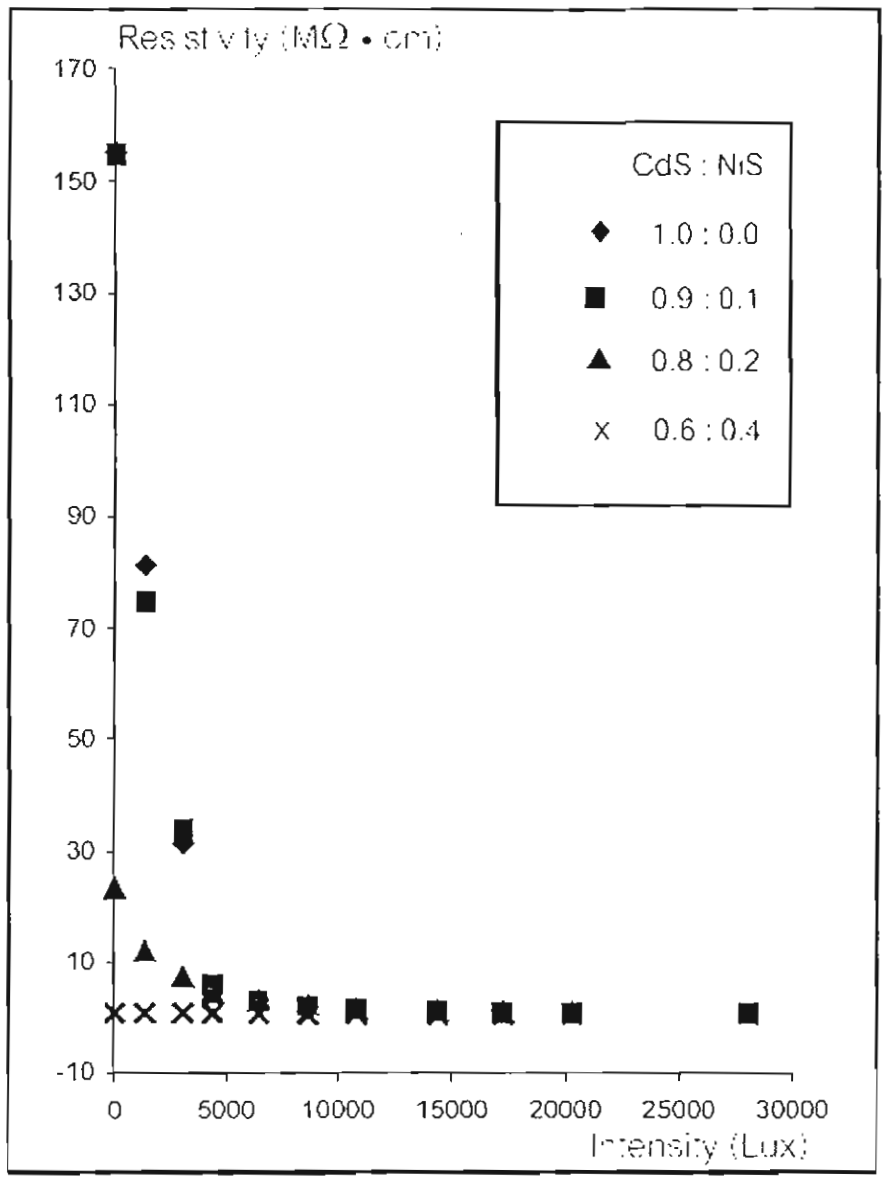

Fig. 2. The relationship between the intensity of light source and the resistivity of CdS:Ni films.

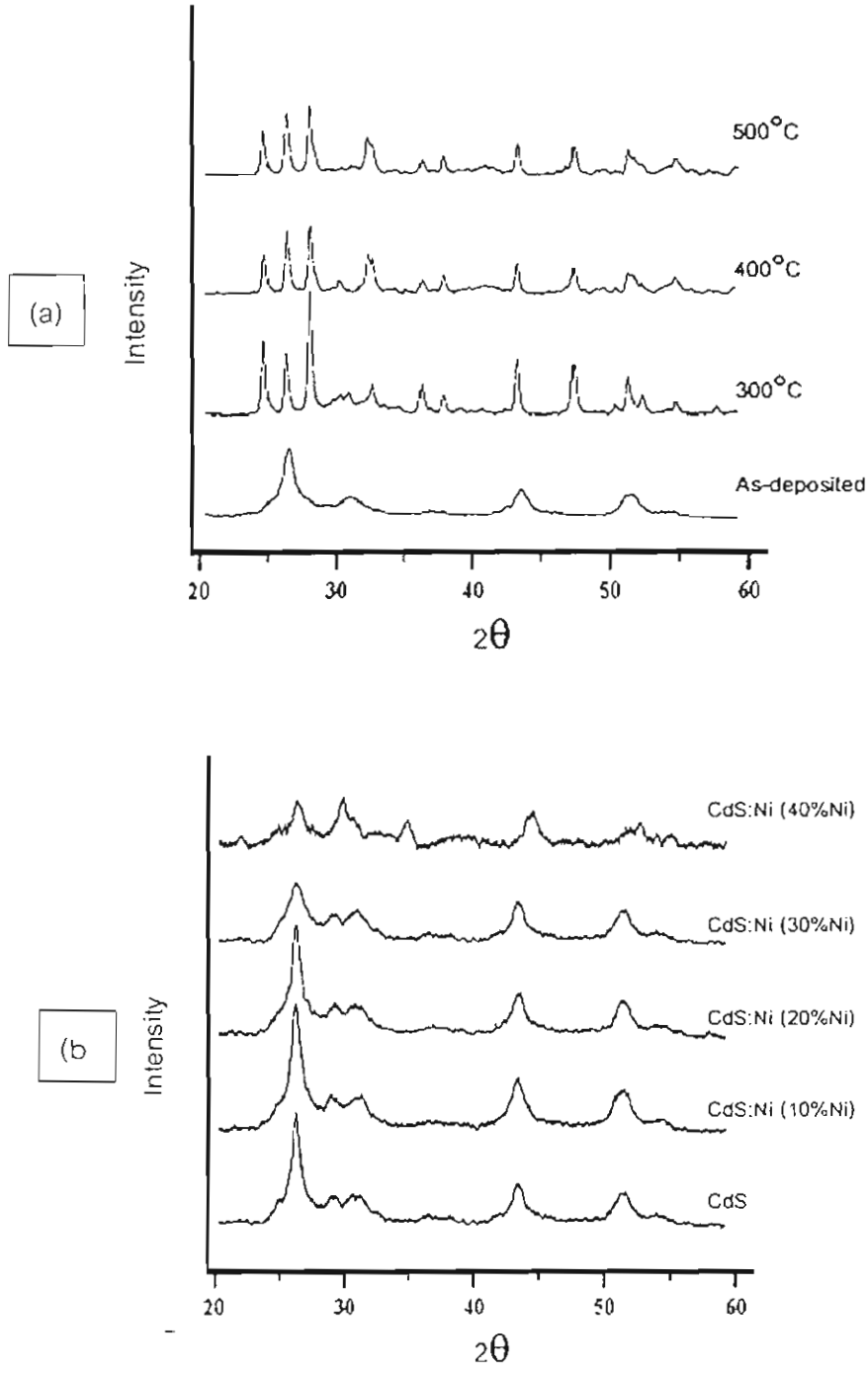

Fig. 3. X-ray diffractograms of CdS and CdS:Ni films.

(a) undoped CdS films at, 300°C, 400°C and 500°C.

(b) CdS and CdS:Ni films at 28°C.

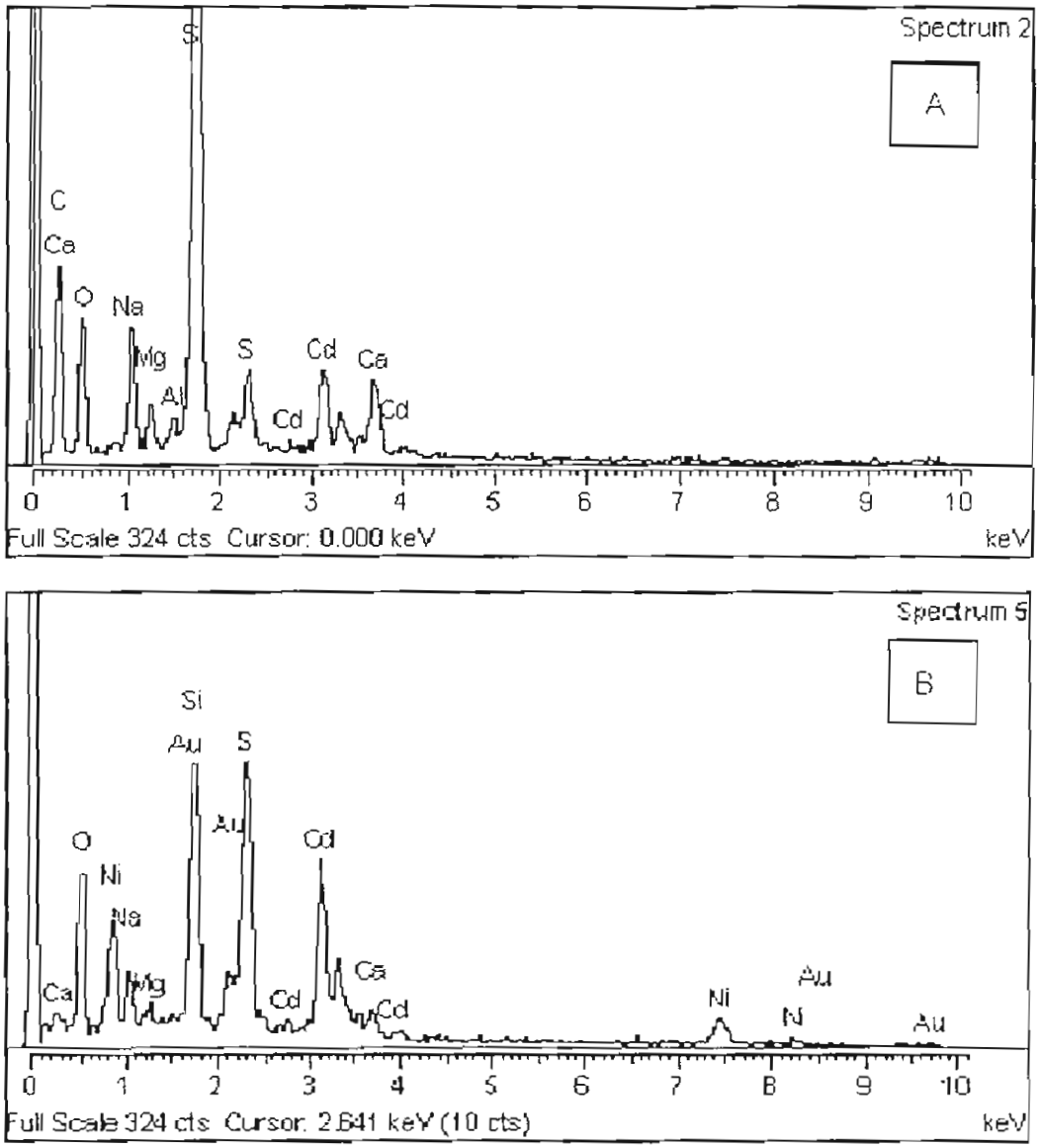

Fig. 4. EDS spectra of CdS and CdS:NiS films. (A) CdS film and (B) CdS:Ni film.

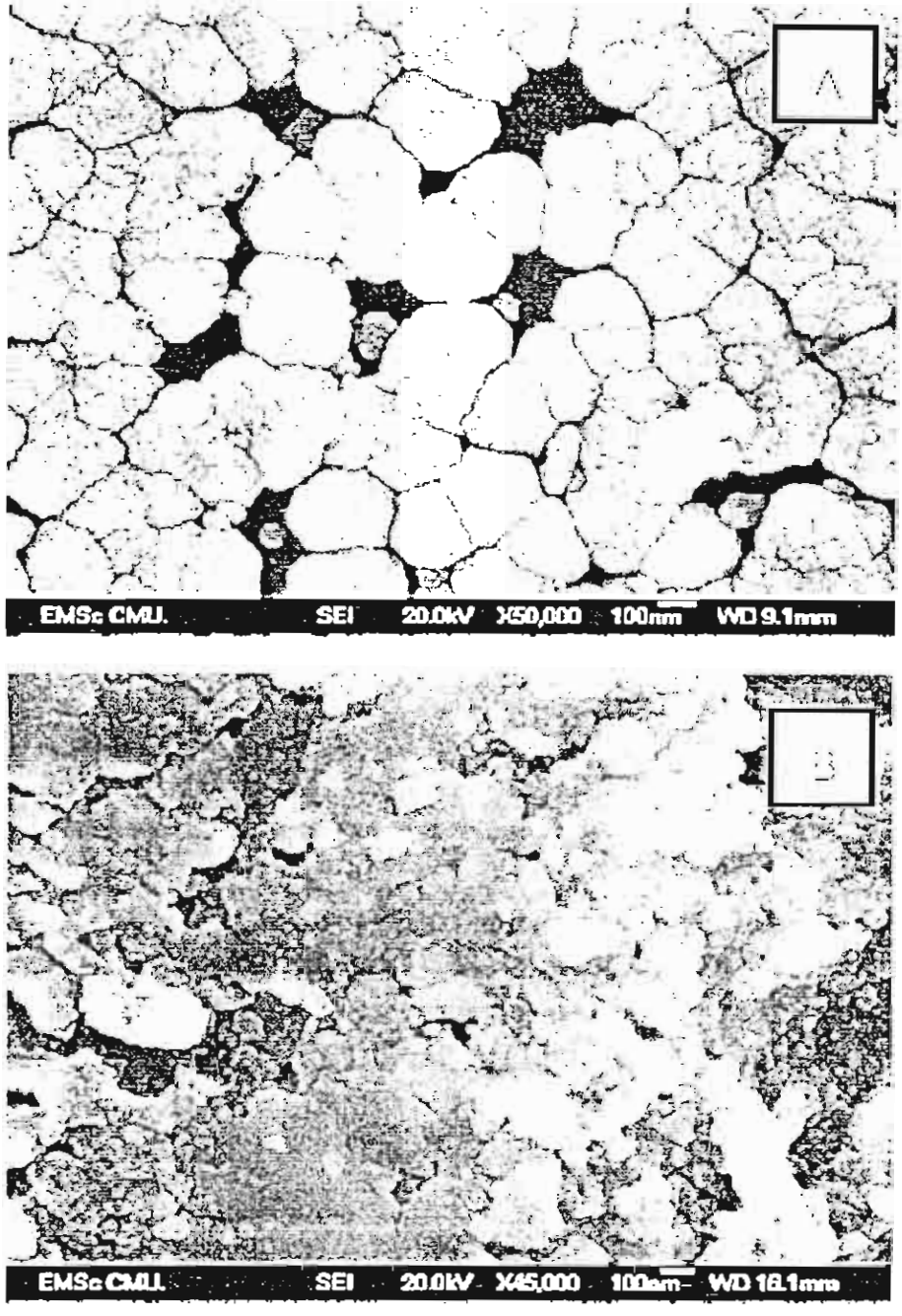

Fig. 5. The surface morphologies of CdS and CdS:Ni from SEM (A) CdS, (B) CdS :Ni.

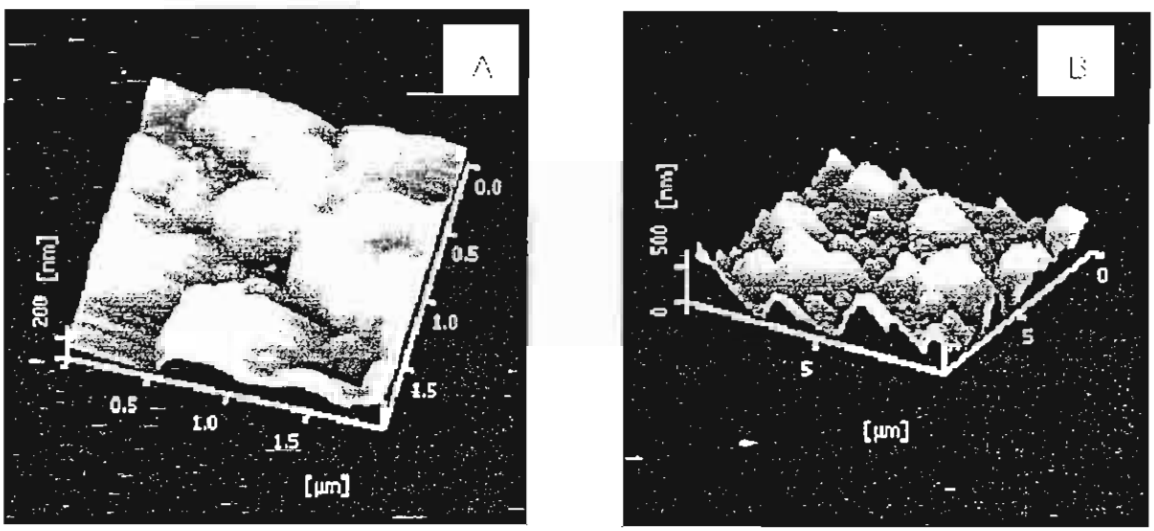

Fig. 6. The surface morphologies of CdS and CdS:Ni from AFM (A) CdS, (B) CdS :Ni.

Table 1. The resistivity values of CdS and CdS:Ni films.

Sample	The resistivity in dark (Ω cm) (0 Lux)	The resistivity in light (Ω cm) (28100 Lux)
CdS	1.55×10^{8}	1.82×10^{6}
CdS:Ni (at 10%)	1.54×10^{8}	8.56×10^{5}
CdS:Ni (at 20%)	2.34×10^{7}	6.84×10^{5}
CdS:Ni (at 30%)	7.90×10^{5}	6.02×10^{5}
CdS:Ni (at 40%)	0.54×10^{3}	0.54×10^{3}

Table 2. The surface charaterization of CdS and CdS:Ni films observed from AFM.

Sample	Rounghness (nm)	Thickness (nm)
CdS	246	69
CdS:Ni(10%Ni)	389	143
CdS:Ni(20%Ni)	432	144
CdS:Ni(30%Ni)	560	168
CdS:Ni(40%Ni)	647	164

เอกสารหมายเลข 2.5

Journals
Editorial Office

Springer

Dr. J. Tontragoon
Chiang Mai University
Department Of Physics
Faculty Of Science
MSEL
Chiang Mai
50200 Thailand

Date: 03 February 2005

Our ref.: JMSL10585-04 J3AUT1 76894
Dielectric Properties of Liquid Phase Sintered
0.98BaTiO3-0.02Ba(Mg1/3Nb2/3)O3 Ceramic
MUNPAKDEE/TONTRAKOON/SIRIWITAYIKORN/TUNKASIRI

Dear Dr. Tontragoon:

I am pleased to inform you that your
manuscript has been accepted for publication
and will appear in one of the next issues of the
JOURNAL OF MATERIALS SCIENCE LETTERS

Any queries concerning the production of your manuscript
should be sent to:

Mrs. Angela DePina
Springer
JMSL
101 Philip Drive
Assinippi Park
Norwell, MA 02061 U.S.A.
Email address: angela.depina@springer-sbm.com

Please remember to quote the manuscript number
JMSL10585-04 at all times. Thank you.

It would be greatly appreciated if you could provide us with
an electronic version of your paper (please see the enclosed
instructions). Thank you.

Sincerely yours,
Springer

Betty Pinney & Amiee DeSouza
Editorial Office JMSL
Email address: jms@springer-sbm.com

P.S.: If you would like to submit your accepted paper
to the Open Choice program, please access the following
URL: http://www.springeronline.com/openchoice

Dielectric properties of low firing $0.98BaTiO_3$-$0.02Ba(Mg_{1/3}Nb_{2/3})O_3$ with PbO/Li_2CO_3-Bi_2O_3 ceramics

A. Munpakdee, J. Tontragoon and T. Tunkasiri

Department of Physics, Faculty of Science. Chiang Mai University, Chiang Mai, 50200, THAILAND

In a previous paper(1) we discussed the additions to barium titanate with barium magnesium niobate ($Ba(Mg_{1/3}Nb_{2/3})O_3$: BMN) and their effects on dielectric properties of the material. Preparation was carried out via a solid solution which would rather be costly on the manufacturing scale while Weill *et al* (2,3) employed the chemincal method. It is the dielectric properties of barium titanate doped which give rise to this interest. Our earlier work showed that composition containing mostly barium titanate with 2 mol% of BMN reached a higher dielectric constant than pure barium titanate. The barium titanate modified was often used as capacitor dielectrics however, disadvantage of barium titanate was sintering of high temperature about 1300 °C, reduce sintering temperature by using flux was interesting the last few years. In order to reduce sintering temperature down to about 1000 °C the powder small amount of fluxing agents such as Bi_2O_3, PbO and Li_2CO_3(4-8) have been used. To promote densification by liquid phase sintering at lower temperatures. Unfortunately, lower sintering temperature are often accompanied by a significant decrease in dielectric constant. In some case, however, the reaction between the base and flux was found to produce dielectric properties advantageous for using in capacitor.

The objection of this work are to obtain both low firing and high dielectric constant of barim titanate doped with barium magnesium niobate based with some suitable dopants by solid solution method.

Experimental procedures.

The specimens studied in this investigation were fabricated according to formula 0.98 $BaTiO_3$ – $0.02Ba(Mg_{1/3}Nb_{2/3})O_3$. The purity of the starting raw materials was 99% and the specimens were prepared by the mixed oxides method. They were ball milled with zirconia ball in ethyl alcohol for 24 h and dired in an oven. The powder was calcined at 1200 °C for 2 h in air. The calcined powders were ball milled again with fluxing agents as xLi_2CO_3–xBi_2O_3+yPbO (where x = 5.26, 2.63, 1.315 wt% and y = 1.75, 0.875, 0.4375 wt%) for 24 h. Sample composition are shown in Table 1. After dried, green compact samples were sintered at various temperature for 2 h in air. They were heated by controlling the furnace temperature at the rate of 5 °C/min. The densities of all sintered pellets were measure volumetrically and determined. The calcined and sintered specimens were analyzed by x-ray diffractometer. The sintered pellets were polish on different grades of silicon carbind papers to obtain paralled surfaces. Sample discs were electroded using silver paste for dielectric measurement. Evolution of dielectric constant against the temperature was measured at various ambient temperature rang from room temperature to 200 °C, using an LCR meter.

Table 1. Sample composition

Code	Amount of fluxing agent
A	$0.98BaTiO_3 - 0.02Ba(Mg_{1/3}Nb_{2/3})O_3$ (No flux)
pbl	$5.26wt\%(Li_2CO_3 - Bi_2O_3) - 1.75wt\%$ PbO
2pbl	$2.63wt\%(Li_2CO_3 - Bi_2O_3) - 0.875wt\%$ PbO
4pbl	$1.315wt\%(Li_2CO_3 - Bi_2O_3) - 0.437wt\%$ PbO

Result and Discussion

The different kind of additives are added simultaneously, densification will be faster since more liquid phase is present. Moreover, using monovalent carbonate and trivalent oxides as liquid phase to correct the instability by way of charge compensation. So, in this study, Li_2CO_3, PbO and Bi_2O_3 with melting temperatures between 700 °C, 880 °C and 850 °C are selected as the liquid phase formers in the sintering 0.98BT-0.02 BMN ceramics.

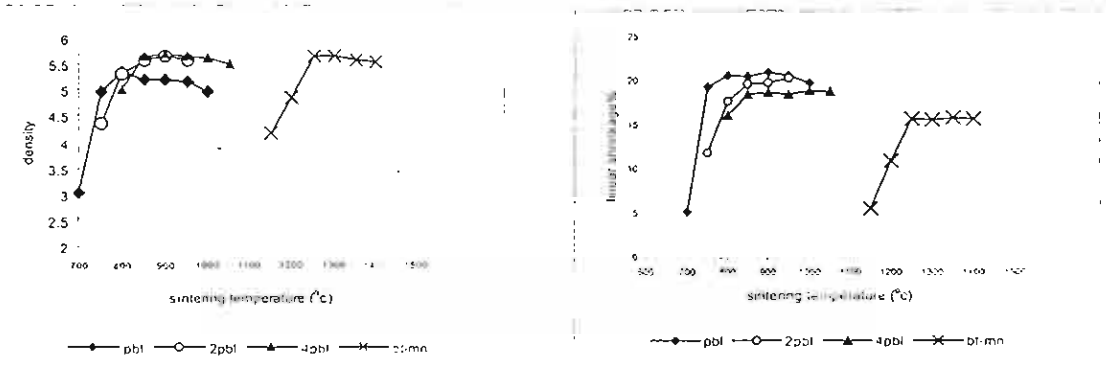

Figure 1. shows the relative densities and linear shrinkage of 0.98BT-0.2BMN sintered with different amount of PbO, $LiCO_3$, Bi_2O_3. Versus the sintering temperature.

In liquid phase sintering, the microflow of the liquid phase will rearrange the grain configuration so that it can eventually approach a denser structure. This flow gives to densification and accelerates the sintering process which is the first stage of liquid phase sintering. Linear shrinkage and density are shown in Figure 1. The linear shrinkage also tends to be saturated after sintering at 850 °C and the more liquid phase former added, the larger will be the shrinkage. In case, densities are up side down. A higher amount of fluxing agent gives lower density products as a consequence of mainly glassy phase to occurred during sintering if often accompanied by significant decrease in density compared with undoped sample. The slight decrease in density and shrinkage at high temperatures, can be attributed to the vaporization of additives. However, all of amount of fluxing agents is sufficient for sintering 0.98BT-0.02BMN ceramics below 1000 °C.

Through XRD, the phase of all the sintered ceramics were perovskite are shown in Figure 2. The sharp lines observed indicate good crystallinity which matched with BT phase. The analysis was carried out base on the Joint Committee on Powder Diffraction Standard (JCPDS). The trace of $Bi_4Ti_3O_{12}$ was observed in $PbO/Bi_2O_3/ Li_2CO_3$ added samples. The shift of the diffraction peak can be usualized as the shift of d-space and thus the change of the lattice constant of 0.98BT-0.02BMN due to the modification by Bi_2O_3/Li_2CO_3. It was found that tetragonal BT structure become cubic at room temperature when highest of amount of fluxing agents were added.

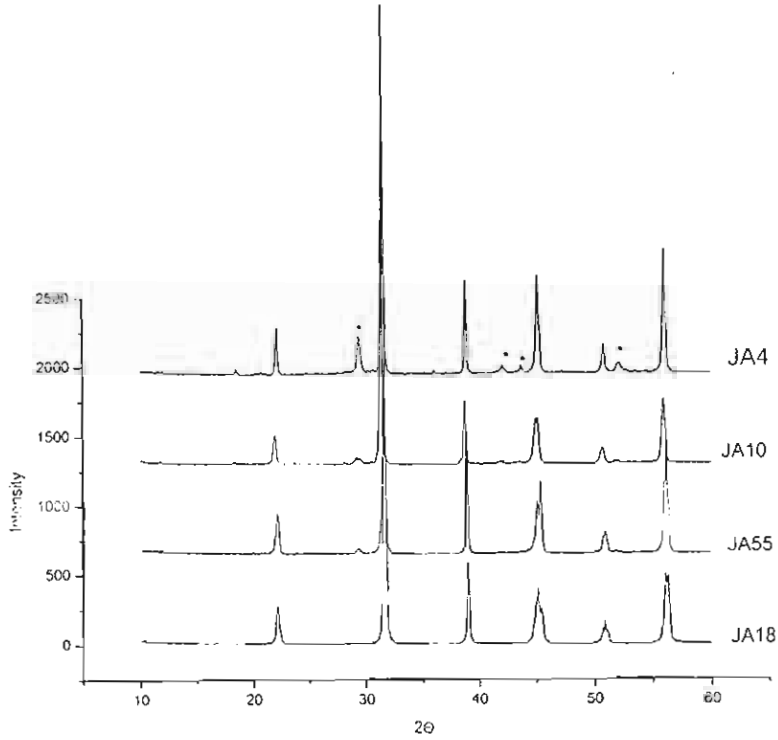

Figure 2. XRD pattern of ceramics of flux-sintered ceramic. (* $Bi_4Ti_3O_{12}$)

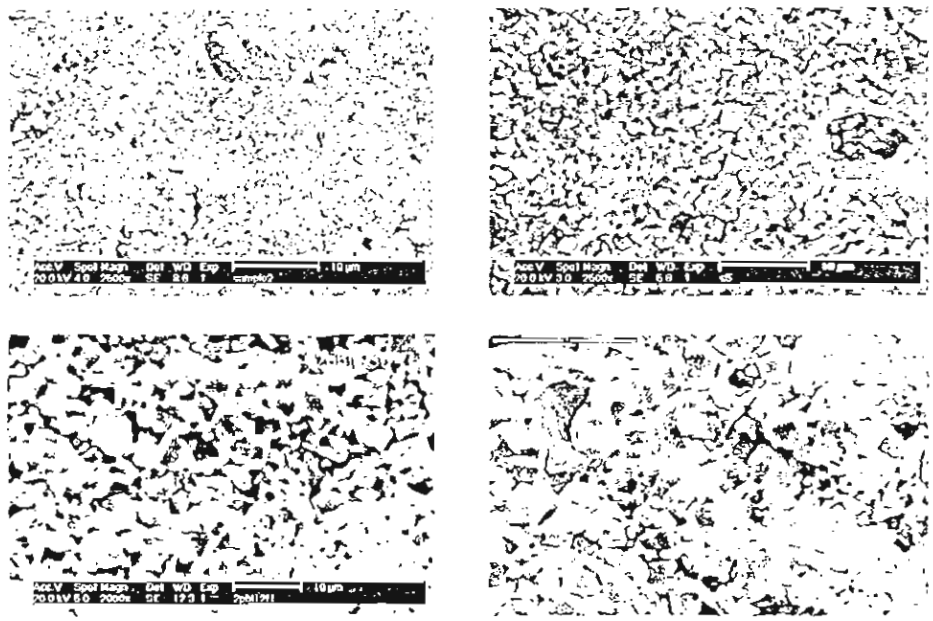

Figure 3. Typical microstructure of flux-sintered ceramic.

The actions of liquid phase formers on sintering are disclosed by observing the microstructures of specimens. One can also see that more amount fluxing agents added simultaneously, densification will be faster since more liquid phase (Figure 3). In case of highest flux-added (pbl), densification is fast occurred with sintering at 800 °C, the liquid phase coats grains and provides interconnection among them. With decreasing on grain size with increasing of fluxing agents and sintering temperature are observed (6,7,9). So, Bismuth and Lithium oxide have been added to $BaTiO_3$ to enhance sintering without grain growth. The rich in Bi-content was found at GB, detected by energy dispersive X-ray analysis(EDX), and are formed by substitution to Ba ion in lattice. This result is confirmed by XRD techniques.

Table 2. Dielectric characteristics of flux-added 0.98BT-0.02BMN ceramics.

composition	sintering temperature	ε_r	T_c	dielectric loss	ρ (Ω.cm)
A	1300	40,000	98	1	4.5×10^{6}
	1350	25,000	95	0.35	4.9×10^{5}
	1400	16,000	103	0.25	6.3×10^{6}
4pbl	850	6245	77	1.25	3.3×10^{9}
	900	9410	80	1.25	3.610^{7}
	950	9570	83	8	3.2×10^{7}
	1000	10,080	84	1	5.2×10^{8}
	1050	14,650	85	8	1.2×10^{8}
2pbl	750	1962	35	0.3	32×10^{6}
	800	2,200	100	40	0.32×10^{6}
	850	10,252	84	50	0.83×10^{6}
	900	17,327	94	25	0.56×10^{6}
	950	30,485	83	20	5.3×10^{6}
pbl	750	3,645	flat	50	1.2×10^{10}
	800	2,500	flat	2	1.63×10^{8}
	850	2,500	flat	2	2.15×10^{9}
	900	2,500	flat	5	2.15×10^{9}
	950	3,595	78	0.9	3.4×10^{8}
	1000	18,000	-	200	9×10^{4}

The effect of doping on dielectric characteristics, the substituting and interstitial process of additive ions must be occurred into bulk. These maybe A-or B-site substitution and the possibility of either octahedral or tetrahedral interstitial packing by doping into ABO_3 perovskite structure. Which effect is dominant will depend on valency and radius of doping ion. It is believed that Bi^{3+}, Pb^{2+} and Li^{+} undergo A-site substitution.(9-12) The dielectric properties of flux-added 0.98BT-0.02BMN ceramic with different sintering temperatures are tabulated in Table 2 and Figure 4. From the result, the highest ε_r value was about 30,000 for ceramic containing 2.63 wt% (Li_2CO_3-Bi_2O_3)-0.83wt%PbO sintered at 950 °C. Effect of Bi^{3+} substituted at A-site was shown in Figure 4. At high Bi_2O_3 amount the permittivity peak was depressed and broadened. Moreover, in the Bi^{3+} state tended to shift the T_c downward. However, the interstitial effect with Li^{+} can be confirmed by anomalous increase of dielectric loss when temperature is higher than T_c.

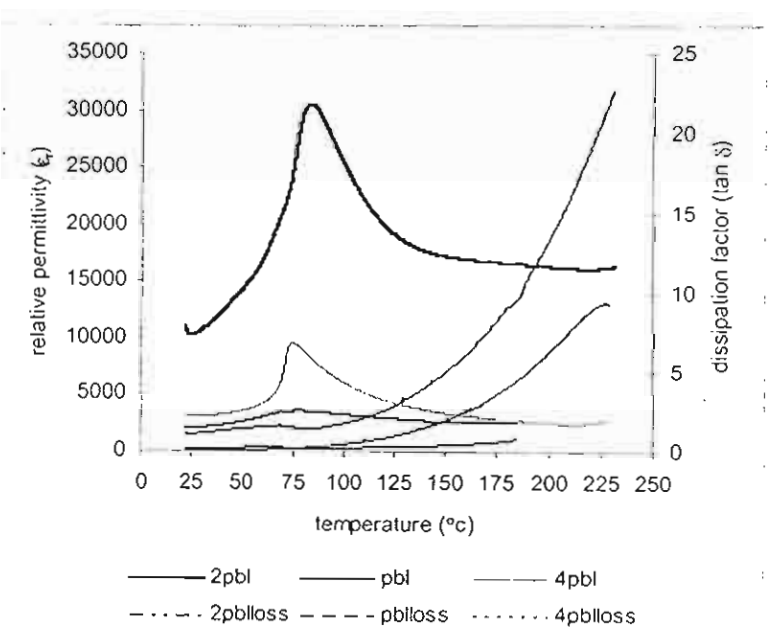

Figure 4. Change of dielectric constant (at 1 kHz) and dissipation factor (tanδ) against temperature of flux-added 0.98BT-0.02BMN ceramics at 950 °C.

Conclusion

Li_2CO_3/ Bi_2O_3 (equal ratio) and PbO were used as liquid phase sintering in $0.98BaTiO_3 - 0.02Ba(Mg_{1/3}Nb_{2/3})O_3$ system to accelerate the densification process without grain growth. Phase transformation between tetragonal to cubic at room temperature at highest amount of fluxing agents but smaller grain size were found. Effect of Bi^{3+} and Li^{+} on dielectric properties were found by substitution and interstitial process at A-site in perovskite structure. To cause T_c shifted downward and broaden peak of dielectric characteristic. The optimum condition from this work is contain 2.63 wt% (Li_2CO_3-Bi_2O_3)-0.83wt%PbO sintered at 950 °C. The highest relative permittivity was about 30000.

References

1. Munpakdee, A., Tontragoon, J., Siriwitayakorn, K. and Tunkasiri, T., Effect of $Ba(Mg_{1/3}Nb_{2/3})O_3$ on Microstructure and dielectric properties of barium titanate ceramics., J. Mats. Sci. Lett. 22 2003 1307-1310.
2. Weill, F., Rehspringer, J, L., Crystallographic Study of $BaTiO_3$-$Ba(M_{1/3}N_{2/3})O_3$ Solid Solution (M=Co or Mg and N=Nb or Ta), *J. Mater. Sci.*, 1992; **27**: 2316-2320.
3. Weill, F., Rehspringer, J, L., Dielectric Characterisation of $BaTiO_3$-$Ba(M_{1/3}N_{2/3})O_3$ Solid Solution (M=Co or Mg and N=Nb or Ta), *J. Mater. Sci.*, 1992; **27**: 2321-2325.
4. Burn, I., Flux-sintered $BaTiO_3$ dielectrics, J. Mats. Sci.,17,1982,1398-1408.
5. Ernest, M. and McDaniel, C.,L., The system Bi_2O_3- B_2O_3, J. Amer. Ceram. Soc., 45,1962,355-360.

6. Maher, G., H., Liquid phase assisted sintering of ceramic dielectric for low fired MLC application, J. Glass for electronic application. ,365-386.

7. Li Q., Jianquan, Q., Wang, Y., Zhilun, G. and Li, L., Improvement of temperature-stable $BaTiO_3$ –based dielectrics by addition of Li_2CO_3 and Co_2O_3, J. Eur. Ceram. Soc., 21,2001,2217-2220.

8. Chen, G. F. and Fu, S. L., Dielectric properties of low-fitting $Pb(Mg_{1/3}Nb_{2/3})_{1-x}$ TiO_3- Bi_2O_3 / Li_2O ceramics, J. Mats. Sci., 25,1990,424-430.

9. Cheng, S-Y., Fu, S. L. and Wei, C. C., Low- temperature sintering of PZT ceramics, J. Ceram. Inter.,13,1987,223-231.

10. Cheng, S.Y., Fu, S.L., Wei, C. C. and Ke, G. M., The properties of low-temperature fired piezoelectric ceramics, J. Mats. Sci., 21,1986, 571-576.

11. Kim, K. T. and Kim, C. I., Structural and dielectric properties of Bi-doped $Ba_{0.6}Sr_{0.4}TiO_3$ thin films fabricated by sol-gel method, J. Microelectronic Engineering., 1, 2002, (Impress).

12. Zhilin, G., Longtu, L., Suhua, G. and Xiaowen, Z., Low-Temperature Sintering of Lead-Based Piezoelectric Ceramics, J. Am. Ceram. Soc., 72, 1989, 486-491.

เอกสารหมายเลข 2.6

MSRL : Materials Science Research Laboratory, DEPARTMENT OF PHYSICS
FACULTY OF SCIENCE, CHIANG MAI UNIVERSITY, CHIANG MAI, 50200 THAILAND
TEL. (6653) 943376, 942470 FAX (6653) 357512 E-mail : tawee@chiangmai.ac.th

4th January 2005

Ref. Manuscript no. 04L84 entitled "Structural and physical properties of Nd-doped $Pb(Zr_{0.52}Ti_{0.48})O_3$ ceramics."

Dear Prof. George W. Taylor,

Referring to the reference above, we have revised the manuscript according to the points made by the referee.

Enclosed please find 3 copies of the revised manuscripts and 1 CD-R of the article.

Looking forward to hearing from you.

Sincerely yours,

(Tawee Tunkasiri)

Structural and physical properties of Nd-doped $Pb(Zr_{0.52}Ti_{0.48})O_3$ ceramics

W. Thamjaree, W. Nhuapeng, and T. Tunkasiri

Department of Physics, Faculty of Science, Chiang Mai University, Chiang Mai 50200, Thailand

Lead zirconate titanate (PZT) ceramics (Zr/Ti = 52/48) have been modified with different quantities of neodymium oxide (Nd_2O_3). The preparation was carried out via the solid-state-reaction route. The samples were calcined and sintered at 850 °C and 1200°C, respectively. The structural evolution and the microstructure were investigated using an X-ray diffractometer (XRD) and a scanning electron microscope (SEM), respectively. The physical properties such as dielectric constants, piezoelectric coefficients, density etc. were also studied.

INTRODUCTION

Lead zirconate titanate [$Pb(Zr_xTi_{1-x})O_3$, PZT] ceramics have been intensively studied due to their applications in electronics, microphone, ignitors, ultrasonic transducers, accelerometers, piezoelectric sonar, radio and communication filter [1-4]. Many studies have been carried out to enhance the piezoelectric properties for some technological demand. Various dopants were added into the PZT ceramics as well as the ratios of Zr/Ti were varied in order to improve their piezoelectricity. He and Li [5] doped the $Pb_{0.95}Sr_{0.05}(Zr_{0.52}Ti_{0.48})O_3$ and $Pb(Zr_{0.53}Ti_{0.47})_{0.98}(Sb_{2/3}Mn_{1/3})_{0.02}O_3$ with various quantities of $MnCO_3$ (x = 0-7.5 mol%). They found that for the low concentration of Mn ion (less than 0.5 mol%), k_p and d_{33} of the samples increased. On the other hand, Qm was found to increase without any significant change in k_p and d_{33} if Mn ion was added in the range of 0.5-1.5 mol%. Moreover, the piezoelectric properties deteriorated when the concentration is more than 1.5 mol%. Garg and Goel [6] employed 2.0 mol% rare-earth oxides (M_2O_3) where M = Er, Gd, Eu, Nd and La to modify the $Pb_{1-(3x-2)}M_x(Zr_{0.40}Ti_{0.60})O_3$ using solid-state-reaction route. They found that the additive preferably goes to the A site with increasing ionic radius. Garg and Agrawal [7] and Shannigrahi et al. [8] improved the electrical properties of $Pb_{0.98}M_{0.02}(Zr_{0.535}Ti_{0.465})_{0.995}O_3$ and $Pb_{1-z}Nd_z(Zr_{0.60}Ti_{0.40})_{1-z/4}O_3$ by adding Nd_2O_3 where the Nd_2O_3 quantities were used at 0.02, 0.07, 0.08 and 0.10 mol. Since PZT ceramics have five different phases including, orthorhombic and tetragonal

antiferroelectric phases ($x > 0.9$), two different ferroelectric rhombohedral phases($x > 0.53$), and a ferroelectric tetragonal phase ($x < 0.53$). The rhombohedral phases have a mutual phase transition at Zr-content dependent temperatures. At room temperature, the high-temperature rhombohedral phase covers the Zr-composition range of $0.53 < x < 0.64$. Above the Curie temperature of about 350 °C, paraelectric PZTs always have the cubic perovskite structure. The composition at the phase boundary between the ferroelectric tetragonal and high-temperature rhombohedral phase are very important effects on the piezoelectric properties of PZT around this composition value [9]. Especially, the composition where $PbZrO_3$:$PbTiO_3$ is 1:1, the domain structure has a very important effect on behavior of piezoceramics. Therefore, it is reported that different ratios of Pb:Zr:Ti result in structural change with composition at constant temperatures in a solid solution range [10]. For example at about 350 °C the $Pb(Zr_xTi_{1-x})O_3$ system has a tetragonal unit cell where x less than 0.53 and changes to high temperature rhombohedral where x more than 0.53. As a result, this affects their electric properties significantly. The coupling coefficient and dielectric constant show remarkably high values when $x = 0.52$ [11]. Therefore, it would be very interesting to attempt to achieve better piezoelectric properties for PZT ceramic at exactly $x = 0.52$ using a wider range of Nd_2O_3 for doping. This paper reports the authors' work on the production of this type of PZT ceramics and characterization of their physical properties.

EXPERIMENTAL PROCEDURE

PZT ceramics with the morphotropic phase boundary (Zr/Ti = 52/48) incorporated with various amounts of Nd_2O_3 (0.1, 0.3, 1.5 and 2.7 mol%) were prepared via the conventional solid-state-reaction route. Lead oxide (PbO ~ 99%, Fluka), zirconium oxide (ZrO_2 ~ 99%, Fluka), titanium dioxide (TiO_2 ~ 99%, Reidel) and neodymium oxide (Nd_2O_3 ~ 99%, Reidel) were employed as precursors. They were weighed according to appropriate molar fractions, mixed and wet milled (in ethanol) for 24 h in the zirconia grinding media. The mixtures were dried and calcined at 850 °C. The mixtures were then reground and formed into circular disks with diameter of 15 mm. and thickness of 2.5 mm. 2 wt% polyvinyl alcohol (Fluka) was employed as binder. The samples were sintered at 1200 °C with heating/cooling rate of 5 °C/min in a close alumina crucible with a lead atmosphere provided by lead zirconate (PZ) powder. The polished samples were electroded and poled in an electric field of 10 kV/mm for 30 min in silicone oil at 120 °C. The planar coupling coefficient (k_p), dielectric constant (ε_r), loss angle (tan δ) were measured (using Hewlett Packard 4192 LF impedance analyzer and 16048 A test lead). An X-ray diffractometer (XRD, Philips) and a scanning electron microscope (SEM, Philips XL 30 ESEM) were employed to study phase evolution and microstructure of the samples, respectively.

RESULTS AND DISCUSSION

The XRD patterns of the ceramics with Nd amount of 0 to 2.7 mol% and a typical pattern of the 1.5 mol% Nd doped sample are shown in Fig. 1. The analysis was carried out based on the Joint Committee on Powder Diffraction Standards (JCPDS). From the calcined sample at 850 °C, the second phases of $Nd_{0.667}TiO_3$ [13] and $Pb_{1-1.5x}Nd_x(Zr_{0.65}Ti_{0.35})O_3$ [14] were detected together with tetragonal PZT phase and small trends of unknown peaks which may be from the unreacted of starting powders. The tetragonal $Pb(Zr_{0.52}Ti_{0.48})O_3$ phases [12] were found in all patterns of the ceramics samples which is corresponding to JCPDS file no 33-784. However, these phases disappeared in the ceramic samples. It is seen that the single phase of tetragonal perovskite PZT structure could be obtained from undoped and doped samples with Nd content of lower than 0.3 mol%. The second phases of $Pb_2Ti_2O_6$ [15], $Nd_2Zr_2O_7$ [16] and trace of unreacted Nd_2O_3 [17] were found in ceramic samples when the amount of Nd dopant was higher than 1.5 mol%. The $Pb_2Ti_2O_6$ phase was also found by Hirashima et al. [18] though their preparation of PZT powder was carried out by metal alkoxide method. In our present work, it is found that both tetragonal and rhombohedral PZT phases appeared when the amount of Nd_2O_3 were in the range of 0-0.3 mol%, but tetragonal is more outstanding than rhombohedral phase. However, the rhombohedral distinctively separated from tetragonal phase as the amount of Nd was greater than 0.3 mol% which can be observed from the extra peak of (102)R. Garg and Agrawal [7] and Nasar et al. [19] also found both

rhombohedral and tetragonal PZT phase in their work. The appearance of the tetragonal phase in the PZT ceramics agrees well with our previous work [20]. The piezoelectric, dielectric and other physical properties are tabulated in the Table 1. The results from Garg and Goel [6], Garg and Agrawal [7] and Shannigrahi et al. [8] are also presented for the sake of compararison.

From the Table, it may be concluded that the d_{31} increased with the increasing amounts of Nd_2O_3 upto 1.5 mol%. It tends to drop slightly at higher quantity. These are probably due to the occurrence of the drop of density and the existing of second phase (see Fig. 1). The values of ε_r obtained here decrease with increasing Nd_2O_3 contents, (from 29,200 down to 4450). It should be noted that the values are higher than those obtained by Garg and Goel [6], Garg and Agrawal [7] and Shannigrahi et al. [5] who prepared sample by mixed oxide method with excess PbO and acetate alkoxide sol-gel technique, respectively. Similar trend was found in the T_c values. The fall of these values may be due to the formation of microscopic heterogeneity, second phase and internal stress in the compounds. Moreover, the coating of glassy phase around the grains may exhibit the lower dielectric constant of these materials. Consequently, it may be assumed that the addition of Nd-dopant in the PZT system has a significant effect on properties of the ceramics such as unit-cell size, spontaneous polarization and resistivity. The densities and shrinkages of the ceramics samples were relatively constant, whereas the tan δ, k_{31} and k_p values

obtained in our work show slightly decrease, though not significantly. Our results are comparable to those of Garg and Agrawal [7], though the ratios of Zr/Ti of their samples are slightly different.

Fig. 2. shows the surfaces of the as-sintered of the undoped and doped ceramics. It can be concluded that the grain size tends to decrease (from 8.2 μm down to 1.1 μm) with increasing Nd_2O_3 dopant as generally expected. Though at the Nd_2O_3 quantities higher than 0.3 mol%, the grain size are almost constant (slightly over 1 μm). Furthermore, there is a trend that the values of ε_r drop with increasing grain size. This agrees very well with Randall et al. [21].

CONCLUSIONS

In this work, it has been found that the addition of the Nd-dopant has the effect to phase transformation of PZT system. The rhombohedral phase was found together with tetragonal phase and the second phase disappeared in the sintered samples. With high quantities of Nd (over 1.5 mol%), however, new second phases and trace of unreacted Nd_2O_3 were found. The piezoelectric coefficients obtained in our works are comparable to those obtained by others, whereas the dielectric constants are higher.

Acknowledgement

The authors would like to express their sincere thanks to the Thailand Research Fund for the funding of this project. The authors would also like to thank Asst. Dr. S. Wiboolsake and Dr. A. Chaipanich for their useful comments and correction the manuscript.

References

1. H. Zeming, J.M. Ruifang Ahang and T. Li, *J. Eur. Ceram. Soc.* **23,** 1943-1947 (2003).
2. T. Tunkasiri, *Smart Mater. Struct.* **3,** 243-247 (1994).
3. V.F. Janas, and A. Safari, *J. Am. Ceram. Soc.* **78**[11], 2945-2955 (1995).
4. G.H. Haertling, *J. Am. Ceram. Soc.* **82**[4], 797-818 (1999).
5. L.X. He and C.E. Li, *J. Mats. Sci.* **35,** 2477-2480 (2000).
6. A. Garg and T.C. Goel, *J. Mats. Sci: Mats in Elect.* **11**, 225-228 (2000).
7. A. Garg and D.C. Argrawal, *Mats. Sci. and Eng. B.* **86**, 134-143 (2001).
8. S.R. Shannigrahi, R.N.P. Dhoudhary and H.N. Acharya, *Mats. Sci. Eng. B* **56,** 31-39 (1999).
9. J. Lappalainen and V. Lantto, *App. Surf. Sci.* **154-155**, 118-122(2000).
10. A.J. Moulson and J.M. Herbert, *Electroceramics* (Wiley & Sons Ltd. 1st edition, 1990) p.277.

11. A.J. Moulson and J.M. Herbert, *Electroceramics* (Wiley & Sons Ltd. 2nd edition, 2003) p.356.

12. Powder Diffraction File, Card No.33-784, Joint Committee on Powder Diffraction Standards, International Centre for Diffraction Data, Swarthmore, PA.

13. Powder Diffraction File, Card No.49-247, Joint Committee on Powder Diffraction Standards, International Centre for Diffraction Data, Swarthmore, PA.

14. Powder Diffraction File, Card No.50-227, Joint Committee on Powder Diffraction Standards, International Centre for Diffraction Data, Swarthmore, PA.

15. Powder Diffraction File, Card No.26-142, Joint Committee on Powder Diffraction Standards, International Centre for Diffraction Data, Swarthmore, PA.

16. Powder Diffraction File, Card No.78-1618, Joint Committee on Powder Diffraction Standards, International Centre for Diffraction Data, Swarthmore, PA.

17. Powder Diffraction File, Card No.75-2255, Joint Committee on Powder Diffraction Standards, International Centre for Diffraction Data, Swarthmore, PA.

18. H. Hirashima, E. Onishi and M. Nakagawa, *J. Non-Crys. Solids* **121**[1-3], 404-406 (1990).

19. S.R. Nasar, M. Cerqueira, E. Longo, J.A. Varela and A. Beltran, *J. Eur. Ceram. Soc.* **22**, 209-218 (2002).

20. W. Thamjaree, W. Nhuapeng and T. Tunkasiri, *Ferr. Lett. Sec.* **31**[3-4], 79-85 (2004).

21. C.A. Randall, N. Kim, J.P. Kucera, W. Cao and T.R. Shrout, *J. Am. Ceram. Soc.* **81**[3], 677-688(1998).

Table 1. The piezoelectric, dielectric and physical properties of PZT doped with Nd sintered at 1200 °C

Quantity of dopant–Nd (mol%)	Density (%)	Shrinkage (%)	T_C (°C)	ε_r	tan δ	d_{31} (pC/N)	k_{31}	k_p
0.1	92	14.42	378	29,200	0.01	38.8	0.21	0.31
0.3	95	15.23	370	17,800	0.03	42.8	0.21	0.31
1.5	94	16.01	250	8,114	0.01	48.3	0.20	0.30
2.7	93	15.74	250	4,450	0.002	26.3	0.18	0.27
2.0 [6]	97	-	-	680	-	-	-	-
2.0 [7]	-	-	371	3490	0.03	128	0.29	0.49
0.07 [8]	97	-	196	5878	0.03	-	-	-

N.B. - means they were not shown in the original papers.

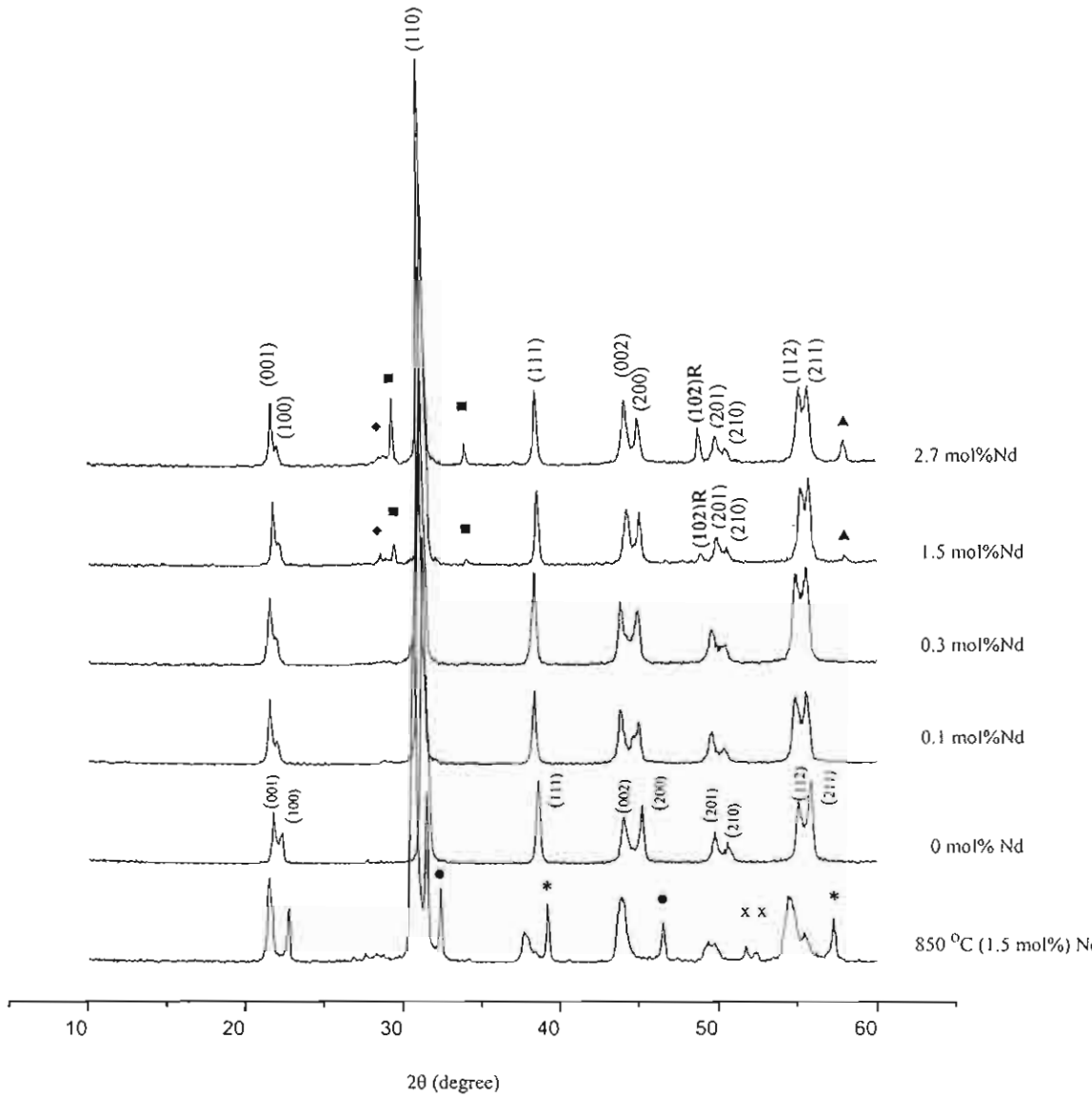

Fig 1. The top 5 X-ray diffractograms are the undoped and Nd-doped ceramics, sintered at 1200 °C. The bottom plot is an XRD pattern of 1.5 mol% Nd doped sample calcined at 850 °C.

(♦) Nd_2O_3 (102)R Rhombohedral

(■) $Pb_2Ti_2O_6$

(▲) $Nd_2Zr_2O_7$

(•) $Nd_{0.667}TiO_3$

(*) $[Pb_{1-1.5x}Nd_x(Zr_{0.65}Ti_{0.35})]O_3$

(x) unknown

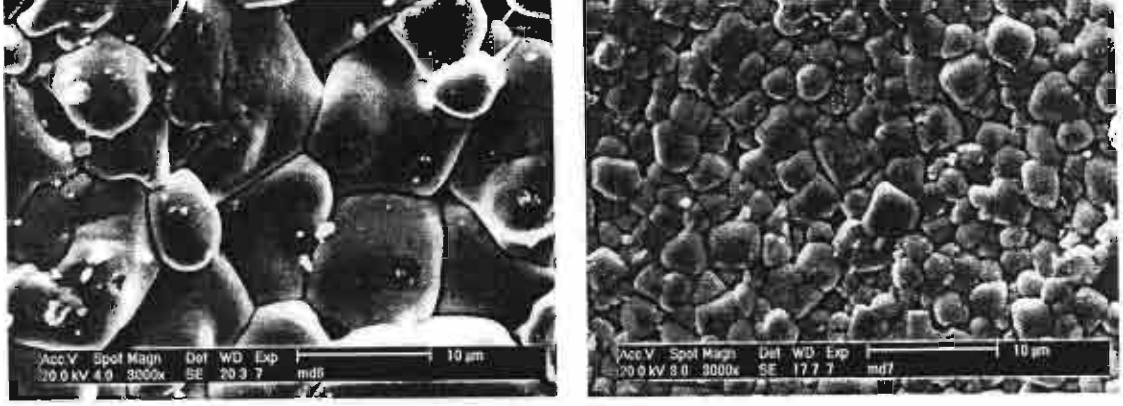

(a) (b)

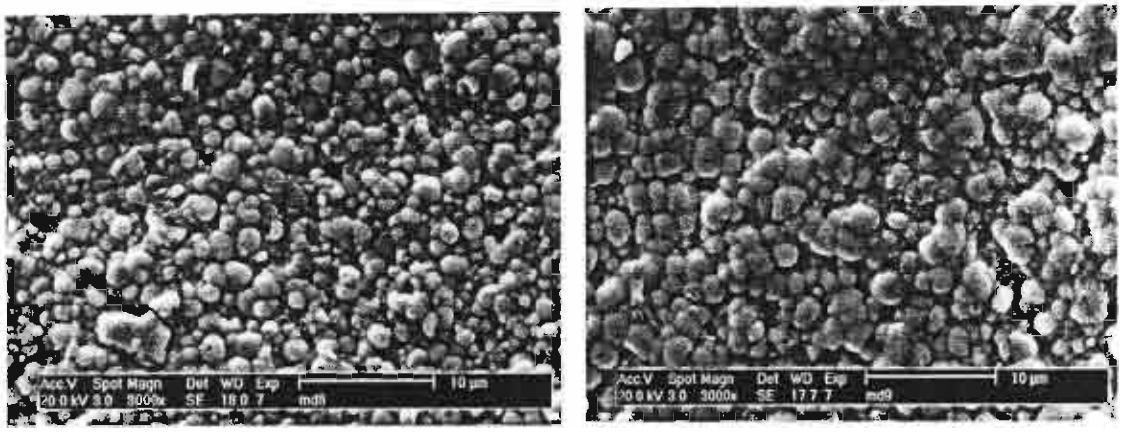

(c) (d)

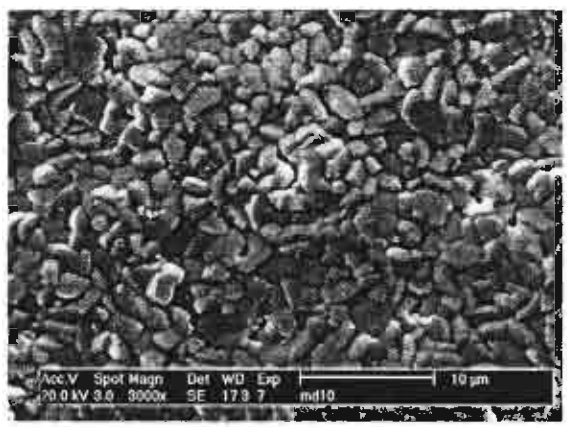

(e)

Fig. 2 SEM micrographs of as sintered surface of PZT ceramics sintered at 1200°C doped with (a) 0 (b) 0.1 (c) 0.3 (d) 1.5 and (e) 2.7 mol% of Nd_2O_3

List of Figure

Figure 1. The top 5 X-ray diffractograms are the undoped and Nd-doped ceramics, sinter at 1200 °C . The bottom plot is an XRD pattern of 1.5 ;mol% Nd doped sample calcined at 850 °C.

(•) Nd_2O_3

(■) $Pb_2Ti_2O_6$

(▲) $Nd_2Zr_2O_7$

(•) $Nd_{0.667}TiO_3$

(*) $[Pb_{1-1.5x}Nd_x(Zr_{0.65}Ti_{0.35})]O_3$

(x) unknown

(102)R Rhombohedral

Figure 2. SEM micrographs of as sintered surface of PZT ceramics doped with (a) 0 (b) 0.1 (c) 0.3 (d) 1.5 and (e) 2.7 mol% of Nd_2O_3 sintered at 1200 °C.

Table 1. The piezoelectric, dielectric and physical properties of PZT doped with Nd sintered at 1200 °C

N.B.

Figure 1. should appear after paragraph 1, page 5

Figure 2. should appear after paragraph 1, page 7

Table 1. should appear after paragraph 2, page 6

เอกสารหมายเลข 3

เลขที่สิทธิบัตร 18359

สป/200 - ข

สิทธิบัตรการประดิษฐ์

อาศัยอำนาจตามความในพระราชบัญญัติสิทธิบัตร พ.ศ. 2522 อธิบดีกรมทรัพย์สินทางปัญญาออกสิทธิบัตรฉบับนี้ให้แก่

สำนักงานพัฒนาวิทยาศาสตร์และเทคโนโลยีแห่งชาติ

สำหรับการประดิษฐ์ตามรายละเอียดการประดิษฐ์ ข้อถือสิทธิ และรูปเขียน (ถ้ามี) ปรากฏในสิทธิบัตรนี้

เลขที่คำขอ ๐๐๓๕๙๓

วันขอรับสิทธิบัตร 15 กุมภาพันธ์ 2544

ผู้ประดิษฐ์ นายทวี ตันฆศิริ และคณะ

ชื่อที่แสดงถึงการประดิษฐ์ สารประกอบเพียโซอิเล็กทริกชนิดมีกลไกสำหรับใช้ในสวนกระจะเทียบ และกรรมวิธีผลิตสารประกอบดังกล่าว

ให้ผู้ทรงสิทธิ[illegible]และหน้าที่ตามกฎหมายว่าด้วยสิทธิบัตรทุกประการ

ออกให้ ณ [illegible] 12 เดือน เมษายน พ.ศ. 2548

หมดอายุ ณ [illegible] 14 เดือน กุมภาพันธ์ พ.ศ. 2564

(ลงชื่อ) .....

(นายวิเชียร นาวานุเคราะห์)

อธิบดีกรมทรัพย์สินทางปัญญา

ผู้ออกสิทธิบัตร

พนักงานเจ้าหน้าที่

หมายเหตุ 1. ผู้ทรงสิทธิบัตรจะต้องชำระค่าธรรมเนียมรายปีเริ่มแต่ปีที่ 5 ของอายุสิทธิบัตร มิฉะนั้นสิทธิบัตรจะสิ้นอายุ

2. ผู้ทรงสิทธิบัตรจะต้องชำระค่าธรรมเนียมรายปีล่วงหน้าโดยชำระทั้งหมดในคราวเดียวก็ได้

3. การอนุญาตให้ใช้สิทธิตามสิทธิบัตรและการโอนสิทธิบัตรต้องทำเป็นหนังสือและจดทะเบียนต่อพนักงานเจ้าหน้าที่

เอกสารหมายเลข 4

เอกสารหมายเลข 4.1

Subject: RE: Greetings and Report on Recent Development of Asian Ferroelectric Association
From: "Zhu Weiguang \(Prof\)" <EWZHU@ntu.edu.sg>
Date: Sat, July 9, 2005 10:09 am
To: tadashi@takenaka.ee.noda.sut.ac.jp (more)
Cc: yfchen@nju.edu.cn (more)
Priority: Normal
Options: View Full Header | View Printable Version | View Message details

Dear all AFA Executive & Advisory Board Members:

Greetings and wish all of you well. This is a half-year short circulation to report all Board Members on recent development of AFA. Prof. T. Takenaka (Chair), Prof. X. Yao (Immediate-Past-Chair), Prof. W. Zhu (Chair-Elect), and other several board members including Prof. Q. R. Yin, Prof. T. Shiosaki, Prof. T. Y. Tseng met at the 4th Asian Meeting on Electroceramics held 27 - 30 June in Hangzhou of China, exchanged information and views. Below is the brief report on the recent development or change for the past ~ half-year.

5th Asian Meeting on Ferroelectrics (AMF-5). AMF-5 will be held 27-31 August 2006 in Noda of Japan near the Tokyo area. The 1st Call for Papers is ready. For more information, please contact Professor T. Takenaka or find at http://www.amf5.com. For AMF-5, Prof. T. Takenaka is the General Chair, Prof. T. Tsurumi of TIT is the Program Chair, and Prof. T. Shiosaki is the Chair for Prof. Y. Ishibashi Workshop.

Confirmation of Prof. Tawee as the Executive Board Member. Prof. Tawee of Thailand was recommended in the last circulation as the Executive Board Member to represent the Thai's ferroelectric community. There is no any objection has been received since the last circulation about half-year ago, and Prof. Tawee is therefore confirmed as an AFA's Executive Board Member. Let's warmly welcome Prof. Tawee to AFA's Executive Board and congratulate to Prof. Tawee!

Retirement from Executive Board, Change to Advisory Board and New Replacement

* Prof. YAO Xi requested to relinquish his Executive Board Membership, and his request was accepted by the Executive Board Standing/Working Committee. However, the Executive Board Standing/Working Committee asked Prof. YAO Xi to remain as his Immediate-Past-Chair and as a Member of Advisory Board; and Prof. YAO has kindly agreed on it.
* Prof. T. Shiosaki also kindly requested to relinquish his Executive Board Membership, and his request was accepted by the

Executive Board Standing/Working Committee. However, the Executive Board Standing/Working Committee asked Prof. T. Shiosaki as a Member of Advisory Board; and Prof. Shiosaki has kindly accepted it.

* Prof. Yan-Feng CHEN of Nanjing University of China has been proposed and recommended by the Chinese community to replace Prof. YAO Xi as an Executive Board Member for China. Attached please find Prof. Chen's short CV. If any board member has objection, please feel free to contact or email any one of us. If the objection ratio is less than 1/3 by about at the end of this year, Prof. Chen will be confirmed his membership in AFA's Executive Board.

* Prof. T. Tsurumi of Tokyo Institute of Technology has been proposed and recommended by the Japanesee community to replace Prof. T. Shiosaki as an Executive Board Member for Japan. If any board member has objection, please feel free to contact or email any one of us. If the objection ratio is less than 1/3 by about at the end of this year, Prof. Tsurumi will be confirmed his membership in AFA's Executive Board.

Thanks, have a nice weekend and with our best wishes,

T. TAKENAKA	YAO Xi
Weiguang ZHU	
Chair	Immediate-Past-Chair
Chair-Elect	

****
Professor ZHU Weiguang
School of Electrical & Electronic Engineering
BLK S2, B2a-03
Nanyang Technological University
50 Nanyang Avenue
Tel: (65) 6790 4541
Fax: (65) 6792 0415
Email: ewzhu@ntu.edu.sg
****

เอกสารหมายเลข 4.2

Dear Prof. Tawee Tunkasiri,

The manuscript titled

High Curie Temperature Perovskite BiInO₃-PbTiO₃ Ceramics

by

1) Robert Speyer 2) Runrun Duan 3) Edward Alberta 4) Thomas Shrout

has been submitted to Journal of Materials Research. I would like to ask you to serve as reviewer on this paper. In an effort to expedite the review process, please respond to this request by e-mail (reply) as soon as possible (within 1 to 2 working days). I hope that you will agree to review this paper, in which case you will be notified by e-mail within 3 calendar days about how to access the complete manuscript through our online review system. You will receive a personalized UserID and password with which to access the manuscript. I know that our expert reviewers greatly contribute to the high standards of the Journal, and I thank you in advance for accepting this request. If you are unable to review the manuscript, I would greatly appreciate your recommending another expert reviewer.

Sincerely,

Doh-Yeon Kim
JMR Principal Editor

JMR-2004-0123
High Curie Temperature Perovskite BiInO₃-PbTiO₃ Ceramics
Corresponding Author: Prof. Robert Speyer
Contributing Authors: 1) Robert Speyer 2) Runrun Duan 3) Edward Alberta 4) Thomas Shrout

The extent of BiInO₃ substitution in the perovskite system xBiInO₃-(1 - x)PbTiO₃ and the corresponding raise in the Curie temperature were investigated using thermal analysis, X-ray diffraction and electron microscopy. Maximum tetragonal perovskite distortion (c/a = 1.082) was obtained for x = 0.20, with a corresponding Curie temperature of 582[[deg]]C. Phase-pure tetragonal perovskite was obtained for x [[lteq]] 0.25. Compound formation after calcining mixed oxide powders resulted in agglomerated cube-shaped tetragonal perovskite particles, which could be fired to 94.7% of theoretical density (TD) by crushing after calcining, dry pressing and firing. Sol-gel fabrication resulted in nano-sized tetragonal or pseudo-cubic perovskite particles, which after two-step firing, resulted in a tetragonal perovskite microstructure at as high as (x = 0.25) 98.2% of TD.

เอกสารหมายเลข 4.3

PLEASE ACKNOWLEDGE RECEIPT OF THIS MANUSCRIPT FOR YOUR REVIEW.
We need a review as soon as possible.

Manuscript No.: P5-2843

Title: Phase transitions of natural corals monitored by ESR spectroscopy
Author(s): V. Vongsavat, P. Winotai and S. Meejoo

Dear Professor T. Tunkasiri,

The enclosed manuscript (.PDF) has been submitted quite some time ago for publication in NIM B: Beam Interactions with Materials and Atoms. I seem to be unable to locate a suitable referee. I hope that you will consent to review it for us.

It is essential that a timely and careful review be given to all manuscripts in order to maintain a high quality for the Journal. Please consider the originality, quality of presentation, and scientific merit in your review. If you know at the outset that you will be unable to review this manuscript within the next two weeks, please inform our office and suggest another reviewer if possible. You may refer this manuscript to a qualified colleague at your laboratory for review if you wish. You may e-mail (e-mail is preferred), fax or mail your reply to the listed information below.

Your help is greatly appreciated.

Sincerely,

Lynn E. Rehn, Editor, NIMB

Dr. Lynn E. Rehn
Editor, NIMB
Building 223, MS7, Room S-231
Argonne National Laboratory
9700 South Cass Avenue
Argonne, IL 60439 USA

Phone: 630-252-9297 / Fax: 630-252-3308
E-mail: nimb@anl.gov

เอกสารหมายเลข 5

เอกสารหมายเลข 5.1

ผลการประเมินแบบสอบถามการประชุมวิชาการทางฟิสิกส์
เรื่อง "เพียโซอิเล็กตริกเซรามิกที่อุณหภูมิซินเตอร์ต่ำ"

Low Sintering Temperature Ceramics

16 กรกฎาคม 2546

ณ ภาควิชาฟิสิกส์ คณะวิทยาศาสตร์ มหาวิทยาลัยเชียงใหม่

จากการประเมินผู้เข้าร่วมสัมมนาทั้งหมด 60 คน มีผู้ส่งแบบสอบถามจำนวน 58 ชุด แบ่งเป็นเพศชาย 31.0 เปอร์เซนต์ เพศหญิง 69.0 เปอร์เซนต์ โดยมีอาชีพเป็นอาจารย์ ข้าราชการและพนักงาน คิดเป็น 62.1 เปอร์เซนต์ นักศึกษา 34.5 เปอร์เซนต์ และบริษัทเอกชน 3.4 เปอร์เซนต์

ตารางที่ 1 ความน่าสนใจของเนื้อหาสาระของแต่ละหัวข้อบรรยายคิดเป็นเปอร์เซนต์

หัวข้อบรรยาย	ดีมาก	ดี	ปานกลาง	พอใช้	รวม
1. Low Sintering Temperature Ceramics	41.4	41.4	17.2	0	100
2. High Permittivity Ceramics	13.8	72.4	13.8	0	100
3. Barium-Strontium Titanate Ceramics	13.8	75.9	6.9	3.4	100
4. Piezo-pyroelectric and thermal effects	10.3	69.0	13.8	3.9	100
5. PZT thin films prepared by spin coating	27.6	62.1	10.3	0	100
6. Low Temperature Firing PZT (54/46)	31.0	51.7	17.2	0	100
7. Particle Size Measurement by XRD	6.9	55.2	20.7	17.2	100
8. BNT Ceramics	13.8	72.4	13.8	0	100
9. Chemical Synthesis of $BaTi_5O_{11}$ Powders	24.1	62.1	13.8	0	100
10. Spray Pyrolysis	13.8	75.9	10.3	0	100

ตารางที่ 2 วิธีการนำเสนอของแต่ละหัวข้อบรรยายคิดเป็นเปอร์เซนต์

หัวข้อบรรยาย	ดีมาก	ดี	ปานกลาง	พอใช้	รวม
1. Low Sintering Temperature Ceramics	31.0	69.0	0	0	100
2. High Permittivity Ceramics	20.7	72.4	6.9	0	100
3. Barium-Strontium Titanate Ceramics	27.6	65.5	6.9	0	100
4. Piezo-pyroelectric and thermal effects	17.2	72.4	10.3	0	100
5. PZT thin films prepared by spin coating	31.0	69.0	0	0	100
6. Low Temperature Firing PZT (54/46)	27.6	69.0	3.4	0	100
7. Particle Size Measurement by XRD	10.3	55.2	34.5	0	100
8. BNT Ceramics	17.2	82.8	0	0	100
9. Chemical Synthesis of $BaTi_5O_{11}$ Powders	13.8	75.9	10.3	0	100
10. Spray Pyrolysis	24.1	72.4	3.4	0	100

ส่วนความคิดเห็นเรื่องอื่นๆ ผู้เข้าร่วมสัมมนาให้ความเห็นว่าน่าจะมีการจัดประชุมอย่างนี้อีกทุกปี โดยให้เพิ่มจำนวนวันประชุมให้มากขึ้น และควรจัดให้มีการเยี่ยมชมห้องปฏิบัติการด้วย

เอกสารหมายเลข 5.2

รายงานผลการสัมมนาเรื่อง The International Conference on Smart Materials

(SmartMat-'04) -Smart/Intelligent Materials and Nanotechnology-

ระหว่างวันที่ 1-3 ธันวาคม 2547

ณ โรงแรมอิมพีเรียลแม่ปิง จ.เชียงใหม่

จำนวนผู้เข้าร่วมการประชุม 296 คน ดังนี้

	ประเภท	จำนวน
1	Participants	169 คน
2	Students	127 คน

<u>จากสถาบันต่าง ๆ ดังนี้</u>

1. มหาวิทยาลัยเชียงใหม่
2. จุฬาลงกรณ์มหาวิทยาลัย
3. มหาวิทยาลัยเกษตรศาสตร์
4. มหาวิทยาลัยขอนแก่น
5. สถาบันเทคโนโลยีพระจอมเกล้าคุณทหารลาดกระบัง
6. สถาบันเทคโนโลยีพระจอมเกล้าพระนครเหนือ
7. สถาบันเทคโนโลยีพระจอมเกล้าธนบุรี
8. มหาวิทยาลัยมหิดล
9. ศูนย์เทคโนโลยีโลหะและวัสดุแห่งชาติ
10. มหาวิทยาลัยรามคำแหง
11. มหาวิทยาลัยศิลปากร
12. มหาวิทยาลัยเทคโนโลยีสุรนารี
13. มหาวิทยาลัยธรรมศาสตร์
14. วิทยาลัยปิโตรเลียมและปิโตรเคมี
15. มหาวิทยาลัยทักษิณ
16. มหาวิทยาลัยบูรพา
17. มหาวิทยาลัยราชภัฏนครราชสีมา
18. มหาวิทยาลัยนเรศวร

19. มหาวิทยาลัยแม่ฟ้าหลวง
20. มหาวิทยาลัยแม่โจ้
21. มหาวิทยาลัยสงขลานครินทร์
22. มหาวิทยาลัยศรีนครินทร์วิโรฒ
23. มหาวิทยาลัยอุบลราชธานี
24. มหาวิทยาลัยวลัยลักษณ์
25. มหาวิทยาลัยราชภัฏบ้านสมเด็จเจ้าพระยา
26. สถาบันเทคโนโลยีนานาชาติสิรินธร
27. สถาบันวิจัยวิทยาศาสตร์และเทคโนโลยีแห่งประเทศไทย
28. ศูนย์ศิลปาชีพบบางไทรในสมเด็จพระนางเจ้าสิริกิติ์ฯ
29. บริษัท บางกอกโพลีเอทธีลีน จำกัด (มหาชน)
30. บริษัท ยูเนี่ยนนิฟโก้ จำกัด
31. บริษัทโอเชียนกลาส จำกัด
32. Asian Institute of Technology / Thailand
33. Aston University / UK
34. Cambridge University / UK
35. Indian Institute of Technology Delhi / India
36. Nanyang Technological University / Singapore
37. National Technology of Singapore / Singapore
38. RMIT University / Australia
39. Shandong University / China
40. Sultan Qaboos University / Oman
41. Tokyo University / Japan
42. University of Bath / UK
43. University of Berscia / Italy
44. University of Bologna / Italy
45. Victoria University of Wellington / New Zealand

จำนวนผู้เข้าร่วมเสนอผลงานการประชุม SmartMat-'04
จำนวน 227 ราย ดังนี้

1	Oral presentation	89 ราย
2	Poster presentation	138 ราย

จำนวน Guest Speakers ของการประชุม SmartMat-'04
จำนวน 18 ราย ดังนี้

3	Plenary Speakers	5 คน
4	Invited Speakers	13 คน

Plenary Speakers

1. Robert E. Newnham
2. Supapan Seraphin
3. Kenji Uchino
4. Anthony K. Cheetham
5. Ron Stevens

Invited Speakers

1. Ram P. Tandon
2. Yao Xi
3. Brian J. Tighe
4. Tawee Tunkasiri
5. John Wang
6. Amar S. Bhalla
7. David P. Cann
8. Derek C. Sinclair
9. Geoffrey R. Mitchell
10. Qi Zhang
11. Weiguang Zhu
12. Ahmad Safari
13. Paul Lawrence

จำนวนผู้เข้าร่วมประชุมการประชุม SmarMat-'04

จำนวน 296 คน แบ่งเป็น

	ประเภท	จำนวน
1	Participants	169 คน
2	Students	127 คน

จำนวน Guest Speakers ในการประชุม SmarMat-'04

จำนวน 19 คน แบ่งเป็น

1	Plenary Speakers	5 คน
2	Invited Speakers	14 คน

จำนวนผู้เข้าร่วมเสนอผลงานประชุมการประชุม SmarMat-'04

จำนวน 227 ราย แบ่งเป็น

1	Oral presentation	89 ราย
2	Poster presentation	138 ราย

บทความบางส่วนที่เผยแพร่ในการประชุม

บทความที่ 1

Progress in Electroceramics in Thailand

Tawee Tunkasiri

Research in Electroceramics in Thailand, has actually started since 1987. Work has been carried out in universities/institutes mainly on property and structure of Piezoelectric ceramics such as barium titanate ($BaTiO_3$, BT) and lead zirconate titanate ($Pb(Zr_{0.48}Ti_{0.52})O_3$, PZT. With high permittivity and rapid change in resistance at Curie temperature, enable BT ceramics to be employed as capacitors and thermistors. Also with appropriate compositions barium based ceramics can be employed in microwave circuits. Many research works have been carried out in a few institutes/universities on PZT compounds. Due to their high planar coupling coefficient enables PZT ceramics to be fabricated in ultrasonic cleaners, igniters, buzzers...etc.

Regarding to the processing, mixed oxides route has been chosen for simplicity. However, chemical route (Co-precipitation, Oxalate...etc.) has been used to obtain smaller particles, higher purity and more precise compositions.

The relation of microstructure and the physical properties of ceramics has been studied, mainly employing electron microscopy (SEM, TEM). X-ray line broadening method has also been used to measure the particle size of the staring powder. Inorder to bring down some physical properties, the study of composite materials such as piezoceramic (PZT) – polymers (HDPE, Epoxy resin) has been done in some universities. Thin sheets of the PZT-polymer-composite (0-3 type) can be achieved via calendering method.

Other materials, such as zinc oxide varistors (employed as surge arrestors) and the solar cell group such as thin film of CdS, $Cd_{1-x}\ Zn_x\ S$ and $CuIn_{1-x}\ Ga_x\ Se_2$ have been studied in some universities.

บทความที่ 2

Low Temperature Sintering Piezoelectric Ceramics

ทวี ตันฆศิริ

ประโยชน์ของ Piezoelectric Ceramics

ในโลกปัจจุบันเป็นการยากที่จะดำรงชีวิตอยู่โดยไม่พึ่งพาวัสดุที่สร้างขึ้นมา ยกตัวอย่าง เช่น กระดาษ สิ่งที่ทำด้วยไม้ สิ่งที่ทำด้วยโลหะ แก้ว แม้ในร่างกายก็ยังมีวัสดุที่มนุษย์สร้างขึ้นมาอยู่ในร่าง เช่น วัสดุที่อุดในฟัน ข้อต่อเซรามิก เลนซ์ตา ลิ้นหัวใจ เป็นต้น สิ่งต่างๆ เหล่านี้ถูกสร้างขึ้นเพื่อปฏิบัติการบางสิ่งในร่างกาย เพื่อให้ชีวิตดำรงอยู่ได้ในห้วงอวกาศก็ยังมีดาวเทียมที่มนุษย์สร้างขึ้นวิ่งวนรอบโลก รอบดาวเคราะห์ต่างๆ ในชีวิตประจำวันเราต้องพึ่งพาอุปกรณ์ต่างๆ อย่างมากมาย ดังรูปที่ 1.1 จะเห็นได้ว่าในบ้านเรือนที่อยู่อาศัยเช่น ที่จุดก๊าซ เซลล์สุริยะ อุปกรณ์ในรถยนต์ เป็นต้น อาจจะกล่าวได้ว่ามนุษย์ชาติในโลกปัจจุบันดำรงชีวิตอยู่ในท่ามกลางวัสดุทั้งสิ้น เป็นที่แน่ชัดแล้วว่าวัสดุเป็นสิ่งที่มีประโยชน์หลายๆ ด้านอย่างมหาศาล สามารถสร้างขึ้นในกระบวนการทางวิทยาศาสตร์ สมบัติต่างๆ ของวัสดุ รวมทั้งโครงสร้างจึงต้องศึกษาและนำสมบัติที่เด่นของวัสดุเหล่านั้นมาใช้ให้เป็นประโยชน์ สมบัติของวัสดุที่สำคัญเช่น ความต้านทานทางไฟฟ้า ไดอิเล็กทริก ความหนาแน่น การขยายตัวเมื่ออุณหภูมิเปลี่ยนไป ฯลฯ ซึ่งเป็นสมบัติทางฟิสิกส์ทั้งสิ้น ข้อแตกต่างระหว่างนักฟิสิกส์ และนักวัสดุศาสตร์จะแตกต่างกันที่นักวัสดุมักจะพิจารณาศึกษาโครงสร้างจุลภาค (microstructure) ซึ่งอยู่ในช่วง 10^{-6} ม. หรือในช่วงของไมครอน (micron, μm) แต่ในขณะที่นักฟิสิกส์มักจะสนใจแต่ช่วงของ 10^{-10} ม. หรืออังสตรอม (Angstrom, A) หรือช่วงของ 10^{-9} ม. หรือนาโนมิเตอร์ (nonometer, n)

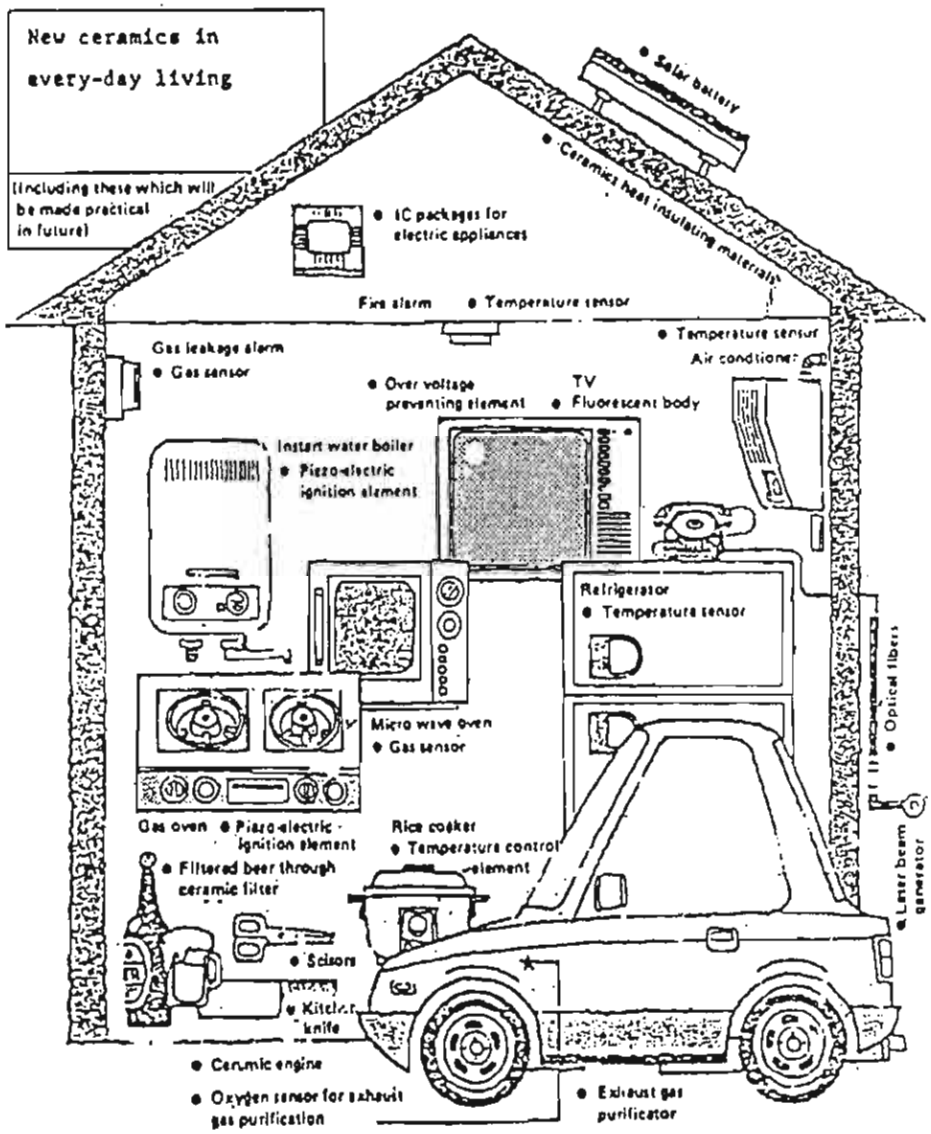

รูปที่ 1.1 ตัวอย่างการใช้เซรามิกยุคใหม่ในชีวิตประจำวัน

แผนภาพ (diagram) ของวัสดุอาจแบ่งออกได้ตามรูปที่ 1.2

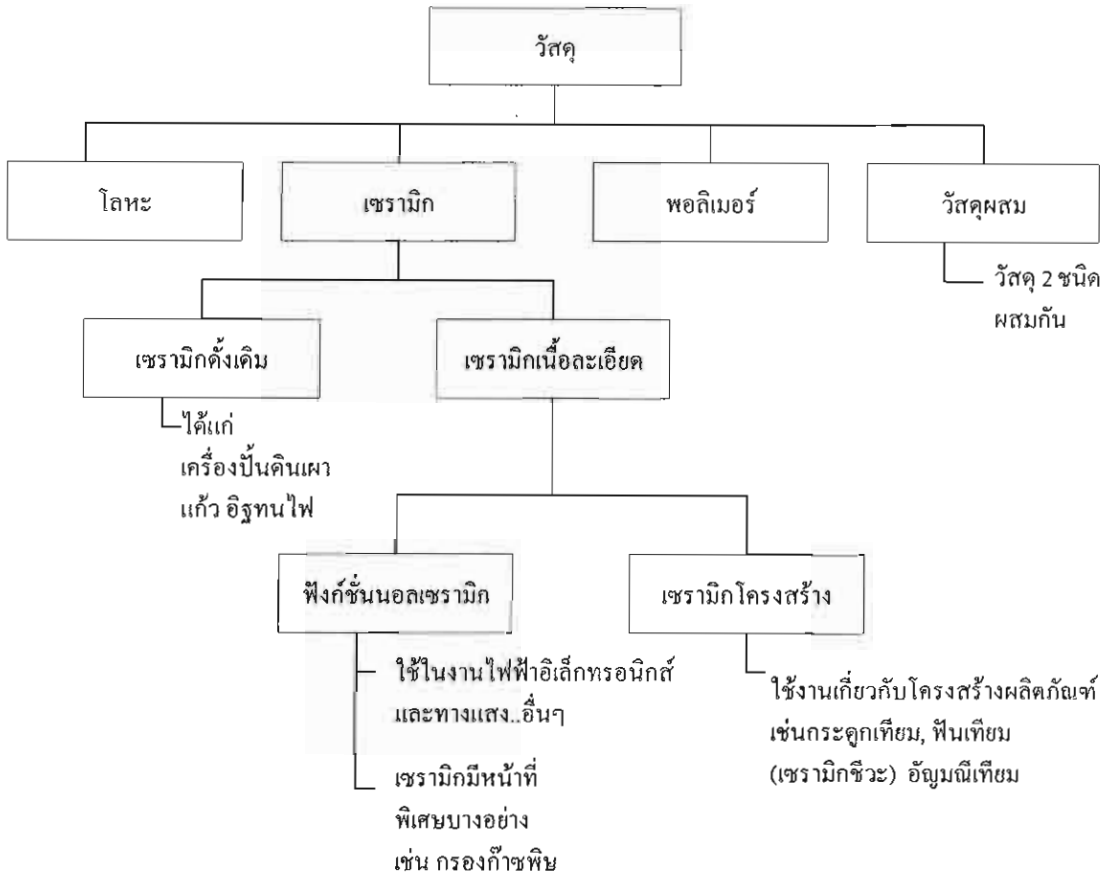

รูปที่ 1.2 แผนภาพของวัสดุ (ดัดแปลงจาก [1])

จากรูปที่ 1.2 จะเห็นว่าวัสดุอาจจะแบ่งออกเป็น 4 กลุ่ม ได้แก่ โลหะ พอลิเมอร์เซรามิก และวัสดุผสม เซรามิกยังแบ่งได้เป็น 2 ชนิดหลัก คือ เซรามิกดั้งเดิม (classical ceramics) ซึ่งได้แก่ เครื่องปั้นดินเผา แก้ว ผลิตภัณฑ์ที่ใช้ในบ้าน อิฐต่างๆ และเซรามิกเนื้อละเอียด (fine ceramics) เซรามิกดั้งเดิมสร้างจากวัตถุดิบตามธรรมชาติ เช่นดินเหนียวแร่ธาตุต่างๆ ขณะที่เซรามิกเนื้อละเอียดสร้างจากสารประกอบทางเคมีที่บริสุทธิ์สูง (> 99.99%) กรรมวิธีการผลิตยุ่งยากซึ่งจะกล่าวภายหลัง เซรามิกเนื้อละเอียด บางทีเรียกว่าเซรามิกยุคใหม่ (new ceramics) ยังแบ่งย่อยออกไปอีกเป็นฟังก์ชั่น

นอลเซรามิก (functional ceramics) จะเป็นกลุ่มที่ใช้ประโยชน์ทางไฟฟ้าอิเล็กทรอนิกส์ทางแสง และหน้าที่พิเศษบางอย่างเช่นที่กรองก๊าซพิษ อีกกลุ่มหนึ่งจะเป็นกลุ่มที่มีหน้าที่เกี่ยวกับโครงสร้าง เรียกเซรามิกโครงสร้าง (structural ceramics) เช่น กลุ่มที่เข้าไปอยู่ในร่างกาย บางทีเรียกเซรามิกชีวะ (bio ceramics) เช่นกระดูกเทียม ฟันเทียม และกลุ่มอื่น เช่น อัญมณี เป็นต้น ข้อแตกต่างที่สำคัญของเซรามิกดั้งเดิม และเซรามิกเนื้อละเอียดคือความพรุน (porosity) ในเนื้อผลิตภัณฑ์เซรามิกเนื้อละเอียด ความพรุนจะน้อยกว่ามาก หรือรูในเนื้อผลิตภัณฑ์มีน้อยกว่า สมบัติต่างๆ ของเซรามิกเนื้อละเอียดโดยเฉพาะกลุ่มฟังก์ชั่นนอลจะควบคุมโดยการควบคุมขนาดเกรน (grain size) เส้นขอบเกรน ด้วยกรรมวิธีทางวิทยาศาสตร์ รายละเอียดนี้จะกล่าวในภายหลังด้วยสาเหตุที่ว่าเซรามิกเนื้อละเอียดสร้างจากการผสมของสารประกอบทางเคมี จึงทำให้ผลิตภัณฑ์ทางด้านนี้มีมากมายหลายชนิดที่ใช้ทำประโยชน์เฉพาะด้านต่างๆ ดังในรูปที่ 1.1 ปัจจุบันมีโรงงานที่ผลิตอุปกรณ์ต่างๆ ทางเซรามิกมากมาย โดยเฉพาะทางด้านไฟฟ้าอิเล็กทรอนิกส์เนื่องจากเป็นสิ่งจำเป็นในวงจรต่างๆ มากมาย หากเราเปิดฝาด้านหลังโทรทัศน์ออกมาจะพบแผ่นวงจรต่างๆ มีชิ้นส่วนเล็กๆ หลายร้อยตัวประกอบอยู่ ชิ้นส่วนต่างๆ เหล่านั้นคือฟังก์ชั่นนอลเซรามิกทั้งสิ้น ความต้องการทางการค้าของชิ้นส่วนเหล่านี้ ค้าขายไปทั่วโลก ฟิชเชอร์ (Fisher) [2] ได้สำรวจและประเมินไว้ว่าในปี ค.ศ.1983 ความต้องการชิ้นส่วนต่างๆ ด้านนี้ค้าขายกันทั่วโลกอยู่ในระดับ 5,000 ล้านเยน ถึง 100,000 ล้านเยน (ต่อปี) ขึ้นกับชนิดของอุปกรณ์และจะเพิ่มขึ้นประมาณ 10-20% ต่อปี ในปัจจุบันตลาดสหรัฐอเมริกา มูลค่าชิ้นส่วนของ Advanced Ceramics มีค่าประมาณ 5.5 ล้านเหรียญสหรัฐ 76% ของมูลค่านี้เป็นชิ้นส่วนของอิเล็กทรอนิกส์เซรามิก และคาดว่าจะมีค่าในปี ค.ศ. 2005 นี้ ถึง 10 หมื่นล้านเหรียญ

จากภาพที่ 1.1 จะพบว่า อุปกรณ์ในชีวิตประจำวันรวมถึงในอุตสาหกรรม จะประกอบด้วย Piezoelectric ceramics เช่น ที่จุดก๊าซ, เครื่องทำความสะอาดเหนือเสียง ซึ่งใช้ในวงการแพทย์ และอุตสาหกรรมทั่วไป ใช้ในโทรศัพท์ ใช้เป็นอุปกรณ์ที่เตือนเมื่อรถถอยหลัง อุปกรณ์โซนาร์ เครื่องสลายนิ่ว เป็นต้น สมบัติของสารเพียโซอิเล็กตริกนี้ อาจอธิบายโดยง่ายว่าเป็นการเปลี่ยนแปลงของพลังงาน 2 ชนิด กล่าวคือ

พลังงานไฟฟ้า เป็น พลังงานกล

พลังงานกล เป็น พลังงานไฟฟ้า

การค้นพบและพัฒนาที่สำคัญ อาจสรุปได้ดังนี้

1880-1882	Pierre และ Jacques Curie พบสมบัติเพียโซอิเล็กตริกใน ควอทซ์, Rochelle salts
1882-1917	นำไปใช้เป็นทรานสดิวเซอร์ เกิด resonance ที่ 50 Hz. และเกิดการใช้ใน sonar
1920-1940	นำไปใช้ในการตรวจรอยแยกในเหล็ก และเกิดการสร้าง actuator ขึ้น
1940-1965	นำไปพัฒนาเป็นที่จุดเตาก๊าซ
ในปัจจุบัน	มีการพัฒนาไปมาก โดยเฉพาะในวงการแพทย์ เช่น เครื่องวัดความดัน เครื่องขูดหินปูน เครื่องกระตุ้นหัวใจ เครื่องนวด ultrasound เป็นต้น

สารประกอบที่ใช้ส่วนใหญ่มีตะกั่วเป็นฐาน เช่น

Lead titanate ($PbTiO_3$)

Lead niobate ($PbNb_2O_6$)

Lead magnesium niobate ($PbMgNbO_3$)

เป็นต้น

จะพบว่าส่วนใหญ่แล้วจะใช้สารตะกั่ว ทำให้สิ่งแวดล้อมเป็นพิษ ใช้อุณหภูมิในการ sinter สูง (> 1350 °C) ทำให้สิ้นเปลืองอย่างมาก ในงานนี้จึงมีวัตถุประสงค์ในการทำให้สารดังกล่าวมาอุณหภูมิ sinter ต่ำลง

ในโครงการวิจัยนี้มุ่งที่จะทำสาร PZT และ BT เป็นหลัก

1. Thick film ceramics with sintering aids
2. PLZT thin film
3. Composite materials
4. Lead-free piezo compound

Thick film ceramics with sintering aids

ในการทำฟิล์มเซรามิกหนา 10-10 mm จะต้องใช้ผงเริ่มต้นขนาดเล็กมาก ผงที่มีขนาดเล็กมีแนวโน้มทำให้อุณหภูมิซินเตอร์ลดลง ดังนั้นใน sub project นี้มีขั้นตอนดังนี้

1. สร้างผงเริ่มต้นที่เล็กมากขนาด < 1 mm โดยวิธีต่างๆ เช่น Spray dry techniques
2. สร้างแผ่นฟิล์มบาง (ก่อนนำไปเผา) ด้วย Tape casting หรือ spin coating

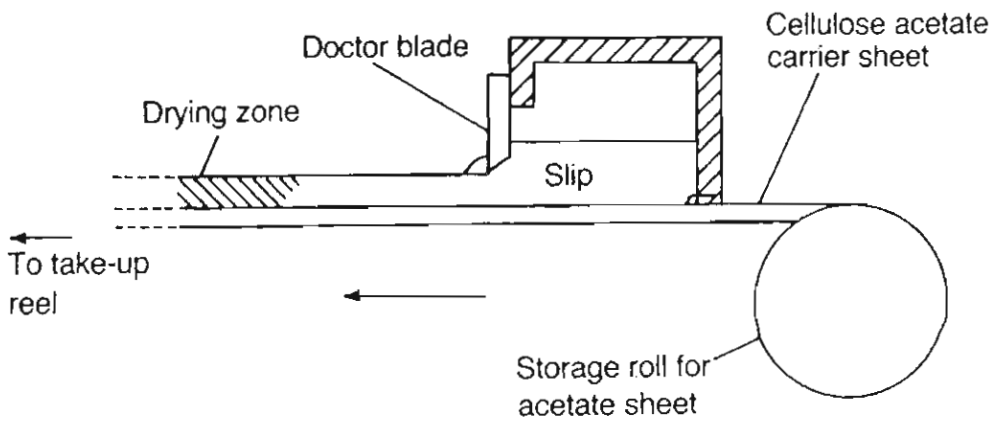

เครื่อง Tape casting

PLZT thin film

สาร PZT ที่เจือด้วย lanthanum (La) เป็นสารประกอบที่มีประโยชน์ด้าน Electro-Optics และวงจรอิเล็กทรอนิกส์อื่นๆ ในโครงการย่อยนี้มีวัตถุประสงค์ที่จะทำแผ่นฟิล์มบาง PLZT โดยวิธี Sol-Gel และ spin coating ~ 10 μm

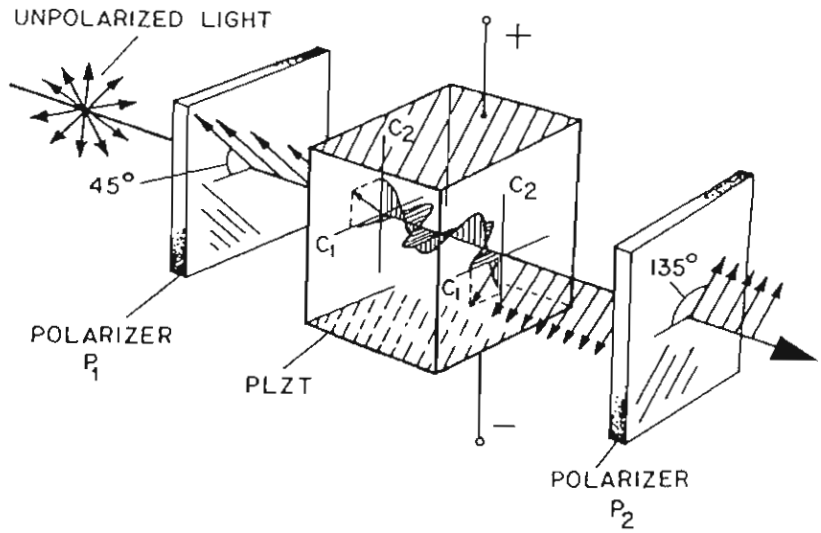

ความหน่วงของออฟติกเฟสในอิเล็กโทรออฟติกเซรามิกที่ถูกกระตุ้น ในรูปแสดงสภาวะเปิดที่ voltage ครึ่งหนึ่งของคลื่น (half-wave) ใช้ประโยชน์ในอุตสาหกรรมด้าน Electro-optics

Composite materials

บางกรณีสารประกอบบางชนิดมีสมบัติที่ยังไม่สามารถนำมาประยุกต์ใช้ได้ดีตามต้องการ ในโครงการนี้มีวัตถุประสงค์ที่จะทำวัสดุผสม เช่น PZT+ Polymer เป็นต้น เพื่อทำให้วัสดุมีสมบัติเหมาะสมกับการประยุกต์ใช้ เช่น เป็นตัวกลางให้คลื่นเชิงกลผ่านระหว่างเซรามิก (ความหนาแน่นสูง) เข้าสู่ร่างกายมนุษย์ (ความหนาแน่นต่ำ)

Lead-free piezo compound

จากการที่ PZT จะประกอบด้วยตะกั่วเป็นฐาน ทำให้มีอัตราเสี่ยงต่อสิ่งแวดล้อม ในโครงการนี้จึงมีวัตถุประสงค์ในการทำสารที่ไม่มีตะกั่วเป็นหลัก อาจประกอบด้วย BaSrTiO3 และสาร ประกอบ cadmium sulphide ที่ใช้ทำเซลล์สุริยะ

บทบาทของวัสดุในอนาคต [3]

ตามที่สหประชาชาติได้คาดคะเนไว้ว่า ในสหัสวรรษใหม่นี้ จำนวนประชากรของโลกจะเพิ่มขึ้นอย่างรวดเร็ว อาจถึงหมื่นล้านคนใน ค.ศ. 2150 ดังนั้นปัญหาที่ตามมาในด้านต่างๆ เช่น การขาดแคลนอาหาร น้ำดื่ม การทำลายป่า ปัญหาด้านเศรษฐกิจ การเมือง เป็นต้น ปัญหาบางชนิดนำมาซึ่งการค้นคว้าวิจัยและพัฒนานำเอาวัสดุมาใช้ เช่นต้องสร้างอ่างเก็บน้ำที่ใหญ่ มีการชลประทานเพียงพอ ทำให้วัสดุด้านซีเมนต์ต้องมีคุณภาพยิ่งขึ้น มีความแข็งแกร่งกว่าซีเมนต์ธรรมดา ที่กรองน้ำเซรามิกก็อาจจะต้องพัฒนาให้กรองเชื้อโรค หรือมีประเภท antibacterials tiles ซึ่งเป็นเซรามิกที่ฉาบด้วยแผ่นฟิล์มของ metal catalyst บางชนิด ที่ทำลายผนังเซลล์ของบักเตรีได้

ความก้าวหน้าทางโทรคมนาคมจะไวยิ่งขึ้นทำให้อุตสาหกรรมไมโครอิเล็กทรอนิกส์ต่างๆ มีมากขึ้น และมีขนาดเล็กลง กำลังการผลิตจะมากยิ่งขึ้น เป็น exponential อุปกรณ์เหล่านี้ได้แก่ กลุ่ม sensors ต่างๆ กลุ่ม composite transducers, thermistors capacitors, multilayer capacitors และ actuators เป็นต้น

ชิ้นส่วนบางอย่างจะต้องมีสมรรถภาพดียิ่งขึ้น เช่น Multilayer capacitors อาจมีขนาดเล็กเพียง 1 มม. หนาเพียง 1 μm กลุ่ม sensors และสารเพียโซอิเล็กตริกเซรามิก (PZT) หรือ composite ระหว่าง PZT และ polymer เช่น ไม่เพียงแต่ sensing ยังวิเคราะห์สัญญาณ ซึ่งบางทีเรียก Smart materials และหากทำหน้าที่ sensing วิเคราะห์สัญญาณที่รับและ respond ทันที กลุ่มเหล่านี้บางทีเรียกว่า Intelligent Materials ซึ่งจะใกล้เคียงกับระบบประสาทของมนุษย์เข้าไปทุกที และในอนาคตวัสดุบางชนิดอาจจะสามารถ respond ให้ถูกต้องตามทำนองคลองธรรมได้ด้วย

ทางด้านอาหารที่บริโภคโดยเฉพาะกลุ่มของสัตว์ทะเล เช่น ปลา จะหายากยิ่งขึ้น ดังนั้นอาจจะต้องมีการทำฟาร์มขนาดใหญ่ที่เลี้ยงปลาทะเล สาร PZT อาจจะนำมาดัดแปลงให้ทำหน้าที่เป็น sonar และสื่อสารกับปลาได้

ทางด้านที่พักอาศัยก็จะพัฒนาให้สะดวกสลายได้ด้วยวัสดุที่มีสมรรถภาพต่างๆ เช่น ควบคุมความชื้น อุณหภูมิให้พอเหมาะ หน้าต่างสามารถเปิดรับแสงอาทิตย์ในตอนเช้า และปิดในตอนกลางคืน

ในด้านสุขภาพอนามัยมนุษย์จะแข็งแรงยิ่งขึ้นด้วยการพัฒนาให้ gene ที่อ่อนแอถูกแทนที่หรือสร้างใหม่ด้วย gene ที่แข็งแรง กลุ่ม robots จะมีมากขึ้น โดยสรุปมนุษย์ในสหัสวรรษหน้าจะมีความเป็นอยู่ที่ดีขึ้น มีอายุยืนยาว และกระทำสิ่งต่างๆ ถูกต้องตามทำนองคลองธรรม

บรรณานุกรม

1. Cooke, B. and Sang, D. Physics of Materials. The University of Leeds, second edition (1989).

2. Fisher, G. Ceram. Bull. 64(1)(1983)34.

3. Newnham, R. E., Ceramic Focus. 1999. No.2, P.15.

บทความที่ 3

High Permittivity Ceramics

จีระพงษ์ ตันตระกูล

ในปัจจุบันเทคโนโลยีด้านอิเล็กทรอนิกส์กำลังได้รับความสนใจศึกษาและค้นคว้ากันอย่างกว้างขวางเพื่อให้ได้อุปกรณ์อิเล็กทรอนิกส์ที่มีคุณภาพดียิ่งขึ้น อุปกรณ์อิเล็กทรอนิกส์เซรามิกเป็นอุปกรณ์ที่มีเซรามิกเป็นองค์ประกอบ และอุปกรณ์อิเล็กทรอนิกส์เซรามิกที่มีอยู่ในวงจรอิเล็กทรอนิกส์เสมอได้แก่ ตัวเก็บประจุไฟฟ้า (capacitors) และตัวต้านทาน (resistors) ตัวเก็บประจุไฟฟ้าที่มีสารไดอิเล็กตริก (dielectrics) คั่นอยู่ระหว่างขั้วไฟฟ้าทั้งสองเป็นเซรามิกส์นั้นมีการผลิตเป็นจำนวนมากในแต่ละปี ไดอิเล็กตริกเซรามิก (dielectric ceramics) ส่วนใหญ่เป็นสารเฟร์โรอิเล็กตริกเซรามิกส์ (ferroelectric ceramics) เช่น แบเรียมไทเทเนต ($BaTiO_3$, BT) เลดแมกนีเซียมไนโอเบต $\{Pb(Mg_{1/3}Nb_{2/3})O_3$, PMN$\}$ และเลดซิงค์ไนโอเบต $\{Pb(Zn_{1/2}Nb_{2/3})O_3$, PZN$\}$ เป็นต้น แบเรียมไทเทเนตถูกนำมาใช้เป็นองค์ประกอบของตัวเก็บประจุไฟฟ้ามาตั้งแต่เริ่มต้นที่ค้นพบในปี 1941 มาจนถึงปัจจุบันนี้ และมีแนวโน้มจะมีความสำคัญมากขึ้น เพราะ PMN และ PZN เป็นสารที่มีตะกั่วเป็นองค์ประกอบ ซึ่งเป็นอันตรายต่อสิ่งแวดล้อมจึงอาจถูกห้ามใช้ในอนาคต

ตัวเก็บประจุไฟฟ้าจะมีปริมาณของประจุไฟฟ้า (Q) ที่เก็บอยู่ที่แผ่นตัวนำไฟฟ้าแต่ละแผ่นแปรผันโดยตรงกับค่าความต่างศักย์ไฟฟ้า (V) ระหว่างแผ่นตัวนำไฟฟ้าทั้ง 2 นั้น

$$Q = CV \qquad (1)$$

โดยที่ C เป็นค่าคงที่เรียกว่า capacitance (C) ซึ่งจะมีค่าขึ้นอยู่กับชนิดของสาร dielectric (ε) ที่คั่นอยู่ระหว่างแผ่นตัวนำไฟฟ้าทั้ง 2 ขนาดของพื้นที่ (A) ของแผ่นตัวนำไฟฟ้าและระยะห่าง (d) ระหว่างแผ่นตัวนำไฟฟ้าทั้ง 2

$$C = \frac{\varepsilon A}{d} \qquad (2)$$

ε ของสาร dielectric คือค่า permittivity ของสาร dielectric ซึ่ง $\varepsilon = \varepsilon_0 \varepsilon_r$ โดย ε_0 คือค่า permittivity ของ free space และ ε_r คือค่า relative permittivity หรือ dielectric constant

$$Q = \varepsilon_0 \varepsilon_r \left(\frac{A}{d}\right) V \qquad (3)$$

ปริมาณ volume efficiency ของตัวเก็บประจุไฟฟ้า (B_{eff}) คือค่า capacitance (C) ต่อหนึ่งหน่วยปริมาตรของตัวเก็บประจุไฟฟ้านั้น

$$B_{eff} = \frac{C}{vol} = \frac{\varepsilon_0 \varepsilon_r}{d^2} \qquad (4)$$

จำนวนพลังงานที่เก็บอยู่ในตัวเก็บประจุไฟฟ้า (E)

$$E = \frac{1}{2} C V^2$$

จำนวนพลังงาน E ต่อหนึ่งหน่วยปริมาตรของตัวเก็บประจุไฟฟ้านั้น

$$U = \frac{E}{vol} = \frac{1}{2} B_{eff} V^2 = \frac{1}{2} \varepsilon_0 \varepsilon_r \left(\frac{V}{d}\right)^2 \qquad (5)$$

ผลคูณของ B_{eff} กับ V คือ figure of merit

$$\text{Figure of merit} = B_{eff} V$$

$$= \frac{\varepsilon_0 \varepsilon_r}{d^2} V = \frac{Q}{vol} \qquad (6)$$

จากสมการ (6) ต้องการ fique of merit ที่มีค่ามากๆ B_{eff} จะต้องมีค่ามากตามไปด้วย ซึ่งหมายความว่าสาร dielectric ต้องมีค่า ε_r มาก และ d น้อยๆ แต่เราไม่สามารทำให้ค่า d เป็นศูนย์ได้ เพราะ applied voltage (V) จะต้องมีค่าน้อยกว่า breakdown voltage ของสาร dielectrics

แบเรียมไทเทเนต (BT) มีโครงสร้างของผลึกเหมือนกับแร่ perovskite ($CaTiO_3$) ลักษณะของ unit cell เป็นแบบ cubic เมื่อมีอุณหภูมิสูงกว่า Curie point (ประมาณ 130 °C) และเมื่อมีอุณหภูมิต่ำกว่า Curie point จะมีโครงสร้างเปลี่ยนเป็น tetragonal single crystal ของ BT มีค่า ε_r ณ อุณหภูมิต่างๆ ดังรูปที่ 1 และ BT ceramics มีค่า ε_r ณ อุณหภูมิต่างๆ ดังรูปที่ 2

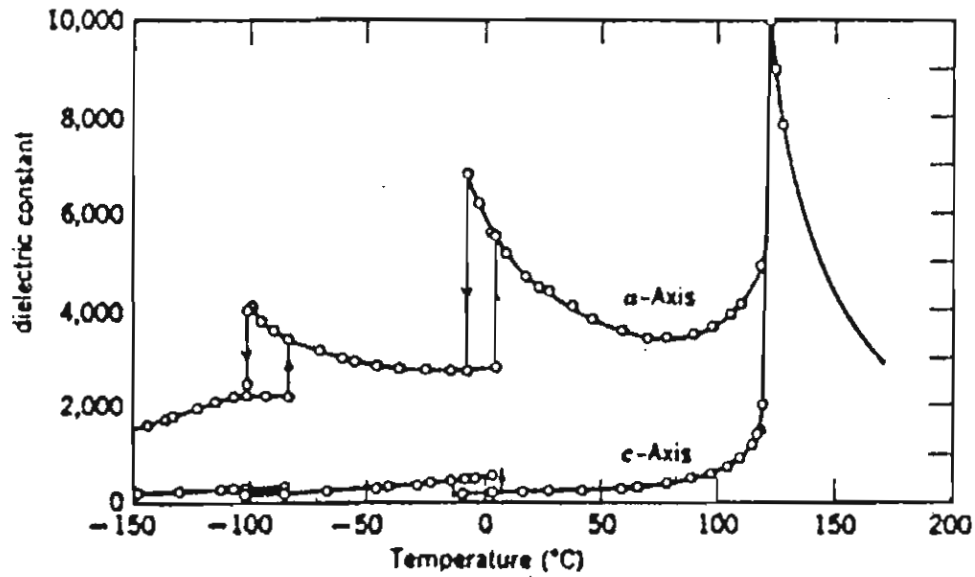

รูปที่ 1 Dielectric constant of Barium titanate ceramic as a function of temperature[2]

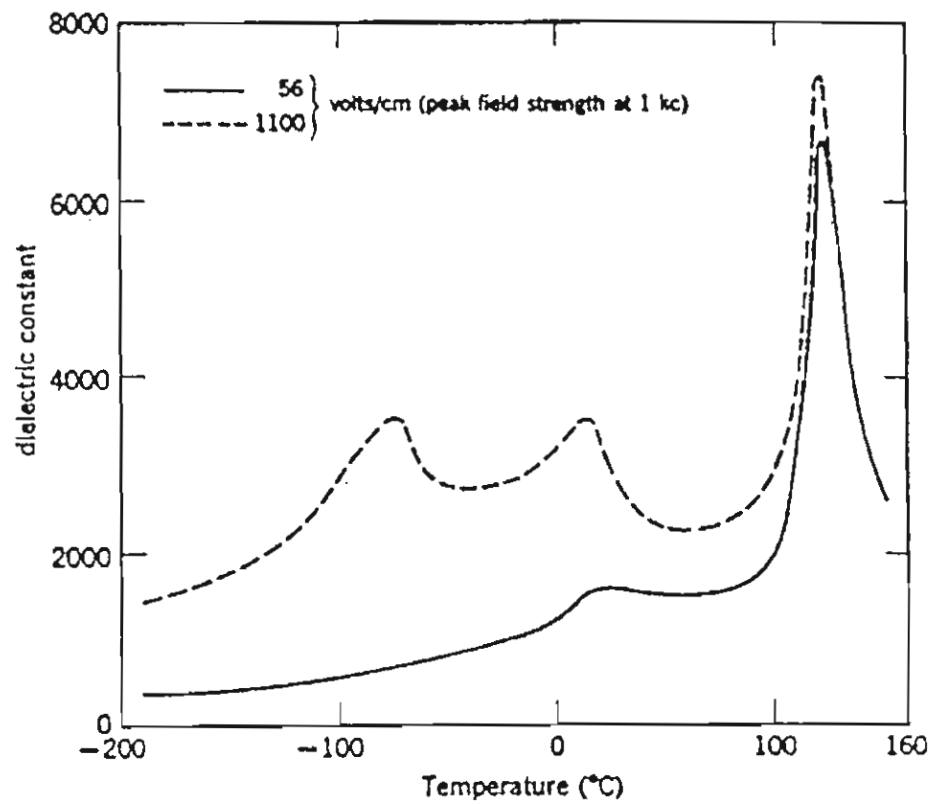

รูปที่ 2 Temperature dependence of dielectric constant[1]

จากรูปที่ 1 และ 2 ค่า ε_r ของ BT มีค่าสูงเมื่ออุณหภูมิเข้าใกล้ Curie point และมี peak ที่ Curie point และสมบัติของ BT สามารถเปลี่ยนแปลงแก้ไขได้โดยเติม additive ลงไปใน BT ดังตัวอย่างต่อไปนี้

Neirman (3) ได้เตรียมเซรามิกที่มีส่วนผสมของ $(1-x)BaTiO_3+(x)BaZrO_3$ โดย x มีค่าระหว่าง 0.0.25 ทำการ sintering ที่ 1250-1400 °C ได้ $\varepsilon_r > 12,000$ เมื่อ $x = 0.2$

Hennings (4) ได้เตรียมเซรามิกที่มีส่วนประกอบเป็น $Ba(Ti_{1-y}Zr_y)O_3$ พบว่าเมื่อ $Y = 0.13$ มีค่า $\varepsilon_r > 16,000$ แต่ถ้าเติม CaO ลงไป 13 mol% จะได้ $\varepsilon_r \approx 3,000$

Weill (5) ได้เตรียมเซรามิกที่มีส่วนประกอบเป็น $(1-x)BaTiO_3-(x)Ba(Mg_{1/3}Nb_{2/3})O_3$ และ $(1-x)BaTiO_3-(x)Ba(Co_{1/3}Nb_{2/3})O_3$ เมื่อ X มีค่าระหว่าง 0-0.1 โดยวิธีทางเคมีแล้วนำไป sintering ที่ 1250-1500 °C ได้เซรามิกมีค่า $\varepsilon_r \approx 220,000$ เมื่อเติม $Ba(Mg_{1/3}Nb_{2/3})O_3$ ที่มีค่า $X = 0.04$ และ $\varepsilon_r \approx 650,000$ เมื่อเติม $Ba(Co_{1/3}Nb_{2/3})O_3$ ที่มีค่า $X = 0.03$

จากตัวอย่างที่กล่าวมาข้างบนนี้ Weill สามารถเตรียมเซรามิกได้ ε_r สูงมาก จึงได้นำส่วนประกอบของเซรามิก $(1-x)BaTiO_3-(x)Ba(Mg_{1/3}Nb_{2/3})O_3$ มาทดลองเตรียมโดยวิธี solid state reaction เมื่อ $0 \leq x \leq 0.06$ ได้เซรามิกมีสมบัติดังตารางที่ 1

ตารางที่ 1 Physical properties of BMN doped BT ceramics. (T_C = Curie temperature)

Sintering Temperature T_s (°C)	Shrinkage (%)	Density (g/cm^3)	x	Dielectric Constant (ε_r)	T_C (°C)
1300	13.71	5.84	0.01	9,600	126
1350	13.47	5.84		10,000	119
1400	13.65	5.86		8,500	120
1300	15.81	5.85	0.02	43,000	98
1350	15.72	5.81		32,000	95
1400	15.93	5.80		16,000	103
1400	15.60	5.80	0.03	9,500	74
1450	15.46	5.84		10,000	73
1400	15.95	5.61	0.04	12,000	54
1450	15.90	5.76		14,300	54
1400	15.68	5.81	0.05	21,000	~30
1450	15.62	5.82		15,000	~30
1400	16.27	5.80	0.06	15,000	~30
1450	16.90	5.76		9,300	~30

และกราฟแสดงการเปลี่ยนแปลงของค่า ε_r และ dissipation factor (tanδ) ดังรูปที่ 3

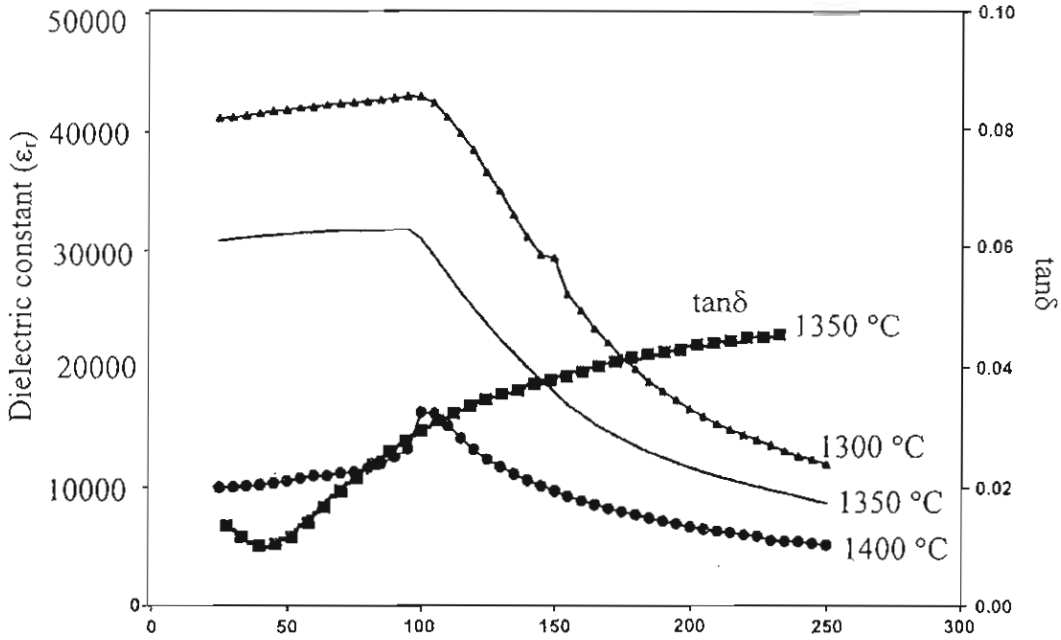

รูปที่ 3 Changes of dielectric constant (at 1 kHz) and dissipation factor (tanδ) against temperature of 2 mol% BMN doped BT ceramics at various sintering temperature.

จากรูปที่ 3 จะเห็นว่าค่า ε_r มีค่าประมาณ 43,000 และเกือบจะคงที่ในช่วงอุณหภูมิ 25-100 °C และมีค่า tanδ หรือ dielectric loss หรือ dissipation factor ต่ำ จึงเหมาะที่จะนำไปใช้ทำเป็นตัวเก็บประจุฟ้าสอดคล้องกับความต้องการในปัจจุบันที่ต้องการตัวเก็บประจุไฟฟ้าที่มีขนาดเล็ก และมีค่า capacitance สูง

เอกสารอ้างอิง

1. D.W. Richerson, *Modern Ceramic Engineering*, Marcel Dekber, New York, 1992.
2. A.J. Moulson and J.M. Herbert, *Electroceramics*, Chapman and Hall, London, 1990.
3. S.M. Neirman, The Curie Point Temperature of $Ba(Ti_{1-x}Zr_x)O_3$ Solid Solution, *J.Mater.Sci.*,**23**,3973-3980(1988).
4. D. Hennings, A.Schnel and G.Simon, Diffuse Ferroelecric Phase Transition in $Ba(Ti_{1-y}Zr_y)O_3$ Ceramics, J.Am.Ceram.Soc., 65[11], 539-544 (1982).
5. F. Weill, J.L. Rehspringer, P. Poix and J.C. Bernier, *J.Mater.Sci.*,**27**, 2321(1992).

Based on the DTA and XRD data, it may be concluded that, over a wide range of calcinations conditions, single phase $ZrTiO_4$ cannot be straightforwardly formed via a solid state mixed oxide synthetic route. Between 1100 and 1150 °C, TiO_2 anatase is transformed into the rutile phase. After 1200 °C, ZrO_2 totally disappeared, yet, up to 1240 °C, TiO_2 is remaining. A large temperature decrease observed at temperature greater than 1275 °C may be attribute to the crystallization of $ZrTiO_4$. The experimental work carried out here suggests that the optimal calcination conditions for single phase $ZrTiO_4$ is 1300 °C for 4 h with heating/cooling rates as fast as 20 °C/min.

The morphological evolution during calcination was investigated by scanning electron microscopy (SEM). Micrographs of ZT powders calcined at various temperatures from 1100 to 1300 °C for 4 h are shown in Fig. 5. In general, the particles are agglomerated and basically irregular in shape, with a substantial variation in particle size, particularly in samples calcined at high temperatures. The range of particle diameter was found to be about 0.2–1.0, 0.2–1.5, 0.3–2.0 and 0.5–3.0 μm for the samples calcined at 1100, 1175, 1200 and 1300 °C for 4 h, respectively. The results indicate that averaged particle size and degree of agglomeration tend to increase with calcination temperature. Moreover, the grain shape tends towards greater sphericity at higher temperatures. Energy dispersive X-ray (EDX) analysis showed the calcined compositions of the powder calcined at 1300 °C for 4 h with heating/cooling rates of 20 °C/min. to be $ZrTiO_4$, in agreement with XRD results.

4. Conclusions

Single-phase of zirconium titanate powders may be produced by employing a solid state reaction process using oxides as starting materials. Evidence has been obtained for a 100% yield of an orthorhombic $ZrTiO_4$ at a calcination temperature of 1300 °C for 4 h with heating/cooling rates of 20 °C/min. The resulting ZT powders consist of agglomerated particles of 0.5 to 3.0 μm in size, which are rounded in morphology.

Acknowledgements

The authors would like to acknowledge the Thailand Research Fund (TRF) for the financial support. One of the authors (R. T.) wishes to thanks the University of Ubon Ratchatanee and The Ministry of University Affair, Thailand for the scholarship.

References

[1] K. Wakino, K. Minai, H. Tamura, J. Am. Ceram. Soc. 67 (1984) 278–281.
[2] A.J. Moulson, J.M. Herbert, Electroceramics, Chapman & Hall, New York, 1990.
[3] M. Leoni, M. Viviani, G. Battilana, A.M. Fiorello, M. Viticoli, J. Eur. Ceram. Soc. 21 (2001) 1739–1741.
[4] K. Tanabe, Solid Acids and Bases: Their Catalytic Activity, Academic Press, New York, 1970.
[5] F.J. Parker, J. Am. Ceram. Soc. 73 (1990) 929–932.
[6] D.A. Chang, P. Lin, T. Tseng, J. Appl. Phys. 77 (1995) 4445–4447.
[7] M.K. Jain, M.C. Bhatnagar, G.L. Sharma, Sens. Actuators, B 55 (1999) 17–25.
[8] B.V. Cockeram, D.P. Measures, A.J. Mueller, Thin Solid Films 355–356 (1999) 17–25.
[9] R.E. Newnham, J. Am. Ceram. Soc. 50 (1967) 216.
[10] P. Bordet, A. Mchale, A. Santoro, R.S. Roth, J. Solid State Chem. 64 (1986) 30–46.
[11] A. Yamamoto, T. Yamada, H. Ikawa, O. Fukunaga, K. Tanaka, F. Marumo, Acta Crystallogr. C47 (1991) 1588–1591.
[12] R. Ruh, G.W. Hollenberg, E.G. Charles, V.A. Pale, J. Am. Ceram. Soc. 59 (1976) 495–499.
[13] S. Hirano, T. Hayashi, A. Hattori, J. Am. Ceram. Soc. 74 (1991) 1320–1324.
[14] J.A. Navio, F.J. Marchena, M. Macias, P.J. Sánchez-Soto, P. Pichat, J. Mater. Sci. 27 (1992) 2463–2467.
[15] A. Bianco, M. Paci, R. Freer, J. Eur. Ceram. Soc. 18 (1998) 1235–1243.
[16] M. Daturi, A. Cremona, F. Milella, G. Busca, E. Vogna, J. Eur. Ceram. Soc. 18 (1998) 1079–1087.
[17] G. Wolfram, H.E. Göbel, Mater. Res. Bull. 16 (1981) 1455–1463.
[18] A.E. Mchale, R.S. Roth, J. Am. Ceram. Soc. 66 (1983) C18–C20.
[19] Y. Park 105 (1998) 735–738.
[20] D. Houivet, J.E. Fallah, J.M. Haussonne, J. Eur. Ceram. Soc. 19 (1999) 1095–1099.
[21] P.J. Sánchez-Soto, M.A. Arilés, G. Colón, M. Macias, J.A. Navio, Mater. Lett. 20 (1994) 339.
[22] C.L. Wang, H.Y. Lee, F. Azough, J. Mater. Sci. 32 (1997) 1693–1701.
[23] F. Azough, R. Freer, J. Petzelt, J. Mater. Sci. 28 (1993) 2273–2276.

เอกสารหมายเลข 1.3